

**GENERATION OF HYDROGEN FROM SODIUM-
BOROHYDRIDE USING VARIOUS CATALYSTS AND
ADDITIVES FOR FUEL CELL APPLICATIONS**

Ph.D. THESIS

by

PRASHANT KUMAR SINGH



**DEPARTMENT OF CHEMICAL ENGINEERING
INDIAN INSTITUTE OF TECHNOLOGY ROORKEE
ROORKEE-247667 (INDIA)
JANUARY, 2020**



GENERATION OF HYDROGEN FROM SODIUM-BOROHYDRIDE USING VARIOUS CATALYSTS AND ADDITIVES FOR FUEL CELL APPLICATIONS

A THESIS

Submitted in partial fulfilment of the requirements for the award of the degree

of

DOCTOR OF PHILOSOPHY

in

CHEMICAL ENGINEERING

by

PRASHANT KUMAR SINGH



**DEPARTMENT OF CHEMICAL ENGINEERING
INDIAN INSTITUTE OF TECHNOLOGY ROORKEE
ROORKEE-247667 (INDIA)
JANUARY, 2020**



© INDIAN INSTITUTE OF TECHNOLOGY ROORKEE, ROORKEE-2020
ALL RIGHTS RESERVED



INDIAN INSTITUTE OF TECHNOLOGY ROORKEE

STUDENT'S DECLARATION

I hereby certify that the work presented in the thesis "GENERATION OF HYDROGEN FROM SODIUM-BOROHYDRIDE USING VARIOUS CATALYSTS AND ADDITIVES FOR FUEL CELL APPLICATIONS" is my own work carried out during a period from January 2014 to January, 2020 under the supervision of Dr. Taraknath Das, Assistant Professor, Department of Chemical Engineering, Indian Institute of Technology Roorkee, Roorkee.

The matter presented in this thesis has not been submitted by me for the award of any other degree of this or any other Institution.

Prashant Kumar Singh

(PRASHANT KUMAR SINGH)

SUPERVISOR'S DECLARATION

This is to certify that the above mentioned work is carried out under my supervision.

Dr. Taraknath Das

(Dr. Taraknath Das)
Supervisor

The Ph.D. Viva-Voce Examination of Mr. Prashant Kumar Singh, Research Scholar, has been held on 24th January, 2020.

Somla

Chairman, SRC

Prashant Kumar Singh

Signature of External Examiner

This is to certify that the student has made all the corrections in the thesis.

Dr. Taraknath Das

Signature of Supervisor

Dated: 24/01/2020

डा० तारकनाथ दास/Dr. Taraknath Das
सहायक प्राध्यापक/Assistant Professor
रासायनिक अभियांत्रिकी विभाग
Department of Chemical Engineering
भारतीय प्रौद्योगिकी संस्थान रुड़की
Indian Institute of Technology Roorkee
रुड़की/Roorkee-247 667(U.K.) INDIA

Somla

Head of the Department
विभागाध्यक्ष/H.O.D.

रासायनिक अभियांत्रिकी विभाग
Dept. of Chemical Engineering
भारतीय प्रौद्योगिकी संस्थान रुड़की/I. I. T. Roorkee
रुड़की/Roorkee-247 667 (INDIA)

ABSTRACT

The cobalt boride is used as catalyst for various important chemical reactions such as hydrogenation of alkenes, citral, aldehyde, and reduction of nitrogen oxide, water splitting reaction, ODH of propane, Oxygen Evolution Reaction, Na-O₂ batteries, and hydrogen generation. The unsupported and supported cobalt-boride catalysts have been prepared by considering various method of synthesis. The supports used for the synthesis of supported catalysts are ceria, carbon nanotubes, activated carbon, silica, titania, and alumina. The active component of these catalysts is cobalt-boride and the species dispersed over the support differently.

The objectives of the present thesis work were to study the generation of hydrogen from sodium-borohydride using various catalysts/additives for fuel cell applications. The generation of hydrogen was considered by a) hydrolysis of sodium borohydride solution using supported/bulk metal-boride catalysts, and b) thermolysis of sodium borohydride using metal halides additives.

Metal-boride catalysts were active for the hydrolysis of sodium borohydride at room temperature. The bulk metal-boride catalysts (CoB, NiB, and FeB) were synthesized by simple reduction precipitation method. The supported metal boride catalysts (CoB/SiO₂) were synthesized by two-step reduction precipitation followed by impregnation method. The surface area of the metal-boride catalysts was also increased by using various support materials. Since the metal-boride catalysts are not active for thermolysis of sodium borohydride for the generation of hydrogen. The metal halide additive/catalysts composite mixtures were active for the thermolysis of sodium borohydride at low temperature. The metal-halides additives/catalysts were used for the thermolysis study are MnCl₂, CaCl₂, and ZnCl₂. The sodium-borohydride/additive composite mixtures were prepared by facile solution method. The

bulk (CoB) or supported metal-boride (CoB/SiO₂) catalysts or the composite mixture (xMnCl₂/NaBH₄) were characterized using various characterization techniques to improve our understanding of hydrogen generation from sodium borohydride by considering various factors such as metal loading, effect of calcination temperature, effect of supports of catalysts, and the effect of thermolysis temperature to find the most suitable additive. Moreover, the synthesized catalysts and composite materials were characterized by BET, XRD, FE-SEM, in situ UV-vis spectrophotometer, FTIR and Raman spectroscopy.

A series of CoB, FeB, and NiB catalysts were prepared by the chemical reduction method using base stabilized sodium borohydride solution as a reducing agent. The CoB catalyst was most stable and highly dispersed even at high calcination temperature. The hydrolysis study suggested that CoB catalyst was most effective and suitable for the generation of hydrogen from hydrolysis of sodium borohydride. The generation of hydrogen using base stabilized CoB-BS catalysts was most active using both the base/without base stabilized sodium-borohydride solution. The generation of hydrogen using base stabilized sodium borohydride solution using various catalysts was as follows: CoB-BS > NiB-BS > FeB-BS.

The effect of support on the CoB catalysts were examined and studied. The supported cobalt boride catalysts (xCoB/SiO₂, xCoB/Al₂O₃, xCoB/MgO) were prepared by two-step impregnation-reduction method. The synthesized catalysts were studied for the hydrolysis of based stabilized sodium-borohydride solution for the generation of hydrogen. The synthesized catalysts were characterized by using BET, XRD, and Raman spectroscopy techniques. Various parameters such as catalysts loading, effects of calcination temperature, effect of supports were considered. The synthesized catalysts were calcined at various calcination temperature from 373 K to 773 K. The study suggested that the support plays a significant role on enhancing the generation of hydrogen from base stabilized sodium borohydride solution. Moreover, the calcination temperature also played a significant role in enhancing the catalytic

performance. It was necessary to calcine the CoB impregnated support at moderate temperature before reduction of the cobalt so that an active CoB is dispersed and anchored with the support properly. The study suggested that the surface area gradually increased with increasing calcination temperature up to 573 K and further increasing calcination temperature the surface area decreased for the catalysts xCoB/(support). However, all the calcined samples were highly amorphous in nature even at 673 K and started formation of crystalline phase at 773 K in 50CoB/Al₂O₃. It was also observed that a Co₃O₄ species formed with the CoB in all catalysts during the second step of catalyst synthesis (reduction step). The most active catalyst was found to be 50CoB/SiO₂ calcined at 573 K. The order of catalytic activity for the generation of hydrogen for all catalysts: 50CoB/SiO₂ > 50CoB/Al₂O₃ > CoB > 50CoB/MgO.

The effect of additives/catalysts for the thermolysis of sodium borohydride is also important for the generation of hydrogen. A series of MnCl₂ impregnated sodium borohydride composite mixture was prepared by facile solution method at room temperature. The additive loading was varied from 10 wt% to 50 wt% during the synthesis of composite materials. Other additives were also used such as CaCl₂ and ZnCl₂. However, the 20 wt% of additive was an optimum loading for the synthesis of 20MnCl₂/NaBH₄ composite mixture. The generation of hydrogen was obtained from the material 20MnCl₂/NaBH₄ at 373 K. The generation of hydrogen increased with increasing thermolysis temperature (373 K to 823 K). However, the study suggested that the generation of hydrogen was incomplete at 373 K from the material 20MnCl₂/NaBH₄. The most effective additive was found to be CaCl₂. The addition of additive assists in lowering the thermolysis temperature of NaBH₄ for the generation of hydrogen. The effect of additive considering various additives as follows: 20CaCl₂/NaBH₄ > 20MnCl₂/NaBH₄ > 20ZnCl₂/NaBH₄. The FTIR analysis and thermolysis study suggested that the generation of hydrogen was incomplete at low temperature (373 K).

Thus, the generation of hydrogen from sodium borohydride (hydrolysis/thermolysis) using various catalysts (supported/bulk) and metal-chloride additives with the information obtained from various characterization studies of BET, XRD, FTIR, FE-SEM, and Raman spectroscopy, the effect of various parameters could be established. The parameters included the effect of metal in metal boride catalysts, effect of calcination temperature, effect of supports, and effect of various additives.



Acknowledgements

I would like to take this opportunity to express my deep sense of thank to my supervisor, **Dr. Taraknath Das** (Assistant Professor, Department of Chemical Engineering, Indian Institute of Technology (IIT) Roorkee) who has introduced me to the field of hydrogen generation using heterogeneous catalysts and for constantly supporting me with essential research facilities. His support in terms of thorough guidance on the fundamentals of the subject helped me evolve and tackle every academically difficult situation of my Ph.D. It is an honour to have had the great opportunity to work with him. I would also like to thank to all other professors in the Department of Chemical Engineering, Indian Institute of Technology Roorkee, for their valuable suggestions and critical comments during the evaluation of my thesis, moreover, the valuable guidance, sharing of knowledge and academic support during my research.

I highly acknowledge the help of staff members of Instrument Analysis Laboratory (CHED) and Institute Instrument Center, IIT Roorkee, especially Mr. Satyapal Singh, Mr. Shiv Kumar and Mr. Arvind Kumar in carrying out the catalyst characterization studies.

I would further express my deep gratitude to my father Late **Mr. Fanish Singh** who passed away during my Ph.D., my mother **Mrs. Shashiprabha Singh**, without whose blessings and constant support my Ph.D. would have been impossible. A special acknowledge to **Dr. Surendra Kumar** (Former Professor CHED IIT Roorkee) and **Dr. Y. S. Negi** (Dean Saharnpur campus, IIT Roorkee) for his constant support and encouragement during my tenure as a Ph.D scholar in IIT Roorkee. I would also like to thank my laboratory mates in IIT Roorkee; Mr. Pradeep Kumar Yadav, Mr. Vijendra Kumar Yadav, Mr. Mamleshwar Kumar, Ms. Akanksha Singh Rajput and Mr. Kaustuv Bhattacharya, also a special mention of some of my colleagues Dr. Aniruddha Sanyal, Dr. Anil Kumar Verma, Mr. Mohd. Asif, Mr. Abhishekh Kumar Lal, Mr. Amit Singh and Dr. Lovjeet Singh for their constant support both in personal and professional affairs during my stay in Indian Institute of Technology Roorkee. Last but not the least; I would express my deep gratitude to **Mr. Praveen Kumar Singh, Mr. Savitendra Pratap Singh, Mr. Ravi Krishnan, Dr. Surendra Pratap Yadav, Mr. Rajoo Yadav and Mr. Ratnesh Singh** for being my constant emotional support at every tough phase of my Ph.D.

PRASHANT KUMAR SINGH



TABLE OF CONTENTS

Abstract		i-iv
Acknowledgements		v
Table Of Contents		vii-ix
List of Schemes		x
List of Tables		x
List of Figures		xi-xiv
Nomenclature		xv
Publications		xvi
Chapter		
1.	Review on Various Catalysts/Additives: Its Application To Hydrogen Storage and Generation from Sodium Borohydride	1-21
1.1	Introduction	1
1.2	Various modes of Hydrogen storage	1
1.3	Literature Review on Chemical Hydrides and Metal hydrides	3
1.4	Hydrogen Generation Study	4
1.4.1	Hydrolysis Study and Use of Various Catalysts	5
1.4.2	Thermolysis Study and Use of Various Additives/Catalysts	7
1.5	Kinetics and Hydrogen Generation Mechanism (Hydrolysis / Thermolysis)	10
1.6	Applications of Hydrogen Energy	11
1.7	Industrial Methods of Production of NaBH ₄	12
1.7.1	The Brown-Schlesinger Process	12
1.7.2	The Bayer Process	13
1.8	Characterizations of Sodium Borohydrides and the Metal-Boride/Metal Halides Catalysts	14
1.8.1	BET Surface Area Analysis	14
1.8.2	XRD Analysis	14
1.8.3	UV-Vis Analysis	16
1.8.4	FE-SEM Analysis	16
1.8.5	Raman Study	17
1.8.6	FTIR Study	17
1.8.7	TGA Analysis	18
1.9	Summary	18
1.10	Research Objectives	19
1.11	Thesis Outline and Organization	20
2.	Generation of Hydrogen from NaBH₄ Solution using Metal-Boride (CoB, FeB, NiB) Catalysts	22-44
2.1	Abstract	22
2.2	Introduction	22

2.3	Experimental Method	25
2.3.1	Catalysts Preparation	25
2.3.2	Characterization Studies	26
2.3.3	In-situ Chemical Reduction of metal chloride in UV-vis Spectrometer	26
2.3.4	Hydrogen generation study	26
2.4	Results and discussion	27
2.4.1	BET surface area analysis	27
2.4.2	<i>In Situ</i> UV-vis spectroscopy analysis during catalyst synthesis	27
2.4.3	FTIR Spectra Analysis	28
2.4.4	X-ray Diffraction analysis	29
2.5	Hydrogen generation study	30
2.5.1	Hydrogen generation using various metal-boride catalysts	30
2.5.2	The effect of base during catalysts synthesis and generation of hydrogen over various metal-boride catalysts	31
2.5.3	Hydrogen generation and effect of calcination temperature	31
2.6	Conclusions	32
3.	Hydrolysis of Sodium Borohydride Using Supported Cobalt Boride Catalyst For The Generation of Hydrogen	45-62
3.1	Abstract	45
3.2	Introduction	45
3.3	Experimental Method	47
3.3.1	Preparation of Catalysts	47
3.3.2	Catalyst characterization Studies	48
3.3.3	Hydrogen generation study	49
3.4	Results and discussion	49
3.4.1	Surface area analysis	49
3.4.2	Powdered X-ray diffraction (P-XRD) analysis	50
3.4.3	Raman analysis	50
3.5	Hydrogen generation study	51
3.5.1	Effect of cobalt boride loading with supports and generation of hydrogen	52
3.5.2	Effect of calcination temperature and generation of hydrogen	52
3.5.3	Effect of supports and generation of hydrogen	53
3.6	Conclusions	53
4.	Generation of Hydrogen from Sodium Borohydride at Low Temperature using Metal Halides Additive	63-84
4.1	Abstract	63
4.2	Introduction	63
4.3	Experimental	66
4.3.1	Material Preparation	66
4.3.2	Synthesized Material characterizations	67
4.3.3	Thermal decomposition behaviour and hydrogen generation study	67

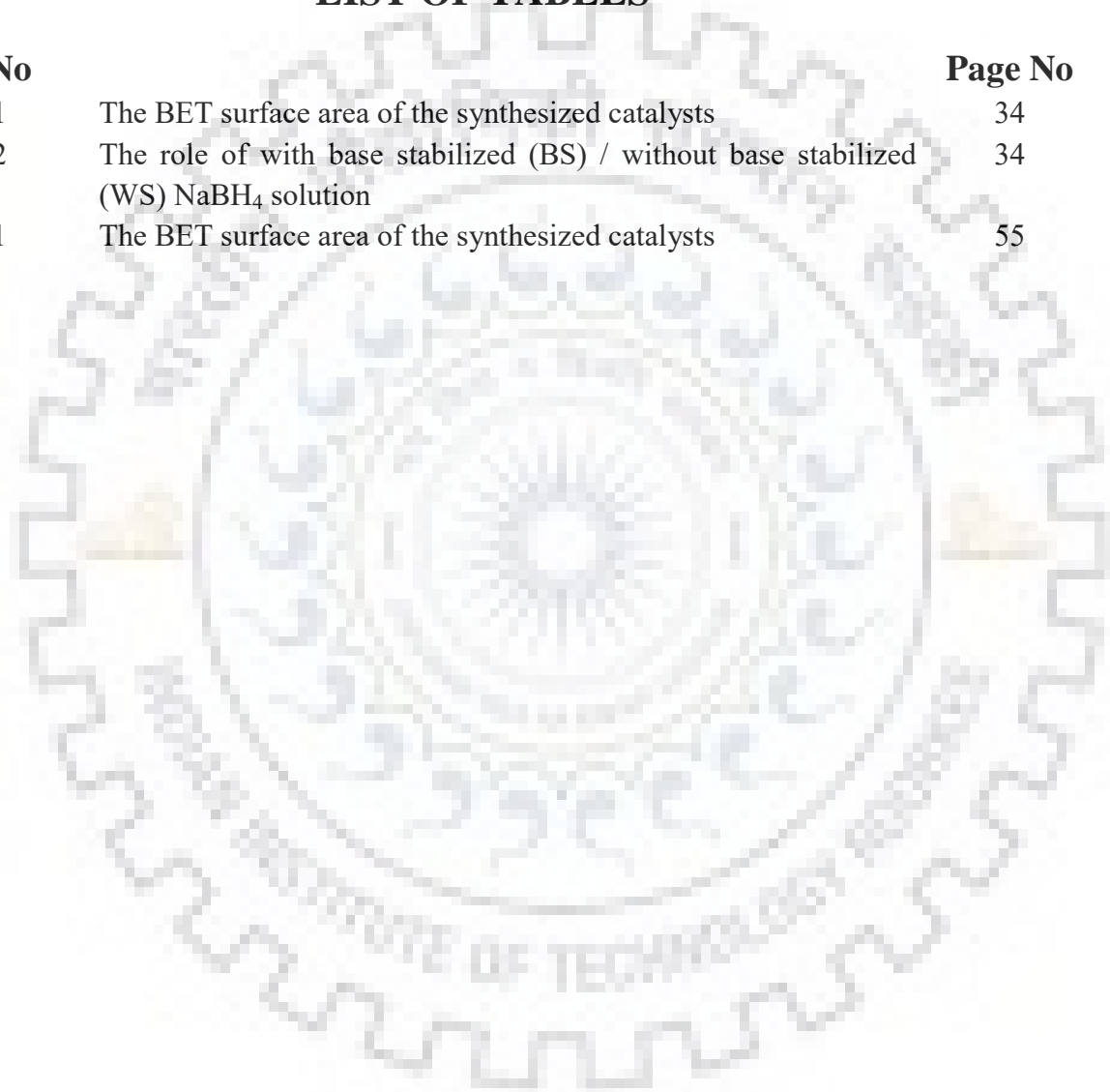
4.4	Results and Discussion	68
4.4.1	Powdered X-ray diffraction (P-XRD) studies	68
4.4.2	Field Emission Scanning Electron Microscopy (FE-SEM) Studies	69
4.4.3	Thermo Gravimetric Analysis (TGA) Studies	69
4.4.4	Raman analysis	69
4.5	Thermolysis and FTIR analysis	70
4.5.1	The effect of temperature on pure NaBH ₄ and 20MnCl ₂ /NaBH ₄	70
4.5.2	Effect of additive loading and thermolysis of xMnCl ₂ /NaBH ₄	71
4.5.3	Effect of various additives over 20(additives)/NaBH ₄	71
4.6	Conclusions	72
5.	Conclusions and recommendations	85-89
5.1	Conclusions	85
5.2	Recommendations	87
	References	90-112
	Appendices	113-163
	Appendix A	113
	Appendix B	116
	Appendix C	130
	Appendix D	138
	Appendix E	144

LIST OF SCHEMES

Table No		Page No
Scheme 2.1	The generation of H ₂ using metal boride catalysts	35
Scheme 3.1	The experimental set-up for the thermolysis of xMnCl ₂ /NaBH ₄ mixture for the generation of hydrogen	73

LIST OF TABLES

Table No		Page No
Table 2.1	The BET surface area of the synthesized catalysts	34
Table 2.2	The role of with base stabilized (BS) / without base stabilized (WS) NaBH ₄ solution	34
Table 3.1	The BET surface area of the synthesized catalysts	55



LIST OF FIGURES

Figure No		Page No
Figure 2.1	<i>In situ</i> reduction of CoCl ₂ and synthesis of CoB-BS catalyst using base stabilized NaBH ₄ solution a) CoCl ₂ solutions (1.75 ml), b) subsequent addition of 0.3 ml, c) 0.6 ml, d) 1.0 ml, e) 1.4 ml, f) 1.6 ml, g) 2.0 ml of base stabilized NaBH ₄ solution. The <i>in-situ</i> chemical reduction was performed by using 0.002 (M) CoCl ₂ solutions and a base stabilized 0.005 (M) NaBH ₄ solutions	36
Figure 2.2	<i>In situ</i> reduction of NiCl ₂ and synthesis of NiB-BS catalyst using base stabilized NaBH ₄ solution a) NiCl ₂ solutions (1.75 ml), b) subsequent addition of 0.3ml, c) 0.6 ml, d) 0.9 ml, e) 1.2 ml of base stabilized NaBH ₄ solution. The <i>in-situ</i> chemical reduction was performed by using 0.002 (M) NiCl ₂ solutions and a base stabilized 0.005 (M) NaBH ₄ solutions.	37
Figure 2.3	Ex-situ reduction of FeCl ₃ and synthesis of FeB-BS catalyst using base stabilized NaBH ₄ solution a) FeCl ₃ solution (0.25 (M) 4.0 ml), b) subsequent addition of 0.3 ml, c) 0.6 ml, d) 1.0 ml, e) 2.0 ml, f) 3.5 ml, g) 4.5 ml NaBH ₄ solution	38
Figure 2.4	Ambient FTIR spectra of base stabilized catalysts a) FeB-BS, b) NiB-BS and c) CoB-BS calcined at 393 K for 2 h	39
Figure 2.5	X-Ray diffraction patterns of a) CoB-BS, b) FeB-BS, and c) NiB-BS catalysts calcined at 393 K for 2 h	40
Figure 2.6	XRD patterns of CoB-BS catalyst calcined with various calcinations temperature at a) desecrator dried, b) 383 K, c) 473 K, d) 573 K, e) 673 K, and f) 773 K for 1 h	41
Figure 2.7	The generation of hydrogen with time using 10 mg of each catalysts a) CoB-BS, b) NiB-BS and c) FeB-BS at 303 K, A) The generation of hydrogen using base stabilized (BS) 0.25 (M) NaBH ₄ solution and B) The generation of hydrogen using without base stabilized (WS) 0.25 (M) NaBH ₄ solution	42
Figure 2.8	The rate of hydrogen with time using 10 mg of each catalyst at 303 K; A) NiB-WS, B) FeB-BS, C) CoB-BS. The generation of hydrogen was studied using with (BS) or (WS) base stabilized 0.25 (M) NaBH ₄ solutions	43
Figure 2.9	The generation of hydrogen at 303 K using CoB-BS catalyst synthesized with different calcinations temperature at a) desecrator dried, b) 383 K, c) 473 K, d) 573 K, e) 673 K, and f) 773 K for 1 h. The generation of hydrogen was studied using with base stabilized (BS) 0.25 (M) NaBH ₄ solutions	44
Figure 3.1	X-ray diffraction patterns of a) xCoB/SiO ₂ with different loading (5 wt% to 50 wt%) calcined at 573 K, b) 50CoB/SiO ₂ with various calcination temperature (oven dried to 773 K), and c) 50CoB/(support) with various supports (SiO ₂ , Al ₂ O ₃ , MgO)	56

	calcined at 573 K. Where, x was weight percent of CoB in support (5 wt%, 10 wt%, 20 wt%, 30 wt%, 40 wt%, and 50 wt%)	
Figure 3.2	The Raman spectra of a) $x\text{CoCl}_2/\text{SiO}_2$ samples calcined at 573 K for 2 h, b) after reduction with NaBH_4 solution of each catalyst reported in Figure2 a. Where the x was the wt% of CoCl_2 impregnated over the support. (x = 5 wt%, 10 wt%, 20 wt%, 30 wt%, 40 wt% and 50 wt%)	57
Figure 3.3	The Raman spectra of a) $50\text{CoCl}_2/\text{SiO}_2$ samples calcined at various temperature for 2 h, b) reduction with NaBH_4 solution of each catalysts reported in Figure3 a	58
Figure 3.4	The Raman spectra of a) $50\text{CoCl}_2/(\text{support})$ samples calcined at 573 K, b) after reduction the same sample with NaBH_4 solution, the catalysts reported in Figure4 a. The supports used were SiO_2 , Al_2O_3 , and MgO	59
Figure 3.5	The generation of hydrogen using $x\text{CoB}/\text{SiO}_2$ catalysts with changing total loading of CoB and bulk CoB catalyst. The generation of hydrogen study was conducted with the temperature at 303 K using 20 mg of catalyst. The catalyst was calcined at 573 K followed by reduction with NaBH_4 solution	60
Figure 3.6	The generation of hydrogen using $50\text{CoB}/\text{SiO}_2$ catalyst with changing calcinations temperature from oven dried to 773 K. The generation of hydrogen study was conducted with the temperature at 303 K using 20 mg of catalyst calcined at 573 K followed by reduction with NaBH_4 solution	61
Figure 3.7	The generation of hydrogen using $50\text{CoB}/(\text{support})$ catalysts with changing supports (SiO_2 , Al_2O_3 , and MgO). The generation of hydrogen study was conducted with the temperature at 303 K using 20 mg of catalyst calcined at 573 K followed by reduction with NaBH_4 solution	62
Figure 4.1	The XRD Patterns of p- NaBH_4 at various decomposition temperatures at (a) 373 K, (b) 473 K, (c) 573 K, (d) 673 K and (e) 773 K, for 1 h at each temperature with the flow of nitrogen gas (15 ml/min flow rate) in reactor (HVC-DRM-5). The P-XRD patterns were collected after cool down each material at room temperature	74
Figure 4.2	The P-XRD patterns of $20\text{MnCl}_2/\text{NaBH}_4$ at various decomposition temperatures at (a) 303 K, (b) 373 K, (c) 473 K, (d) 573 K, (e) 673 K, (f) 773 K and (g) 823 K for 1 h at each temperature with the flow of nitrogen gas (15 ml/min flow rate) in reactor (HVC-DRM-5). The XRD patterns were collected after cool down each material at room temperature	75
Figure 4.3	The XRD Patterns of various materials (a) p- NaBH_4 , (b) $10\text{MnCl}_2/\text{NaBH}_4$, (c) $20\text{MnCl}_2/\text{NaBH}_4$, (d) $30\text{MnCl}_2/\text{NaBH}_4$, (e) $40\text{MnCl}_2/\text{NaBH}_4$ and (f) $50\text{MnCl}_2/\text{NaBH}_4$. The XRD patterns for	76

	each composite materials mixer were collected at room temperature	
Figure 4.4	The P-XRD Patterns of various materials (a) p-NaBH ₄ (b) 20MnCl ₂ /NaBH ₄ , (c) 20ZnCl ₂ /NaBH ₄ and (d) 20CaCl ₂ /NaBH ₄ . The XRD patterns for each composite material were collected at room temperature	77
Figure 4.5	Field Emission Scanning Electron Microscopy (FE-SEM) images of various materials (a) p-NaBH ₄ , (b) 10MnCl ₂ /NaBH ₄ , (c) 20MnCl ₂ /NaBH ₄ (d) 30MnCl ₂ /NaBH ₄ , (e) 40MnCl ₂ /NaBH ₄ and (f) 50MnCl ₂ /NaBH ₄	78
Figure 4.6	Thermo Gravimetric Analysis (TGA) of (a) 20MnCl ₂ /NaBH ₄ , (b) 30MnCl ₂ /NaBH ₄ , (c) 40MnCl ₂ /NaBH ₄ , (d) 50MnCl ₂ /NaBH ₄ , (e) 10MnCl ₂ /NaBH ₄ and (f) p-NaBH ₄	79
Figure 4.7	The Raman spectra of various materials (a) p-NaBH ₄ , (b) 20ZnCl ₂ /NaBH ₄ , (c) 20MnCl ₂ /NaBH ₄ , and (d) 20CaCl ₂ /NaBH ₄ . The spectra for each composite material were collected at room temperature	80
Figure 4.8	(A) The FTIR spectra of p-NaBH ₄ at various decomposition temperature with the flow of nitrogen gas flow through reactor (HVC-DRM-5) at (a) 303 K, (b) 373 K, (c) 473 K, (d) 573 K, (e) 673 K and (f)773 K for 1 h at each temperature, (B) The Generation of hydrogen from p-NaBH ₄ at different decomposition temperature after 5 min, (C) The generation of hydrogen from p-NaBH ₄ at different thermal decomposition temperature (a) 373 K, (b) 473 K, (c) 573 K, (d) 673 K, (e) 773 K and (f) 823 K	81
Figure 4.9	(A) The FTIR spectra of 20MnCl ₂ /NaBH ₄ at various decomposition temperature with nitrogen gas flow through reactor (HVC-DRM-5) for 1 h at (a) 303 K, (b) 373 K, (c) 473 K, (d) 573 K, (e) 673 K, (f) 773 K, (g) 823 K, (B) The generation of hydrogen from 20MnCl ₂ /NaBH ₄ at different thermal decomposition temperature after 5 min, (C) The generation of hydrogen from 20MnCl ₂ /NaBH ₄ at different thermal decomposition temperature (a) 373 K, (b) 473 K, (c) 573 K, (d) 673 K, (e) 773 K, (f) 823 K	82
Figure 4.10	(A) The FTIR spectra of x wt% of MnCl ₂ doped in xMnCl ₂ /NaBH ₄ samples by changing the weight percentage of additive MnCl ₂ over NaBH ₄ samples (a) p-NaBH ₄ , (b) 10MnCl ₂ /NaBH ₄ , (c) 20MnCl ₂ /NaBH ₄ , (d) 30MnCl ₂ /NaBH ₄ , (e) 40MnCl ₂ /NaBH ₄ and (f) 50MnCl ₂ /NaBH ₄ at 373 K temperature after thermolysis. All spectra were collected at room temperature post thermolysis of the material. (B) The Generation of hydrogen after 5 min of thermolysis in the flow of nitrogen gas and (C) The detail generation of hydrogen for 5 to 60 min of run at each	83

decomposition temperature . The sample was taken ~ 50 mg for each analysis

Figure 4.11

Generation of hydrogen with 20 Wt% of additive (20M-Cl₂/NaBH₄) at 373 K after 5 min reaction in nitrogen control environment in reactor (HVC-DRM-5). Where, x is the loading of additives (M = Mn, Ca and Zn)

84



NOMENCLATURE

Symbol	Nomenclature
ODH	Oxidative Dehydrogenation
PdH	Palladium hydride
MOF	Metal–organic Framework
BET	Brunauer-Emmett-Teller
XRD	X-Ray Diffraction
TPD	Temperature Programmed Desorption
TPR	Temperature-programmed Reduction
TGA	Thermal Gravimetric Analysis
TG/MS	Thermal Gravimetric Mass Spectrometry
DTA	Differential Thermal Analysis
SEM	Scanning Electron Microscopy
FE-SEM	Field Emission Scanning Electron Microscopy
FTIR	Fourier Transform Infrared Spectroscopy
UV-VIS	Ultraviolet–visible Spectroscopy
XPS	X-ray Photoelectron Spectroscopy
DSC	Differential Scanning Calorimetry
NMR	Nuclear Magnetic Resonance
DFT	Density Functional Theory



PUBLICATIONS

INTERNATIONAL JOURNALS

- Prashant Kumar Singh, Taraknath Das, Generation of hydrogen from NaBH_4 solution using metal-boride (CoB, FeB, NiB) catalysts, International journal of hydrogen energy 42 (2017) 29360-29369. (Impact Factor: 4.084)
- Prashant Kumar Singh, Ishwar Sharan, Mamleshwar Kumar, Taraknath Das, Generation of hydrogen from sodium borohydride at low temperature using metal halides additive, International journal of hydrogen energy 42 (2019) 20191-20202. (Impact Factor: 4.084)
- Prashant Kumar Singh, Taraknath Das, Hydrolysis of sodium borohydride using supported cobalt boride catalyst for the generation of hydrogen, 2019 (under review)

INTERNATIONAL AND NATIONAL CONFERENCES

- (Chemcon-2016)(P. K. Singh, T. Das, "Generation of hydrogen using Co, Fe, and Ni boride catalysts from NaBH_4 solution", 27-30th Dec,2016, Chemcon2016, India)
- (WHEC-2016) (P. K. Singh, A. Jain, T. Das, "Generation and storage of hydrogen from NaBH_4 solution using metal boride catalysts" June 13-16, 2016, 21st WHEC-2016, Zaragoza, Spain)
- (Hypothesis-XIII 2018) (P. K. Singh, Ishwar Sharan, T.Das," Thermolysis of sodium borohydride at low temperature using metal halides as additive", 24-27th July, 2018, Hypothesis-XIII 2018, NTU, Singapore)

REVIEW ON VARIOUS CATALYSTS/ADDITIVES: ITS APPLICATION TO HYDROGEN STORAGE AND GENERATION FROM SODIUM BOROHYDRIDE

1.1 Introduction

Hydrogen is a light, green, renewable, environmentally friendly and efficient source of energy carrier and produces only water as a byproduct after combustion. The chemical energy per unit mass of hydrogen (142 MJ/kg or 39.4 kWh/kg) is three times larger than other chemical fuels (the heating value of methane (13.9 kWh/kg) and petrol (12.4 kWh/kg)) [Schlapbach and Zuttel, 2001; Zuttel, 2004]. The hydrogen atom is utmost abundant in the earth, and no molecular hydrogen exists. However, it is available in various forms such as water, hydrocarbons and other various compounds. Presently, 96 % of hydrogen is being produced from fossil resources. Hydrogen is produced from various sources like thermolysis of water [Zuttel, 2004], electrolysis of water [Zheng et al., 2019; Kovendhan et al., 2019; Lei et al., 2019; Qureshy et al., 2019], photocatalysis of water [Wang et al., 2019], reforming of methane [Yadav and Das, 2019; Soykal et al., 2012], and ethanol [Nanda et al., 2019], conversion of biomass [Azadi et al., 2014; Chang et al., 2011; Sharma, 2019; Siddiqui and Dincer 2019], coal [Siriwardane et al., 2019; Ma et al., 2019; Yang et al., 2019; Barbuzzaa et al., 2019], and waste-materials [Soria et al., 2019; Irfan et al., 2019; Acar and Dincer, 2019].

1.2 Various modes of Hydrogen storage

As a light, environmentally friendly and renewable source of energy, hydrogen has been considered the most efficient fuel for hydrogen-powered fuel cell applications [Schlapbach and Zuttel, 2001; Zuttel, 2004]. Hydrogen based fuel cell system is not merely delayed due to lack of storage technology. Many other factors are associated such as viable hydrogen generation technology, safety & public acceptance, and commercial competitiveness with Li-Ion battery. However, hydrogen is being used as clean fuel only for the space program. Since, for on-board energy storage, vehicles need compact, light and safe storage vessel. Moreover, a combustion engine burns about 24 kg of petrol to run a range of 400 km. The same range can be meeting with 8 kg of hydrogen in the combustion engine and 4 kg of hydrogen in an electrical car with fuel cell [Schlapbach and Zuttel, 2001]. Therefore, the easy and safe storage of hydrogen is essential for onboard vehicle application. The purpose of storage of hydrogen is the reduction of volume or increase the density of hydrogen gas. Since 1 kg of hydrogen gas takes 11 m³ of

volume at ambient temperature and pressure [Zuttel, 2004]. However, hydrogen has been stored in various ways such as liquefied hydrogen in cryogenic storage vessels, gas phase as compressed hydrogen, solid-state as a metal-hydride and adsorption in porous materials (MOF, carbon nano-tubes (CNT), fullerenes, activated carbon, clathrates, and graphene sheet). Depending upon the application and the storage size, various types of hydrogen storage systems have been considered. A large scale stationary storage system for production sites, a stationary small scale storage system for distribution sites, and mobile small storage system for onboard vehicles have been used. Vehicle tanks have been used to store hydrogen for road vehicles. Since hydrogen is a low-density fuel, as a result always requires large volumes for high-pressure heavy storage tanks (gas phase storage), extremely low temperature (liquid phase storage), or as metal hydride (solid-phase storage).

The most important consideration for the storage vessel for such high pressure compressed hydrogen storage tank is preferred must be lightweight, inexpensive, and able to withstand the embrittlement with hydrogen. In high-pressure storage tank (200 to 450 bar) internal volume required is 225 liters to store 4 kg of hydrogen (volumetric density, $\rho_v < 40 \text{ kgH}_2/\text{m}^3$). However, hydrogen stored in higher pressure tanks, the cost is high, less practicality, unsafe and unacceptable by the general public [Zuttel, 2004]. Moreover, In addition to the safety of gaseous hydrogen itself a flammable, the high-pressure storage vessel leads to severe safety problems.

The liquid phase storage of hydrogen by Cryo-cooling or liquefaction at low temperature is another possibility of storage of hydrogen. The liquid hydrogen is being used for the launching process of the space shuttle. Since, the storage of hydrogen such as compressed gas or liquefaction is not suitable for portable or automotive application due to their low hydrogen storage densities (volumetric density, $\rho_v \sim 70.8 \text{ kg/m}^3$ at $-253 \text{ }^\circ\text{C}$) [Parker, 2010]. The liquid hydrogen has been considered for various hydrogen-fueled cars, such as BMW model (750 hL), freedom car, Toyota and Honda. The advantage in the process is that the store hydrogen ~ 2.6 times the energy per unit mass as gasoline; however, the disadvantage is that it needs about 4 times the volume for a given amount of energy [Grochala and Edwards, 2004]. Moreover, the challenge is the energy-efficiency of the liquefaction process and thermal insulation of the cryogenic storage vessel due to boil-off of hydrogen [Schlapbach and Zuttel, 2001; Ren et al., 2017].

Each storage mechanism has fundamental limits, such as gaseous hydrogen requires a large volume, liquid hydrogen evaporates easily, and metal hydrides add significant weight to the system and adsorbent materials do not hold enough hydrogen. Thus, solid-state storage is

recently found as the safest and most effective way of routinely handling hydrogen [Grochala and Edwards, 2004; Durbin and Jugroot, 2013]. Hydrogen can be supply and stored at room temperature and atmospheric pressure as chemical/metal hydrides [Schlapbach and Zuttel, 2001]. In this particular method of storage, the volumetric density of hydrogen (volumetric density, $\rho_v \sim 150 \text{ kg/m}^3$ at 1 bar and $>100 \text{ }^\circ\text{C}$) is improved as compared to other modes of storages [Parker, 2010; Mao et al., 2012]. However, the most important criterion of the storage of hydrogen in various forms is the reversibility nature of hydrogen uptake and release [Grochala and Edwards, 2004]. The hydrogen in metal hydrides like PdH or LaNi_5H_6 is stable and reversible. In this particular form of storage, hydrogen atom occupies the interstitial site in the metal lattice without the formation of any bond with the metal atom. These hydrides are not suitable due to very high mass of metal. The gravimetric density of hydrogen in metal hydride could be improved by using B or Al atom. The most promising material for hydrogen storage with high volumetric and gravimetric hydrogen density is found to be borohydrides and alanates. The hydrogen density of $\text{Al}(\text{BH}_4)_3$ (150 kg/m^3) is almost double than that of the liquid hydrogen [Parker, 2010]. In spite of the improved storage capacity, the metal hydrides decompose at high temperature and produce various side products are such as ammonia, halides, and diborane. Moreover, the interesting properties observed with the hydrogen storage materials or metal hydrides that the materials follow low activation energy barrier with low decomposition temperature are very unstable which store hydrogen irreversibly and the materials are thermodynamically very stable with high activation energy barrier and high decomposition temperature that store hydrogen reversibly. The destabilization of metal hydrides or decrease dehydrogenation temperature to release hydrogen is possible by the addition of the second cation or increase the electronegativity of the cation. As results, the thrust materials should be catalytically enhanced thermodynamically slightly stable with low decomposition that store hydrogen reversibly. It has been reported that the catalyst-supported LiAlH_4 generate hydrogen at room temperature, however, the nature of catalysts and the detailed mechanism of catalytic action are unknown for alanates. Thus, to search a catalytically improve the reversibility of hydrogen storage material is under research and development [Grochala and Edwards, 2004; Durbin and Jugroot, 2013; Dasi and Bhattacharya, 2015; Ren et al., 2017].

1.3 Literature Review on Chemical Hydrides and Metal hydrides

The solid-state storage of hydrogen is one of the most promising ways of storage of hydrogen. As results a lot of attention is given on development and synthesis of chemical hydrides or metal hydrides consists of the high volumetric and gravimetric storage capacity of

hydrogen operates at low temperature, and that should be reversible. The most promising chemical hydride is considered to be $\text{NH}_3\text{-BH}_3$ (AB) (19.6 wt %), and N_2H_4 (hydrazine, 12.6 wt %). Borazine is being released as a by-product during the dehydrogenation of ammonia-borane [Dasi and Bhattacharya, 2015]. However, in spite of high content of hydrogen, due to slow kinetics and unfavourable thermodynamics associated with the release of hydrogen, it is limited to use of these chemical hydrides as potential hydrogen storage materials. There are various types of metal hydrides that have also been reported such as simple metal hydrides consist of one metal with hydrogen (MH_x , MgH_2 , PdH_x), intermetallic hydrides (consists of two or more metals with hydrogen) ($\text{A}_m\text{B}_n\text{H}_x$, NaAlH_4), complex metal hydrides (N or B containing hydrides) (Li_2NH , LiBH_4) [Durbin and Jugroot, 2013]. Moreover, various metal hydrides have been studied for the storage and generation of hydrogen such as LiAlH_4 , NaAlH_4 , LiBH_4 , KBH_4 , MgH_2 , PdH_x , $\text{Ca}(\text{BH}_4)_2$, $\text{Mg}(\text{BH}_4)_2$, and NaBH_4 [Zuttel, 2004; Mao and Gregory, 2015; Hsueh et al., 2011; Niaz et al., 2015; Berg and Arean, 2008]. The palladium hydride can adsorb a sufficient amount of hydrogen in a reversible process at room temperature and atmospheric pressure, however, Pd is costly and heavy metal did not yield good gravimetric efficiency. The magnesium hydride a lightweight alkaline earth metals store a large amount of hydrogen (~ 7.7 wt%), however, due to strong metal-hydrogen bond, the desorption temperature is unfavourable (~ 300 °C) [Dasi and Bhattacharya, 2015; Berg and Arean, 2008]. Various metal hydrides have been considered to be release hydrogen by reaction with water such as CaH_2 , LiBH_4 , NaBH_4 , and magnesium, aluminium-based powdered materials [Berg and Arean, 2008]. Among the various hydrogen storage materials, NaBH_4 has been considered to be a promising hydrogen storage material, since its cost is low and the material having high hydrogen density (~ 10.6 wt %). However, due to high decomposition temperature (500 °C at 1 atm), little focus has been given on sodium borohydride as compared to other borohydrides (Li, Mg, and Ca) as hydrogen storage material [Mao and Gregory, 2015].

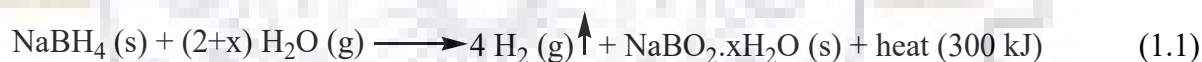
1.4 Hydrogen Generation Study

Hydrogen can be stored in room temperature and atmospheric pressure. The storage of hydrogen in the solid-state as sodium borohydride is one of the promising routes of storage. The storage of hydrogen in sodium borohydrides is ~ 10.6 wt %. The generation of hydrogen from sodium borohydride is possible either by hydrolysis (reaction with water in presence of a catalyst) or thermolysis study (thermal heating in presence of additive or catalyst) for the direct use of hydrogen in fuel cell application [Hsueh et al., 2011; Niaz et al., 2015; Berg and Arean, 2008; Alfonso et al., 2009; Jeon and Cho, 2006; Paskevicius et al., 2013; Ren et al., 2017]. The thermal hydrolysis is not attractive for portable applications due to high-temperature stability

of metal hydride even at 500 °C and the gravimetric hydrogen storage capacity of hydrolysis based storage system is lower than theoretical (~10.6 wt %) due to excess water required to dissolve NaBH₄ and formation of by-product (NaBO₂) in storage vessels during hydrogen generation [Zuttel, 2004; Mao and Gregory, 2015; Alfonso et al., 2009; Demirci et al., 2009]. In spite of a few limitations in each mode of storage and generation of hydrogen from sodium borohydride is preferred due to low cost and high hydrogen storage capacity.

1.4.1 Hydrolysis Study and Use of Various Catalysts

The alkaline solution of sodium borohydride in water constitutes a super-efficient storage system (~9.2 wt% of H₂) and pure water contains ~ 11.1 wt% of hydrogen. The control of hydrogen evolution from the solution is possible by using a proper catalyst [Grochala and Edwards, 2004]. Thus, the catalytic hydrolysis of aqueous metal hydride solution to generate hydrogen is a promising method [Amendola et al., 2000]. The hydrolysis process is not taken seriously for automobile applications. However, the hydrolysis process is very fast and it takes 2.5 or 16 min to complete in the presence of a catalyst, in spite of a promising reaction process, it is not reversible [Durbin and Jugroot, 2013]. The exothermic hydrolysis reaction is followed as per below reaction 1.1 [Alfonso et al., 2009; Amendola et al., 2000; Ingersoll et al., 2007].



Moreover, the metal hydride is stable in solution (sodium hydroxide solution) (hydrolysis process) and catalyst is required for the generation of hydrogen. The catalysts commonly used are Pt, Co, Ni, Mn, Fe, Cu, Ru, Fe-B, Co-B, Ni-B, Co-Ni-B, Co-Cu-B, Co-Ce-B, Co-Cr-B, Co-La-Zr-B, Co-Ru-B, Pt-LiCoO₂, CoB/SiO₂, Co/IR-120, Pt/C, Pt/TiO₂, Rh/TiO₂, Silica-Sulphuric Acid catalyst, Pd/C, and Ru-RuO₂/C catalysts [Zuttel, 2004; Hsueh et al., 2011; Jeong et al., 2005; Dai et al., 2008; Chang et al., 2014; Fernandes et al., 2009; Fernandes et al., 2009a; Diang et al., 2010; Tuan et al., 2013; Zhang and Mohring, 2009; Singh and Xu, 2009; Peng et al., 2013; Liu and Li, 2009; Demirci and Garin, 2008; Zou et al., 2011; Figen and Coskuner, 2013; Kalidindi et al., 2008; Patel et al., 2008; Cheng et al., 2015; Zhang et al., 2013; Yang et al., 2011]. Among the commercially available carbon-supported ruthenium catalyst has been reported most efficient.

Various catalysts have been studied and reported to use for the hydrolysis of sodium borohydride for the generation of hydrogen. It has been reported that the metal-metal oxide (Pt-TiO₂, Pt-CoO, Pt-LiCoO₂) catalysts are very active [Liu et al., 2008]. The catalyst is synthesized by both conventional impregnation method and supercritical method using carbon dioxide [Kojima et al., 2002]. It has been reported by using ruthenium supported on anion

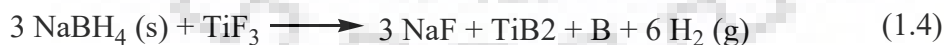
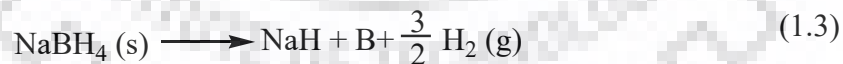
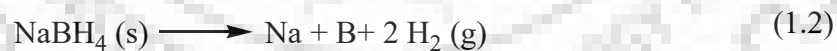
exchange resin bed catalyst is also highly active. The catalyst is reusable for hydrogen generation. The study is basically by considering various parameters such as the effect of sodium hydroxide concentration, sodium borohydride concentration, and reaction temperatures [Demirci and Garin, 2008; Zou et al., 2011; Liu et al., 2008; Kojima et al., 2002; Amendola et al., 2000]. The Fe-B catalyst fabricated by hybrid capacitive adsorption-chemical reduction method is active for the generation of hydrogen [Tuan et al., 2013]. The NiB (nickel boride) catalyst is also active for the generation of hydrogen from aqueous sodium borohydride solution [Sahin et al., 2014; Pinto et al., 2006; Sahin et al., 2013]. The low-cost Co-B (cobalt boride) catalyst has been used with a 2 W polymer electrolyte membrane fuel cell (PEMFC) stack which operated and successfully powered a cellular phone [Hsueh et al., 2011].

Few studies have been done on hydrogen generation using NaBH_4 on various metal-doped catalysts [Fernandes et al., 2009; Fernandes et al., 2009a; Ding et al., 2010]. The hydrogen generation using NaBH_4 hydrolysis study has been done using silica sulfuric acid (SSA) catalyst, and aqueous acid (HNO_3 , Acetic Acid, HCl) [Ingersoll et al., 2007; Brack et al., 2015]. It has been proposed that the activation energy is obtained for NaBH_4 hydrolysis reaction very low. Also, it has been reported that the hydrolysis rate is improved in the presence of the prepared catalyst. It has been studied on hydrogen generation using transition metal-doped Co-B catalyst. The hydrogen generation reaction is studied by using various metals like Ni, Mo, W as doping. It has been reported that the un-doped catalyst undergoes crystallization and decomposed faster at high temperature. Cr, W, Mo, and Cu offered considerable promoting effects on the efficiency of the Co-B catalyst by increasing the H_2 generation rate by 3-4 times as compared to un-doped catalyst [Ding et al., 2010; Manna et al., 2015]. A few other related studies on catalytic hydrogen generation have been done by using various metals as catalysts [Alfonso et al., 2009]. It has been reported that the rate of hydrogen generation using Ni-Co-B catalyst strongly dependent on the concentration of base, sodium borohydride, and reaction temperature. The synthesized catalysts have been studied using various characterization techniques, eg., SEM, XRD, XPS, FTIR [Chang et al., 2014; Fernandes et al., 2009; Figen and Coskuner, 2013; Patel et al., 2008; Yang et al., 2011]. However, no publications that deals with the hydrogen generation using sodium borohydride and the *in situ* UV-vis spectroscopy for catalyst synthesis [Kalidindi et al., 2008; Metin et al., 2009; Palmer et al., 2009]. The NaBH_4 is hydrolyzed slowly with water, and this hydrolysis process can be stabilized in the presence of sodium hydroxide. The mechanism of the self-hydrolysis process has been described; however, the mechanism is still poorly understood [Zuttel, 2004; Alfonso et al., 2009]. Moreover, the supported ruthenium catalyst is costly and looks for a cheaper one which would be used as an alternative. The advantage of hydrolysis

process is that half of the generated hydrogen produced from water by reaction with NaBH₄, moreover, the solution is non-flammable, stable in air for months, generation occurs only in presence of catalysts, reaction product (water) environmentally safety, and that can be recycled back to NaBH₄ [Amendola et al., 2000].

1.4.2 Thermolysis Study and Use of Various Additives/Catalysts

Various metal/chemical hydrides have been studied as hydrogen storage materials and consequence hydrogen release [Berg and Arean, 2008; Jeon and Cho, 2006; Paskevicius et al., 2013; Jain et al., 2010]. The thermolysis of NaBH₄ has been studied extensively and the hydrogen has been stored at room temperature and atmospheric pressure [Urgnani et al., 2008; Chong et al., 2011; Cakanyildirim and Guru, 2009; Mahato et al., 2015; Petitpas et al., 2014; Aceves et al., 2013; Rivarolo et al., 2018; Jain et al., 2010; Murthy, 2012; Zhang et al., 2011; Varin et al., 2017; Kumar et al., 2017]. The desorption rate of hydrogen increased with increasing thermolysis temperature. The theoretical hydrogen desorption is ~ 1.11 wt%, suggesting that a small amount of sodium borohydride not decomposed at 100 °C [Zhang et al., 2011]. However, the release or desorption of hydrogen is a very complex process and important. Since, a small amount of diborane (B₂H₆) as byproducts is released during the reaction of NaBH₄ using ZnF₂ as additives [Jeon and Cho, 2006; Zhang et al., 2011]. Also, the formation of elemental boron (B) is reported during the thermolysis of NaBH₄. Moreover, sodium metal (Na) is also evaporated out at high temperature during the thermolysis of NaBH₄ [Kumar et al., 2017]. The complete thermolysis reaction of NaBH₄ and in presence of TiF₃ additive at 300 °C is proposed as per below reactions 1.2, 1.3 and 1.4 [Mao and Gregory, 2015; Urgnani et al., 2008].



The hydrogen desorption from other various metal hydrides decomposes at high temperatures such as >600 °C for LiH, 285 °C for MgH₂. The metal hydride Ca(BH₄)₂ decompose at 367 °C, Mg(BH₄)₂ at 320 °C, LiBH₄ at 380 °C, and NaBH₄ decomposes at 505 °C. The ammonia borane decomposes in three stages and the decomposition temperatures are 110, 150, and 400-900 °C by the formation of intermediate species polyaminoborane, [NH₂BH₂]_n, polyiminoborane, [NHBH]_n, and boron nitride. Sometimes, toxic gas like borazine (N₃B₃H₆) is released during thermal decomposition. The thermal decomposition temperature of the metal hydride has been reduced and studied by the addition of various transition metal complexes are KBF₄, NaBF₄, TiF₃, ZnF₂, MnF₃, FeF₃ [Grochala and Edwards, 2004; Bai et al.,

2014]. The hydrogen release in $\text{NaBH}_4\text{-MnF}_3$ system began at $130\text{ }^\circ\text{C}$, FeF_3 decreased the temperature to $161\text{ }^\circ\text{C}$, and TiF_3 to $200\text{ }^\circ\text{C}$. The Ni-Co-B acts as a catalyst and reduced the decomposition temperature of $\text{NaNH}_2\text{-NaBH}_4$ below $250\text{ }^\circ\text{C}$. The reversible hydrogen storage and thermal decomposition of metal hydrides have been studied by considering sodium-doped fullerene, Ni/Si/ Al_2O_3 , reduced graphene oxide, mesoporous carbon scaffold, the addition of boron [Mao and Gregory, 2015; Humphries et al., 2013; Nale et al., 2016; Wang et al., 2014]. The decomposition reaction is studied by using in situ XRD, TPD, Raman, FTIR, DT/TGA, DSC, ^{11}B NMR. The mechanism of the thermolysis process has been described; however, the mechanism is still poorly understood [Kim et al., 2008; Zhang et al., 2010].

The thermal decomposition of metal hydride has been studied by considering various materials. It has been studied that the effect of the addition of boron in metal borohydrides MBH_4 ($\text{M} = \text{Li}, \text{Na}, \text{Ca}$). The addition of boron changed slightly the rate of hydrogen release [Pendolino, 2012]. It is also studied and investigated by considering various metal chlorides and reported that the thermal decomposition temperature of sodium borohydride lowered significantly by the addition of ZnCl_2 , MnCl_2 and NiCl_2 [Mao and Gregory, 2015; Jeon and Cho, 2006]. The thermal decomposition of metal hydride is investigated by considering a series of monometallic borohydrides and borohydride eutectic mixtures. Each system behaves differently concerning the physical behaviour upon melting. The molten phases can exhibit colour changes, bubbling, and in some cases frothing, or even liquid-solid phase transitions during hydrogen release. The hydrogen release from solid-state NaBH_4 by considering experimental and computational methods is also reported [Urgnani et al., 2008] and a multi-step reaction followed after annealing in both isothermal and scanning conditions. Moreover, it is reported the destabilization of NaBH_4 possible by using transition metal fluorides and for pure NaBH_4 hydrogen released temperature possessed at $430\text{ }^\circ\text{C}$. The hydrogen release in the $\text{NaBH}_4\text{-MnF}_3$ system began as low as $130\text{ }^\circ\text{C}$, FeF_3 decreased the temperature to $161\text{ }^\circ\text{C}$, and TiF_3 to $200\text{ }^\circ\text{C}$ [Bai et al., 2014]. The effect of chloride substitution between NaBH_4 and transition metal chlorides (Cu, Zn, and Cd) is studied. The product identified is $\text{Na}(\text{BH}_4)_{1-x}\text{Cl}_x$ and the lowest decomposition temperature is found for the Zn containing sample ($103\text{ }^\circ\text{C}$), while Cd leads to the highest value ($521\text{ }^\circ\text{C}$) [Jansa et al., 2012]. The thermal decomposition of composite $\text{NaNH}_2\text{-NaBH}_4$ by using Ni-Co-B catalyst is studied and the reversible hydrogen storage is possible by milled of NaBH_4 with Ni containing additives ($\text{Ni-Si-Al}_2\text{O}_3$). It is reported that the Ni containing additives enhanced the thermal desorption significantly at least $60\text{ }^\circ\text{C}$ lower, also reported that the Pd nanoparticles decreased the desorption temperature at least $85\text{ }^\circ\text{C}$ ($420\text{ }^\circ\text{C}$). The thermal decomposition temperature has been reported to be reduced

by the addition of sodium doped fullerene, reduced graphene oxide and mesoporous carbon scaffold [Humphries et al., 2013; Nale et al., 2016; Wang et al., 2014].

Lightweight $\text{NaNH}_2\text{-NaBH}_4$ hydrogen storage materials have been synthesized via liquid phase ball milling under the co-protection of argon and cyclohexane as solvent [Bai et al., 2014]. The NaBH_4 hydrazines have been synthesized by using tetrahydrofuran (THF) as a solvent via a facile solution synthesis approach [Mao et al., 2015; Kim et al., 2008; Mao et al., 2015]. Moreover, the diethyl ether is an appropriate solvent for the metathesis reaction between NaBH_4 and ZnCl_2 [Jeon et al., 2006]. The solvent is removed under vacuum. It vibrational the effect of temperature and pressure on metal complex hydrides, $\text{NaAlH}_4\text{-TiCl}_3$ using in situ Raman cell. The formation and decomposition of chemical structures under high pressure via Raman scattering is also reported [Ferrer et al., 2011; Cerny et al., 2009]. The formation and studied of $\text{NaBH}_4\text{-ZnF}_2$ at low temperature below $100\text{ }^\circ\text{C}$ using Raman analysis and reported the formation of elemental B which is due to the decomposition of B_2H_6 [Zhang et al., 2011].

A few studies have been done on hydrogen generation using NaBH_4 on various metal-doped catalysts and the thermolysis study that deals with the hydrogen storage and generation from sodium borohydride using ZrCl_2 as additive [Kumar et al., 2017; Manna et al., 2015; Fernandes et al., 2011; Ingersol et al., 2007]. A 3D numerical model for predicting the hydrogen absorption process performance of cylindrical metal hydride tank (MHT) filled with TiZrVFeCrMn hydrogen storage material is reported. The performance of the MHT is analyzed based on numerical simulation [Bhogilla et al., 2017]. The lithium hydride reported as a potential hydrogen storage material by considering a theoretical approach. In the study, it is reported the structural stability of LiH using a DFT framework on LiH.H_2 , LiH.3H_2 , and LiH.4H_2 [Banger et al., 2018]. The thermal dehydrogenation of $\text{Mg(BH}_4)_2$ using ZrCl_4 as an additive in vacuum and argon gas flow conditions is also reported. They reported that the hydrogen release started at $235\text{ }^\circ\text{C}$ for pure- $\text{Mg(BH}_4)_2$ and the ZrCl_4 catalyzed $\text{Mg(BH}_4)_2$ down to $197\text{ }^\circ\text{C}$ [Kumar et al., 2017] and a solid-state hydrogen storage device with a finned tube heat exchanger is considered during the study. In the study, it is reported that LaNi_5 hydrating alloy as solid-state adsorbing material for hydrogen at 15 bar pressure and 288 K temperature. It is also reported that the charging copper flakes inside the storage vessel increase the absorption efficiency and decreases the charging time [Bai et al., 2014; Singh et al., 2017]. The CNT doped polyolithiated molecule is studied as potential hydrogen storage materials. In the study, a DFT calculation is considered to investigate the structure and stability of CNT functionalized with various polyolithiated molecules (PLMs) like CLi_n and their hydrogen storage properties [Panigrahi et al., 2018]. Ambient hydrogen storage in porous materials with exposed metal sites is reported and a cross-linked porous polymeric complexes

(phloroglucinol-terephthalaldehyde framework (PTF)) work with exposed metal sites (Cr and Mg) are synthesized and studied as hydrogen storage material at room temperature at 298 K with 100 bar pressure. In the study, it is reported that cross-linked framework provides high structural stability with rigid chelated ligands to support the further exposure of the metal species [Pareek et al., 2014]. The Mg-based nanocomposites containing different concentrations of NiMnAl alloy is also studied to improve the dehydrogenation kinetics of MgH₂ and it is reported that the onset temperature of hydrogen absorption decreased to about 40 °C with increasing the concentration of NiMnAl in MgH₂ from 25 to 50 wt% [Meena et al., 2017]. The effect on specific capacity and de-hydrogenation efficiency MgH₂ doped with La, Ce, Al, Li, and Ni using DFT calculation is reported [Chakrabarti et al., 2017]. The thermodynamics and kinetics of Mg-Li alloy for an MgH₂ based anode material for Li-ion batteries are studied and a single-phase Li₃Mg₇ is studied by ball-milling of LiH and MgH₂ as a precursor of Li and Mg followed by dehydrogenation at 400 °C under dynamic vacuum conditions. The hydrogenation-dehydrogenation kinetics is remarkably improved by doping with ZrCl₄ as a catalyst [Kumar et al., 2017]. The dehydrogenation kinetics by considering doping at various layers of MgH₂ surface using first-principles based calculations (DFT) is reported and the doping influences on dehydrogenation and Al and Sc are the best possible dopant in lowering the desorption temperature [Kumar et al., 2017]. A multiple Li⁺ and Mg²⁺ decorated polycyclic aromatic hydrocarbons (PAHs) for reversible hydrogen storage materials using DFT calculation are studied and it has been reported that all the complexes possess high gravimetric storage capacity, and are found to be maximum for Mg²⁺ decorated anthracene [Ghosh et al., 2017].

1.5 Kinetics and Hydrogen Generation Mechanism (Hydrolysis/Thermolysis)

Understanding and controlling the release of hydrogen during the hydrolysis of NaBH₄ is crucial to the success of the technology. The hydrolysis of sodium borohydride for the generation of hydrogen is an irreversible process. The hydrolysis process is a highly exothermic reaction [Zou et al., 2011]. The hydrolysis of NaBH₄ has been studied by considering various acid, and metal-based (cobalt, nickel, copper, palladium, ruthenium) catalysts, the effect of temperature, pH, NaBH₄ concentration on reaction kinetics. The various mechanisms also have been proposed, however, the pathways are not completely understood. The rate of hydrolysis reaction is decreased with the formation of metaborate anion (B(OH)₄⁻ or NaB(OH)₄ or NaBO₂ · 2H₂O. The tetrahydroxyborate anion formed at strongly basic conditions (pH > 9) and boric acid yields under acidic conditions (pH < 9). The rate is slow probably due to the solubility and mobility inhibition by NaBO₂, and lower the availability of

water. Many studies have been initiated to recycle the byproduct metaborate into sodium borohydride [Alfonso et al., 2009; Demirci et al., 2009; Cakanyildirim et al., 2009; Hsueh et al., 2009; Li et al., 2003; Cakanyildirim et al., 2010; Cakanyildirim et al., 2012; Liu et al., 2009]. The hydrolysis kinetics depends on various parameters such as base concentration, NaBH_4 concentration, solution temperature, and the ratio of hydride to catalysts. The reaction followed zero-order kinetics concerning the high hydride/catalyst molar ratio and first-order kinetics at low hydride/catalyst molar ratio. This might be because at high hydride/catalyst ratio, the BH_4^- induced dynamic saturation of the active sites on the catalysts, and the catalyst's surface is not covered completely at low hydride/catalyst ratio [Patel et al., 2009]. Moreover, the reaction order (fractional/negative) is reported to be -0.41 for NaBH_4 and +0.68 for H_2O over the Ni-supported BMR07 catalysts. The activation energy is also reported for the study ~ 52 kJ/mol over a temperature range 273 to 303 K [Jeong et al., 2005; Chang et al., 2014; Ding et al., 2010; Peng et al., 2013; Demirci and Garin, 2008; Cheng et al., 2015; Zhang et al., 2013; Manna et al., 2015; Zhang et al., 2007; Dai et al., 2008].

The simple hydride decomposes upon heating via reversible thermolysis. The simple hydrides consist of a metal or alloy which is hydrating under high pressure. The complex hydride decomposes and produces hydrogen upon heating, however, the reversibility is not possible always. The hydrides are mixed with a binder or inert materials to form a pellet to down the thermolysis temperature, as a result, the mass of the component and net hydrogen storage efficiency reduces [Gorchala and Edwards, 2004; Alfonso et al., 2009]. A high temperature is required to initiate the reaction and thermolysis offers high energy density as compared to hydrolysis. The melting point of NaBH_4 is reported to be 505°C and it appears to be a constant function of the H_2 pressure. In the study, about 1wt% of H_2 is being released in comparison to a total of 10.4 wt% at the end of the complete decomposition reaction. Since the thermolysis is a multistep process, the evolution of hydrogen starts at low temperature (240°C) and continues by several steps at different temperatures. The most significant hydrogen emission starts at 450°C and continues at higher temperatures [Urgnani et al., 2008; Mao et al., 2012]. The activation energy in the thermolysis is reported to be ~ 180 kJ/mol and ~ 275 kJ/mol in the presence and absence of additives, respectively [Kumar et al., 2017].

1.6 Applications of Hydrogen Energy

Hydrogen is an ideal synthetic fuel, since, it is lightweight, highly abundant, and its oxidation product, water is environmentally friendly, however, efficient storage technique remains challenging. Thus, the search for innovative materials with high-storage capacity is focused in the present study. The use of hydrogen by either in a combustion engine with air and

the efficiency of transformation of chemical energy to mechanical through thermal energy are limited to ~ 25%. The same hydrogen converts electrochemically with oxygen from the air in a fuel cell, which produces electricity (and heat) and drives an electric engine, the efficiency reached ~50-60%. Thus, the application of hydrogen energy is directly associated with the use to fuel cell for the small portable electronic devices (mobile phones, laptop, computer), hydrogen fuel cell buses, and vehicle (electric car) application [Hsueh et al., 2011; Alfonso et al. 2009; Ren et al., 2017; Jeong et al., 2005]. However, the cryogenic liquid hydrogen with the super-insulated tank is developed in space technology. The liquid hydrogen has been used in the launching process of the space shuttle and Ariane, a Lockheed military-type aircraft, a Tupolev supersonic aircraft, and BMW car. [Schlapbach and Zuttel, 2001; Parker, 2010; Durbin and Jugroot, 2013]. The demand on the hydrogen storage system is vast and the group Darnell studied the markets for the fuel cell for commercial portable device required power < 1 kW. The devices are portable computers, cell phones, satellite phones, mobile communications, camcorders, and digital cameras. The devices used by public transport like cars, buses, trains, and aeroplanes. The hydrogen storage device considering the chemical/metal hydrides has been developed with various types of hydrogen generator that extract hydrogen using catalytic hydrolysis of sodium borohydride alkaline solution in the presence of a catalyst. The components used for the hydrogen generator are a suitable catalyst, hydrogen chamber, byproduct separator, reactor, pump, cooling fan, valves, the controller [Kim, 2014; Kojima et al., 2004; Kim and Kim, 2015; Gang et al., 2017]. Metal hydride based hydrogen storage device using cooling tube reaction bed filled with $\text{LaNi}_{4.7}\text{Al}_{0.3}$ alloy with thermal management has been carried out by various researchers, still, there is a significant lag in the experimentally developed a robust system for the hydrogen storage and hydrogen generator for real-life application [Kumar et al., 2019]. However, the technology is not viable and well established so far [Alfonso et al., 2009].

1.7 Industrial Methods of Production of NaBH_4

The sodium borohydride is produced industrially using two most common processes are 1) The Brown-Schlesinger process and 2) The Bayer process. The details of the process are discussed.

1.7.1 The Brown-Schlesinger Process

The Schlesinger process is known as the Rohm and Haas Process. In the process, the sodium borohydride is produced expensive due to multiple steps process and the process is highly energetic. In the method of synthesis, sodium hydride and trimethyl borate undergo a

rapid reaction at 225-275 °C and produce the sodium borohydride of high purity (90-96%) and high yield (94%). An industrial process, trimethyl borate is added to sodium hydride (produced from the reaction of metal sodium and hydrogen gas) dispersed in hydrocarbon oil at 250 °C. The hydrocarbon oil phase is separated with the addition of water and sodium methylate (NaOCH₃) hydrolyzes to methanol and sodium hydroxide. The product methanol is further recovered by distillation and further convert into trimethyl borate. The sodium borohydride is in the remaining alkaline solution with a concentration of NaBH₄ (12%) and NaOH (40%). The solid sodium borohydride is recovered by extraction with iso-propylamine and precipitation [Alfonso et al., 2009; Cakanyildirim et al., 2009; Li et al., 2003; Cakanyildirim and Guru, 2012; Schlesinger et al., 1953]. The key reaction 1.5 for the process of production of sodium borohydride is given below.



1.7.2 The Bayer Process

The sodium borohydride has also been prepared commercially by using the Bayer process. In the batch process, a mixture of dehydrated borax, quartz, and sodium metal under hydrogen heated in the presence of silica. The process has many complications (like explosion risks) which restricted to the process for commercial-scale of production. In addition to that, the disposal of sodium silicate is another issue of the process [Alfonso et al., 2009]. The key reaction 1.6 for the process of production of sodium borohydride is given below.



Moreover, the NaBH₄ is synthesized using a ball milling process considering below reaction at high temperature (480 °C) and pressure (10 to 30 MPa). In this particular method, a known quantity of NaBO₂, NaH, and SiO₂ ternary mixture added into a ball mill and mixed the mixture for 4 h at a rate of 400 rpm. The mixture then transformed into pellet under static pressure 10 to 30 MPa in an Ar-filled glove box, followed by calcination at 480 °C for 5 h under 0.1 MPa in Ar atmospheres. The details reaction 1.7 is given below [Schlesinger et al., 1953].



1.8 Characterizations of Sodium Borohydrides and the Metal-Boride/Metal Halides Catalysts

The synthesized catalysts for the hydrolysis of sodium borohydride using various methods and the composite materials considering the thermolysis of sodium borohydride for the generation of hydrogen has been studied by using various characterization techniques.

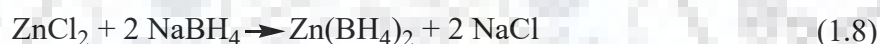
1.8.1 BET Surface Area Analysis

The specific surface area of CoB catalyst is reported to be 77 m²/g [Jeong et al., 2005]. The Cr modified CoB catalysts have been synthesized by chemical reduction at room temperature. In the study, Cr/Co molar ratio is varied to find the Cr doping on surface modification and performance of the catalytic activity. In the study, the BET surface area of the synthesized catalysts is obtained. It has been reported that the surface area increased with the addition of Cr in Co-Cr-B catalysts. As a result, the generation of hydrogen is also increased as the surface area of the catalyst increased [Fernandes et al., 2009]. A facile method is used for the synthesis of Ru nanoparticles deposited montmorillonite (MMT), Ru/MMT catalyst for the generation of hydrogen from the hydrolysis of sodium borohydride. In the study, the specific surface area of the catalysts is obtained as fresh and used both the catalyst after 10 runs. It has been observed that the specific surface area decreased by 9.2% after 10 cycles, and the decrease in specific surface area is due to the incorporation of byproduct sodium metaborate in montmorillonite (MMT) mesopores [Peng et al., 2013]. The generation of hydrogen from the hydrolysis of sodium borohydride is studied using Ni(0) catalyst prepared in the presence of the plasma method. It has been observed that in the presence of plasma treatment the specific surface area of the catalyst increased. In the plasma method, the catalyst possesses a higher metal dispersion during synthesis [Sahin et al., 2013].

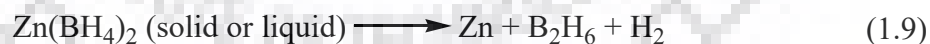
1.8.2 XRD Analysis

The XRD analysis of the synthesized CoB catalysts for the hydrolysis of sodium borohydride is reported. The study suggested that the formation of amorphous structure of CoB ($2\theta = 45^\circ$) at low calcination temperature and the grain size increased with increasing the calcination temperature [Dai et al., 2008; Fernandes et al., 2009; Fernandes et al., 2009a; Figen and Coskuner, 2013; Kalidindi et al., 2008; Patel et al., 2008; Yang et al., 2011]. The diffraction peak for FeB catalyst is assigned at 34.5° [Tuan et al., 2013] and the NiB at various locations [Kalidindi et al., 2008; Ingersoll et al., 2007].

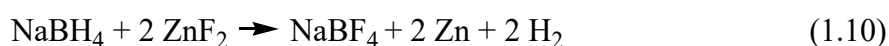
The XRD pattern of the pure NaBH₄ is reported in the open literature [Hsueh et al., 2009; Cakanyildirim and Guru, 2012]. A multi-step decomposition reaction has been observed in both isothermal and heating experiments. The evolution of H₂ begins at 240 °C with multiple steps with changing temperature and continues at a higher temperature. The significant amount of hydrogen is released at 450 °C [Urgnani et al., 2008]. The thermal decomposition of the material 2NaBH₄-MgH₂ by changing the decomposition temperature under static vacuum is also reported. The dehydrogenation of sodium borohydride in the presence of MgH₂ is studied in the presence of various inert gases (Ar) under 1 bar and vacuum. It is reported that during the decomposition of NaBH₄ the formation of Na₂B₁₂H₁₂ or B₁₂H₁₂²⁻ anion [Mao and Gregory, 2015]. The material NaBH₄-ZnCl₂ ball milled for 30 min and the XRD pattern is obtained of the final product. The study suggested that after ball milling the formation of Zn(BH₄)₂, neither the ZnCl₂ or NaBH₄ is observed. The study suggested that after ball milling following reaction 1.8 is followed.



The sample (Zn(BH₄)₂-NaCl) is heated at 150 °C for 3 days and it is observed the presence of NaCl in XRD study, neither crystalline or amorphous boron (B) detected. However, a considerable amount of Zn is detected after keeping the sample inside a glove box for a week at room temperature, suggested the following reaction. The XRD patterns of the sodium borohydride with zinc chloride after ball milling the formation of zinc borohydride is confirmed and reported. However, the thermolysis study suggested that the zinc borohydride decomposes at low temperature with the production of diborane, boron, and hydrogen at 85 to 140 °C is expressed in reaction 1.9. The material is not suitable for reversible storage of hydrogen for onboard applications [Jeon and Cho, 2006].



The thermolysis of NaBH₄ in presence of ZnF₂ reagent is reported at 100 °C. The initial dehydrogenation temperature below 100 °C is favourable kinetics with the formation of NaBF₄, Zn, and intermediate product NaZnF₃. The dehydrogenation is reported at various temperatures such as 85 °C, 92 °C, and 100 °C. The high reaction temperature is favoured for the elimination of B₂H₆. The Zn(BH₄)₂ melts at 85°C underflow of argon is not suitable materials for reversible hydrogen storage material for onboard applications [Jeon and Cho, 2006]. The decomposition mechanism during the release of hydrogen in NaBH₄/ZnF₂ at 120 °C is expressed in reaction 1.10 as follows [Zhang et al., 2011].



The hydrogen desorption rate is very low and the rate increased with increasing the thermolysis temperature. The desorbed hydrogen are 0.89 wt% at 85 °C, 1.24 wt% at 92 °C, and 1.23 wt% at 100 °C after 60 min of operation [Mao and Gregory, 2015; Zhang et al., 2011].

1.8.3 UV-Vis Analysis

The reduction of metal ions (cobalt chloride) in the presence of sodium borohydride has been studied using UV-vis electronic absorption spectra analysis. It has been reported that the formation of Co (0) metal from Co (II) chloride and the nanosize metallic cobalt is active for the generation of hydrogen from the hydrolysis of sodium borohydride and ammonia borane. The band of Co (II) at 510 nm disappeared during the reduction and a broad absorption feature is observed due to surface plasmon resonance of Co (0) nanoclusters at 295 nm [Metin and Ozkar, 2009]. The electronic band of iron ion (Fe^{3+}) is at 313, 400, 520, 552, 665 nm and 860 nm [Palmer et al., 2009]. The broad transition band of Ni^{2+} ions is reported at 450 nm [Chen and Kim, 2008].

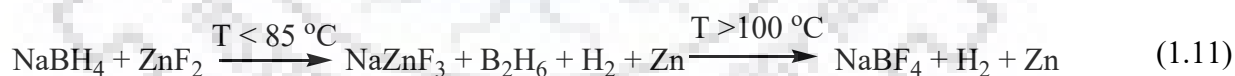
1.8.4 FE-SEM Analysis

The SEM images of the pure NaBH_4 is reported like chunky with rock-like morphology and the Co^{2+} impregnated IR-120 catalyst is granular and ball like morphology [Hsueh et al., 2011]. The SEM images of the CoB catalyst is reported to be a plate-like structure [Jeong et al., 2005]. The image of CoB/Ni foam catalyst is prepared by a modified electroless plating method to form a smooth surface to a coarse and porous structure [Dai et al., 2008]. The SEM images of various supported CoCeB catalyst is reported to be a large disorderly crowd. The TiO_2 supported catalyst is well-dispersed nanoparticles and most of the particles are spherical and regular shape [Chang et al., 2014; Fernandes et al., 2009]. The pure CoB catalyst powder shows a particle-like morphology with spherical shape agglomerate as small particles. The addition of Cr into CoB is transformed into less agglomeration and enhances more active surface sites [Fernandes et al., 2009; Fernandes et al., 2011; Ingersoll et al., 2007; Dai et al., 2008].

The SEM images of the transition metal chloride impregnated NaBH_4 is obtained and it is suggested that the metal chloride distributed homogeneously in sodium borohydride [Jansa et al., 2012]. The SEM image of pure NaBH_4 crystal is reported to be regular, and round shaped. The additive MnCl_2 is agglomerates of fibrous, thinner particles [Varin et al., 2017].

1.8.5 Raman Study

The Raman bands of the synthesized CoB catalysts have been reported to be at 270 cm^{-1} and 800 cm^{-1} [Kim, 2014]. The investigation of metal borohydride using various vibrational spectroscopies has been reported extensively [Parker, 2010; Petitpas et al., 2014]. Moreover, the temperature dependence of the band position of metal-borohydrides is also reported. There is a non-linear thermal expansion of the orthorhombic phase and synchronous in phase rotation of BH_4^- ions in the plane and antiphase rotation between planes [Parker, 2010]. The observed frequencies of borohydride ion (tetrahedral) reported as 313 cm^{-1} (vibrational modes), 1274 cm^{-1} (ν_2 , symmetric bending mode), 2192 cm^{-1} , 2218 cm^{-1} (ν_4 , asymmetric bending mode), and 2340 cm^{-1} (ν_1 , B-H stretching mode) [Parker, 2010; Zhang et al., 2011]. It is reported that the size or electronegativity of cation affects the vibration frequency of the anion, BH_4^- ions of bending and stretching. Moreover, the electronegativity of the cation also affects the thermal decomposition temperature of metal-borohydride. The hydrogen decomposition (thermal decomposition) of various metal hydrides (M-BH_4) (where, M: Li, Na, K, Rb, and Cs) is studied using various salts and it is reported that the order of decomposition is $\text{Li (653 K)} < \text{Na (838 K)} < \text{K (857 K)} < \text{Rb, Cs (873 K)}$. Moreover, the vibration of the line-width of ν_2 with temperature is reported. It decreases with increasing cation size. This is maybe due to the available space for the (disordered) tetrahedral (BH_4^-) anions in the octahedral alkaline metal cavities increases when passing from Na to Cs compound [Parker, 2010]. The thermal decomposition of NaBH_4 in presence of ZnF_2 is reported at different temperatures from $85\text{ }^\circ\text{C}$ to $100\text{ }^\circ\text{C}$. With increasing thermolysis temperature the proposed reaction scheme 1.11 is as follows.



A small amount of B_2H_6 decomposed as B trace is detected by Raman spectra of the products at low temperature. The Raman spectra suggested the presence of B-H, B-F and B icosahedra vibration modes [Zhang et al., 2011].

1.8.6 FTIR Study

The FTIR spectrum of the B_2O_3 and CoB catalyst is reported at room temperature. The bands 1404 cm^{-1} (B-O vibration), $1200\text{-}948\text{ cm}^{-1}$ (B-O asymmetric stretching), 671 cm^{-1} (B-O-B deformation band) are associated to B_2O_3 present in the CoB catalyst [Figen and Coskuner, 2013; Cakanyildirim and Guru, 2009].

The vibrational spectra of FTIR for the sodium borohydride, CoB catalysts, and additive Metal halides are studied and reported extensively [Parker, 2010; Figen and Coskuner, 2013; Patel et al., 2010]. The FTIR spectra of $\text{Mn}(\text{BH}_4)_2$ synthesized using NaBH_4 and MnCl_2 is reported [Varin et al., 2017]. The observed frequencies and assignment for borohydrides (BH_4^-) are reported as 1110 cm^{-1} of deformation or bending mode (BH_2) and 2284 cm^{-1} of stretching mode of B-H bond. The bands at 1409 cm^{-1} (Zn-H), 1634 cm^{-1} (Na-H), 1670 cm^{-1} (Zn-Cl) are reported for the materials ($\text{ZnCl}_2 + \text{NaBH}_4$). The bands at 1614 , 2083 cm^{-1} (B-H bridge stretching), 2200 , and 2300 cm^{-1} (bidentate terminal stretching of B-H bond) are BH_4^- ions [Jeon and Cho, 2006; Figen and Coskuner, 2013; Patel et al., 2008; Varin et al., 2017; Zhang et al., 2010; Hsueh et al., 2009; Mao et al., 2012].

1.8.7 TGA Analysis

The TG (Thermal Gravimetric) analysis of the synthesized materials studied and the release gases hydrogen (H_2) and diborane (B_2H_6) is reported [Jeon and Cho, 2006; Paskevicius et al., 2013; Zhang et al., 2010]. The study suggested that pure NaBH_4 melts at $505\text{ }^\circ\text{C}$ and decomposes with release hydrogen gas at $534 \pm 10\text{ }^\circ\text{C}$ under 1 atm hydrogen back pressure [Paskevicius et al., 2013]. The other various materials (KBH_4 , $\text{Mg}(\text{BH}_4)_2$, $\text{Ca}(\text{BH}_4)_2$, $\text{Mn}(\text{BH}_4)_2$, $\text{LiBH}_4\text{-NaBH}_4$, $\text{LiBH}_4\text{-KBH}_4$, $\text{LiBH}_4\text{-Mg}(\text{BH}_4)_2$, $\text{LiBH}_4\text{-Ca}(\text{BH}_4)_2$, $\text{LiBH}_4\text{-Mn}(\text{BH}_4)_2$, $\text{NaBH}_4\text{-KBH}_4$, and $\text{LiBH}_4\text{-NaBH}_4\text{-KBH}_4$) also reported by considering the TGA/DSC analysis and MS data of H_2 and B_2H_6 release [Paskevicius et al., 2013]. The TG/MS analysis of $\text{Zn}(\text{BH}_4)_2 + \text{NaCl}$ is reported and the decomposition started at $85\text{ }^\circ\text{C}$ and completed at $140\text{ }^\circ\text{C}$. The compound $\text{Zn}(\text{BH}_4)_2$ melts and slow decomposition reaction occurs. The MS study suggested the formation of B_2H_6 significant amount [Jeon and Cho, 2006]. The TG analysis of $\text{MgH}_2\text{-AB}$ is obtained and reported. The material decomposes at 88 , 92 , and $108\text{ }^\circ\text{C}$. However, the ball-milling for the mixtures of alkaline-earth metal hydride (MgH_2 or CaH_2) and ammonia borane yields hydrogen at $78\text{ }^\circ\text{C}$ and $72\text{ }^\circ\text{C}$ without generation of unwanted byproduct diborane [Zhang et al., 2010].

1.9 Summary

The advantage of the hydrolysis process is that half of the generated hydrogen produced from water. The NaBH_4 is hydrolyzed slowly with water, and the hydrolysis process can be stabilized in the presence of sodium hydroxide. The mechanism of the self-hydrolysis process has been described; however, the mechanism is still poorly understood. Moreover, the supported ruthenium catalyst is costly and looks for a cheaper one which would be used as an alternative. The development of metal-boride catalysts (supported or unsupported) (CoB and

other metal-boride) for the hydrolysis of sodium borohydride will be studied by choosing various metals, supports, loading, and calcination temperature.

The thermolysis of sodium borohydride is reported by considering various catalysts/additives (metal halides) for the generation of hydrogen. The thermal decomposition temperature of metal-borohydride is lowered in the presence of catalysts/additives. The generation of hydrogen is very slow and very low at low temperature. Thus, to develop a suitable additive/catalyst for the generation of hydrogen from sodium borohydride as prospective hydrogen storage material considering different factors (thermolysis temperature, the effect of various additives, and method of synthesis) as the outline of the thesis and its organization is given below.

1.10 Research Objectives

The objectives of the present thesis work are to study the generation of hydrogen from sodium-borohydride using various catalysts/additives for fuel cell applications. The generation of hydrogen is considered by a) hydrolysis of sodium borohydride solution using supported/bulk metal-boride catalysts, and b) thermolysis of sodium borohydride using metal halides additives.

The aims of the hydrolysis/thermolysis studies are as follows:

- To synthesis of metal boride catalysts (Co-B, Ni-B, Fe-B) using liquid-phase chemical reduction method.
- To monitor the catalytic activity and generation of hydrogen from with (BS)/without (WS) base stabilized sodium borohydride solution by considering various parameters like the effect of various metals in metal-boride catalysts, the effect of the base, calcination temperature during the synthesis of catalyst.
- To monitor the catalyst synthesis process by using an in-situ UV-vis spectrometer.
- To characterize the synthesized catalysts by using BET, XRD and FTIR spectroscopy.
- To prepare a series of supported cobalt boride catalysts by two steps impregnation-reduction method. The supports considered to synthesis the supported cobalt boride ($x\text{CoB}/(\text{Support})$) catalysts are SiO_2 , Al_2O_3 , and MgO .
- To study the thermolysis of sodium borohydride at low temperature using metal halides additives. The additives used for the study are metal halides (MnCl_2 , CaCl_2 , and ZnCl_2).
- To synthesize the composite materials by the facile solution method.
- To consider the thermolysis study by changing various parameters such as an effect of decomposition temperature, decomposition time, various additives, and the effect of total loading of additives.

- To characterize the synthesized catalysts and composite materials using various characterization techniques such as BET, XRD, TGA, FE-SEM, FTIR, and Raman spectroscopy analysis.

1.11 Thesis Outline and Organization

The generation of hydrogen from sodium borohydride is consists of two ways, a) hydrolysis of sodium borohydride in presence of metal-boride catalysts, and b) thermolysis of sodium borohydride in presence of metal halide catalysts/additives.

A systematic study is required to ascertain the effect of metals, calcination temperature, supports during the synthesis of metal-boride catalysts for the generation of hydrogen from hydrolysis of sodium borohydride at low temperature. Understanding of various factors will be achieved by the choice of a few characterization techniques analyzed in conjunction with the hydrogen generation study. The metal-boride (CoB/NiB/FeB) catalysts will be synthesized by the chemical reduction-precipitation method and characterized under ambient conditions by determining the specific surface area, XRD patterns, and surface morphology by FE-SEM, and UV-vis spectra. The generation of hydrogen in the presence of synthesized metal boride catalyst from the based stabilized sodium borohydride solution for the generation of hydrogen will provide important information.

Moreover, find suitable additive/catalysts for the generation of hydrogen from sodium borohydride at low temperature during thermolysis. The synthesis of $\text{NaBH}_4\text{-MnCl}_2$ composite mixture using a facile solution method and the synthesized materials will be characterized by various characterization techniques. The XRD analysis and Ex-situ FTIR study during the decomposition of sodium borohydride-additive mixture for the generation of hydrogen will provide the nature of decomposition of sodium borohydride at low and high temperature.

Thus, the thesis is divided into 5 chapters and the current one is Chapter-1. The generation of hydrogen from hydrolysis of sodium borohydride solution using various characterization techniques (BET, XRD, and FTIR) are tested over CoB/NiB/FeB catalysts and discussed in Chapter-2. The catalytic activity and generation of hydrogen from with (BS)/without (WS) base stabilized sodium borohydride solution is monitored by considering various parameters like the effect of metals in metal-boride catalysts, effect of the base, calcination temperature the during the synthesis of catalyst is monitored. The synthesis of catalyst is monitored by in situ UV-vis spectrometer. Chapter-3 deals with the effect of support on supported CoB catalysts. The supports considered for the synthesis of supported CoB catalysts are MgO , Al_2O_3 , and SiO_2 . The effect of calcination temperature during the synthesis of

supported CoB catalysts is monitored. Chapter-4 deals with the thermolysis of NaBH_4 during the generation of hydrogen using various additives or catalysts. The additives used for the study are MnCl_2 , CaCl_2 , and ZnCl_2 . The synthesis method is used as the facile solution method. The synthesized composite materials are characterized by XRD, FE-SEM and FTIR analysis. Finally, the conclusions of the present work along with the future recommendation are given in Chapter-5.



GENERATION OF HYDROGEN FROM NaBH_4 SOLUTION USING METAL-BORIDE (CoB, FeB, NiB) CATALYSTS

2.1 Abstract

A series of CoB, FeB and NiB catalysts were prepared by the chemical reduction method using base stabilized sodium borohydride solution as reducing reagent. The synthesized catalysts were characterized by using XRD, BET and FTIR spectroscopy. The UV-vis spectroscopy was used for *in-situ* synthesis of metal boride catalysts. With (BS)/without (WS) base stabilized NaBH_4 solution was used during synthesis of metal boride catalysts as well as generation of hydrogen from the solution. The surface area gradually increased with increasing calcinations temperature upto 573 K and furthers increasing calcinations temperature the surface area decreased for the catalysts CoB-BS. The generation of hydrogen using base stabilized NaBH_4 solution (BS) with the catalyst was followed as CoB-BS > NiB-BS > FeB-BS and the generation of hydrogen using without base stabilized NaBH_4 solution (WS) with the catalyst was followed as CoB-BS > FeB-BS > NiB-BS. However, the generation of hydrogen was highest for CoB-BS catalyst using both of with/without base stabilized NaBH_4 solution.

2.2 Introduction

Hydrogen has been used as an alternate energy carriers as sources of sustainable energy. Hydrogen contents the highest energy density per unit mass and produced water after its burning. The storage safe transportation and supply of hydrogen are key-technology for the hydrogen based energy sectors due to increasing demand of portable electronic device like cell phones, satellite phones and motor vehicles in transportation sector with high power density [Hsueh et al., 2011; Alfonso et al., 2009; Jeong et al., 2005; Singh and Xu, 2009; Jena, 2011; Li et al., 2012]. The hydrogen powered fuel cell technology has been delayed due to lack of efficient hydrogen storage technology. However, hydrogen is being used as clean fuel only for the space program. Therefore, the easy and safe storage of hydrogen is essential for onboard vehicle application should allow a driving about 400-500 km, and very fast refuelling [Alfonso et al., 2009]. As a result the strong demand of hydrogen for hydrogen derived vehicles using PEMFC (Polymer electrolyte membrane fuel cell) or DBFC (Direct borohydride fuel cell) stack as portable power source is under demand [Hsueh et al., 2011; Alfonso et al., 2009; Jena,

2011; Li et al., 2012]. Most of the research trend has been focused on the development of hydrogen storage materials. The storage may be either in gas phase, liquid or solid forms. The various mode of storage of hydrogen are used basically in compressed high pressure gas tanks or highly insulated cryogenic liquid hydrogen tanks, in hydrogen storing alloys, on activated carbon, metal organic frameworks, and porous solids like zeolites, organic polymers, clostrates encapsulation, and various metal hydrides [Alfonso et al., 2009; Jena, 2011]. The metal hydrides are mainly formed using metals with hydrogen under appropriate temperature and high pressure. The most commonly studied metal hydrides are $\text{PdH}_{0.6}$, CaH_2 , FeTiH_2 , $\text{Zr-V}_2\text{H}_{5.5}$, Mg_2NiH_4 , MgH_2 , NaAlH_4 , KBH_4 , CoNi_5H_4 , LaNi_5H_6 , $\text{Al}(\text{BH}_4)_3$, $\text{Mg}(\text{NH}_3)_6\text{Cl}_2$, LiH , LiAlH_4 , LiBH_4 , NaAlH_4 , NaBH_4 and complex chemical hydride like $\text{NH}_2\text{-NH}_2$, $\text{NH}_3\text{-BH}_3$ (AB), Guanidinium borohydride ($\text{C}(\text{NH}_2)_3\text{BH}_4$ or GBH) [Schlapbach and Zuttel; 2001; Berg and Areal, 2008; Alfonso et al., 2009; Singh and Xu, 2009; Jena, 2011; Li et al., 2012]. These metal hydrides generate hydrogen on demand reversibly either by thermal heating or hydrolysis [Alfonso et al., 2009; Drozd et al., 2007; Kumar et al., 2017; Kumar et al., 2017]. The heat treatment is required in thermal heating process which is difficult to control. Moreover, the evaporation of sodium metal is one of the major issues on thermolysis [Kumar et al., 2017]. The most interesting aspect of the hydrolysis process is that the generation of hydrogen is very fast on demand by using catalyst and the half of the hydrogen generated through dissociation of water. A catalyst is required to accelerate the hydrolysis process at room temperature. The recycling of obtained by-product (NaBO_2) is possible in presence of magnesium hydride (MgH_2) or magnesium silicide (Mg_2Si) at high temperature and pressure [Mao and Gregory, 2015; Kojima and Haga, 2003; Demirci et al., 2009]. However, a limited study has been reported in open literature.

The hydrolysis reaction is accelerated by various metal-boride catalysts such as CoB, NiB, Fe-B, Ru-B, pure metals like Ru, Rh, Pt, Ni, Mn, Fe, Cu, Co, Zn, $\text{Co}(\text{OH})_2$, Rh_xNi_y , Pt-Rh alloys, Ru/anion exchange resin, Fe-Co-B on Ni-foam, Co-Mo-Ru-B, Co-Cu-B, Co-Cr-B, Co-P-B, Co-Ni-P, Ni-Co-B, Co_3O_4 nano powder as precursor, CoO, CoOOH, $\text{CoCO}_3\text{-Co}(\text{OH})_2$, CoB, Rh/ TiO_2 , Pt/ TiO_2 , Co-B/ TiO_2 , Co/ Al_2O_3 , Co-B/ SiO_2 , Co/AC, Zr-Co/C, Ni/ SiO_2 and Ni-Ag/ SiO_2 [Schlapbach and Zuttel; 2001; Hsueh et al., 2011; Jeong et al., 2005; Singh and Xu, 2009; Kalidindi et al., 2008; Patel et al., 2008; Chang et al., 2015; Zhang et al., 2013; Yang et al., 2011; Metin and Ozakr, 2009; Chen and Kim, 2008; Groven et al, 2013; Pfeil et al., 2014; Patel et al., 2010; Zhao et al., 2007; Si et al., 2010; Sahiner and Yasar, 2014; Wang et al., 2014; Liang et al., 2010; Wu et al., 2011; Walter et al., 2008; Tuan et al., 2013; Wu and Ge, 2011; Netskina et al., 2015; Figen et al., Fernandes et al., 2009; Muir et al., 2014; Das et al., 2013; Umegaki et al., 2013; Kim et al., 2014; Dippolito et al., 2015; Palmer et al., 2009; Liu and Li,

2008; Ozerova et al., 2012]. The catalysts have been prepared by various methods like ball milling [Drozd et al., 2007], solution combustion [Groven et al., 2013; Pfeil et al., 2014], pulsed laser deposition [Patel et al., 2010], impregnation-chemical reduction [Zhang et al., 2013; Zhao et al., 2007], incipient wetness impregnation [Yang et al., 2011], electroplating [Liang et al., 2010; Muir et al., 2014], chemical reduction method [Pfeil et al., 2014; Wang et al., 2014; Wu et al., 2011; Tuan et al., 2013; Wu and Ge, 2011; Netskina et al., 2015; Fernandes et al., 2009; Kim et al., 2014] and precipitation oxidation method [Ozerova et al., 2012]. The metal boride catalysts have been synthesized using chemical reduction method by addition of NaOH with an optimum concentration. The precipitation of metal boride during preparation is dependent upon the pH of the solution by formation of undesired metal hydroxide [Liu and Li, 2008]. Even the activity of the synthesized catalysts is strongly dependent on the precursor used [Wu et al., 2008; Jeong et al., 2007; Akdim et al., 2009], and calcinations temperature during synthesis [Si et al., 2010; Wu et al., 2011; Lee et al., 2007; Wu et al., 2005].

The properties of synthesized catalysts have been characterized by using various characterization techniques like BET [Si et al., 2010; Das et al., 2013], TPR [Zhang et al., 2013], SEM [Hsueh et al., 2011; Jeong et al., 2005; Patel et al., 2008; Cheng et al., 2015; Zhang et al., 2013; Metin and Ozkar, 2009; Chen and Kim, 2008; Kim and Kim, 2015; Groven et al., 2013; Pfeil et al., 2014; Patel et al., 2010; Zhao et al., 2007; Si et al., 2010; Wang et al., 2014; Liang et al., 2010; Wu et al., 2011; Walter et al., 2008; Tuan et al., 2013; Wu and Ge, 2011; Fernandes et al., 2009; Muir et al., 2014; Ozerova et al., 2012; Wu et al., 2008; Jeong et al., 2007; Akdim et al., 2009; Lee et al., 2007; Wu et al., 2005; Ocon et al., 2013], XRD [Patel et al., 2008; Cheng et al., 2015; Zhang et al., 2013; Yang et al., 2011; Dai et al., 2008; Drozd et al., 2007; Kumar et al., 2017; Kojima and Haga, 2003; Groven et al., 2013; Pfeil et al., 2014; Patel et al., 2010; Zhao et al., 2007; Si et al., 2010; Wang et al., 2014; Liang et al., 2010; Wu et al., 2011; Walter et al., 2008; Tuan et al., 2013; Netskina et al., 2015; Fernandes et al., 2009; Muir et al., 2014; Das et al., 2013; Ozerova et al., 2012; Ocon et al., 2013; Yan et al., 2009], B-NMR [Drozd et al., 2007; Patel et al., 2010], FTIR [Hsueh et al., 2011; Patel et al., 2008; Pfeil et al., 2014; Patel et al., 2010; Netskina et al., 2015; Figen et al., 2013; Das et al., 2013; Ozerova et al., 2012], UV-vis spectroscopy [Kalidindi et al., 2008; Metin and Ozkar, 2009; Chen and Kim, 2008; Das et al., 2013; Umegaki et al., 2013; Kim et al., 2014; Dippolito et al., 2015; Palmer et al., 2009; Ozerova et al., 2012; Glavee et al., 1995; Zheng et al., 2015; Wang et al., 2014; Logager et al., 1992]. The generation of hydrogen using the prepared catalysts has been tested by considering various parameters like solution temperatures, catalyst loading,

NaBH₄ solution concentration, and NaOH concentration [Jeong et al., 2005; Kojima et al., 2002].

The aims of the present study was to synthesize of metal boride catalysts (Co-B, Ni-B, Fe-B) using liquid phase chemical reduction method. The catalytic activity and generation of hydrogen from with (BS)/without (WS) base stabilized sodium borohydride solution was monitored by considering various parameter like, effect of various metals in metal-boride catalysts, effect of base, calcinations temperature during synthesis of catalyst was monitored. The catalyst synthesis was monitored by in-situ UV-vis spectrometer. The synthesized catalysts were characterized by using BET, XRD and FTIR spectroscopy. It was expected that the present study will provide useful information for the generation of hydrogen using with (BS)/without (WS) base stabilized sodium borohydride solution.

2.3 EXPERIMENTAL METHOD

2.3.1 Catalysts Preparation

The chemicals were used for the synthesis of catalysts and generation of hydrogen are Cobalt chloride (Merck 98%), Nickel chloride (Thomas Baker 97%), Ferric chloride (Thomas Baker 97%), Sodium borohydride (Merck 96%) and Sodium hydroxide (Thomas Baker). All chemicals were used as received. The synthesis of catalyst was studied using two different solutions 1) with base stabilized (BS) 0.25 (M) NaBH₄ and 2) without base stabilized (WS) 0.25 (M) NaBH₄ solutions. The metal boride catalysts (Co-B, Ni-B, and Fe-B) were prepared by chemical reduction method [Jeong et al., 2005]. In chemical reduction method a known volume of 0.25 (M) cobalt chloride solutions was taken in a beaker by maintaining 273 K using an ice bath. A known volume of 0.1 (M) sodium hydroxide (BS) stabilized 0.25 (M) sodium borohydride solution was added drop-wise to the solution with stirring speed 500 rpm using a magnetic stirrer. During addition of the base stabilized (BS) sodium borohydride solution a black precipitate was appeared once the reaction was completed the black precipitate was separated by filtration, followed by keeping in a dessicator for 12 h. The synthesized sample was named as CoB-BS catalyst. Similarly, by considering the nickel chloride and iron chloride the NiB-BS and FeB-BS catalysts were also prepared. The synthesized samples were denoted as CoB-BS, FeB-BS and NiB-BS.

Similarly a set of cobalt, iron and nickel boride samples were prepared using metal chloride solution and without base stabilized (WS) sodium borohydride solution. The synthesized samples were denoted as CoB-WS, FeB-WS and NiB-WS.

The desiccator dried CoB-BS (base stabilized) sample was divided into six sets using alumina crucibles. The samples were calcined using a muffle furnace in presence of air at various temperatures 383 K, 473 K, 573 K, 673 K and 773 K for 1 h.

2.3.2 Characterization Studies

The surface area of all prepared samples was determined by using surface area analyzer in a single point BET analyzer (Micromeritics Chemisorb 2720, USA). The crystalline phase was determined by X-Ray diffraction (Bruker AXS Diffractometer D8, Germany) using $\text{CuK}\alpha$ irradiation of X-ray wavelength $\lambda = 1.541 \text{ \AA}$ with two theta value of 20 to 80 and a scan rate of 2 degree per minute. The step size was used 0.02 for all samples. The FTIR spectra of the prepared catalysts were obtained under ambient condition using a FTIR spectrometer (Thermo-Fisher Scientific, Nicolet 6700). All spectra were collected in the range of 4000 to 400 cm^{-1} . The synthesis of catalyst by chemical reduction method was monitored in cuvette by using UV-vis spectrometer (Shimadzu UV spectrometer, UV-1800). All spectra were collected in the range of 190 to 1100 nm. Both the solutions were diluted during chemical reduction using *in-situ* UV-vis study.

2.3.3 In-situ Chemical Reduction of metal chloride in UV-vis Spectrometer

The reduction of cobalt chloride using base (NaOH) stabilized (BS) sodium borohydride solution and sodium borohydride solution without base stabilized (WS) was monitored using *in-situ* UV-vis spectrometer. The 0.25 (M) metal chloride solution was prepared and diluted into 0.002 (M) prior to the *in-situ* UV-vis measurement. The 0.25 (M) base stabilized sodium borohydride solutions were diluted into 0.005 (M). Prior to the reduction the cobalt chloride solution was kept in an ice bath. In this study, a known volume of cobalt chloride solutions was taken in a cuvette and the spectra were collected. A known volume of base stabilized sodium borohydride solution was taken in a separating funnel and black precipitate was appeared by drop-wise addition of base stabilized sodium borohydride solution. The spectra were collected after each addition of base stabilized sodium borohydride solution till the reduction was completed. Similarly, the reduction was performed by considering the nickel chloride and iron chloride solution and spectra were also collected.

2.3.4 Hydrogen generation study

The synthesized catalyst was pelleted in a pelletizer and about 10 mg of synthesized catalyst was taken in a batch reactor for each run. The generation of hydrogen was studied using two different solutions 1) with base stabilized (BS) 0.25 (M) NaBH_4 and 2) without base

stabilized (WS) 0.25 (M) NaBH₄ solutions. With (BS) or (WS) base stabilized sodium borohydride solution was injected inside the reactor by using a syringe. The generation of hydrogen by using with (BS) or without (WS) base stabilized sodium borohydride solution was conducted in a closed cap Duran type bottle (considered as reactor) at room temperature (~303 K) and the generated hydrogen was collected in a U-tube by downward water displacement method. The collection of hydrogen was monitored for a particular duration of time using a stop watch. The generation of hydrogen was measured using all prepared catalysts. The experimental details were shown in Scheme-2.1.

2.4 Results and discussion

2.4.1 BET surface area analysis

The surface areas of the synthesized metal-boride samples were obtained and the obtained results were tabulated in Table-2.1. In the Table-2.1 it was indicated that the surface area depending upon the metal used for the synthesis of metal boride catalyst. The CoB-BS catalysts possessed highest surface area, followed by FeB-BS and NiB-BS which was prepared by using the base stabilized sodium borohydride solution (BS). However, the CoB-WS catalyst possessed highest surface area, followed by NiB-WS and FeB-WS which was prepared by using without base stabilized sodium borohydride solution (WS). The desiccator dried CoB-BS a catalyst was calcined at various temperatures, and the surface area of the catalyst gradually increased with increasing calcination temperature. The surface area increased upto the calcination temperature 573 K and then decreases further increasing the calcination temperatures. The obtained results suggested that the catalyst CoB-BS synthesized by base stabilized sodium borohydride solution was highly amorphous while the NiB-BS was crystalline in nature and possessed low surface area.

2.4.2 *In Situ* UV-vis spectroscopy analysis during catalyst synthesis

The Uv-vis spectrum for the cobalt chloride solution (0.25 (M)) diluted into 0.002 (M) was obtained and are shown in Fig.2.1. The spectrum of the cobalt chloride solution possessed various bands are 470 and 517 nm. These bands suggested the presence of Co⁺² ions in the solution [Das et al., 2013; Ozerova et al., 2012]. The intensity of the bands gradually decreased with subsequent addition of base stabilized sodium borohydride solution (0.3 ml, 0.005M) dropwise to the solution. A black precipitate appeared after addition of sodium borohydride solution. Further addition of sodium borohydride sodium borohydride solution the bands due to presence of Co⁺² ions disappeared gradually and it was completed after addition of ~2 ml of 0.005 (M) sodium borohydride solutions. Moreover, on further addition of base stabilized

sodium borohydride solution no changes were observed. These results suggested the formation of cobalt-boride catalysts due to complete chemical reduction of Co^{+2} ions with sodium borohydride. The formation of cobalt-boride was indicated by the presence of noise at 332 nm in the spectrum.

The UV-vis spectrum for the nickel chloride solution 0.002 (M) was obtained and are shown in Fig.2.2. The spectrum of nickel chloride solution possessed bands at 395 nm and 649 nm. These bands were suggested the presence of Ni^{+2} ions in the solution [Umegaki et al., 2013]. The intensity of the bands gradually decreased with addition of base stabilized sodium borohydride solution (0.3 ml, 0.005 (M)) dropwise to the solution. A black precipitate appeared by addition of borohydride solution. Further, on addition of borohydride solution (upto 1.2 ml) these bands disappeared completely which suggested the complete reduction of nickel ions and formation of nickel-boride along with the nano-nickel particles [Sahiner and Yasar, 2014].

The Ex-situ UV-vis spectrum for the iron chloride solution of 0.25 (M) was obtained and shown in Fig.2.3. The spectrum of iron chloride solution possesses bands at 450 and 805 nm. These bands were suggested the presence of Fe^{+3} ions in the solution [Kim et al., 2014]. The chemical reduction of Fe^{+3} in solution and formation of iron-boride gradually started by addition 0.25 (M) base stabilized sodium borohydride solution to the ferric chloride solution. The intensity of these bands gradually disappeared by appearing bands at 435 nm and then 398 nm. Suggested the reduction of Fe^{+3} ions and formation of iron boride along with iron nanoparticles; further on addition of sodium borohydride solution a new band appeared at 249 nm [Khan et al., 2016]. The presence of band suggested the formation of Fe^{+2} ions in the solution and the band remain unaltered on further addition of base stabilized NaBH_4 solution upto 4.5 ml. The study suggested the incomplete reduction of Fe^{+3} ions during chemical reduction and synthesis of FeB-BS catalyst.

The *In-situ* UV-vis study for the CoB-WS, NiB-WS and FeB-WS using without base stabilized sodium borohydride solution was also studied. The *In-situ* UV-vis spectrum is not shown here for brevity. However, the observed phenomena were similar as discussed above for each catalyst, except the synthesis of iron-boride sample. The Fe^{+3} ions reduced to form FeB-WS along with nano-iron particles.

2.4.3 FTIR Spectra Analysis

The FTIR spectra of the synthesized samples are shown in Fig.2.4. The FTIR spectra for the dessicator dried samples CoB-BS, NiB-BS and FeB-BS possessed various bands. The bands at 1023, 1253, 1393, 1632 and 3388 cm^{-1} appeared with CoB-BS catalyst. The bands at 1023, 1253, 1632 and 3388 cm^{-1} were due to presence of hydrous borate species (BO_2^-) during

synthesis of CoB-BS catalyst by chemical reduction method [Patel et al., 2008; Patel et al., 2010; Netskina et al., 2015; Figen and Coskuner, 2013]. The bands at 1632 and 3388 cm^{-1} were suggested the presence of adsorbed water in the sample [Demirci et al., 2009; Netskina et al., 2015; Ozerova et al., 2012; Carneiro et al., 2010]. The bands at 1632 cm^{-1} suggested the deformation band of water molecule and the band 3388 cm^{-1} suggested the band of O-H vibration. Similarly, the FTIR spectra of the other synthesized catalysts NiB-BS and FeB-BS were obtained. The presence of adsorbed water and borate was observed in all samples; however, the presence of hydrous borate was more prominent in case of FeB-BS sample. The adsorbed water and hydroxyl band was very strong in case of FeB-BS catalyst. Thus, the observed spectra suggested the presence of borate and water with the synthesized catalyst.

2.4.4 X-ray Diffraction analysis

The X-ray diffraction patterns of the synthesized CoB-BS, FeB-BS and NiB-BS catalysts were obtained and shown in Fig.2.5. The samples were calcined at 393 K for 2 h. before the measurement. The obtained patterns of the cobalt boride catalyst suggested that the sample was highly amorphous in nature. Similarly, the XRD patterns of the nickel-boride and iron-boride were obtained. The XRD patterns of iron-boride catalyst showed a peak position of two-theta value at 35.34, suggested the presence of $\text{Fe}(\text{OH})_3$ in the catalyst iron-boride [Wu et al., 2008]. However, the catalyst was amorphous in nature. In case of nickel-boride catalyst the peaks were obtained at 45.34 and 60.40, suggested the formation of crystalline feature of nickel-boride in the sample during synthesis [Zhang et al., 2014].

The dessicator dried sample (CoB-BS) were divided equally into six alumina crucibles and calcined various temperature at 383 K, 473 K, 573 K, 673 K and 773 K for 1 h in muffle furnace in presence of air. The XRD patterns of the cobalt-boride catalyst was obtained and calcined at various temperatures shown in Fig.2.6. The pattern suggested the formation of cobalt-boride catalysts was amorphous in nature upto calcinations temperature 673 K. The crystalline features were started to form at 773 K. The crystalline features of CoB-BS indicated by the peak at 36.9 (two theta value). Thus, the result suggested that cobalt-boride catalysts synthesized were amorphous in nature, and remains amorphous till the temperature reached to 673 K. The effect of calcinations temperature over CoB-BS catalysts suggested the formation of more stable CoB-BS and absence of any metal nano-cobalt. The XRD patterns for other catalysts (without base stabilized CoB-WS, NiB-WS and FeB-WS) were also obtained and showed no significant changes however, the patterns are not shown here for brevity.

The XRD patterns of the NiB-BS and FeB-BS catalysts were also calcined similarly at various calcinations temperature as shown above for CoB-BS catalysts. The details Figure was

shown in Fig. A1 (appendix A material). The effect of calcinations temperature suggested that the formation of nano-nickel metals along with NiB-BS during the *in-situ* reduction NiCl_2 using NaBH_4 solution. However, the metal nano-nickel was highly dispersed in the sample. The effect of calcinations temperature suggested the presence of metal nano-nickel that transformed into nickel oxide [Sahiner et al., 2014; Yousefi et al., 2016; Varkolu et al., 2017; Lo and Hwang, 1994]. The similar phenomena were suggested for the iron-boride catalysts, however, not shown here for brevity [Khan et al., 2016].

2.5 Hydrogen generation study

The generation of hydrogen using sodium borohydride solution using various metal boride catalysts was studied at room temperature (303 K). The effects of base and calcination temperature were studied during synthesis of metal boride catalysts. Moreover, the effect of base in sodium borohydride solution was studied for the generation of hydrogen. The generation of hydrogen was studied using two different solutions 1) with base (BS) stabilized 0.25 (M) NaBH_4 and 2) without base (WS) stabilized 0.25 (M) NaBH_4 solutions. The amount of catalysts was taken 10 mg for each study and temperature were maintained constant throughout the operation using an isothermal water jacketed bath at 298 K. The details generation of hydrogen are discussed below.

2.5.1 Hydrogen generation using various metal-boride catalysts

The synthesized catalysts (CoB-BS, NiB-BS and FeB-BS) were studied for hydrogen generation reaction using with (BS) or without (WS) base stabilized sodium borohydride solution. The generation of hydrogen using various catalysts (CoB-BS, NiB-BS and FeB-BS) over the base (BS) and without stabilized (WS) solution were obtained and shown in Fig.2.7A and Fig.2.7B, respectively. The obtained result in Fig.2.7A was the generation of hydrogen using base stabilized (BS) sodium borohydride solution. The obtained results suggested the highest rate of generation of hydrogen were obtained by using cobalt-boride catalyst, followed by iron-boride and the nickel-boride. However, the rate of generation of hydrogen for iron-boride catalyst was higher as compared to nickel-boride catalyst upto time 2000 sec; later nickel-boride possessed higher activity than iron-boride catalyst. The order of activity followed as $\text{CoB-BS} > \text{NiB-BS} > \text{FeB-BS}$.

The generation of hydrogen was studied using the same catalysts using without base stabilized (WS) sodium borohydride solution and obtained results are shown in Fig.2.7B. The obtained results suggested that all synthesized catalysts were active and the order of activity followed as $\text{CoB-BS} > \text{FeB-BS} > \text{NiB-BS}$. However, the cobalt-boride catalyst was most active and the generation of hydrogen was highest while the sodium borohydride solution was

considered as base stabilized (BS) (solution 1) as compared to the solution used without base stabilized (WS) (solution 2). Thus, the base stabilized sodium borohydride solution was more effective for generation of hydrogen. The activity of cobalt-boride in base stabilized sodium borohydride (BS) and sodium borohydride solution without base stabilized (WS) was followed as CoB-BS (1) > CoB-BS(2).

2.5.2 The effect of base during catalysts synthesis and generation of hydrogen over various metal-boride catalysts

The metal boride catalysts (NiB-BS, FeB-BS and CoB-BS) and (NiB-WS, FeB-WS and CoB-WS) were synthesized using with base stabilized (BS) and without base stabilized (WS) sodium borohydride solution, respectively. All the synthesized catalysts were used for the generation of hydrogen using 1) with base (BS) and 2) without base (WS) stabilized sodium borohydride solutions. The details activities of catalysts for generation of hydrogen are shown in Fig.A2 and Fig.A3 (appendix A material). The generation of hydrogen by considering catalysts (NiB-BS, FeB-BS and CoB-BS) with two different solutions base stabilized (BS) (solution 1) and without base stabilized (WS) (solution 2) were shown in Fig.A2 and the generation of hydrogen by considering catalysts (NiB-WS, FeB-WS and CoB-WS) with two different solutions base stabilized (BS) and without base stabilized (WS) were shown in Fig.A3. The obtained best combination from Fig.A2 and Fig.A3 are shown in Fig.2.8. In Fig. 2.8 the obtained results suggested that NiB-WS was more active as compared to NiB-BS catalyst and generates more hydrogen while the solution was considered as WS (without base stabilized). In case of Iron-boride and Cobalt-boride catalysts the most active was FeB-BS and CoB-BS respectively. However, the WS solution was most effective and generated more hydrogen as compared to BS solution with the FeB-BS catalyst. The CoB-BS was most effective among all catalysts using BS solution during generation of hydrogen. Thus, the study suggested that the BS solution was most effective and suitable solution while the catalysts used CoB-BS for hydrogen generation. The details preferred solutions during catalyst synthesis and hydrogen generation for each catalyst are tabulated in Table-2.2.

2.5.3 Hydrogen generation and effect of calcination temperature

The synthesized CoB-BS catalyst was obtained by chemical reduction method and the obtained catalyst was calcined at various calcination temperatures 383 K, 473K, 573 K, 673 K and 773 K. The generation of hydrogen using base stabilized (BS) sodium borohydride solution over the CoB-BS catalysts at various calcination temperatures were obtained and shown in Fig.2.9. The results in Fig.2.9 suggested that the generation of hydrogen gradually increases

with increasing calcinations temperature upto 573 K. The generation of hydrogen decreases with further increasing calcinations temperature. The catalyst was least active while the catalyst was calcined at 773 K for 1 h. However, the catalyst calcined at 573 K was most active for generation of hydrogen as compared to the other CoB-BS catalysts calcined at lower/higher calcinations temperatures. The results of hydrogen generation study were consistent with the BET surface area of all calcined CoB-BS catalysts. Thus, the results suggested that the calcinations temperature was very crucial while synthesis of CoB-BS catalyst used for generation of hydrogen.

2.6 Conclusions

A series of metal boride (CoB-BS, NiB-BS, FeB-BS and CoB-WS, NiB-WS, FeB-WS) catalysts were synthesized by chemical reduction method using with base stabilized (BS) or without base stabilized (WS) sodium borohydride solution and the CoB-BS catalyst was calcined at various temperatures. The catalyst synthesis by chemical reduction method suggested the gradually reduction of Co^{+2} ions and Ni^{+2} ions disappeared completely while the reduction was completed during synthesis of CoB-BS and NiB-BS catalyst respectively. The Fe^{+3} ions reduced to Fe^{+2} ions and finally Fe^{+2} during synthesis of iron-boride catalyst. However, the reduction was incomplete. Also the present study suggested the presence of borate (BO_2^-) species and adsorbed moisture with the metal boride catalysts. A highly amorphous phase was obtained for the CoB-BS and FeB-BS catalysts and little crystalline features of NiB-BS were obtained during synthesis of catalysts. However, the CoB-BS catalysts were calcined at various temperatures and the catalyst remain amorphous in nature with the temperature upto 673 K and the formation of crystalline phase started while reached the temperature at 773 K. The formation of metal nano-particles during the metal-boride catalysts synthesis reduced the catalytic activity of NiB and FeB catalysts.

The hydrogen generation was studied using the synthesized catalysts and it was revealed that the CoB-BS was most active followed by the other metal boride catalysts (FeB-BS and NiB-BS). The catalytic activity was followed as CoB-BS (1) > NiB-BS > FeB-BS while the generation hydrogen was studied using base stabilized (BS) sodium borohydride solution. The catalytic activity was different and followed as CoB-BS (2) > FeB-BS > NiB-BS while the study was performed using without base stabilized (WS) sodium borohydride solution. However, the hydrogen generation rate was higher with the base stabilized (BS) sodium borohydride solution as compared to without base stabilized (WS) solution and the rate was followed as CoB-BS (1) > CoB-BS (2). The generation of hydrogen using without base (WS) stabilized sodium borohydride solution was most suitable solution for the NiB-WS catalyst and for the FeB-BS catalyst. Moreover, the calcination temperature played a

significant role for the generation of hydrogen using CoB-BS catalyst. The generation of hydrogen increased with increasing calcination temperature and most active CoB-BS catalyst was obtained while calcined at 573 K.



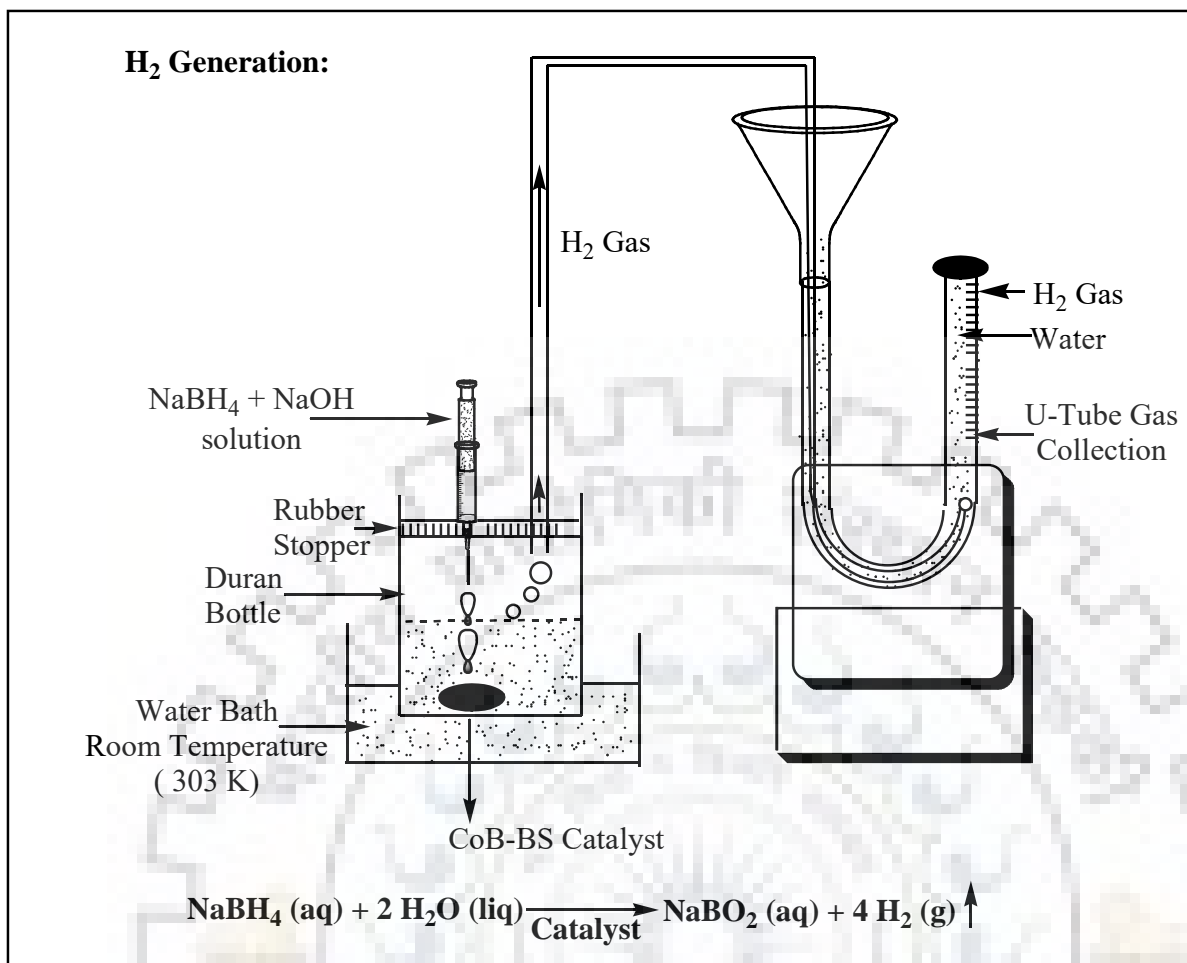
List of Table and Figures:**Table 2.1:** The BET surface area of the synthesized catalysts

(BS: base stabilized, WS: without base stabilized NaBH₄ solution during catalysts synthesis, D.d.: Desiccator dried)

Catalyst	BET surface area (m ² /gm)	Catalyst	BET surface area (m ² /gm)
CoB-BS	52	CoB-BS (D. d.)	50
NiB-BS	43	CoB-BS (383 K)	52
FeB-BS	30	CoB-BS (473 K)	55
CoB-WS	50	CoB-BS (573 K)	70
NiB-WS	44	CoB-BS (673 K)	69
FeB-WS	24	CoB-BS (773 K)	41

Table 2.2: The role of with base stabilized (BS) / without base stabilized (WS) NaBH₄ solution

S. No.	Catalyst	Suggested solution during catalyst synthesis	Suggested solution during H ₂ generation
1	CoB-BS	BS	BS
2	NiB-WS	WS	WS
3	FeB-BS	BS	WS



Scheme 2.1: The generation of H₂ using metal boride catalysts.

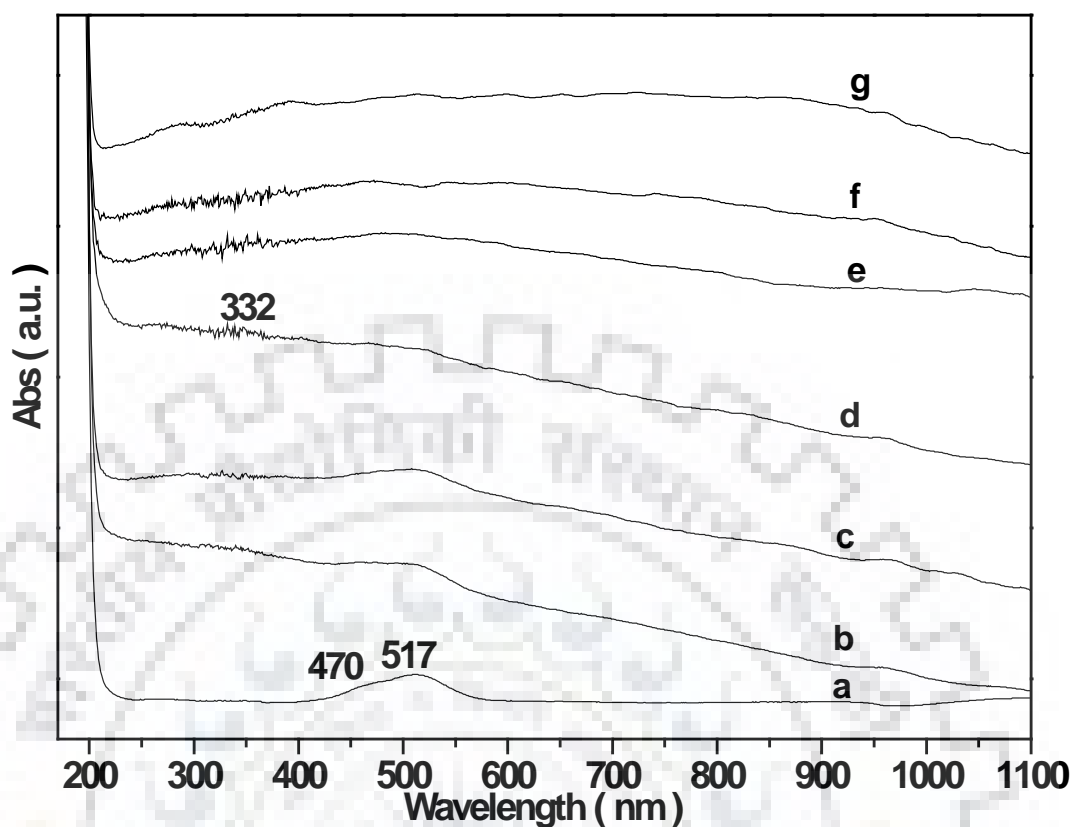


Fig. 2.1: In situ reduction of CoCl_2 and synthesis of CoB-BS catalyst using base stabilized NaBH_4 solution a) CoCl_2 solutions (1.75 ml), b) subsequent addition of 0.3 ml, c) 0.6 ml, d) 1.0 ml, e) 1.4 ml, f) 1.6 ml, g) 2.0 ml of base stabilized NaBH_4 solution. The in-situ chemical reduction was performed by using 0.002 (M) CoCl_2 solutions and a base stabilized 0.005 (M) NaBH_4 solutions.

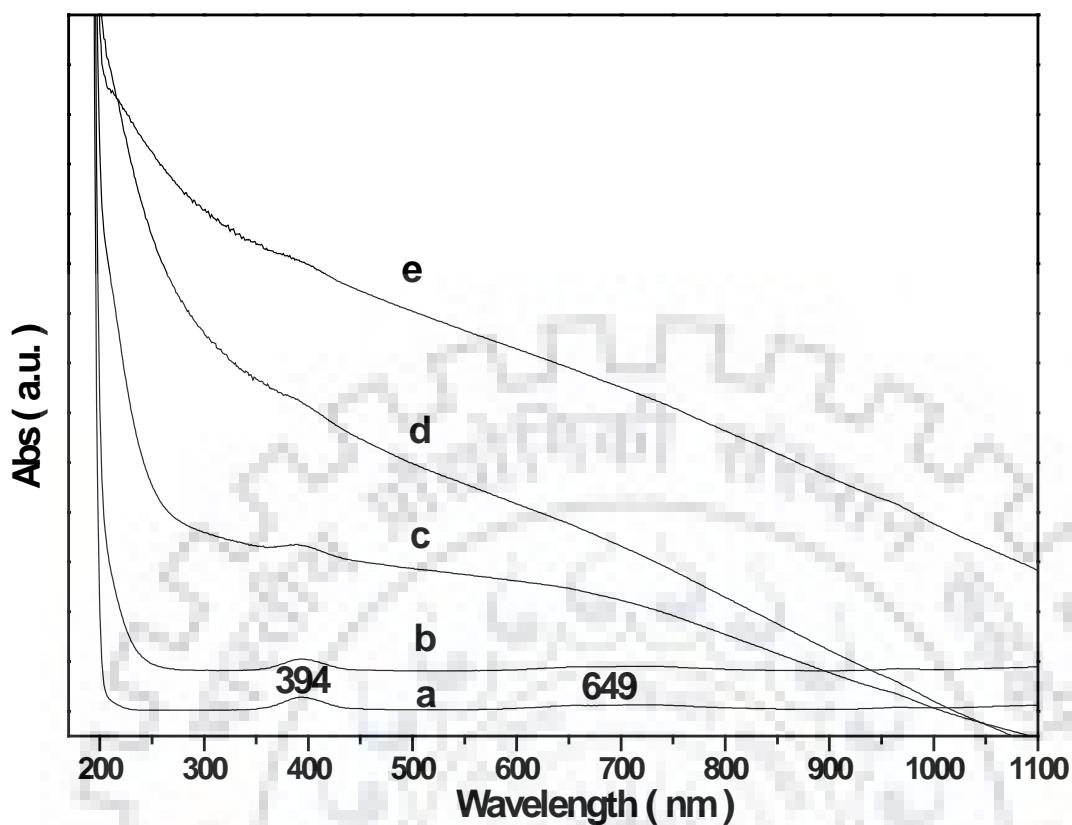


Fig. 2.2: In situ reduction of NiCl₂ and synthesis of NiB-BS catalyst using base stabilized NaBH₄ solution a) NiCl₂ solutions (1.75 ml), b) subsequent addition of 0.3 ml, c) 0.6 ml, d) 0.9 ml, e) 1.2 ml of base stabilized NaBH₄ solution. The in-situ chemical reduction was performed by using 0.002 (M) NiCl₂ solutions and a base stabilized 0.005 (M) NaBH₄ solutions.

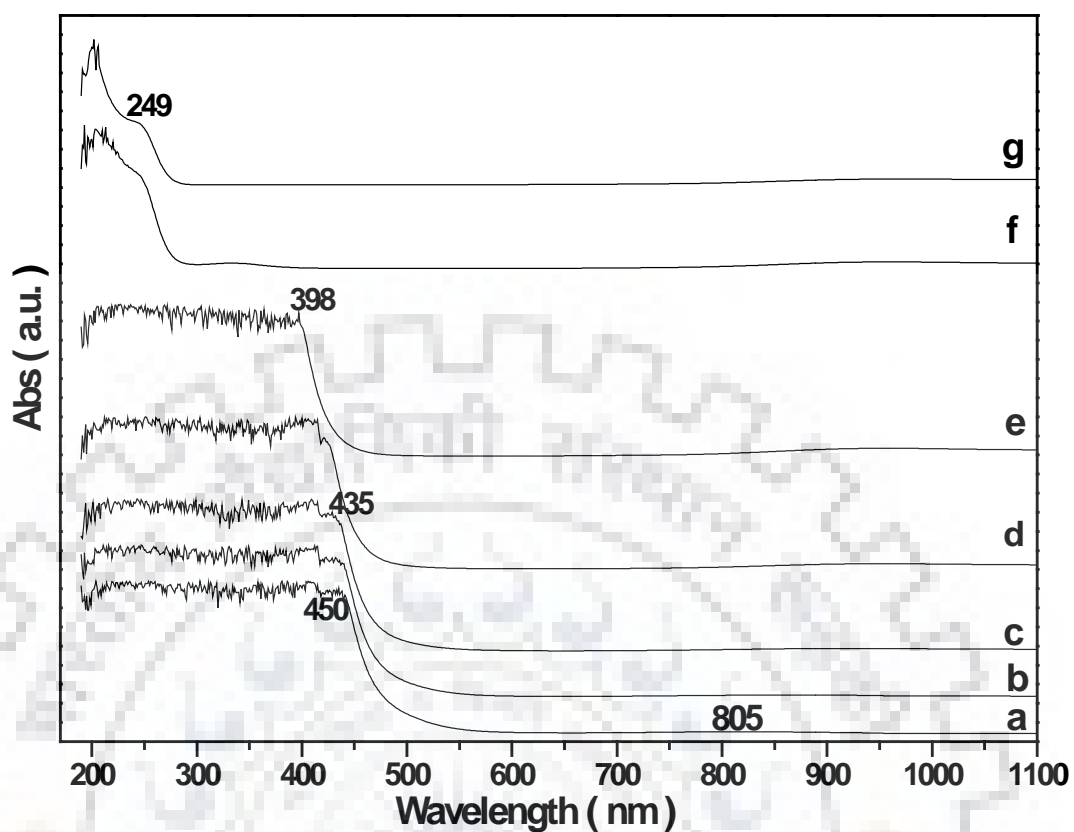


Fig. 2.3: Ex-situ reduction of FeCl_3 and synthesis of FeB-BS catalyst using base stabilized NaBH_4 solution a) FeCl_3 solution (0.25 (M) 4.0 ml), b) subsequent addition of 0.3 ml, c) 0.6 ml, d) 1.0 ml, e) 2.0 ml, f) 3.5 ml, g) 4.5 ml NaBH_4 solution.

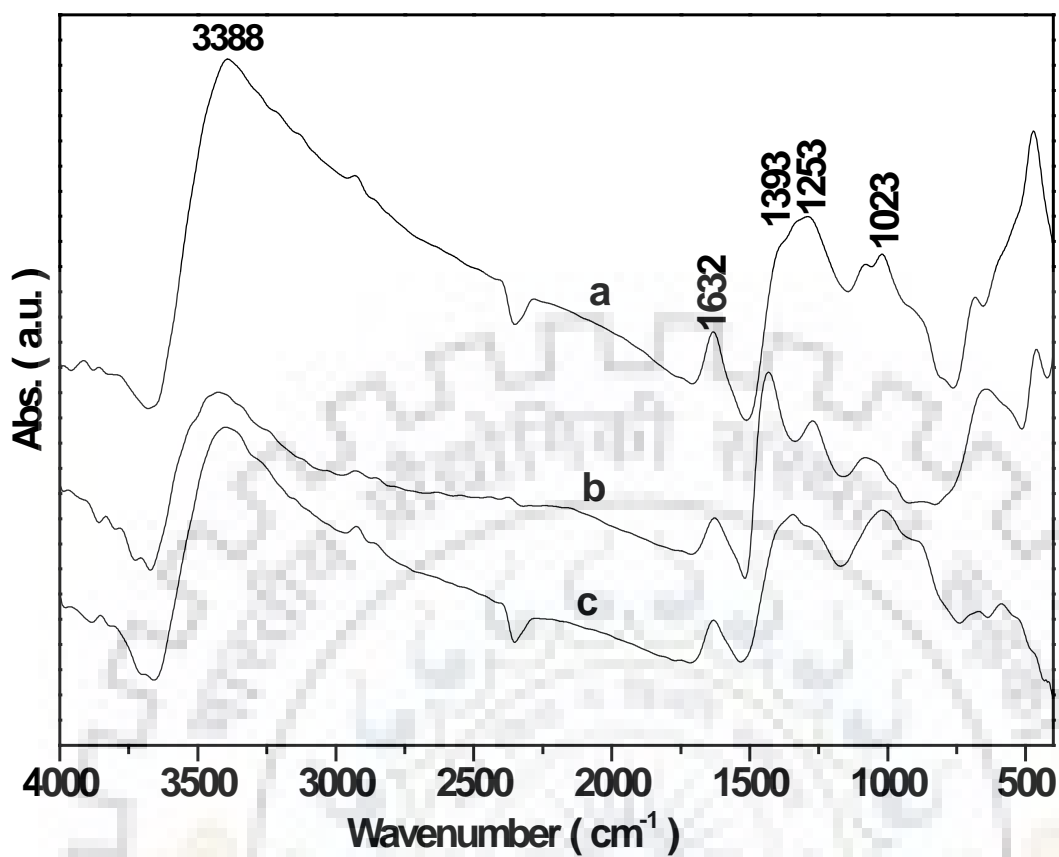


Fig. 2.4: Ambient FTIR spectra of base stabilized catalysts a) FeB-BS, b) NiB-BS and c) CoB-BS calcined at 393 K for 2 h.

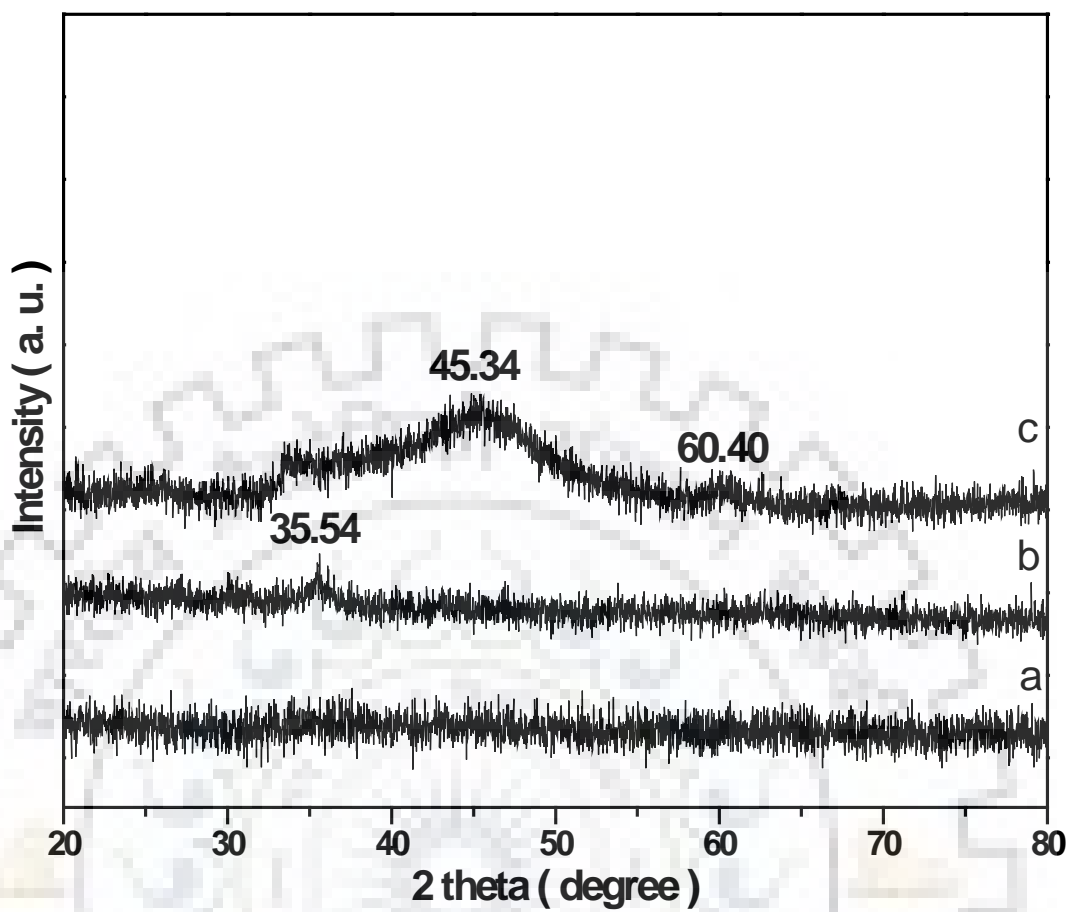


Fig. 2.5: X-Ray diffraction pattern of a) CoB-BS, b) FeB-BS, and c) NiB-BS catalysts calcined at 393 K for 2 h.

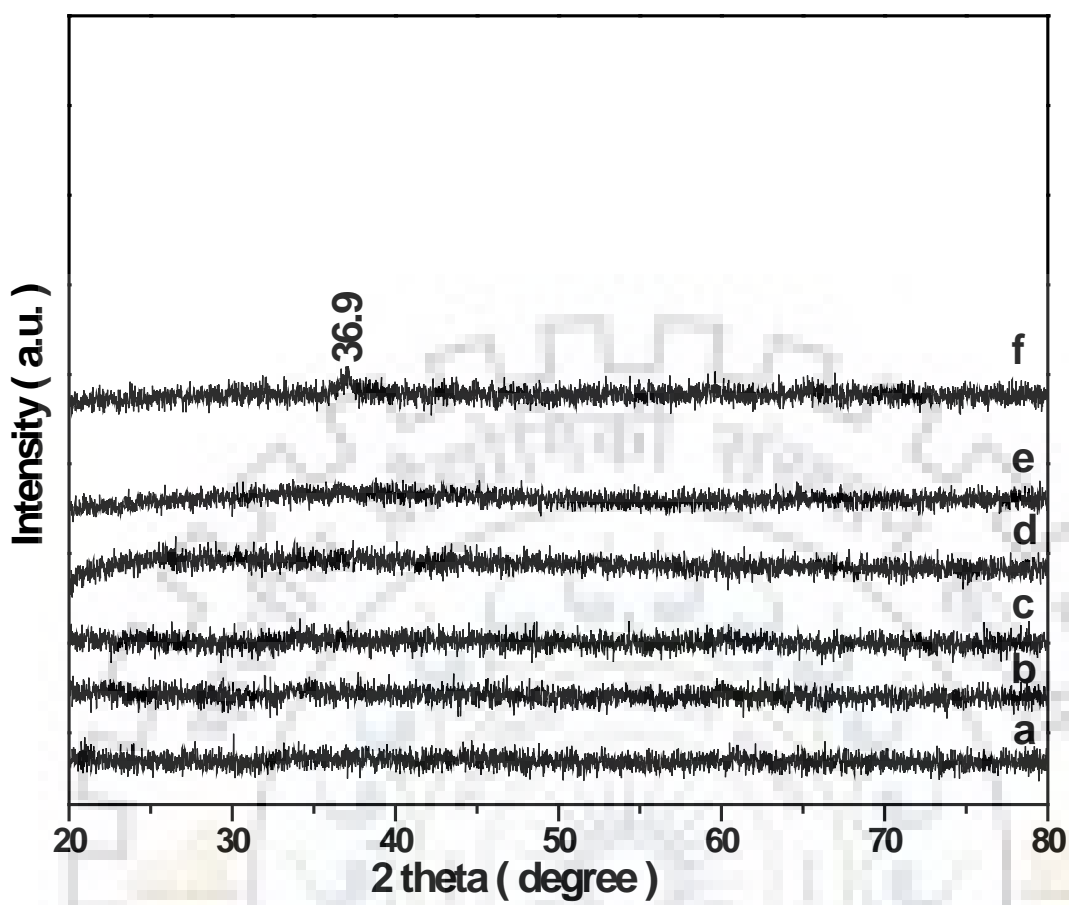


Fig. 2.6: XRD patterns of CoB-BS catalyst calcined with various calcinations temperature at a) desecrator dried, b) 383 K, c) 473 K, d) 573 K, e) 673 K, and f) 773 K for 1 h.

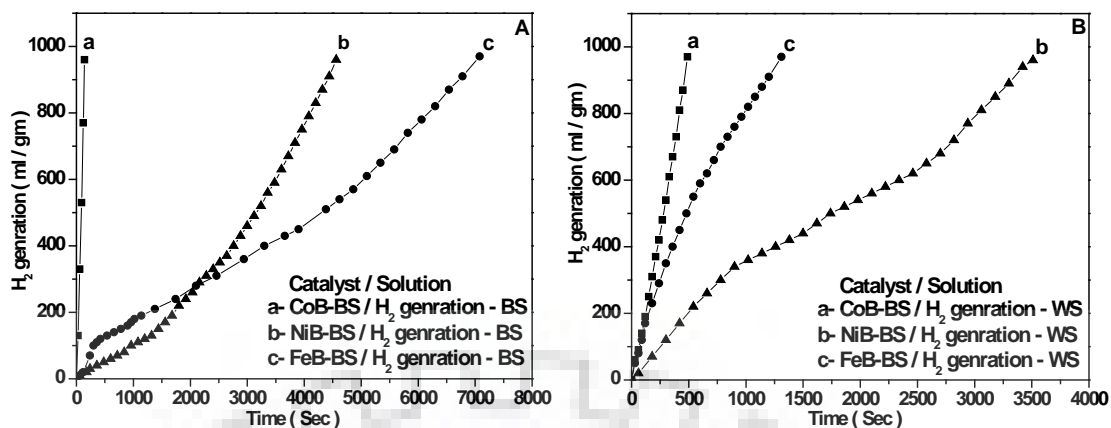


Fig. 2.7: The generation of hydrogen with time using 10 mg of each catalysts a) CoB-BS, b) NiB-BS and c) FeB-BS at 303 K, A) The generation of hydrogen using base stabilized (BS) 0.25 (M) NaBH₄ solution and B) The generation of hydrogen using without base stabilized (WS) 0.25 (M) NaBH₄ solution.

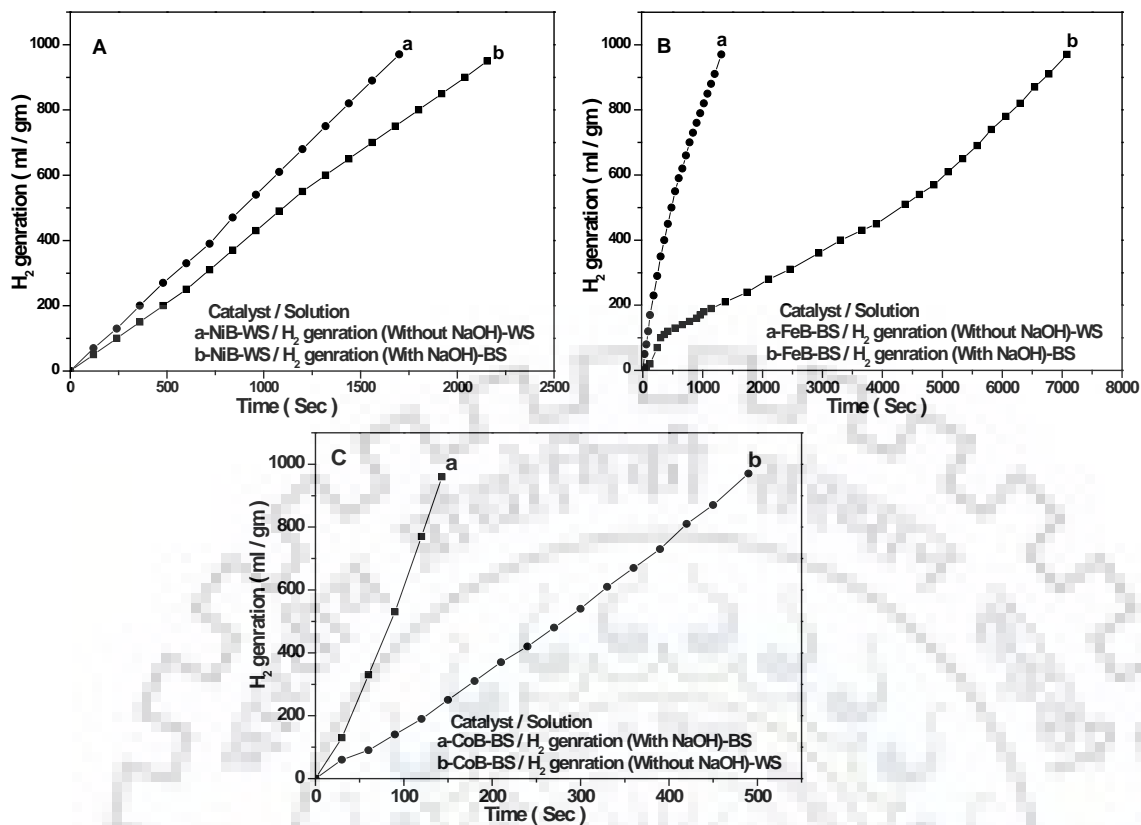


Fig. 2.8: The rate of hydrogen with time using 10 mg of each catalyst at 303 K; A) NiB-WS, B) FeB-BS, C) CoB-BS. The generation of hydrogen was studied using with (BS) (Solution 1) or without (WS) (solution 2) base stabilized 0.25 (M) NaBH₄ solutions.

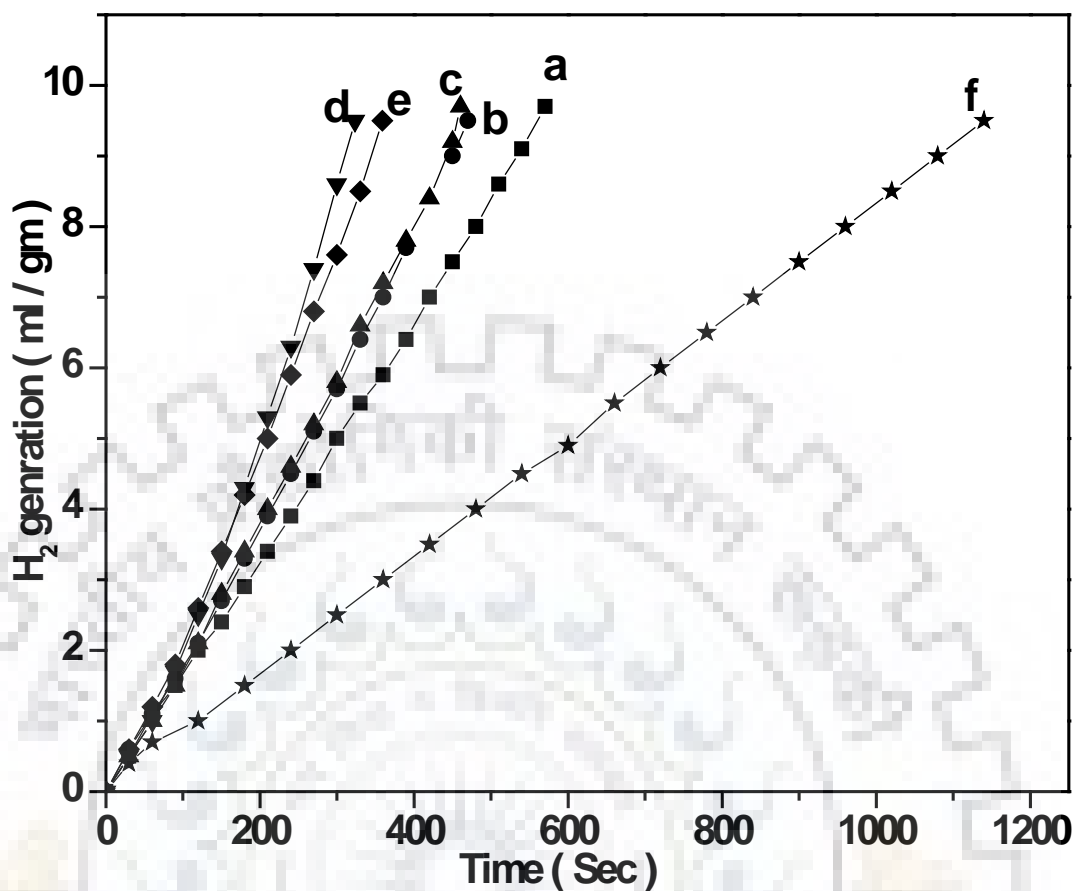


Fig. 2.9: The generation of hydrogen at 303 K using CoB-BS catalyst synthesized with different calcinations temperature at a) desecrator dried, b) 383 K, c) 473 K, d) 573 K, e) 673 K, and f) 773 K for 1 h. The generation of hydrogen was studied using with base stabilized (BS) 0.25 (M) NaBH_4 solutions.

HYDROLYSIS OF SODIUM BOROHYDRIDE USING SUPPORTED COBALT BORIDE CATALYST FOR THE GENERATION OF HYDROGEN

3.1 Abstract

A series of $x\text{CoB}/(\text{support})$ ($x = 5, 10, 20, 30, 40$ and 50) catalysts with changing supports (SiO_2 , Al_2O_3 , and MgO) and bulk CoB catalyst were synthesized by two steps impregnation-reduction method. The prepared catalysts were characterized by using BET surface area, X-ray diffraction (XRD) and Raman spectroscopy. The surface area gradually increased with increasing calcination temperature up to 573 K and further increasing calcination temperature the surface area decreased for the catalysts $50\text{CoB}/\text{SiO}_2$. However, all the calcined samples were highly amorphous in nature even at 773 K . The formation of highly dispersed CoB in $50\text{CoB}/\text{SiO}_2$ was obtained. Moreover, the Co_3O_4 species was formed in the reduction step during the synthesis of supported catalysts. The most active catalyst was found to be $50\text{CoB}/\text{SiO}_2$ catalyst synthesized with calcination temperature at 573 K . The order of catalytic activity for the generation of hydrogen was as follows: $50\text{CoB}/\text{SiO}_2 > 50\text{CoB}/\text{Al}_2\text{O}_3 > \text{CoB} > 50\text{CoB}/\text{MgO}$.

3.2 Introduction

Hydrogen is the most promising energy source to replace the traditional use of fossil fuels. The hydrogen is environmental friendly with less or no disposal of toxic pollutants to the environment. Thus, the promising energy source could be used extensively through hydrogen fuel-cell vehicles, fuel for combustion engines and other various mobile applications. However, due to lack of safety, efficient, lighter, portable and unavailability of the cheap hydrogen storage system with on-demand generation facilities is stopping the use of hydrogen energy system widely [Kojima and Haga, 2003; Bekirogullari et al., 2019; Shi et al., 2019].

The production of hydrogen has been studied by considering various reforming reactions such as dry reforming of methane, steam reforming of ethanol, methane, coke, biomass and other various sources. Thus, the reversible storage of hydrogen is very crucial. Currently, hydrogen has been stored in various ways, for example, liquid hydrogen at cryogenic temperature, compressed gas cylinder with high pressure, clathrate encapsulation and various

metal/chemical hydrides at room temperature and normal pressure [Shi et al., 2019]. The hydrides are widely used such as ammonia borane, lithium borohydride, potassium borohydride, magnesium hydride, sodium hydride and sodium borohydride [Shi et al., 2019]. The use of sodium borohydride has been attracted extensively in recent years due to its high hydrogen storage content (~10.8 wt %) at room temperature [Shi et al., 2019]. The generated by-product sodium metaborate (NaBO_2) is also recycled back to sodium borohydride.

The generation of hydrogen from sodium borohydride is considered mainly by two ways i) thermolysis of sodium borohydride at high temperature using additives, ii) hydrolysis of sodium borohydride at room temperature using various catalysts. The catalysts have been used for the hydrolysis (H_2O) or methanolysis (CH_3OH) of sodium borohydride for the generation of hydrogen are nickel, cobalt, ruthenium, platinum nanoparticles, platinum-ruthenium alloy, low-cost metals and alloys ($\text{LaNi}_{4.5}\text{Mn}_{0.5}$) [Zhao et al., 2007]. The noble metals based catalysts are costly, as result, it is not viable for industrial application and whereas, non-noble metal-based catalysts are lower in cost [Fernandes et al., 2009; Ding et al., 2010; Zhao et al., 2007]. Various metal-boride catalysts for example nickel-boride, cobalt-boride, Co-P-B, cubic CoLaZrB nanoparticles, CoB/rGO , cryogel, organic-inorganic acids are able to enhance the hydrolysis reaction rate [Fernandes et al., 2009; Ding et al., 2010; Zhao et al., 2007; Bekirogullari et al., 2019; Shi et al., 2019]. The hydrolysis reaction is accelerated and promoted by addition of second metals Co-M-B ($\text{M} = \text{Fe, Ni, Cr, Cu, W, Mo, Ru, Mn, Zr, LaZr, P}$) in the CoB catalysts. The second metals act as a promoter (in the form of oxide), which assists to avoid the agglomeration of CoB during synthesis. The addition of promoters enhanced the active surface area and electron transfer by boron to cobalt of CoB catalysts [Fernandes et al., 2009; Fernandes et al., 2009a; Ding et al., 2010; Ingersoll et al., 2007; Wang et al., 2010; Loghmani et al., 2014; Zhuang et al., 2013; Li et al., 2018; Mitov et al., 2007; Seven and Sahiner 2014; Liang et al., 2010; Oh et al., 2019]. Moreover, various supported cobalt boride catalysts have also been studied, for example the supports used are reduced graphene oxide (rGO) [Shi et al., 2019], Cryogel [Seven et al., 2014], Ni-foam [Liang et al., 2010], Cu-substrate [Kim et al., 2009], Co-hydrogel [Seven and Sahiner, 2014], anion exchange resin [Patel et al., 2009], TiO_2 [Cheng et al., 2015; Yang et al., 2011], PVP stabilized cobalt [Metin and Ozkar, 2009], SiO_2 [Yang et al., 2011; Chen and Kim, 2008; Umegaki et al., 2010], carbon nano-sheet [Wen et al., 2019], nano sphere of silica [Umegaki et al., 2009; Chen and Kim, 2008], activated carbon [Zou et al., 2011; Si et al., 2010; Rambabu et al., 2019; Bai et al., 2006], MWCNT [Prasad et al., 2019], $\gamma\text{-Al}_2\text{O}_3$ [Yang et al., 2011; Huang et al., 2008; Li et al., 2014], CoO [Kojima et al., 2002], Pt/TiO_2 [Zou et al., 2007], Pt/LiCoO_2 [Demirci and Grain, 2008], Mont-Morillonite (MMT) (clay mineral), ion exchange resin [Peng et al., 2013]

and ZrO_2 [Fernandes et al., 2009; Fernandes et al., 2009a], The addition of supports assists in strong physical adsorption, dispersion of catalysts on supports, provides high specific surface area, and also improves the acidity/basicity of the catalysts. However, the unsupported cobalt boride catalysts are aggregate easily and difficult to reuse [Yang et al., 2011]. Since, the CoB interacts strongly with the support form supported catalyst that enhances the catalytic activity and the lifetime of the catalysts [Bekirogullari et al., 2019; Rambabu et al., 2019]. Moreover, various supported metal oxides catalysts are shown to be active for the generation of hydrogen from sodium borohydride solution. The platinum nanoparticles encapsulated catalyst, $Fe_3O_4@SiO_2@Pt-TiO_2$ [Ro and Kim, 2019], $Fe_2O_3/OMWCNTs$ [Prasad et al., 2019], $LiCoO_2$, Cu/Co_3O_4 , CoB/CNT [Groven et al., 2013; Wilcox and Groven, 2017; Choi and Chung, 2016; Christie and Lockwood, 1971; Ma et al., 2018; Diallo et al., 2015; Karuppaiah et al., 2018; McNulty et al., 2017; Zied and Alamry, 2019; Bozkurt et al., 2019; Shi et al., 2019], $Co/graphene$ [Guo et al., 2014], CoB/TiO_2 , CoB/CeO_2 [Lu et al., 2012], $NiMo/TiO_2$ [Raikwar et al., 2019], $Mg-FeTi-CNTs$ [Chen et al., 2013], Pd/CNT [Gupta et al., 2009] and CoO_x , Co_3O_4 [Sing and Das, 2017] catalysts are reported very active for the hydrolysis of sodium borohydride.

The Hydrolysis of sodium borohydride for the generation of hydrogen is performed in the presence of suitable catalyst at a considerable rate. The hydrolysis process is accelerated by using a low cost, efficient, stable and suitable catalyst. The aim of the present study was focused on synthesis a series of supported CoB catalysts by incipient wetness impregnation followed by chemical reduction method. The supports used for the study were Al_2O_3 , MgO and SiO_2 . The synthesized catalysts were characterized by specific surface area, XRD, Raman analysis [Groven et al., 2013; Christie and Lockwood, 1971; Ma et al., 2018; Diallo et al., 2015; Karuppaiah et al., 2018]. The generation of hydrogen was monitored by using a glass U-tube hydrogen storage unit. Various parameters tuned for the study such as effect of total loading, effect of supports, and effect of calcination temperature of the synthesized catalysts.

3.3 EXPERIMENTAL METHOD

3.3.1 Preparation of Catalysts

Cobalt chloride (Merck 98%), Sodium borohydride (Loba Chemie 97%) and Sodium hydroxide (Thomas Baker 98%) were used as a precursor for the synthesis of catalysts. Al_2O_3 (Sasol 98%), SiO_2 (Merck 98%) and MgO (Merck 98%) used as supports during catalyst synthesis. Millipore water was used during the synthesis of catalysts and the generation of hydrogen. The cobalt boride supported catalysts (CoB/SiO_2 , CoB/Al_2O_3 , CoB/MgO) were prepared by two-step impregnation-reduction method. The synthesized catalysts were prepared

with different percentage of cobalt chloride loading with various supports. A suitable weight of cobalt chloride was dissolved in Millipore water and mixed thoroughly. Also a suitable amount of SiO₂ support was taken in the beaker and cobalt chloride solution added into SiO₂ support a drop-wise mode under magnetic stirring at ambient temperature for about 1 h with 500 rpm. The prepared sample of cobalt chloride with support was dried into an oven at 373 K for 12 h. The dried sample was divided into six parts for one sample as oven-dried and another five samples were calcined at different temperature (373 K, 473 K, 573 K, 673 K and 773 K) in muffle furnace in presence of air for 2 h at each temperature. The above-calcined sample was put into a beaker by maintaining ambient temperature using a water bath and 20 mL 0.25M sodium borohydride solution (ethanol- Millipore water mixture as solvent, volume ratio = 1:1) was added into the flask in a drop-wise mode using separating funnel to reduce Co²⁺ ions. The suspension was kept under magnetic stirring with 500 rpm. The excess amount of sodium borohydride solution was used in order to fully reduce the cobalt ions. The resultant black precipitate was filtered and washed with Millipore water and ethanol thoroughly. The synthesized catalyst was named as 5CoB/SiO₂. In the same way synthesized the different weight percentage of loading of cobalt chloride in catalyst with SiO₂ support. The synthesized catalysts denoted named as xCoB/SiO₂, where x = 5, 10, 20, 30, 40 and 50.

The supported cobalt boride catalysts with various other supports like Al₂O₃ and MgO were prepared following the above method. In this experiment, the molar ratio of NaBH₄/Co²⁺ fixed at 3:1 to get fully reduce cobalt ions.

3.3.2 Catalyst characterization Studies

The synthesized catalysts using the above technique were characterized to get basic information. The subsequent characterizations techniques used were BET surface area, XRD, and Raman spectroscopy.

The surface area was analyzed by using surface area analyzer in a single point specific surface area analyzer (Smart Sorb 92/93, India) of all the synthesized catalysts and synthesized catalysts were degassed at 423 K for 1 h before analyzing.

The crystalline/amorphous nature of the synthesized catalysts was determined by X-ray diffractometer (Bruker AXS Diffractometer D8, Germany) using CuK α irradiation of X-ray wavelength ($\lambda = 1.5418 \text{ \AA}$) at ambient temperature. The angle of the scan was fixed with the $2\theta = 20^\circ$ to 80° with a scanning speed of $2^\circ/\text{min}$. The step-size was taken 0.02 for all catalysts.

The synthesized catalysts were characterized by using InVia Reflex Raman spectrometer (InVia Reflex Renishaw, UK) with visible laser excitation 532 nm. The spectra were collected

at room temperature within the Raman shift 100 to 2200 cm^{-1} . While the acquisition of spectra, the laser power was kept at 0.05 mW.

3.3.3 Hydrogen generation study

The solution for hydrogen generation was prepared by using a 0.5 gm NaBH_4 and 0.5 gm NaOH was dissolved in 9 ml Millipore water. The pH of the solution was fixed at 9 and the concentration of the aqueous solution was 5% NaBH_4 and 5% NaOH . The aqueous solution was used for hydrolysis reaction. A hydraulic pelletizer used to make the powder sample into pallet and approx 20 mg of synthesized catalyst was loaded in a batch reactor for every single run. A 2.5 ml NaBH_4 base stabilized aqueous solution was used for the generation of hydrogen. Using the base stabilized NaBH_4 aqueous solution for generation of hydrogen was carried out in a closed cap Duran type bottle (batch reactor) at ambient temperature (~ 303 K) and the temperature of reaction system was maintained by water bath. The generated hydrogen volume was measured by U-tube by downward water displacement method. The hydrogen generation was monitored using a stopwatch for a specific duration of time. The detail experimental set up was reported in open literature [Sing and Das, 2017].

3.4 Results and discussion

3.4.1 Surface area analysis

The specific surface area of different wt% of cobalt-boride loading, various calcination temperature and various supported (MgO , SiO_2 and Al_2O_3) cobalt boride catalysts were obtained and the obtained results are tabulated in Table-3.1. In the Table-3.1, shows that the surface area depending upon the wt% of metal loading used during the synthesis of supported metal boride catalysts. The specific surface area gradually decreased as increased cobalt boride loading. The catalyst $50\text{CoB}/\text{SiO}_2$ calcined at 573 K possessed the highest surface area. The surface area of the catalyst $50\text{CoB}/\text{SiO}_2$ increased with increasing calcination temperature up to 573 K and then decreases further increasing the calcination temperatures. The $50\text{CoB}/\text{MgO}$ possessed lowest surface area due to crystalline nature of support MgO and formation of cobalt-magnesia compound. The specific surface area of SiO_2 supported catalyst was higher as compared to alumina or magnesia supported catalyst. The specific surface area of the $50\text{CoB}/\text{SiO}_2$ was obtained with changing the catalyst calcination temperature up to 773 K. The surface area gradually increased as increased the calcination temperature up to the temperature at 573 K, the surface area decreased further increased the calcination temperature. The increased of surface area may be due to the formation of mesopores in the catalysts up to the calcination temperature 573 K, however further increased the calcination temperature the agglomeration of cobalt-boride in the supported catalysts decreased the surface area. Thus, the

optimum calcination temperature was crucial for the synthesis of the supported cobalt boride catalysts.

3.4.2 Powdered X-ray diffraction (P-XRD) analysis

The X-ray diffraction patterns of $x\text{CoB}/\text{SiO}_2$ for different wt% of loading (CoB), various calcination temperature, and effect of various supports (MgO , SiO_2 and Al_2O_3) were obtained and shown in Fig.3.1. In the Fig.3.1a shows the effect of loading of cobalt boride over the support silica, however, the patterns suggested that no distinct feature of CoB was obtained with increasing the loading [Ma et al., 2018]. The XRD patterns (Fig-3.1b) of $50\text{CoB}/\text{SiO}_2$ with increasing the calcination temperature from oven-dried to 773 K, shows amorphous nature of CoB even at high calcination temperature 773 K. The Fig-3.1c suggested the presence of support Al_2O_3 and MgO in supported $50\text{CoB}/\text{Al}_2\text{O}_3$ and $50\text{CoB}/\text{MgO}$ catalysts, respectively. The feature of support silica was absent in $50\text{CoB}/\text{SiO}_2$ catalyst. Thus, the study suggested that the formation of highly dispersed CoB in all synthesized samples.

3.4.3 Raman analysis

The Raman spectra of the different wt% of loading synthesized $x\text{CoCl}_2/\text{SiO}_2$ catalyst calcined followed by reduction with NaBH_4 solution were obtained and shown in Fig.3.2. In Fig.3.2a the CoCl_2 impregnated catalysts with changing loading over the support calcined at 573 K for 2 h. Each calcined catalyst was reduced with NaBH_4 solution and the dried reduced sample shown in Fig.3.2b. In the Fig.3.2a suggested that the peaks at 146, 181, 242, 980 and 1625 cm^{-1} . The peaks 146, 181, 242 suggested the CoCl_2 in sample [Ma et al., 2018]. The bands 980 cm^{-1} was due to formation of CoO in the sample [Li et al., 2016] and 1625 cm^{-1} was due to absorbed moisture or water molecule in the sample after calcination. The calcined sample was reduced in presence of NaBH_4 solution and the obtained spectra shown in Fig.3.2b. The reduced and dried sample shows the peaks at 181, 462, 509, 601 and 665 cm^{-1} suggested the presence of Co_3O_4 species in all reduced samples. The peaks intensity gradually increased as increase the loading of cobalt in the sample. The Raman spectra of the CoB catalyst were also shown. Thus the study suggested that the formation of nano cobalt with the CoB in supported $x\text{CoB}/\text{SiO}_2$ catalysts. The nano cobalt particle was highly active and unstable that transformed into a nano Co_3O_4 crystal with CoB catalyst. The cobalt oxide was highly dispersed and was unable to detect with XRD study. The study also suggested that the Co^{2+} (CoCl_2) ions partially converted into CoO during calcination and the CoO and Co^{2+} ions converted into nano cobalt particles (Co^0) during reduction with sodium borohydride solution during synthesis of catalysts (CoB). The nano cobalt particles were highly unstable and readily converted into higher oxidation state of Co_3O_4 species.

The Raman spectra of $50\text{CoCl}_2/\text{SiO}_2$ calcined at various calcination temperature followed by reduction of the same samples with NaBH_4 solution and the spectra were shown in Fig.3.3a and Fig.3.3b respectively. The analysis of Fig.3.3a suggested the presence of bands at 146, 181, 242, 980 and 1625 cm^{-1} in calcined sample of $50\text{CoCl}_2/\text{SiO}_2$. The oven-dried sample suggested the presence of bands at 146 and 242 cm^{-1} at lower calcination temperature. The band gradually disappears and the band at 181 cm^{-1} dominates as increased the catalyst calcination temperature. All the calcined samples Fig.3.3a were reduced using NaBH_4 solution and shown in Fig.3.3b. The Raman spectra of synthesized samples suggested the presence of Co_3O_4 species. The intensity of the bands gradually increased as increased calcination temperature. The highest intensity was obtained while the sample was calcined at 773 K. The study suggested the formation of larger crystalline of Co_3O_4 as increased the calcination temperature.

The Raman spectra of $50\text{CoCl}_2/(\text{support})$ samples calcined at 573 K for 2 h and after reduction with NaBH_4 solution were obtained and shown in Fig.3.4. The supports used were SiO_2 , Al_2O_3 , and MgO . In the Fig.3.4a the calcined samples of $50\text{CoCl}_2/(\text{support})$ with changing supports. The peaks at 146, 181, 242, 462, and 750 cm^{-1} were obtained with the $50\text{CoCl}_2/\text{MgO}$ samples, and the bands 146, 242, 980 and 1625 cm^{-1} were obtained for $50\text{CoCl}_2/\text{SiO}_2$ catalysts. The band 181 cm^{-1} only was obtained with the $50\text{CoCl}_2/\text{Al}_2\text{O}_3$ catalyst. The bands remain un-altered after reduction with NaBH_4 solution of $50\text{CoCl}_2/\text{MgO}$ catalyst suggests the absence of Co_3O_4 species formation. The Co_3O_4 species was obtained for Al_2O_3 and SiO_2 supported catalysts. However, the intensity of bands due to Co_3O_4 species was more dominant in case of $50\text{CoCl}_2/\text{Al}_2\text{O}_3$ catalyst. The study suggested that the formation of Co_3O_4 species was more in case of Al_2O_3 supported catalyst. A different type of compound formation was obtained with the magnesia supported catalyst. Thus, the study suggested that formation of more CoB species for $50\text{CoB}/\text{SiO}_2$ catalyst as compared to the $50\text{CoB}/\text{Al}_2\text{O}_3$ and $50\text{CoB}/\text{MgO}$ catalysts. The order of Co_3O_4 species formation was as follows: $50\text{CoB}/\text{Al}_2\text{O}_3 > 50\text{CoB}/\text{SiO}_2 > 50\text{CoB}/\text{MgO}$. The order of CoB formation was as follows: $50\text{CoB}/\text{SiO}_2 > 50\text{CoB}/\text{Al}_2\text{O}_3 > 50\text{CoB}/\text{MgO}$.

3.5. Hydrogen generation study

The generation of hydrogen using sodium borohydride with base stabilized solution using various supported cobalt boride catalysts was studied at room temperature (303 K). The effects of wt% of loading, effects calcination temperature (oven-dried, 373 K, 473 K, 573 K, 673 K and 773 K) and effects of supports (MgO , SiO_2 and Al_2O_3) were studied during synthesis of cobalt boride supported catalysts. The catalyst was taken ~20 mg for each

experiment and temperature was maintained constant during the experiment using isothermal water-jacketed water bath at 303 K. The details of study of hydrogen generation were discussed below.

3.5.1 Effect of cobalt boride loading with supports and generation of hydrogen

The generation of hydrogen of the different wt% of loading synthesized $x\text{CoCl}_2/\text{SiO}_2$ sample calcined at 573 K for 2 h followed by reduction with NaBH_4 solution to synthesized $x\text{CoB}/\text{SiO}_2$ catalysts and bulk CoB catalyst were obtained and shown in Fig.3.5. In the Fig.3.5 suggested that the generation of hydrogen gradually increased as increased the loading of CoB in the support SiO_2 . The generation of hydrogen increased up to the loading of 50 wt% of CoB in the support SiO_2 . The generation of hydrogen increased up to the loading $50\text{CoB}/\text{SiO}_2$. Then further increasing the loading of CoB in SiO_2 , the generation of hydrogen increased. The details generation of hydrogen with changing loading was shown in Fig.B1 (appendix B material). The order of activity was followed as: $50\text{CoB}/\text{SiO}_2 > \text{CoB} > 40\text{CoB}/\text{SiO}_2$. Thus, the study suggested that supported CoB catalyst was more active as compared to bulk CoB catalyst.

3.5.2 Effect of calcination temperature and generation of hydrogen

The synthesized $50\text{CoB}/\text{SiO}_2$ catalyst was obtained by two-step impregnation-reduction method and the obtained $50\text{CoCl}_2/\text{SiO}_2$ sample was calcined at various calcination temperatures as oven-dried, 373 K, 473 K, 573 K, 673 K and 773 K followed by reduction of the calcined samples with NaBH_4 solution. The generation of hydrogen of the various calcined $50\text{CoB}/\text{SiO}_2$ catalysts and bulk CoB catalyst were obtained and shown in Fig.3.6. In the Fig.3.6 reveals that the generation of hydrogen gradually increased as increased calcination temperature. The highest generation of hydrogen was obtained while the catalyst calcined at 573 K followed by reduction. Further, increasing the calcination temperature the generation of hydrogen decreased. The order of activity was followed as the catalyst ($50\text{CoB}/\text{SiO}_2$) calcination temperature: $573 \text{ K} > 473 \text{ K} > 373 \text{ K} > 673 \text{ K} > \text{oven-dried} > \text{CoB-bulk-573 K} > 773 \text{ K}$. Thus, the generation of hydrogen study using $50\text{CoB}/\text{SiO}_2$ catalyst by changing the calcination temperature suggested that an optimum calcination temperature was crucial to synthesis a supported $50\text{CoB}/\text{SiO}_2$ catalyst for the highest generation of hydrogen. The most crucial calcination temperature was suggested to be 573 K for the synthesis of $50\text{CoB}/\text{SiO}_2$ catalyst.

3.5.3 Effect of supports and generation of hydrogen

The generation of hydrogen using 50CoB/(support) catalysts with changing supports (SiO_2 , Al_2O_3 , and MgO) and bulk CoB catalyst at calcination temperature 573 K were obtained and shown in Fig.3.7. In the Fig.3.7, reveals that the highest hydrogen generation was obtained with the catalyst 50CoB/ SiO_2 using silica as support. The SiO_2 supported CoB catalyst with 50 wt% loading was the most effective catalyst. The effect of other supports on the generation of hydrogen was followed as: 50CoB/ SiO_2 > 50CoB/ Al_2O_3 > CoB > 50CoB/ MgO . The SiO_2 support was most effective as compared to other supports (Al_2O_3 and MgO). Thus, the study suggested that choosing appropriate support for the synthesis of supported catalyst was very crucial and SiO_2 was most appropriate support for the synthesis of supported cobalt-boride catalyst.

3.6 Conclusions

A series of xCoB/ SiO_2 catalyst was obtained by two-step impregnation-reduction method. Also, a series of the supported catalyst was obtained by using SiO_2 , Al_2O_3 and MgO supports. The most active catalyst was synthesized by changing the catalyst calcination temperature. The specific surface area analysis study reveals that the SiO_2 supported 50CoB/ SiO_2 possessed the highest specific surface area. The oven-dried catalyst 50CoB/ SiO_2 possessed 85 m^2/gm specific surface area. The surface area gradually increased with increasing catalyst calcination temperature up to 573 K and the surface area decreased further increased the calcination temperature. The XRD study suggested the formation of highly dispersed CoB in all the synthesized catalysts. However, no features of other species formation were observed. The Raman spectroscopy analysis of the calcined and NaBH_4 (solution) reduced were obtained and the study suggested that the formation of Co_3O_4 species in all the synthesized catalysts. The Co^{2+} ions partially converted to CoO species during calcination. The study also suggested that the Co^{+2} ions in the calcined catalyst reduced in presence of NaBH_4 solution and formed cobalt nanoparticles which further oxidized to Co_3O_4 species with the CoB. The formation Co_3O_4 species gradually increased as the metal loading increased in support silica. Moreover, the formation of Co_3O_4 species gradually increased as increased catalyst calcination temperature. The formation of Co_3O_4 species was observed for 50CoB/ SiO_2 and 50CoB/ Al_2O_3 catalysts. However, Co_3O_4 species formation was absence for the 50CoB/ MgO catalyst, a different type of supported compound formation was obtained. The hydrogen generation study was monitored using the synthesized catalysts. It was observed that the generation of hydrogen from NaBH_4 solution gradually increased as increased the loading of cobalt in the support silica. The supported catalyst was more active as compared to the bulk CoB catalyst. The order

of activity was followed as: $50\text{CoB}/\text{SiO}_2 > \text{CoB} > 40\text{CoB}/\text{SiO}_2$. The catalyst calcination temperature has also affected the generation of hydrogen. The generation of hydrogen gradually increased as increased the catalyst calcination temperature up to 573 K and then further increasing the calcination temperature the catalytic activity decreased. The effect of supports also influences the catalytic activity of generation of hydrogen. The silica-supported catalyst was most active and effective on the generation of hydrogen. The order of support effect was followed as: $50\text{CoB}/\text{SiO}_2 > 50\text{CoB}/\text{Al}_2\text{O}_3 > \text{CoB} > 50\text{CoB}/\text{MgO}$. The support magnesia was worst as compared to other supports used for the synthesis of supported CoB catalyst. It may be due to the formation of stable complex compound with support magnesia.



List of Table And Figures:

Table 3.1: The BET surface area of the synthesized catalysts

Catalyst	BET surface area (Sq.m/gm)	Catalyst	BET surface area (Sq.m/gm)
5CoB/ SiO ₂ - 573 K	165	50CoB/ SiO ₂ - oven dried	85
10CoB/ SiO ₂ - 573 K	158	50CoB/ SiO ₂ - 373 K	89
20CoB/ SiO ₂ - 573 K	145	50CoB/ SiO ₂ - 473 K	102
30CoB/ SiO ₂ - 573 K	131	50CoB/ SiO ₂ - 573 K	115
40CoB/ SiO ₂ - 573 K	125	50CoB/ SiO ₂ - 673 K	85
50CoB/ SiO ₂ - 573 K	115	50CoB/ SiO ₂ - 773 K	82
50CoB/Al ₂ O ₃ - 573 K	112	SiO ₂	180
50CoB/SiO ₂ - 573 K	115	Al ₂ O ₃	175
50CoB/MgO - 573 K	35	MgO	41

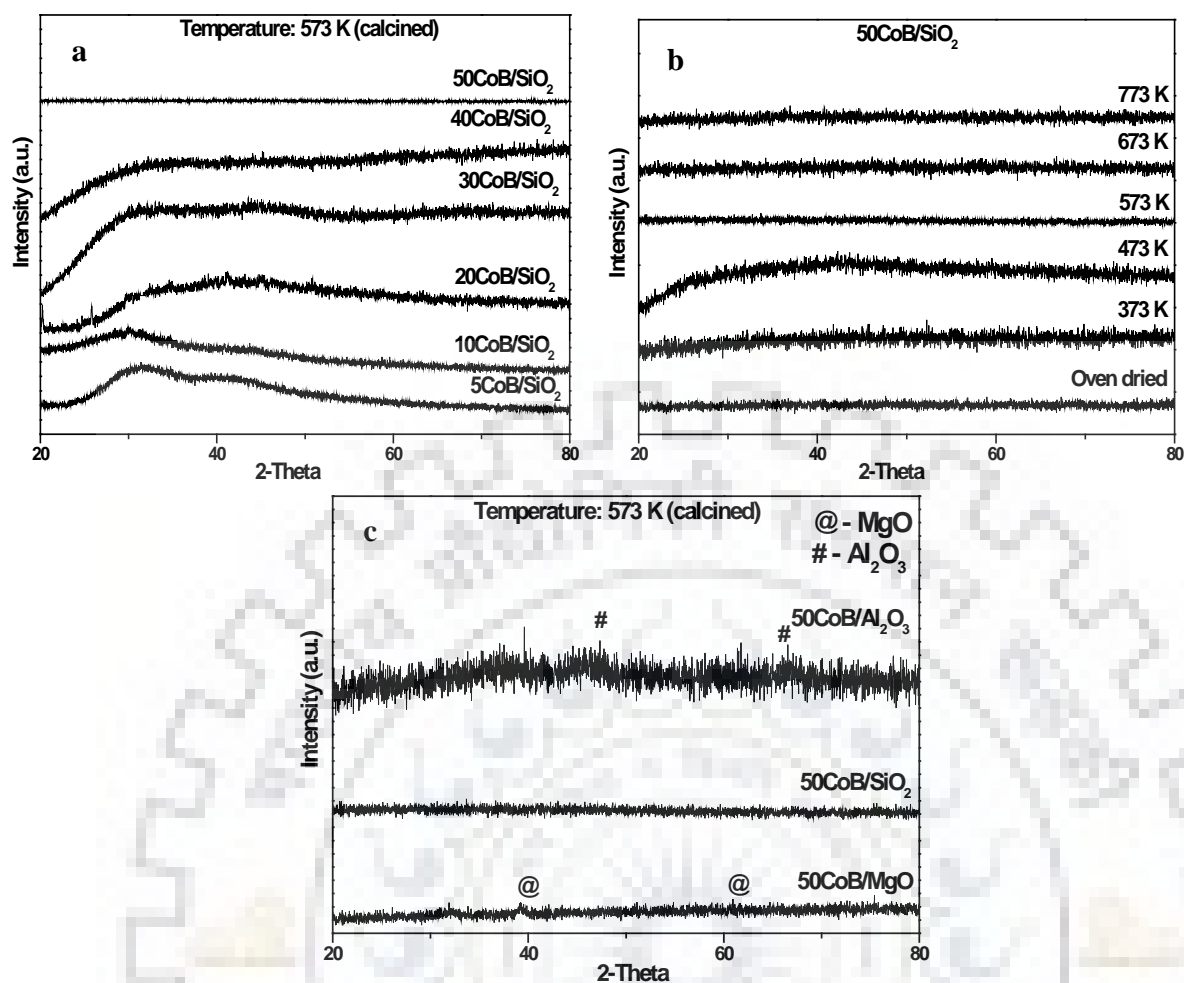


Fig.3.1: X-ray diffraction patterns of a) $x\text{CoB}/\text{SiO}_2$ with different loading (5 wt% to 50 wt%) calcined at 573 K, b) $50\text{CoB}/\text{SiO}_2$ with various calcination temperature (oven-dried to 773 K), and c) $50\text{CoB}/(\text{support})$ with various supports (SiO_2 , Al_2O_3 , MgO) calcined at 573 K. Where, x was weight percent of CoB in support (5 wt%, 10 wt%, 20 wt%, 30 wt%, 40 wt%, and 50 wt%). All the catalysts were calcined at the respective temperature, followed by reduction with NaBH_4 solution.

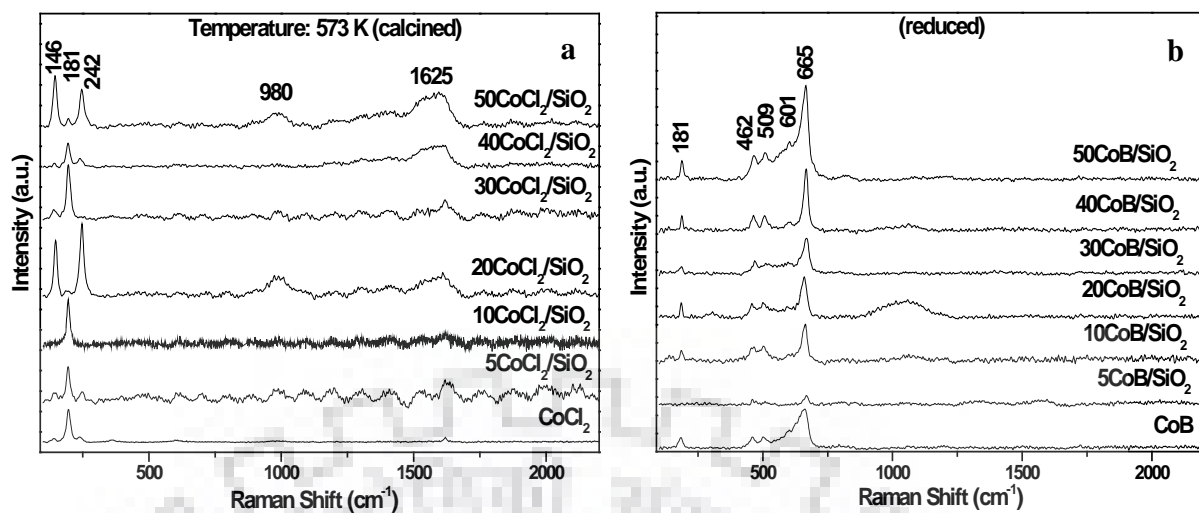


Fig.3.2: The Raman spectra of a) $x\text{CoCl}_2/\text{SiO}_2$ samples calcined at 573 K for 2 h, b) after reduction with NaBH_4 solution of each catalyst reported in Fig.3.2 a. Where the x was the wt% of CoCl_2 impregnated over the support. (x = 5 wt%, 10 wt%, 20 wt%, 30 wt%, 40 wt% and 50 wt%)

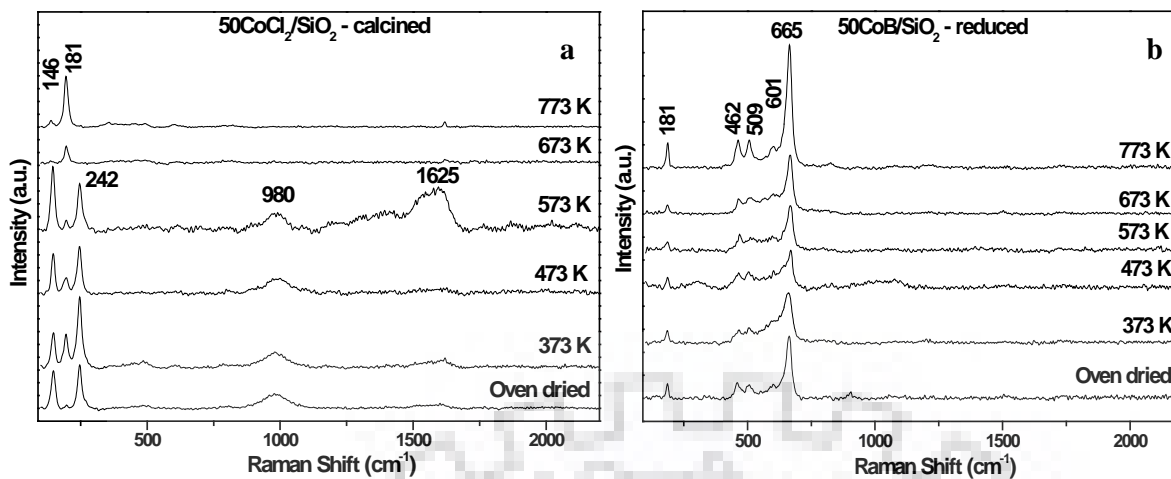


Fig.3.3: The Raman spectra of a) 50CoCl₂/SiO₂ samples calcined at various temperature for 2 h, b) reduction with NaBH₄ solution of each catalyst reported in Fig.3.3 a.

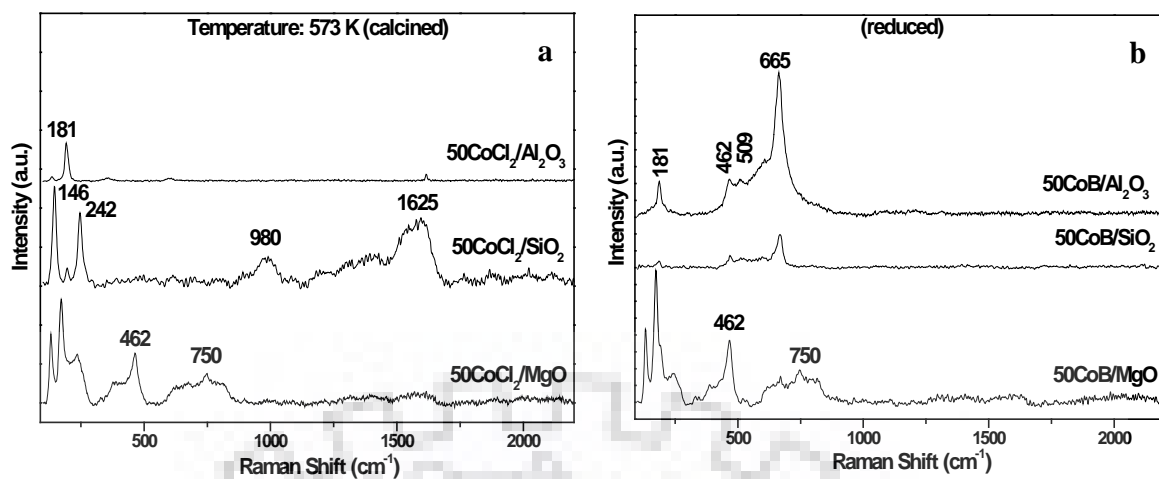


Fig.3.4: The Raman spectra of a) 50CoCl₂/(support) samples calcined at 573 K, b) after reduction the same sample with NaBH₄ solution, the catalysts reported in Fig.3.4 a. The supports used were SiO₂, Al₂O₃, and MgO.

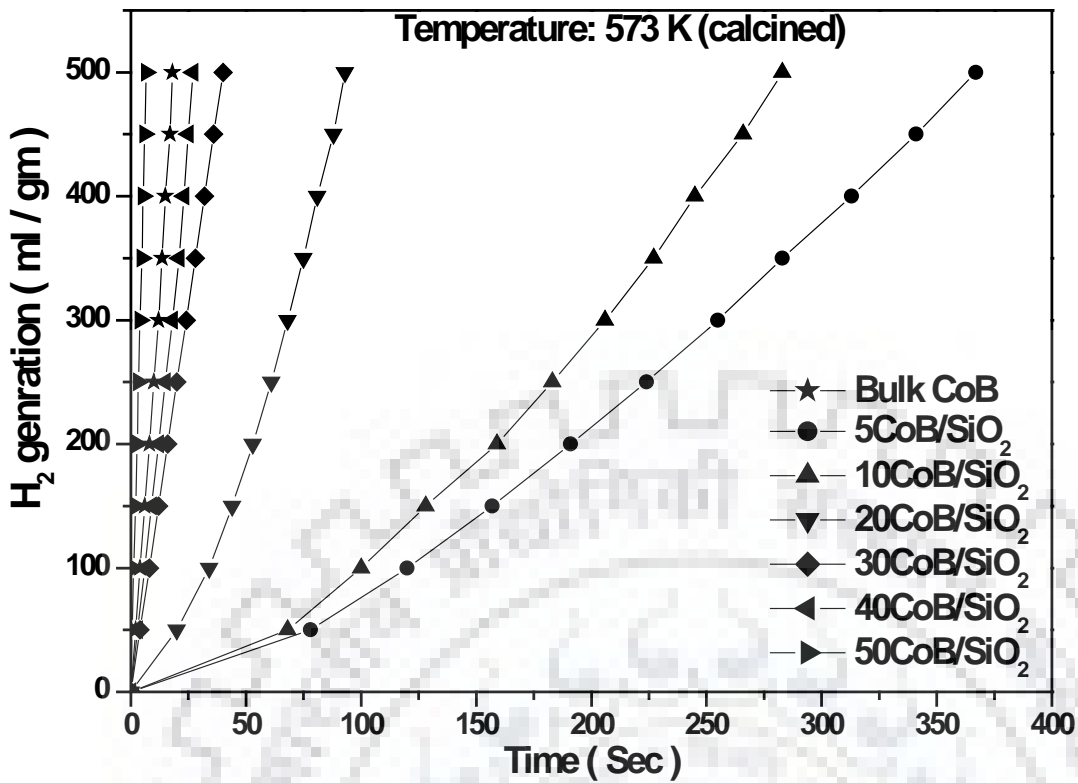


Fig.3.5: The generation of hydrogen using $x\text{CoB}/\text{SiO}_2$ catalysts with changing total loading of CoB and bulk CoB catalyst. The generation of hydrogen study was conducted with the temperature at 303 K using 20 mg of catalyst. The catalyst was calcined at 573 K followed by reduction with NaBH_4 solution.

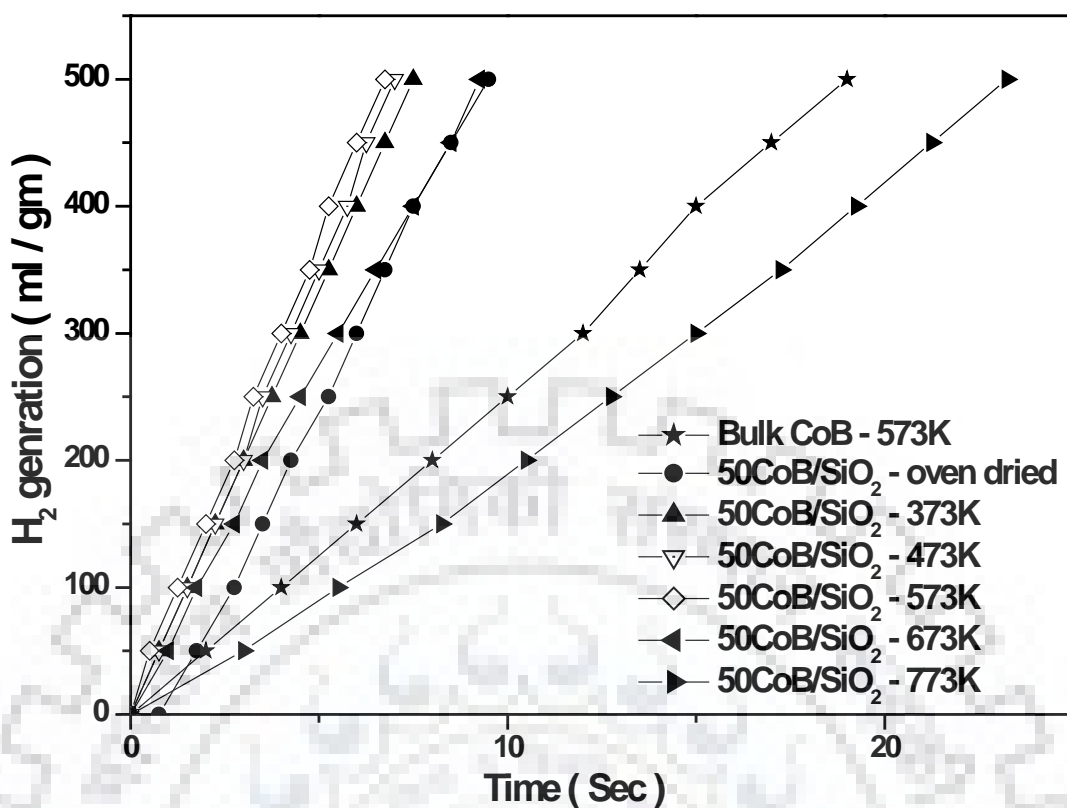


Fig.3.6: The generation of hydrogen using 50CoB/SiO₂ catalyst with changing calcination temperature from oven-dried to 773 K. The generation of hydrogen study was conducted with the temperature at 303 K using 20 mg of catalyst. All catalysts were calcined at the respective calcination temperature followed by reduction with NaBH₄ solution.

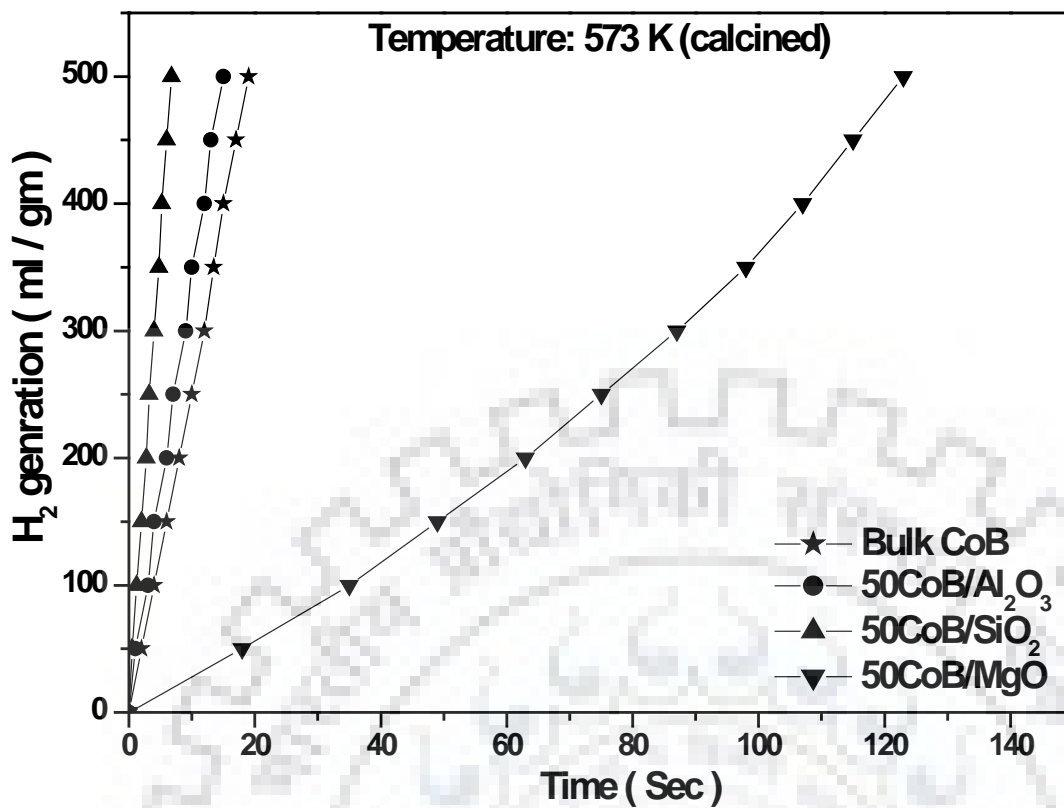


Fig.3.7: The generation of hydrogen using 50CoB/(support) catalysts with changing supports (SiO₂, Al₂O₃, and MgO). The generation of hydrogen study was conducted with the temperature at 303 K using 20 mg of catalyst. All the catalysts were calcined at 573 K followed by reduction with NaBH₄ solution.

GENERATION OF HYDROGEN FROM SODIUM BOROHYDRIDE AT LOW TEMPERATURE USING METAL HALIDES ADDITIVE

4.1 Abstract

A series of MnCl_2 impregnated NaBH_4 composite mixture was synthesized by facile solution method. The weight percent of MnCl_2 varied from 10 wt% to 50 wt% in sodium borohydride during synthesis of the material. The effects of other additives were also studied by considering CaCl_2 , and ZnCl_2 . The synthesized materials were characterized by using X-ray diffraction (XRD), TGA, FE-SEM, Raman spectroscopy, and Fourier Transform Infra-red spectroscopy (FTIR). The generation of hydrogen was monitored by using a Gas Chromatograph. The study suggested that the formation of a homogenous composite mixture and spherical structure of $\text{MnCl}_2/\text{NaBH}_4$ composite material. The optimum loading of additive was found to be 20 wt% MnCl_2 for the generation of hydrogen. The addition of additive assists in lowering the thermal decomposition temperature of sodium borohydride at 373 K. The order of thermolysis performance by addition of various additives was as follows: $20\text{CaCl}_2/\text{NaBH}_4 > 20\text{MnCl}_2/\text{NaBH}_4 > 20\text{ZnCl}_2/\text{NaBH}_4$. However, the FTIR spectra and the thermolysis study suggested that the decomposition of NaBH_4 was incomplete at 373 K even by the addition of additives.

4.2 Introduction

There is a need for alternative and renewable energy resources to overcome the current situation of depletion of fossil fuel and environmental pollution problem. Amongst all energy resources hydrogen is the best, abundant and clean energy carrier. It has no environmental impact as on hydrogen react with environmental oxygen converted into water. Hydrogen has high energy density; however, the problem appears with the storage of hydrogen in a compact way, generation, and utilization of hydrogen in a controlled way [Nale et al., 2016; Varin et al., 2017; Martelli et al., 2010; George and Saxena, 2010; Kim et al., 2006; Chaugule et al., 2015; Chinnapan et al., 2012; Singh and Das, 2017]. Hydrogen can be stored in various forms, for example, gaseous, liquid and solid form. The storage of hydrogen in high-pressure compression and cryogenic liquefaction is not suitable and economical for mobile industries [Mao et al., 2012; Das et al., 2015; Das et al., 2016; Das et al., 2019]. Hydrides have a higher

volumetric density of hydrogen than pressurized hydrogen vessel and cryogenic hydrogen tanks.

The solid phase storage is basically in the form of various metal/chemical hydrides such as metal borohydrides and ammonia borane [Lu et al., 2013; Yao et al., 2014; Yao et al., 2015; Yao et al., 2016; Dai et al., 2011]. Moreover, Several hydrides such as LiAlH_4 , LiBH_4 , CaH_2 , MgH_2 , LiH , $\text{NH}_3\text{-BH}_3$, $\text{Zn}(\text{BH}_4)_2$, KBH_4 , NaBH_4 , $\text{Mg}(\text{BH}_4)_2$, and $\text{Ca}(\text{BH}_4)_2$ having great storage potential for hydrogen. These hydrides may be used in vehicle application for transportation of small distance automobiles. As a promising hydrogen storage material, the gravimetric hydrogen and volumetric hydrogen density of sodium borohydride is ~ 10.8 wt% and $113 \text{ kg H}_2/\text{m}^3$ respectively [Urgnani et al., 2008; Martelli et al., 2010; Chinnappan et al., 2012]. The thermodynamic stability of these metal hydrides is reported very high, for example, the thermal decomposition temperatures of $\text{Mg}(\text{BH}_4)_2$ (593 K), $\text{Ca}(\text{BH}_4)_2$ (640 K), LiBH_4 (653 K), and NaBH_4 (778 K). The multi-step thermal decomposition of NaBH_4 has been reported by considering a Catlab reactor in a continuous heating under He-2.5 wt% H_2 gas flow. Desorption of water is started at 373 K, hydrogen released started at 423 K, and the main hydrogen delivered at 713 K during the thermolysis process. The decomposition process is slow during isothermal heating at 693 K. The reaction is slow for first 50 min and the release of hydrogen reached to maximum and faster after 120 min. The advantages of addition of additives/catalysts (Ti or TiH_2 , TiF_3) with NaBH_4 is very crucial. The ball-milled NaBH_4 is desorbed hydrogen about 1.5 wt%, $\text{NaBH}_4\text{-}0.05\text{Ti}$ (1.65 wt %), $\text{NaBH}_4\text{-}0.05\text{TiH}_2$ (1.85 wt %), and $\text{NaBH}_4\text{-}0.05\text{TiF}_3$ (3.2 wt %) at 713 K within 400 min. The desorbed amount of hydrogen is gradually increased as desorption time and temperature increased [Mao and Gregory, 2015; Urgnani et al., 2008; Chen and Kim, 2008]. The hydrogen is being produced as major product, however, it produces other various intermediate species such as metal sodium, NaH , unreacted NaBH_4 , B_2H_6 (diborane), $\text{B}_3\text{H}_6\text{N}_3$ (borazine), $\text{Na}_2\text{B}_{12}\text{H}_{12}$ (dodecaborane) during decomposition of chemical/metal borohydride at 778 K [Mao and Gregory, 2015; Jeon and Cho, 2006; Urgnani et al., 2008; Chong et al., 2011; Zhang et al., 2011; Kumar et al., 2017; Zhang et al., 2010; Humphries et al., 2013; Bai et al., 2014; Chen and Kim, 2008; Nakamori et al., 2006; Zhang et al., 2013; Khafidz et al., 2016; Olsen et al., 2011; Li et al., 2011]. Thus, it is challenging, and required high temperature during destabilization of metal hydrides to release hydrogen while in use. Several strategies have been considered to destabilize the metal borohydride and improve the nature of reversibility at low temperature. The strategy includes anion substitution, cation substitution, mixed metal borohydride, the synthesis method of reactive hydride composites, and nano-confinement [Mao and Gregory, 2015; Jeon and Cho, 2006; Paskevicius et al., 2013; Chang et al., 2014; Chong et al., 2011; Zhang et al., 2011;

Kumar et al., 2017; Zhang et al., 2010; Pendolino, 2012; Humphries et al., 2013; Nale et al., 2016; Bai et al., 2014; Kumar et al., 2017; Mao et al., 2012; Varin et al., 2017; Martelli et al., 2010; George and Saxena, 2010; Kim et al., 2006; Chaugule et al., 2015; Chinnappan et al., 2012; Singh and Das, 2017; Dai et al., 2011; Nakamori et al., 2006; Zhang et al., 2013; Khafidz et al., 2016; Olsen et al., 2011; Li et al., 2011; Wu et al., 2016; Bai et al., 2017; Kumar et al., 2017; Cho et al., 2006; Jepsen et al., 2013; Knight et al., 2013]. Thus, the evaporation of sodium metal and other species formation during thermolysis of sodium borohydride is reduced by lowering the decomposition temperature, the addition of various additives, catalysts, and chemical modification [Kumar et al., 2017]. Various additives have been used to down the thermal decomposition temperature of metal hydrides such as TiF_3 [Mao and Gregory, 2015; Kalantzopoulos et al., 2014; Mao et al., 2012; Zhang et al., 2013], ZnF_2 [Zhang et al., 2011], ZrCl_4 [Kumar et al., 2017; Kumar et al., 2017; Kumar et al., 2017], SiO_2 , Charge compensation by Li^+ ion [Nakamori et al., 2006], MWCNT, graphene oxide, fullerene [Knight et al., 2013], mesoporous carbon scaffold [Wang et al., 2014], LnF_3 , FeF_3 , MnF_3 , NaBF_4 , NiCl_2 , NiF_2 , ZnF_2 , $\text{Ni-Si/Al}_2\text{O}_3$, fluorographite (FGI), MgH_2 , LiNH_2 , ZnCl_2 , mixed metal cations [Mao and Gregory, 2015; Kalantzopoulos et al., 2014; Wang et al., 2014; Zhang et al., 2013], Ni_3B , NiCo-B , CaF_2 [Zhang et al., 2013], VCl_3 , TiCl_3 , Guanidine (CN_3H_5) [Wu et al., 2016], MgCoB [Bai et al., 2017], Si , Al [Cho et al., 2006], TiO_2 , V_2O_3 , SnO_3 , MgCl_2 , and excessive amorphous boron [Pendolino, 2012].

The composite material have been synthesized using various methods such as SSBM method (solid state ball milling method) [Hino et al., 2007; Buhl et al., 2005; Pei et al., 2017], LPBM method (liquid phase ball milling), planetary ball mill or magneto ball mill with flow of an inert gas medium of argon [Ferrer et al., 2011] and MCAS method (mechano-chemical activation synthesis) [Chong et al., 2011; Kim et al., 2008; Kumar et al., 2017; Zhang et al., 2010; Humphries et al., 2013; Bai et al., 2014; Mao et al., 2015; Varin et al., 2017; Khafidz et al., 2016; Olsen et al., 2011; Wu et al., 2016; Yang et al., 2011; Naik et al., 2009; Toche et al., 2012; Huot et al., 2013], and facile solution method [Mao et al., 2015]. Moreover, various solvents have been used in the facile solution method, for example, THF [Kim et al., 2008; Mao et al., 2015; Wu et al., 2016; Naik et al., 2009], cyclohexane [Bai et al., 2014], diethyl ether [Groven et al., 2013; Li et al., 2011].

The synthesized materials have been characterized by using various methods such as FE-SEM [Soykal et al., 2012; Hino et al., 2007; Qiao and Swihart, 2017], XRD [Jeon and Cho, 2006; Kim et al., 2008; Humphries et al., 2013; Bai et al., 2014; Mao et al., 2015; Kojima and Haga, 2003; Wu et al., 2016; Yang et al., 2011], XPS [Yadav and Das, 2019; Mao et al., 2012], TPD [Humphries et al., 2013; Bai et al., 2014; Zhang et al., 2013; Olsen et al., 2011], Raman

analysis [Zhang et al., 2011; Nakamori et al., 2006; Zhang et al., 2013], B-NMR [Mao and Gregory, 2015; Chong et al., 2011], FTIR [Jeon and Cho, 2006; Urgnani et al., 2008; Zhang et al., 2011; Kumar et al., 2017; Zhang et al., 2010; Bai et al., 2014; Mao et al., 2015; Hsueh et al., 2009; Mao et al., 2012; Kumar et al., 2017; Yang et al., 2011; Gennari et al., 2009; Danna et al., 2014; Sljukic et al., 2013; Buhl et al., 2012; Filinchuk et al., 2008; Choudhury et al., 2009; Concha et al., 2010; Yang et al., 2013; Karabulut et al., 2016], and TGA-DTA [Urgnani et al., 2008; Bai et al., 2014; Mao et al., 2015; Toche et al., 2012].

Since high temperature is required for thermolysis of pure sodium borohydride during generation of hydrogen. A suitable catalyst or additive is required to down the thermolysis temperature. The aim of the present study was to synthesize a series of $x\text{MnCl}_2/\text{NaBH}_4$ homogeneous mixture using a facile solution method. The synthesized materials were characterized by using XRD, FE-SEM, TGA, Raman, and FTIR analysis. The generated hydrogen was monitored using GC (Gas Chromatograph). The thermolysis study was considered by changing various parameters such as an effect of decomposition temperature, decomposition time, various additives, and the effect of total loading of additives.

4.3. EXPERIMENTAL

4.3.1 Material Preparation

The materials purchased for the study were Sodium borohydride (97% of Loba Chemie, India), MnCl_2 (Molychem, India, 98%), ZnCl_2 (Thomas Baker, India, 98%), CaCl_2 (Molychem, India, 98%) and Diethyl ether (Et_2O) (Thomas Baker, India, 99.5%). A homogeneous mixture of $x\text{MnCl}_2/\text{NaBH}_4$ was synthesized by facile solution method [Bai et al., 2014; Varin et al., 2017]. In this method, a known amount of sodium borohydride (~4 g) and manganese chloride each was pestle for 1 h using a mortar to reduce the size and the prepared mixture put into three necks round bottom flask containing 20 ml of diethyl ether (Et_2O). Nitrogen gas passed to purge the air inside the flask. The sample mixture stirred with a rate of 500 rpm at 308 K for 1 h. The solid powder mixture stirred until the solvent diethyl ether evaporated completely from the flask. The dried composite material collected and stored into an airtight culture tube for future use and analysis. The material synthesized in this method denoted as $x\text{MnCl}_2/\text{NaBH}_4$, where, $x = 10\text{wt}\%$, $20\text{wt}\%$, $30\text{wt}\%$, $40\text{wt}\%$, $50\text{wt}\%$ of MnCl_2 in NaBH_4 . Similarly, $20\text{ZnCl}_2/\text{NaBH}_4$ and $20\text{CaCl}_2/\text{NaBH}_4$ were also prepared using the above methods.

4.3.2 Synthesized material characterizations

The composite materials synthesized using the above method was characterized to obtain fundamental information. The following characterizations techniques used were XRD, TGA, FE-SEM, Raman, and FTIR.

The X-ray diffraction study of the synthesized materials was recorded at room temperature using X-ray diffractometer (Bruker AXS Diffractometer D8, Germany) with Cu-K α ($\lambda = 1.5418$ Å) irradiation. The scanning angle used $2\theta = 10^{\circ}$ to 90° with a scanning speed of $2^{\circ}/\text{min}$.

The Field Emission Scanning Electron Microscopy was used to study the surface morphology of synthesized materials using FE-SEM (FE-SEM QUANTA 200 FEG, Netherlands) apparatus. The FE-SEM images were taken at different magnification with the acceleration voltage of the apparatus at 20 kV.

The thermogravimetric analysis of the prepared sample was studied by a TGA/DTA apparatus (SII 6300 EXSTAR, Japan). The thermogravimetric analysis was performed from ambient to 300°C temperature range with a programmable heating rate of $5^{\circ}\text{C}/\text{min}$ in a nitrogen gas flow rate of 50 ml/min through the samples in the apparatus.

The Raman spectra of the synthesized materials were obtained by using InVia Reflex Raman spectrometer (InVia Reflex Renishaw, UK) using visible laser excitation 532 nm. The spectra were collected at ambient temperature with the spectral range 100 to 3200 cm^{-1} . The laser power used 0.01 mW during acquisition of spectra.

The ex-situ FTIR spectra of the prepared samples were obtained at room temperature using FTIR spectrometer (Bruker Tensor-II, Germany) and the *in situ* thermal decompositions of the composite mixture for the generation of hydrogen at various temperatures using a reactor (HVC-DRM-5) (Harrick, USA). The ex-situ FTIR analysis was performed by making a pellet of the used composite materials ($x\text{MnCl}_2/\text{NaBH}_4$) and KBr powder using a pelletizer with a hydraulic press. The spectra were obtained in transmission mode with the resolution at 4 cm^{-1} with 32 scans in the range of 4000 to 500 cm^{-1} .

4.3.3 Thermal decomposition behaviour and hydrogen generation study

The thermal decomposition of composite materials was obtained using a reactor (HVC-DRM-5) connected with a Gas Chromatograph (Centurion Scientific GC5800, India). A sample of ~ 50 mg was put into the reactor (HVC-DRM-5) for the study of thermolysis of synthesized composite materials at various temperatures. The sample was put into the reactor with the flow of nitrogen gas at the flow of 15 ml/min as shown in the scheme-4.1. The isothermal temperature of the reactor was maintained through a Chillier (Siskin Profichill RCC-700,

India) connected with the reactor. The thermolysis temperature was varied from 373 K to 823 K for 1 h hold in each temperature. The generated gases released from the outlet of the reactor were collected at a various time interval with a gas trapper (quartz) and injected the sample immediately to an offline gas chromatograph (GC) equipped with a TCD (thermal conductivity detector) detector. The column used for the separation of the gas mixture was a carbosphere (S.S 3 m long with 1/8" diameter). The carrier gas of the GC was chosen as Ar with the flow of 30 ml/min. The ex-situ FTIR spectra were obtained of the post thermolysis of the sample at each thermolysis temperature.

4.4 Results and Discussion

4.4.1 Powdered X-ray diffraction (P-XRD) studies

The XRD patterns of the pure NaBH_4 materials with the flow of nitrogen gas at various temperatures were obtained and shown in Fig.4.1. Analysis of Fig.4.1 reveals that with increasing the decomposition temperature the peaks due to sodium borohydride was decreased gradually. The peaks were almost disappeared at 773 K. The XRD patterns of the sample $20\text{MnCl}_2/\text{NaBH}_4$ were obtained at various decomposition temperatures and shown in Fig.4.2. Fig.4.2 reveals that the presence of the bands of NaBH_4 species. However, no features of MnCl_2 were obtained in the XRD patterns at low thermolysis temperature. The intensity of the bands due to sodium borohydride in the composite mixture decreased gradually. The details XRD patterns of each additive material shown in Fig.D1 (appendix D materials). Thus, the study suggested that the formation of a homogeneous mixture of additive MnCl_2 and NaBH_4 in the composite mixture, however, no bands due to new composite materials features were obtained.

The XRD patterns of $x\text{MnCl}_2/\text{NaBH}_4$ with different wt% loading of MnCl_2 ($x = 10, 20, 30, 40, 50$ wt %) shown in Fig.4.3. Analysis of Fig.4.3 reveals that the intensity of the peaks gradually decreased on increasing of MnCl_2 loading in NaBH_4 . It also suggested that MnCl_2 was highly dispersed in NaBH_4 and forms a homogeneous composite mixture. The peaks due to MnCl_2 were observed at higher loading. Thus, the study suggested that the additive remain dispersed at lower loading, however, it agglomerated at higher loading. The property of the additive MnCl_2 and NaBH_4 remained unaltered in the homogeneous mixture.

The XRD patterns of the $20\text{X}/\text{NaBH}_4$ (where additives, $\text{X} = \text{ZnCl}_2, \text{MnCl}_2$ and CaCl_2) were obtained using various additives such as $\text{ZnCl}_2, \text{MnCl}_2$, and CaCl_2 shown in Fig.4.4. Analysis of Fig.4.4 suggested that the additive remain dispersed in the NaBH_4 and formed a homogeneous mixture. The NaBH_4 was crystalline in nature and no crystalline features of additive were obtained in the mixture.

4.4.2 Field Emission Scanning Electron Microscopy (FE-SEM) Studies

The FE-SEM results of the studied materials obtained and shown in Fig.4.5. The images of various additives and additives-sodium borohydride composite materials were shown in Fig.D2 (appendix D materials). The analysis of Fig.4.5 revealed that NaBH₄ was crystalline in nature. The larger crystalline sodium borohydride dispersed into smaller crystalline of composite materials while the addition of the additive. The additive MnCl₂ distributed homogeneously with sodium borohydride in 20MnCl₂/NaBH₄ mixture after its synthesis. The distribution of additive and formation of smaller crystalline of composite materials gradually increased as increased the loading of additives with sodium borohydride. The study suggested that the synthesized material mixer was homogeneous in nature. The study is consistent with the XRD study as discussed above. In Fig.D2 suggested that the additive MnCl₂ and CaCl₂ were highly crystalline. However, the additive ZnCl₂ was also crystalline in nature. The XRD pattern of 20ZnCl₂/NaBH₄ was consistent. The ZnCl₂/NaBH₄ was homogeneous and crystalline in nature. However, in the case of 20MnCl₂/NaBH₄ and 20CaCl₂/NaBH₄, the composite materials formed a smaller crystalline structure. Thus, the study suggested that the addition of additives breaks the larger crystalline nature of sodium borohydride and formed smaller crystalline composite materials.

4.4.3 Thermo Gravimetric Analysis (TGA) Studies

The thermo-gravimetric analysis study performed for the xMnCl₂/NaBH₄ with the flow of nitrogen gas at a rate of 200 ml/min with 5 °C/min temperature ramps from ambient temperature to 300 °C and plot was shown in Fig.4.6. The analysis of Fig.4.6 reveals that the percent weight loss was linear and decomposition of pure NaBH₄ was very low even the temperature reached 300 °C. The thermolysis of the material 10MnCl₂/NaBH₄ was also obtained. The percent wt. loss decreased after addition of additive MnCl₂ in NaBH₄ in the sample 10MnCl₂/NaBH₄. The decrease % wt loss in 10MnCl₂/NaBH₄ was may be due to the loss of absorbed surface moisture during synthesis of material. The percent weight loss and thermal decomposition increased with the addition of additives for the sample 20MnCl₂/NaBH₄. However, the percent weight loss gradually decreased with further increasing the wt% of additive in the sample. Thus, the study suggested that the optimum loading of MnCl₂ for the thermolysis of NaBH₄ was obtained for 20MnCl₂/NaBH₄.

4.4.4 Raman analysis

The Raman spectra of the synthesized materials were obtained and shown in Fig.4.7. In the analysis of Fig.4.7 revealed that the presence of P-NaBH₄ material with the bands at 1280,

2198, and 2330 cm^{-1} . These bands were due to the symmetric bending, asymmetric bending and symmetric stretching mode of the B-H bond of BH_4^- species in the sample, respectively [Das et al., 2016]. The magnitude of the B-H bond frequency remains at the same position and no shifting of frequency observed for the samples while additives were added with sodium borohydride. The study suggested that the additive distributed homogeneously with the sodium borohydride during the synthesis of composite materials. The property of the additive MnCl_2 and NaBH_4 remained unaltered in the homogeneous mixture.

4.5 Thermolysis and FTIR analysis

4.5.1 The effect of temperature on pure NaBH_4 and $20\text{MnCl}_2/\text{NaBH}_4$

The FTIR analysis of the p- NaBH_4 at room temperature and the thermal decomposition at different temperature was obtained. The decomposition of p- NaBH_4 obtained with different thermolysis temperature (373 K, 473 K, 573 K, 673 K, 773 K, and 823 K) using (HVC-DRM-5) reactor under the flow of nitrogen gas at 15 ml/min. The FTIR spectra of p- NaBH_4 at each temperature was obtained after 60 min of decomposition time and shown in Fig.4.8A. The corresponding generation of hydrogen after 5 min and 5 to 60 min of the run was shown in Fig.4.8B and Fig.4.8C respectively. The spectra in Fig.4.8A suggested the bands at 3413 cm^{-1} to 3549 cm^{-1} were due to the $\nu^{\text{O-H}}$ stretching, and 1620 cm^{-1} due to bending of adsorbed moisture present in the sample. The bands at 2220 cm^{-1} to 2375 cm^{-1} was due to $\nu^{\text{B-H}}$ stretching, and 1122 cm^{-1} and 614 cm^{-1} was due to the B-H bending of NaBH_4 . The intensity of the adsorbed moisture gradually decreased with increasing the thermolysis temperature. The generation of hydrogen gradually increased with increasing the thermal decomposition temperature. The details study at each temperature up to 60 min of run shown in Fig.4.8C. The thermal decomposition study is consistent with the XRD study. No generation of hydrogen was obtained at 373 K. The study suggested that high temperature required during the thermolysis of p- NaBH_4 for generation of hydrogen [Urgnani et al., 2008].

The FTIR analysis of the $20\text{MnCl}_2/\text{NaBH}_4$ with changing the thermal decomposition temperature was obtained after 60 min of decomposition study and shown in Fig.4.9A. The corresponding generation of hydrogen shown in Fig.4.9B for 5 min at each temperature and for 5 to 60 min of each run was shown in Fig.4.9C. The spectra in Fig.4.9A for $20\text{MnCl}_2/\text{NaBH}_4$, suggested the presence of adsorbed moisture and NaBH_4 in the sample. A new band was observed at 940 cm^{-1} which may be due to MnB in the sample [Kojima and Haga, 2003]. The adsorbed moisture was very less in $20\text{MnCl}_2/\text{NaBH}_4$ as compared to pure NaBH_4 . The intensity of the bands was gradually decreased with increasing decomposition temperature, however, by addition of MnCl_2 with NaBH_4 assists in the generation of hydrogen at low temperature (373

K). The generation of hydrogen increased from 0 wt% to 0.03 wt% at 373 K after 5 min of the run. However, the generation of hydrogen increased from 0.03 wt% to 0.98 wt% at high temperature 823 K. Thus, the study suggested that the addition of additive increased the generation of hydrogen at low temperature. However, the decomposition was incomplete even at high temperature (823 K) for 60 min of the run.

4.5.2 Effect of additive loading and thermolysis of $x\text{MnCl}_2/\text{NaBH}_4$

The analysis of FTIR study by considering the changes of loading of additive in the NaBH_4 on $x\text{MnCl}_2/\text{NaBH}_4$ was investigated at 373 K. The details spectra at 60 min in Fig.4.10A and the generation of hydrogen after 5 min of run and 5 to 60 min of the run were shown in Fig.4.10B and Fig.4.10C, respectively. The highest thermal decomposition was investigated at 373 K temperature for $20\text{MnCl}_2/\text{NaBH}_4$. The decomposition of NaBH_4 obtained temperature at 373 K and the generation of hydrogen was started from the material $x\text{MnCl}_2/\text{NaBH}_4$. However, no generation of hydrogen from pure sodium borohydride was obtained at 373 K. The generation of hydrogen started at 373 K after addition of MnCl_2 with sodium borohydride in $10\text{MnCl}_2/\text{NaBH}_4$. The generation of hydrogen increased further as increased the loading of MnCl_2 up to $20\text{MnCl}_2/\text{NaBH}_4$. However, the generation of hydrogen decreased further with increased the loading of additive in NaBH_4 upto $40\text{MnCl}_2/\text{NaBH}_4$. The generation of hydrogen again increased as increased loading of MnCl_2 in NaBH_4 up to 50wt%. Thus, the optimum additive loading was considered to be 20wt% for $20\text{MnCl}_2/\text{NaBH}_4$ at 373 K for the generation of hydrogen at low temperature. The details thermolysis of $x\text{MnCl}_2/\text{NaBH}_4$ by changing of additive loading was shown in Fig.D3 to Fig.D6 (appendix D materials). The spectral investigation suggested that the generation of hydrogen obtained at low thermolysis temperature at 373 K in presence of an additive, however, the decomposition was incomplete even at 373 K for 60 min of the run.

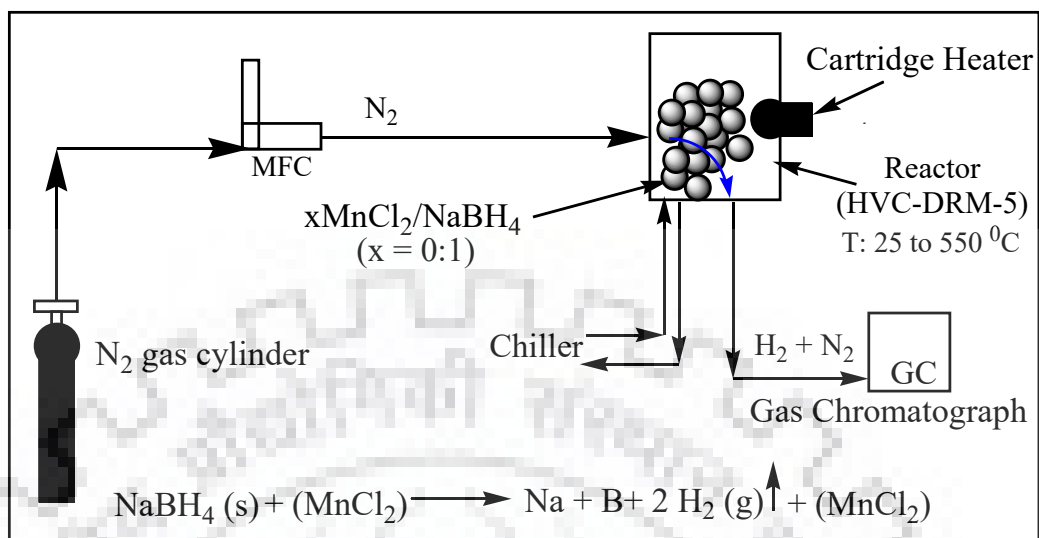
4.5.3 Effect of various additives over $20(\text{additives})/\text{NaBH}_4$

The effect of additives on thermal decomposition of $20(\text{additives})/\text{NaBH}_4$ was obtained and shown in Fig.4.11. The additives used for the study were CaCl_2 , MnCl_2 , and ZnCl_2 with NaBH_4 . The Fig.4.11 reveals that the generation of hydrogen at 373 K was highest for the additive CaCl_2 in $20\text{CaCl}_2/\text{NaBH}_4$ [Gennari et al., 2009; Danna et al., 2014; Slijkic et al., 2013; Buhl et al., 2012]. The order of activity was suggested to be $20\text{CaCl}_2/\text{NaBH}_4 > 20\text{MnCl}_2/\text{NaBH}_4 > 20\text{ZnCl}_2/\text{NaBH}_4$. The details (FTIR spectra) studies of the effect of other additives in NaBH_4 at 373 K were obtained, however, not shown here for brevity. Thus, the study suggested that the choice of a suitable additive for the thermal decomposition of NaBH_4 at low temperature was very crucial for the generation of hydrogen.

4.6 Conclusions

A series of $x\text{MnCl}_2/\text{NaBH}_4$ composite materials were synthesized by using the facile solution method. The synthesized materials were characterized by using XRD, TGA, FE-SEM, Raman and FTIR analysis. The synthesized materials were used as solid phase storage of hydrogen and the generation of hydrogen from the composite material was performed by using various additives. The XRD study suggested that the formation of the crystalline phase of NaBH_4 and the phase gradually decreases its intensity as increased the thermolysis (decomposition) temperature. The highest thermolysis temperature obtained at 823 K. The XRD patterns also suggested that the presence of additive MnCl_2 in $x\text{MnCl}_2/\text{NaBH}_4$ at higher loading in the sample. The addition of other additives of CaCl_2 and ZnCl_2 in NaBH_4 obtained, however, the additives were at highly dispersed in the sample. The FE-SEM images are also consistent with the XRD study. The TGA analysis of the $x\text{MnCl}_2/\text{NaBH}_4$ was obtained and the study suggested that the additive MnCl_2 accelerate the thermolysis process and suggested that the decreases the thermolysis temperature. The optimum loading was obtained at 20 wt% of MnCl_2 in NaBH_4 . The FTIR study also suggested the presence of NaBH_4 species in the composite $x\text{MnCl}_2/\text{NaBH}_4$ samples. The analysis of the study suggested that the hydrogen generates from NaBH_4 at a lower temperature while additive MnCl_2 was added, the generation of hydrogen increased as increased thermolysis temperature. However, the decomposition of NaBH_4 was incomplete even at higher thermolysis temperature. The highest generation of hydrogen was obtained for loading at 20 wt% of MnCl_2 , however the study of thermolysis by changing CaCl_2 and ZnCl_2 additive in NaBH_4 was obtained. The additive CaCl_2 was most effective and the order of activity was as follows: $\text{CaCl}_2 > \text{MnCl}_2 > \text{ZnCl}_2$. However, the details of thermolysis study using the additive CaCl_2 is in progress and will be discussed more details in our future work.

List of Figures:



Scheme-4.1: The experimental set-up for the thermolysis of $x\text{MnCl}_2/\text{NaBH}_4$ mixture for the generation of hydrogen

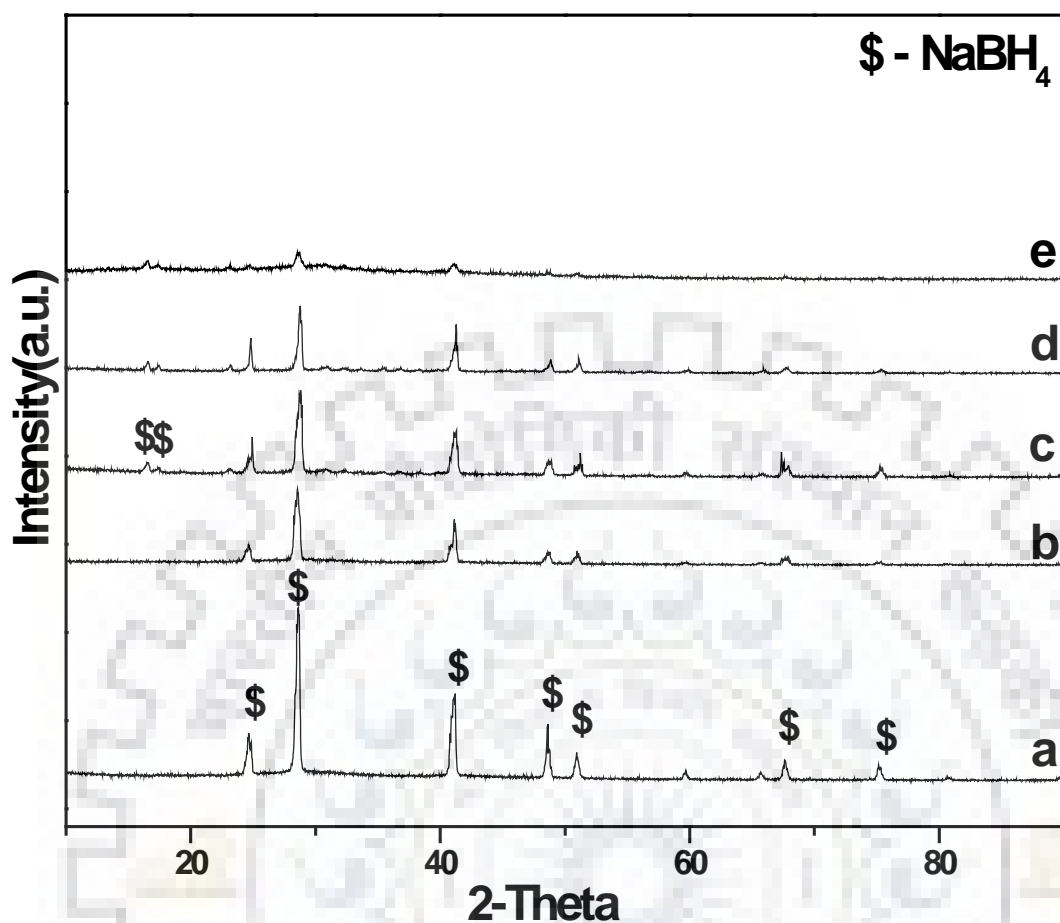


Figure 4.1: The XRD Patterns of p-NaBH₄ at Various Decomposition Temperature at (a) 373 K, (b) 473 K, (c) 573 K, (d) 673 K and (e) 773 K, for 1 h at each temperature with the flow of nitrogen gas (15 ml/min flow rate) in reactor (HVC-DRM-5). The P-XRD patterns were generated after cool down each material at room temperature.

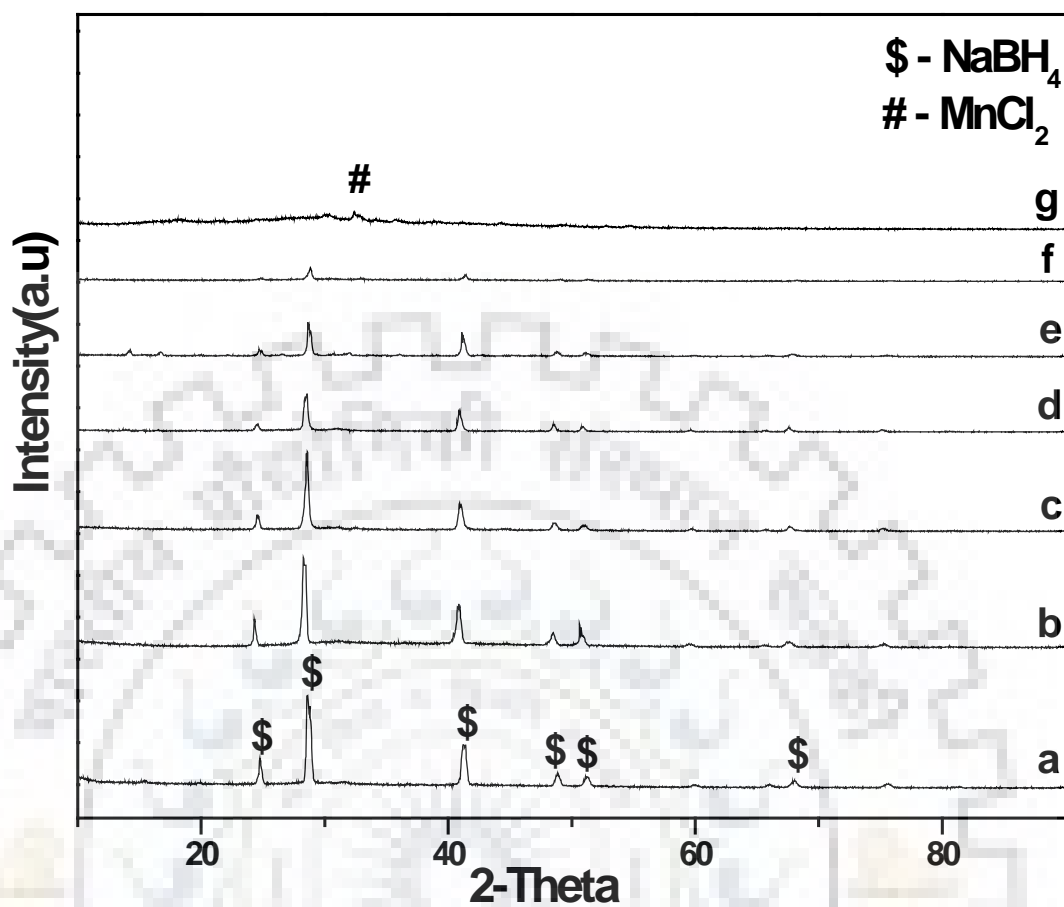


Figure 4.2: The P-XRD patterns of 20MnCl₂/NaBH₄ at various decomposition temperatures at (a) 303 K, (b) 373 K, (c) 473 K, (d) 573 K, (e) 673 K, (f) 773 K and (g) 823 K for 1 h at each temperature with the flow of nitrogen gas (15 ml/min flow rate) in reactor (HVC-DRM-5). The XRD patterns were generated after cool down each material at room temperature.

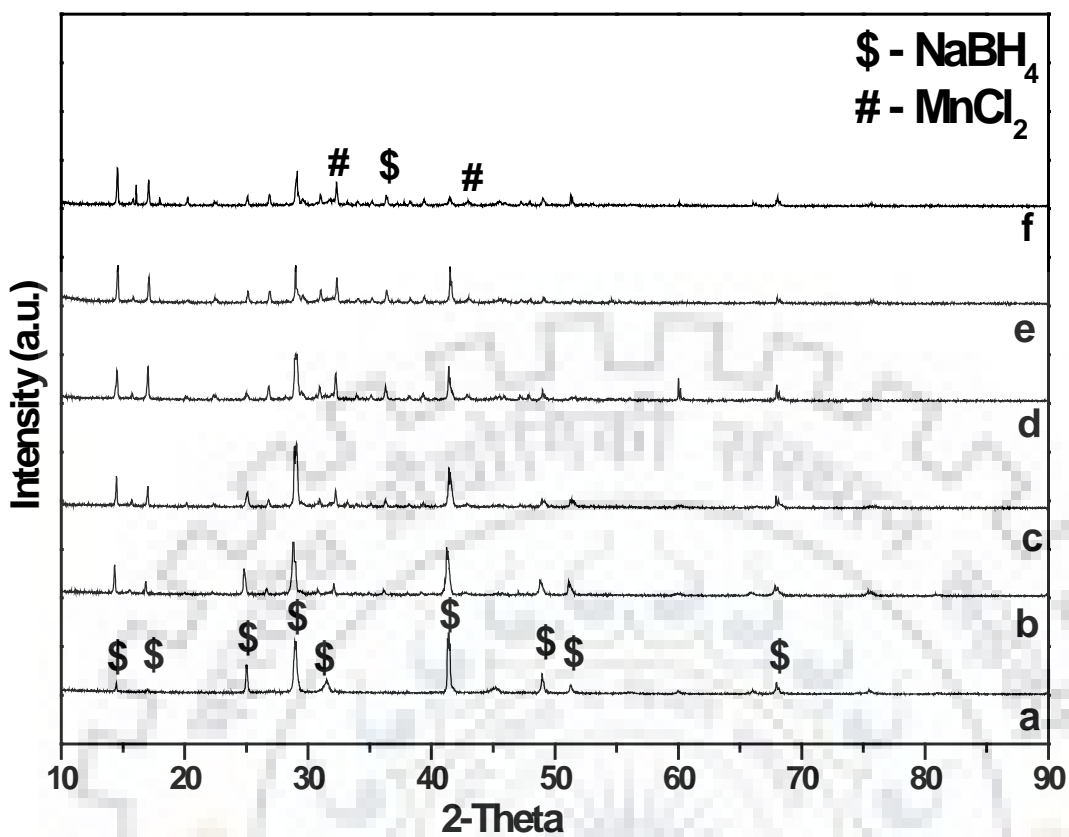


Figure 4.3: The XRD Patterns of various materials (a) p-NaBH₄, (b) 10MnCl₂/NaBH₄, (c) 20MnCl₂/NaBH₄, (d) 30MnCl₂/NaBH₄, (e) 40MnCl₂/NaBH₄ and (f) 50MnCl₂/NaBH₄. The XRD patterns for each composite materials mixer were generated at room temperature.

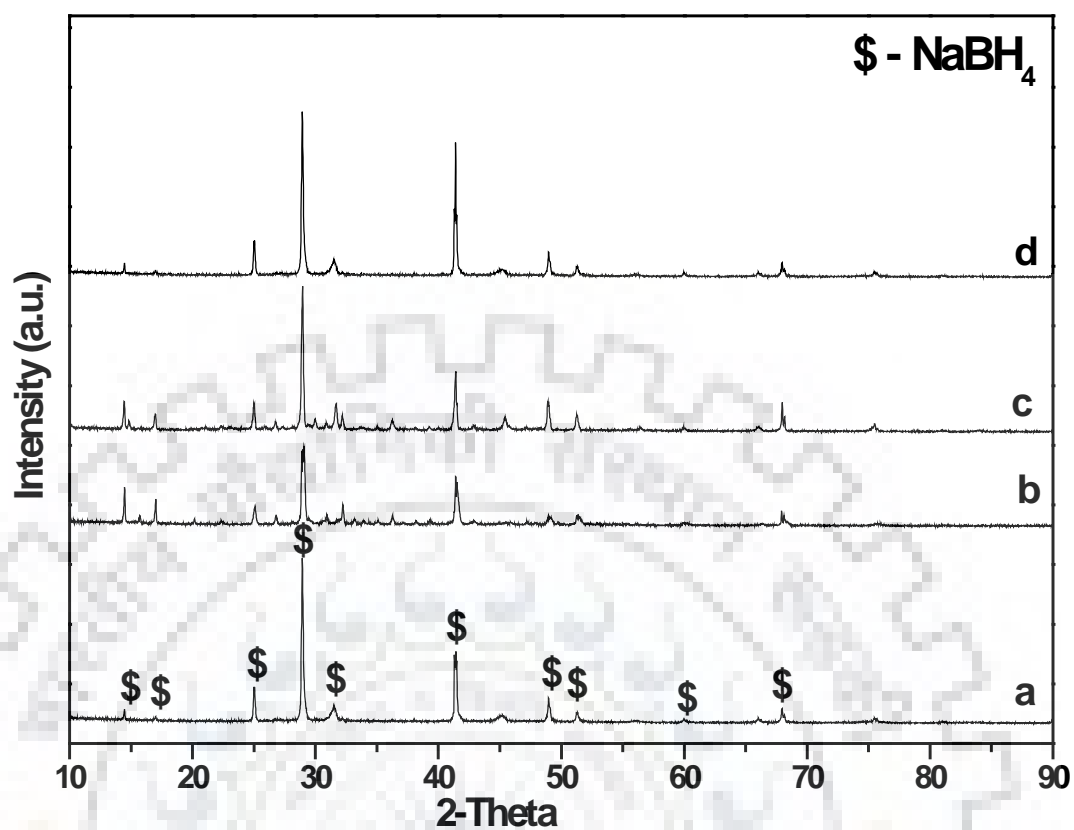


Figure 4.4: The P-XRD Patterns of various materials (a) p-NaBH₄ (b) 20MnCl₂/NaBH₄, (c) 20ZnCl₂/NaBH₄ and (d) 20CaCl₂/NaBH₄. The XRD patterns for each composite material were generated at room temperature.

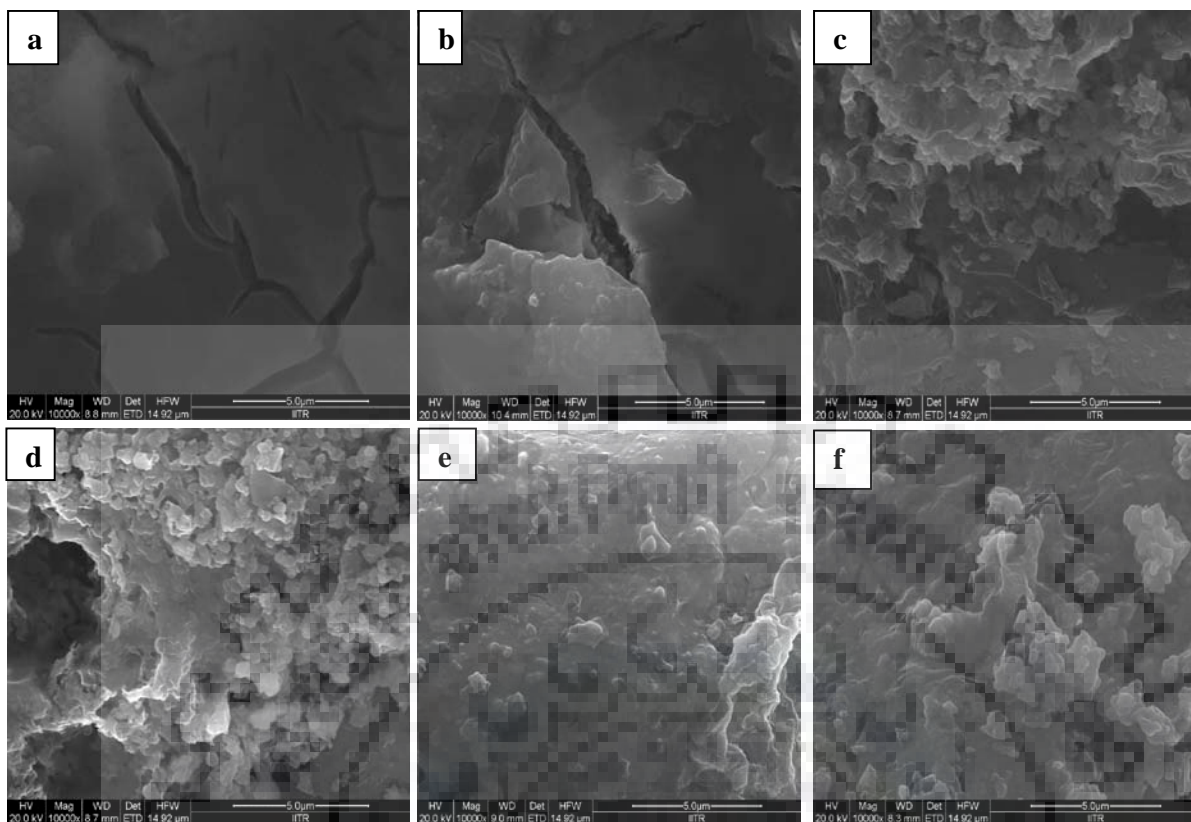


Figure 4.5: Field Emission Scanning Electron Microscopy (FE-SEM) images of various materials (a) p-NaBH₄, (b) 10MnCl₂/NaBH₄, (c) 20MnCl₂/NaBH₄ (d) 30MnCl₂/NaBH₄, (e) 40MnCl₂/NaBH₄ and (f) 50MnCl₂/NaBH₄.

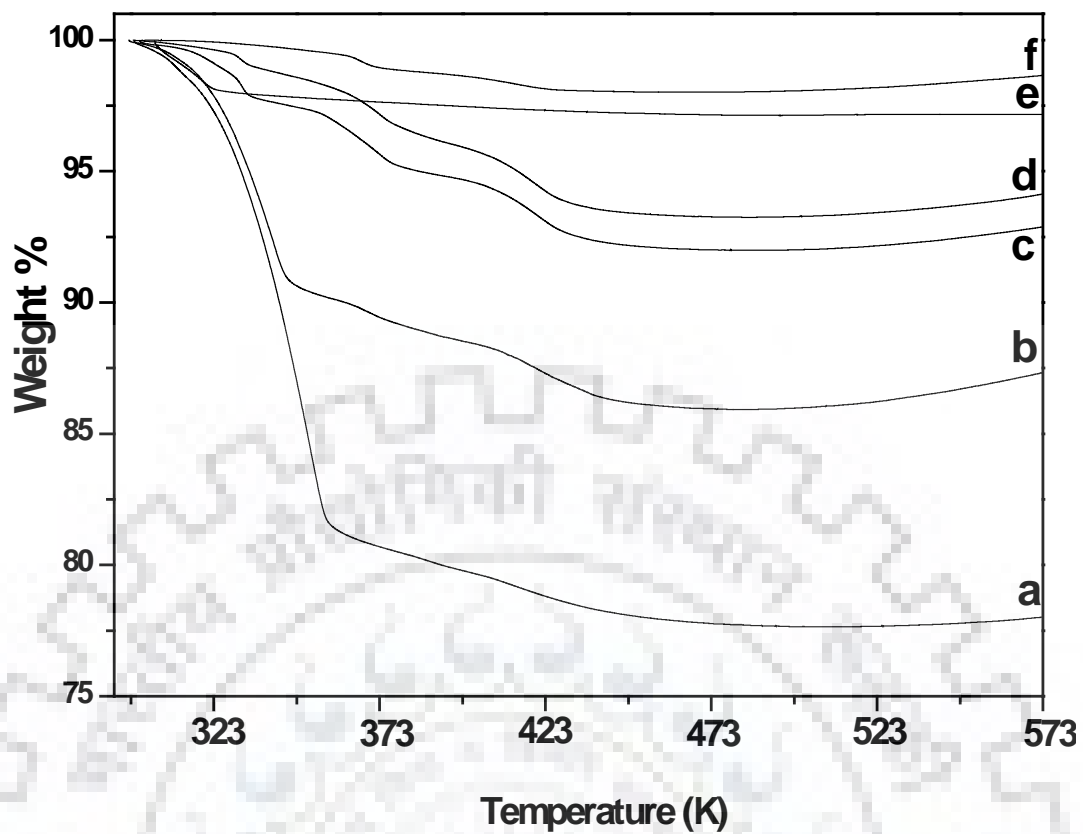


Figure 4.6: Thermo Gravimetric Analysis (TGA) of composite mixture (a) 20MnCl₂/NaBH₄, (b) 30MnCl₂/NaBH₄, (c) 40MnCl₂/NaBH₄, (d) 50MnCl₂/NaBH₄, (e) 10MnCl₂/NaBH₄ and (f) p-NaBH₄. Where heating rate was 5 °C/min.

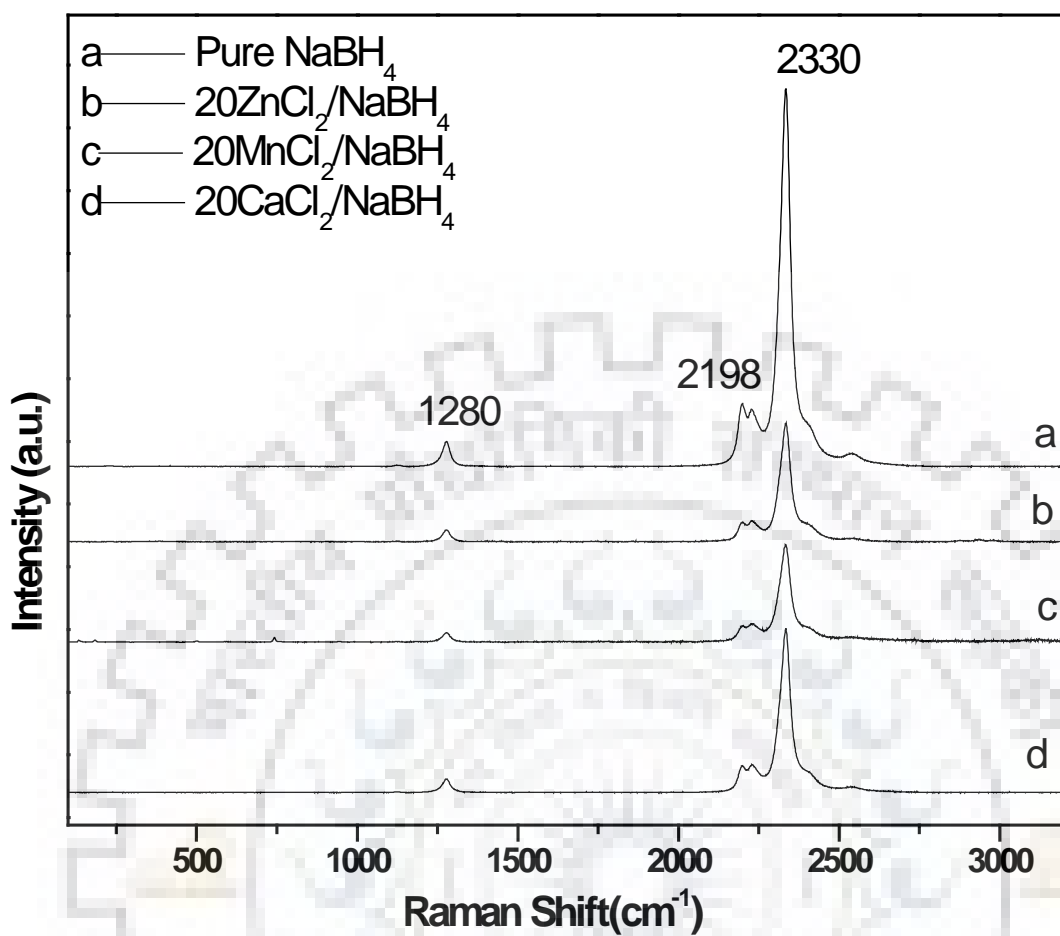


Figure 4.7: The Raman spectra of various materials (a) p-NaBH₄, (b) 20ZnCl₂/NaBH₄, (c) 20MnCl₂/NaBH₄, and (d) 20CaCl₂/NaBH₄. The spectra for each composite material were collected at room temperature.

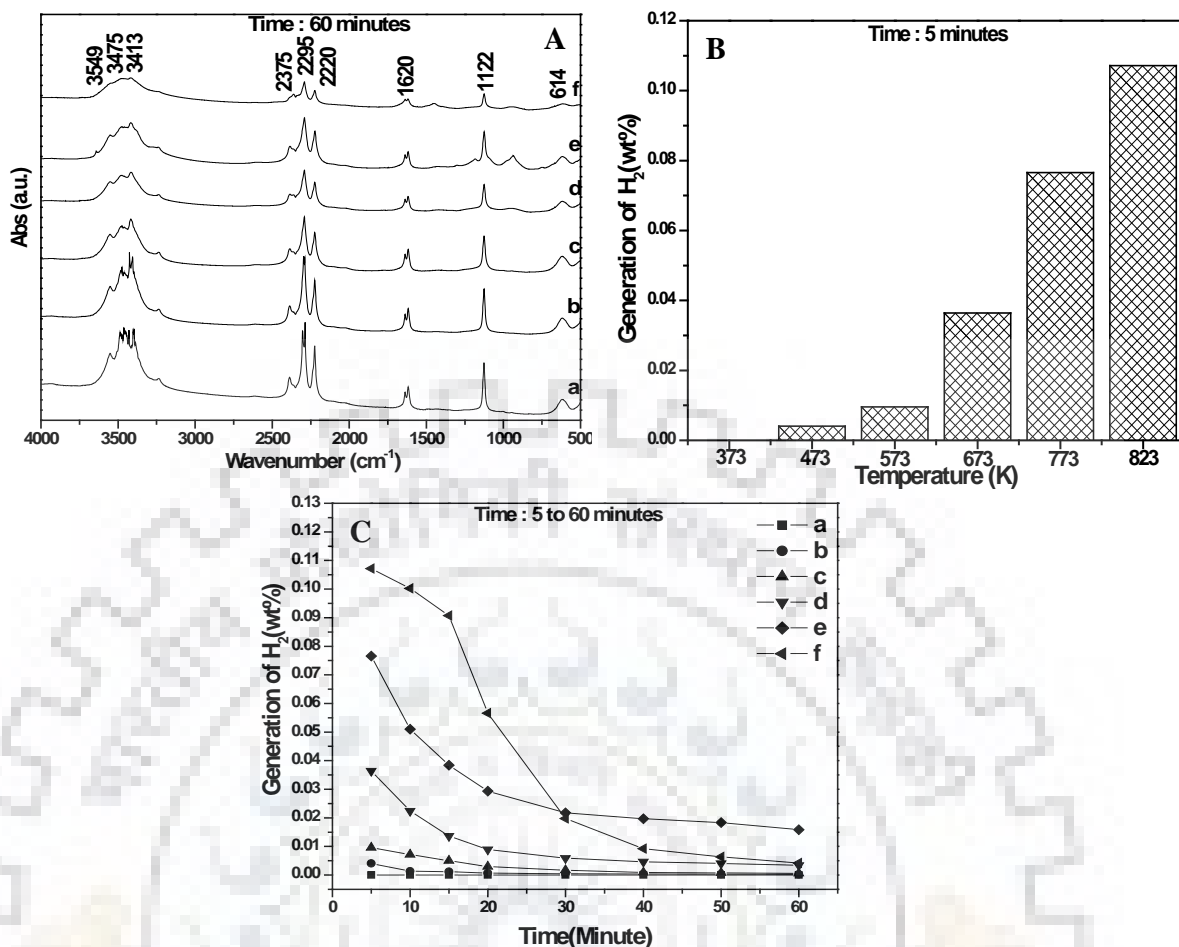


Figure 4.8: (A) The FTIR spectra of p-NaBH₄ at various decomposition temperature with the flow of N₂ gas flow through reactor (HVC-DRM-5) at (a) 303 K, (b) 373 K, (c) 473 K, (d) 573 K, (e) 673 K and (f) 773 K for 1 h at each temperature, (B) The Generation of H₂ from p-NaBH₄ at different decomposition temperature after 5 min, (C) The generation of hydrogen from p-NaBH₄ at different thermal decomposition temperature (a) 373 K, (b) 473 K, (c) 573 K, (d) 673 K, (e) 773 K and (f) 823 K.

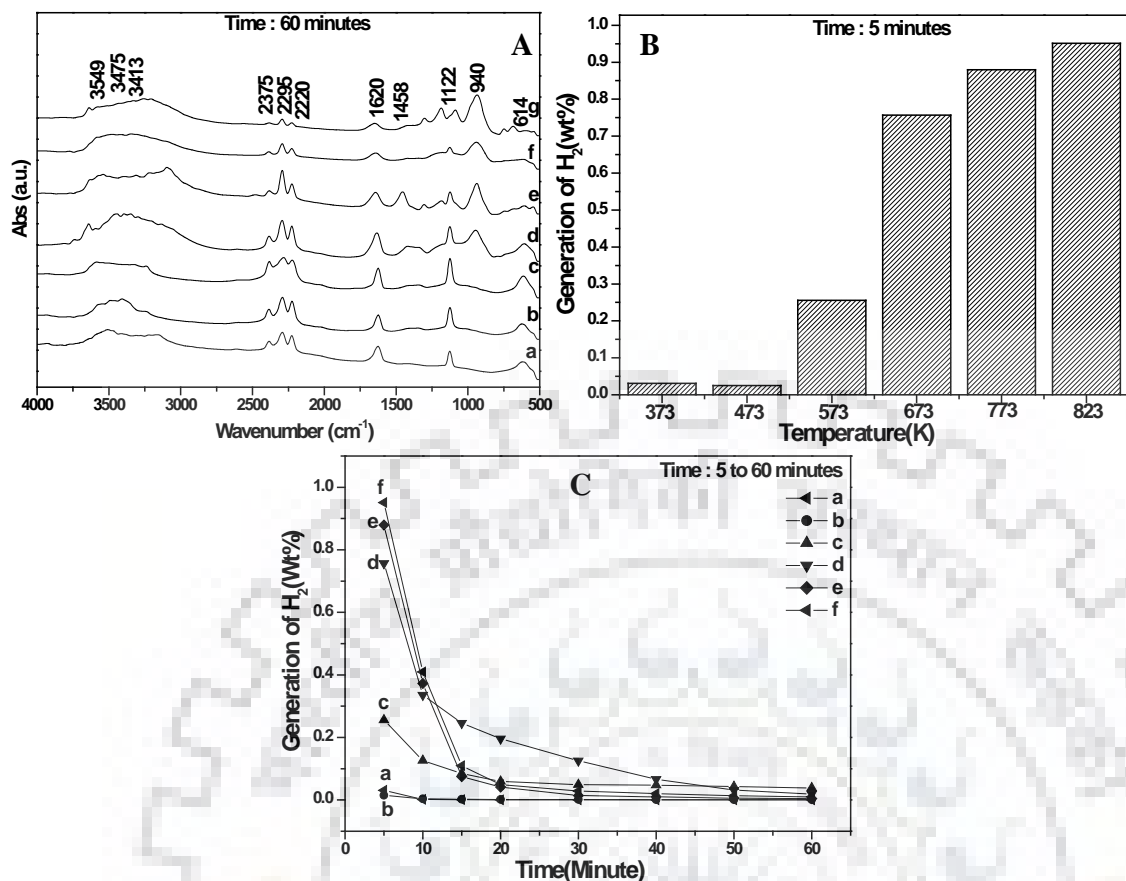


Figure 4.9: (A) The FTIR spectra of 20MnCl₂/NaBH₄ at various decomposition temperature with N₂ gas flow through reactor (HVC-DRM-5) for 1 h at (a) 303K, (b) 373K, (c) 473K, (d) 573K, (e) 673K, (f) 773K, (g) 823K, (B) The generation of hydrogen from 20MnCl₂/NaBH₄ at different thermal decomposition temperature after 5 min, (C) The generation of hydrogen from 20MnCl₂/NaBH₄ at different thermal decomposition temperature (a) 373 K, (b) 473 K, (c) 573 K, (d) 673 K, (e) 773 K, and (f) 823 K.

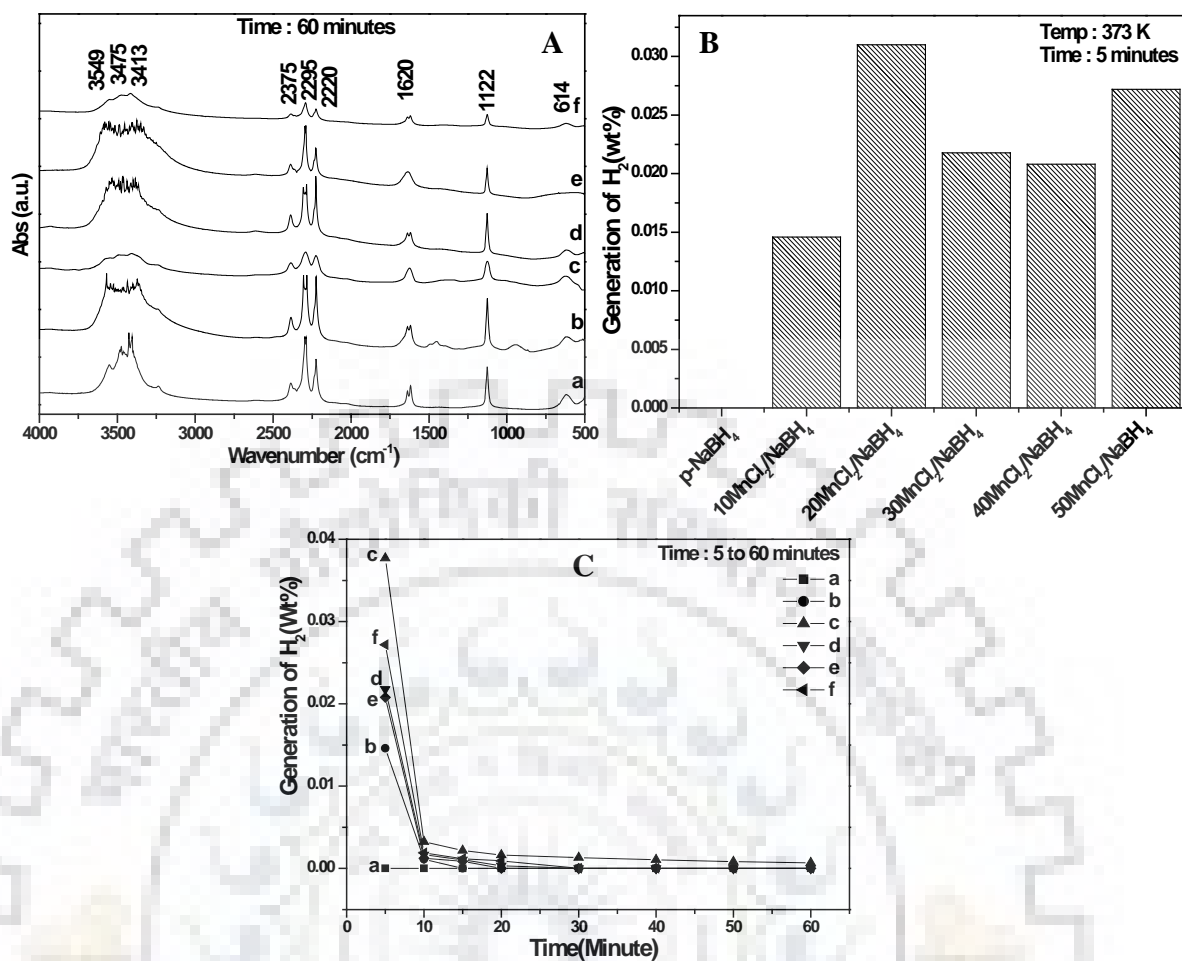


Figure 4.10: (A) The FTIR spectra of x wt% of MnCl₂ doped in xMnCl₂/NaBH₄ samples by changing the weight percentage of additive MnCl₂ over NaBH₄ samples (a) p-NaBH₄, (b) 10MnCl₂/NaBH₄, (c) 20MnCl₂/NaBH₄, (d) 30MnCl₂/NaBH₄, (e) 40MnCl₂/NaBH₄ and (f) 50MnCl₂/NaBH₄ at 373 K temperature after thermolysis. All spectra were collected at room temperature post thermolysis of the material. (B) The Generation of hydrogen after 5 min of thermolysis in the flow of nitrogen gas and (C) The detail generation of hydrogen for 5 to 60 min of run at each decomposition temperature. The sample was taken ~50 mg for each analysis.

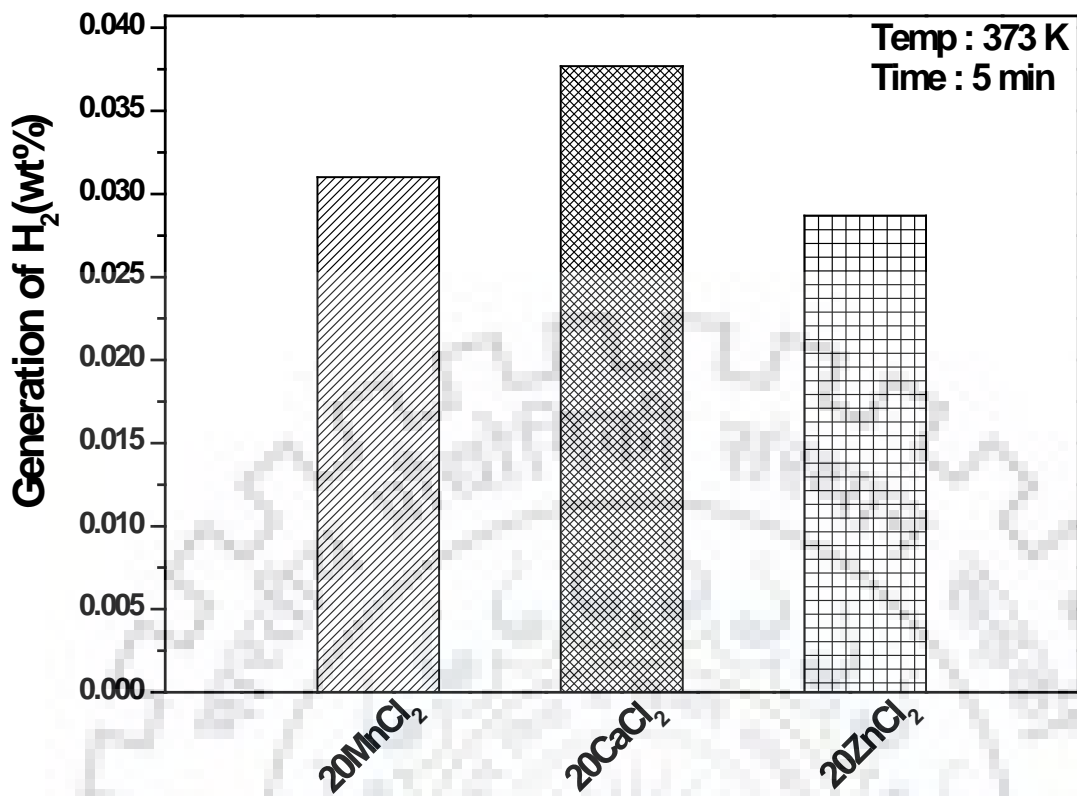


Figure 4.11: Generation of hydrogen with 20 Wt% of additive (20M-Cl₂/NaBH₄) at 373K after 5 min reaction in flow of nitrogen control environment in reactor (HVC-DRM-5). Where, x is the loading of additives (M = Mn, Ca and Zn).

CONCLUSIONS AND RECOMMENDATIONS

5.1 Conclusions

The present study was focused on the generation of hydrogen by considering two routes i) hydrolysis sodium-borohydride using bulk or supported metal-boride catalysts, and ii) thermolysis of sodium-borohydride using metal halide catalyst/additives. The present study considering route i) provides an idea about the *in situ* reduction during synthesis of metal-boride catalysts, effect of various metals in synthesis of metal-boride catalysts, effect of calcinations temperature, effect of base (with/without base stabilized sodium borohydride solution) during catalyst synthesis, and the generation of hydrogen during the hydrolysis of sodium borohydride solution. The catalysts synthesis was monitored by *in situ* UV-vis spectrophotometer. ii) The thermolysis of sodium borohydride with additives at low temperature considering various parameters such as effect of thermolysis temperature, loading of additives, and effect of various additives.

To study the catalytic activity and generation of hydrogen from with (BS)/without (WS) base stabilized sodium borohydride solution was monitored by considering various parameters such as, effect of various metals in metal-boride catalysts, effect of base, calcinations temperature during synthesis of catalysts. To study the various metals in metal-boride catalysts cobalt chloride, nickel chloride and ferric chloride were used. The supported cobalt-boride catalysts with alumina, silica, and magnesia were used to study the effect of support, and to study the effect of catalyst calcinations temperatures, the catalysts calcined at various temperatures 383 K, 473 K, 573 K, 673 K, and 773 K for 1 h.

It was observed that the reduction of Co^{2+} ions and Ni^{+2} ions disappeared completely with sodium borohydride solution by the formation of CoB-BS and NiB-BS catalysts. However, the Fe^{3+} ions reduced to Fe^{2+} ions and finally Fe^{2+} ions during synthesis of iron-boride catalyst. Moreover, the formation of metal nano-particles (nano-nickel) during the synthesis of metal-boride catalysts which is reduced the catalytic activity of NiB and FeB catalysts. Also the study suggested the formation of borate (BO_2^-) species and adsorbed moisture with the metal-boride catalysts. A highly amorphous phase was obtained with the CoB-BS and FeB-BS catalysts and little crystalline features of NiB-BS were obtained during the synthesis of catalysts. The CoB-BS catalysts were calcined at various temperatures and the

catalysts remain amorphous in nature upto 673 K and the formation of crystalline phase started while reached the temperature at 773 K. The generation of hydrogen using the synthesized catalysts was obtained and it was observed that the CoB-BS was most active followed by other catalysts (NiB-BS and FeB-BS). The hydrogen generation rate was higher with the base stabilized (BS) sodium borohydride solution as compared to the without base stabilized (WS) solution and the rate was followed as CoB-BS (BS solution) > CoB-BS (WS solution). Moreover, the calcinations temperature played a significant role for the generation of hydrogen and increases the activity of catalyst. The most active CoB-BS catalyst was obtained while the catalyst was calcined at 573 K.

The generation of hydrogen from sodium borohydride using various supported CoB catalysts were obtained and studied. The supported xCoB/SiO₂ catalyst was obtained by two-step impregnation-reduction method. The supports used for the supported cobalt boride catalysts were Al₂O₃, MgO and SiO₂. The support plays a significant role in synthesis of supported cobalt-boride catalysts. It was obtained that the support silica formed a most active catalysts for the hydrolysis of sodium borohydride solution. The specific surface analysis study reveals that the SiO₂ supported 50CoB/SiO₂ possessed highest specific surface area. The catalyst 50CoB/SiO₂ 573 K sample possessed 115 m²/gm specific surface areas. The surface area gradually increased with increasing catalyst calcination temperature upto 573 K and the decreased further increased calcination temperature for the catalysts xCoB/(support). However, all the calcined samples were highly amorphous in nature even at 673 K and started formation of crystalline phase at 773 K in 50CoB/Al₂O₃. The most active catalyst was found 50CoB/SiO₂ at 573 K calcination temperature. The obtained supported cobalt boride catalysts were characterized using BET, XRD, and Raman analysis. The XRD analysis suggested that the formation of CoB species only in the supported cobalt boride catalysts, however, the study did not show the formation of any other species. The Raman analysis of the study suggested that the formation of Co₃O₄ species during the synthesis of supported CoB catalyst. The study also suggested that the formation of elemental nano cobalt metals with CoB species during *in situ* reduction of cobalt ions with sodium borohydride solution. The nano cobalt metals were highly active during the synthesis of CoB catalysts, which further oxidized to CoO and finally Co₃O₄ species. However, the formation of Co₃O₄ species was obtained in all the final synthesized catalysts (SiO₂ and Al₂O₃). The magnesia supported catalysts showed different types of compound formation. The synthesized catalysts were active for the hydrolysis reaction. The supported catalysts showed a very good activity for the generation of hydrogen energy from the hydrolysis of sodium borohydride solution. The order of catalytic activity were for all catalyst 50CoB/SiO₂ > 50CoB/Al₂O₃ > CoB > 50CoB/MgO. Thus, the study suggested that the support

plays a significant role in the synthesis of supported cobalt boride catalyst for the hydrolysis reaction study.

The thermolysis of sodium-borohydride for the generation of hydrogen using various metal halide catalyst/additive was also studied. The metal halide-sodium borohydride composite mixture was synthesized by facile solution method. The generation of hydrogen from the synthesized composite materials by considering the thermolysis process was monitored. The thermolysis temperature was varied from 373 K to 823 K for 1 h at each temperature. The highest thermolysis was obtained temperature at 823 K. various additives (MnCl_2 , ZnCl_2 , and CaCl_2) were used during synthesis of composite materials. However, the additives were highly dispersed in the sodium-borohydride. The thermolysis of composite materials was monitored by ex-situ FTIR spectra analysis coupling with the GC (Gas Chromatograph analysis) for quantitative analysis. The additive accelerates the thermolysis process and decrease the thermolysis temperature. The optimum loading of additive was found to be 20 wt% at 373 K and the generation of hydrogen increased with increasing the thermolysis temperature. The additive CaCl_2 was found to be most suitable additive with the NaBH_4 for the generation of hydrogen and the order of activity was as follows: $\text{CaCl}_2 > \text{MnCl}_2 > \text{ZnCl}_2$.

Thus, the generation of hydrogen by either hydrolysis of sodium borohydride using bulk or supported metal-boride catalysts or the thermolysis of sodium borohydride using metal-halide additive/catalyst was studied by considering various parameters and characterization techniques. The obtained information was important for the development of catalyst or additive for the generation of hydrogen applicable for the fuel-cell application in mobile industries. The obtained most active catalysts/additive will be used for the development of a small scale hydrogen generator for the continuous supply of hydrogen to fuel cell.

5.2 Recommendations

The present study was aimed on the generation of hydrogen by considering two routes a) hydrolysis sodium-borohydride using metal-boride catalysts, and b) thermolysis of sodium-borohydride using metal halide catalyst/additive. The present study considering route a) provides an idea about the *in situ* reduction during synthesis of metal-boride catalysts, effect of various metals on synthesis of metal-boride catalysts, effect of calcinations temperature, effect of base (with/without) during catalyst synthesis, and the generation of hydrogen during the hydrolysis of sodium borohydride solution. The catalysts synthesis was monitored by *in situ* UV-vis spectrophotometer.

The thermolysis of sodium-borohydride using various metal halide catalyst/additive was also studied. The metal halide-sodium borohydride composite mixture was synthesized by facile solution method. The generation of hydrogen from the synthesized composite materials by considering the thermolysis process was monitored. Various additives (MnCl_2 , ZnCl_2 , and CaCl_2) were used during synthesis of composite materials. The CaCl_2 was obtained as most suitable additive with the NaBH_4 for the generation of hydrogen. However, additional studies are required using various *in situ* spectroscopy techniques to determine the actual phase transformation, mechanism of decomposition during thermolysis of NaBH_4 -additive mixture. Based on the present observations, the following points are suggested for future work:

- i)** The hydrolysis study by considering other various metals (Ru, Ti, Pt, V, W, Mn, Cu, and Zn) for the synthesis of Metal-boride catalysts and considering other non-metal or metal-borohydride (for example: $\text{Ca}(\text{BH}_4)_2$, $\text{Zn}(\text{BH}_4)_2$, and $\text{NH}_3\text{-BH}_3$), mixture of two different non-metal/metal-borohydrides down the thermolysis temperature for the generation of hydrogen.
- ii)** The potential of NaBH_4 can be compared with others hydrogen storage materials such as LiBH_4 , KBH_4 , PdH , LiAlH_4 , MgH_2 etc.
- iii)** The *in situ* FTIR can be used for the collection of FTIR spectra and simultaneous measurement of generation of hydrogen during thermolysis of $\text{NaBH}_4\text{-MCl}_2$ composite mixture.
- iv)** The *in situ* Raman-GC can be used for the collection of Raman spectra and simultaneous measurement of generation of hydrogen (using GC) during thermolysis of $\text{NaBH}_4\text{-MCl}_2$ composite mixture.
- v)** Recycle of sodium metaborate back to sodium borohydride is essential in order to facilitate practical usage of this hydrolysis process for the storage of hydrogen.
- vi)** The building up an experimental setup coupling with H_2 storage system and the H_2 -Fuel cell. The use of generated hydrogen directly in a single set up to see the performance of fuel cell and performance of synthesized catalysts for online generation and use of hydrogen.
- vii)** The studies involving other characterization techniques such as XPS, *in situ* XRD, *in situ* UV-Vis-NIR to elucidate the phase transformation, change of oxidation number under different thermolysis conditions.
- viii)** Synthesis of most active metal-boride catalysts by considering other various methods
- ix)** The synthesis of $\text{NaBH}_4/\text{M-halide}$ composite mixtures by considering other various solvents. The other solvents may be considered such as THF, Cyclohexanone, and Di-methyl ether etc.
- x)** The other halides may be considered such as metal fluoride, metal chloride, metal iodide (M-F , M-Cl , M-I).

xi) The obtained most active catalysts/additive will be used for the development of a small scale hydrogen generator (considering hydrolysis or thermolysis of sodium-borohydride) for the continuous supply of hydrogen for fuel-cell application.



References:

Acar C., Dincer I. (2019). Review and evaluation of hydrogen production options for better environment, *Journal of Cleaner Production* 218: 835-849.

Aceves S. M., Petitpas G., Loza F. E., Matthews M. J., Orozco E. L. (2013) Safe, long range, inexpensive and rapidly refuelable hydrogen vehicles with cryogenic pressure vessels, *International Journal of Hydrogen Energy* 38: 2480-2489.

Akdim O., Demirci U.B., Muller D., Miele P. (2009). Cobalt (II) salts, performing materials for generating hydrogen from sodium borohydride, *International Journal of Hydrogen Energy* 34: 2631-7.

Alfonso E. Y. M., Beaird A. M., Davis T. A., Matthews M. A. (2009). Hydrogen Generation from Chemical Hydrides, *Ind. Eng. Chem. Res.* 48: 3703–3712.

Amendola S. C., Goldman S. L. S., Janjua M. S., Spencer N. C., Kelly M. T., Petillo P. J., Binder M. (2000). A safe, portable, hydrogen gas generator using aqueous borohydride solution and Ru catalyst, *International Journal of Hydrogen Energy* 25: 969-975.

Azadi P., Foroughi H., Dai T., Azadi F., Farnood R. (2014). An integrated hydrolysis-reforming process for the production of hydrogen from wet biomass feedstocks, *Fuel* 117: 1223-1230.

Bai Y., Pei Z. W., Wu F., Yang J. H., Wu C. (2017). Enhanced hydrogen generation by solid-state thermal decomposition of $\text{NaNH}_2\text{-NaBH}_4$ composite promoted with Mg-Co-B catalyst, *J. Mater. Res.* 32: 1203-1209.

Bai Y., Wu C., Wu F., Yi B. (2006). Carbon-supported platinum catalysts for on-site hydrogen generation from NaBH_4 solution, *Materials Letters* 60: 2236-2239.

Bai Y., Zhao L. L., Wang Y., Liu X., Wu F., Wu C. (2014). Light-weight $\text{NaNH}_2\text{-NaBH}_4$ hydrogen storage material synthesized via liquid phase ball milling, *International Journal of Hydrogen Energy* 39: 13576-13582.

Banger S., Nayak V., Verma U. P. (2018). Hydrogen storage in lithium hydride: A theoretical approach, *Journal of Physics and Chemistry of Solids* 115: 6-17.

Barbuzzaa E., Bucetib G., Pozioc A. (2019). Santarellia M., Tosti S., Gasification of wood biomass with renewable hydrogen for the production of synthetic natural gas, *Fuel* 242: 520-531.

Bekirogullari M., Kaya M., Saka C. (2019). Highly efficient Co-B catalysts with *Chlorella Vulgaris* microalgal strain modified using hydrochloric acid as a new support material for hydrogen production from methanolysis of sodium borohydride, *International Journal of Hydrogen Energy* 44: 7262-7275.

Berg A. W. C. V. D., Areat C. O. (2008). Materials for hydrogen storage: current research trends and perspectives, *Chem. Commun.* 668-681.

Bhogilla S. S. (2017). Design of a AB₂-metal hydride cylindrical tank for renewable energy storage, *Journal of Energy Storage* 14: 203-210.

Bozkurt G., Ozer A., Yurtcan A. B. (2019). Development of effective catalysts for hydrogen generation from sodium borohydride: Ru, Pt, Pd nanoparticles supported on Co₃O₄, *Energy* 180: 702-713.

Brack P., Dann S. E., Wijayantha K. G. U. (2015). Heterogeneous and homogenous catalysts for hydrogen generation by hydrolysis of aqueous sodium borohydride (NaBH₄) solutions, *Energy Science and Engineering* 3(3): 174-188.

Buhl J. C., Gesing T. M., Ruscher C.H. (2005). Synthesis, crystal structure and thermal stability of tetrahydroborate sodalite Na₈[AlSiO₄]₆(BH₄)₂, *Microporous and Mesoporous Materials* 80: 57-63.

Buhl J. C., Schomborg L. and Ruscher C. H. (2012). Enclosure of Sodium Tetrahydroborate (NaBH₄) in Solidified Aluminosilicate Gels and Microporous Crystalline Solids for Fuel Processing, <http://dx.doi.org/10.5772/50186>.

Cakanyildirim C., Guru M. (2009). Production of NaBH₄ and hydrogen release with catalyst, *Renewable Energy* 34: 2362-2365.

Cakanyildirim C., Guru M. (2010). Processing of NaBH₄ from NaBO₂ with MgH₂ by ball milling and usage as hydrogen carrier, *Renewable Energy* 35: 1895-1899.

Cakanyildirim C., Guru M. (2012). The Processing of NaBH₄ from Na₂B₄O₇ by Mechanochemical Synthesis and Its Catalytic Dehydrogenation, *Energy Sources Part A* 34: 1104-1113.

Carneiro J. T., Ana Almeida R., Moulijn J. A., Mul G. (2010). Cyclohexane selective photocatalytic oxidation by anatase TiO₂: influence of particle size and crystallinity, *Phys. Chem. Chem. Phys.* 12: 2744-50.

Cerny R., Penin N., Hagemann H., and Filinchuk Y. (2009). The First Crystallographic and Spectroscopic Characterization of a 3d-Metal Borohydride: Mn(BH₄)₂, *J. Phys. Chem. C* 113: 9003-9007.

Chakrabarti S., Biswas K. (2017). Effect on specific capacity and de-hydrogenation efficiency in doped-MgH₂, *International Journal of Hydrogen Energy* 42: 327-329.

Chang A. C. C., Chang H. F., Lin F. J., Lin K. H., Chen C. H. (2011). Biomass gasification for hydrogen production, *International Journal of Hydrogen Energy* 36: 14252-14260.

Chang J., Tian H., Du F. (2014). Investigation into hydrolysis and alcoholysis of sodium borohydride in ethanolewater solutions in the presence of supported Co-Ce-B catalyst, *International Journal of Hydrogen Energy* 39: 13087-13097.

Chaugule A. A., Tamboli A. H., Sheikh F. A., Kim H. (2015). Preparation and application of Sm-Ni oxide doped TiO₂ nanofiber as catalyst in hydrogen production from sodium borohydride hydrolysis, *Colloids and Surfaces A: Physicochem. Eng. Aspects* 484: 242-252.

Chen B. H., Kuo C. H., Ku J. R., Yan P. S., Huang C. J., Jeng M. S., Tsau F. H. (2013). Highly improved with hydrogen storage capacity and fast kinetics in Mg-based nanocomposites by CNTs, *Journal of Alloys and Compounds* 568: 78-83.

Chen Y., Kim H. (2008). Ni/Ag/silica nanocomposite catalysts for hydrogen generation from hydrolysis of NaBH₄ solution, *Materials Letters* 62: 1451-1454.

Chen Y., Kim H. (2008). Use of a nickel-boride-silica nanocomposite catalyst prepared by in-situ reduction for hydrogen production from hydrolysis of sodium borohydride, *Fuel Processing Technology* 89: 966-972.

Cheng J., Xiang C., Zou Y., Chu H., Qiu S., Zhang H., Sunn L., Xu F. (2015). Highly active nanoporous Co-B-TiO₂ framework for hydrolysis of NaBH₄, *Ceramics International* 41: 899-905.

Chinnappan A., Kim H., Baskar C., Hwang I. T. (2012). Hydrogen generation from the hydrolysis of sodium borohydride with new pyridinium dicationic salts containing transition metal complexes, *International Journal of Hydrogen Energy* 37:10240-10248.

Cho Y. W., Shim J. H., Lee B. J. (2006). Thermal destabilization of binary and complex metal hydrides by chemical reaction: A thermodynamic analysis, *Computer Coupling of Phase Diagrams and Thermochemistry* 30: 65-69.

Choi J. and Chung J. (2016). Preparation and Characteristics of Novel Cobalt Oxide Catalysts for Hydrogen Generation from Metal Borohydride Solution, *J. Energy Eng.* 142(3): 04015026.

Chong M., Karkamkar A., Autrey T., Orimo S. I., Jalisatgid S., Jensen C. M. (2011). Reversible dehydrogenation of magnesium borohydride to magnesium triborane in the solid state under moderate conditions, *Chem. Commun.* 47: 1330-1332.

Choudhury P., Srinivasan S. S., Bhethanabotla V. R., Goswami Y., McGrath K., Stefanakos E. K. (2009). Nano-Ni doped Li-Mn-B-H system as a new hydrogen storage candidate. *International Journal of Hydrogen Energy* 34: 346325-6334.

Christie J. H., Lockwood D. J. (1971). Electronic Raman spectrum of Co^{2+} In CoCl_2 , *Chemical Physics Letters* 8: 120-122.

Concha B. M., Chatenet M., Maillard F., Ticianelli E. A., Lima F. H. B., Delima R. B. (2010). In situ infrared (FTIR) study of the mechanism of the borohydride oxidation reaction. *Phys. Chem. Chem. Phys.* 12: 11507-11516.

Dai H. B., Liang Y., Ma L. P., Wang P. (2008). New Insights into Catalytic Hydrolysis Kinetics of Sodium Borohydride from Michaelis-Menten Model, *J. Phys. Chem. C* 112: 15886-15892.

Dai H. B., Liang Y., Wang P. (2011). Effect of trapped hydrogen on the induction period of cobalt-tungsten-boron/nickel foam catalyst in catalytic hydrolysis reaction of sodium borohydride, *Catalysis Today* 170: 27-32.

Dai H. B., Liang Y., Wang P., Cheng H. M. (2008). Amorphous cobalt–boron/nickel foam as an effective catalyst for hydrogen generation from alkaline sodium borohydride solution, *Journal of Power Sources* 177: 17-23.

Danna V., Spyratou A., Sharma M., Hagemann H. (2014). FT-IR spectra of inorganic borohydrides, *Spectrochimica Acta Part A: Molecular and Biomolecular Spectroscopy* 128: 902-906.

Das T., Choi J. G., Oh I. H. (2019). Synthesis of highly effective α -Fe₂O₃ catalyst for the spin conversion of liquid hydrogen, *Proc. Natl. Acad. Sci., India, Sect. A Phys. Sci.* <https://doi.org/10.1007/s40010-019-00599-3>.

Das T., Kweon S. C., Nah I. W., Karng S. W., Choi J. G., Oh I. H. (2015). Spin conversion of hydrogen using supported iron catalysts at cryogenic temperature, *Cryogenics* 69: 36-43.

Das T., Nah I. W., Choi J. G., Oh I. H. (2016). Synthesis of iron oxide catalysts using various methods for the spin conversion of hydrogen, *Reac Kinet Mech Cat* 118: 669-681.

Das T., Sengupta S., Deo G. (2013). Effect of calcination temperature during the synthesis of Co/Al₂O₃ catalyst used for the hydrogenation of CO₂, *Reac Kinet Mech Cat* 110:147-62.

Dasi G. P., Bhattacharya S. (2015). Simulation, Modelling and Design of Hydrogen Storage Materials, *Proc Indian Natn Sci Acad* 81: 939-951.

Demirci U. B., Akdim O., Miele P. (2009). Ten-year efforts and a no-go recommendation for sodium borohydride for on-board automotive hydrogen storage, *International Journal of Hydrogen Energy* 34: 2638-2645.

Demirci U. B., Garin F. (2008). Kinetics of Ru-promoted sulphated zirconia catalysed hydrogen generation by hydrolysis of sodium tetrahydroborate, *Journal of Molecular Catalysis A: Chemical* 279: 57-62.

Demirci U.B., Akdim O., Miele P. (2009). Ten-year efforts and a no-go recommendation for sodium borohydride for on-board automobile hydrogen storage, *International Journal of Hydrogen Energy*, 34: 2638-45.

Diallo A., Beye A. C., Doyle T. B., Park E., Maaza M. (2015). Green synthesis of Co₃O₄ nanoparticles via *Aspalathus linearis*: Physical properties, *Green Chemistry Letters And Reviews* 8 (3-4): 30-36.

Ding X. L., Yuan X., Jia C., Ma Z. F. (2010). Hydrogen generation from catalytic hydrolysis of sodium borohydride solution using Cobalt-Copper-Boride (Co-Cu-B) catalysts, *International Journal of Hydrogen Energy* 35: 11077-11084.

Dippolito V., Andreozzi G. B., Halenius U., Skogby H., Hametner K., Gunther D. (2015). Color mechanisms in spinel: cobalt and iron interplay for the blue color, *Phys Chem Minerals* 42: 431-9.

Drozd V., Saxena S., Garimella S. V., Durygin A. (2007). Hydrogen release from a mixture of NaBH_4 and $\text{Mg}(\text{OH})_2$, *International Journal of Hydrogen Energy* 32: 3370-5.

Durbin D. J., Jugroot C. M. (2013). Review of hydrogen storage techniques for on board vehicle applications, *International Journal of Hydrogen Energy* 38: 14595-14617.

Fernandes R., Patel N., Miotello A. (2009). Hydrogen generation by hydrolysis of alkaline NaBH_4 solution with Cr-promoted Co-B amorphous catalyst, *Applied Catalysis B: Environmental* 92: 68-74.

Fernandes R., Patel N., Miotello A. (2009a). Efficient catalytic properties of Co-Ni-P-B catalyst powders for hydrogen generation by hydrolysis of alkaline solution of NaBH_4 , *International Journal of Hydrogen Energy* 34: 2893-2900.

Fernandes R., Patel N., Miotello A., Filippi M. (2009). Studies on catalytic behavior of Co-Ni-B in hydrogen production by hydrolysis of NaBH_4 , *Journal of Molecular Catalysis A: Chemical* 298: 1-6.

Fernandes R., Patel N., Miotello A., Jaiswal R., Kothari D. C. (2011). Stability, durability, and reusability studies on transition metal-doped Co-B alloy catalysts for hydrogen production, *International Journal of Hydrogen Energy* 36: 13379-13391.

Ferrer R. D., Ziegls F., Klod S., Lindemann I., Voigtlander R., Dunsch L., and Gutfleisch O. (2011). In Situ Raman Cell for High Pressure and Temperature Studies of Metal and Complex Hydrides, *Anal. Chem.* 83: 3199-3204.

Figen A. K., Coskuner B. (2013). A novel perspective for hydrogen generation from ammonia borane (NH_3BH_3) with Co-B catalysts: "Ultrasonic Hydrolysis", *International Journal of Hydrogen Energy* 38: 2824-2835.

Filinchuk Y. and Hagemann H. (2008). Structure and Properties of $\text{NaBH}_4 \cdot 2\text{H}_2\text{O}$ and NaBH_4 , *Eur. J. Inorg. Chem.* 3127-3133.

Gang G. Byeong, Kim H., Kwon S. (2017). "Ground simulation of a hybrid power strategy using fuel cells and solar cells for high-endurance unmanned aerial vehicles ", *Energy* 141: 1547-1554.

Gennari F.C., Albanesi L. F., Rios I. J. (2009). Synthesis and thermal stability of $Zr(BH_4)_4$ and $Zr(BD_4)_4$ produced by mechanochemical processing, *Inorganica Chimica Acta* 362: 3731-3737.

George L., Saxena S. K. (2010). Structural stability of metal hydrides, alanates and borohydrides of alkali and alkali- earth elements: A review, *International Journal of Hydrogen Energy* 35: 5454-5470.

Ghosh A., Debnath T., Ash T., Das A. K. (2017). Multiple Li^+ - and Mg^{2+} -decorated PAHs: potential systems for reversible hydrogen storage, *RSC Adv.* 7: 9521-9533.

Glavee, G. N., Klabunde K. J., Sorensen C. M., Hadjipanayis G. C. (1995). Chemistry of borohydride reduction of iron (II) and iron (III) ions in aqueous and nonaqueous media. Formation on nanoscale Fe, FeB, and Fe_2B powders, *Inorg. Chem.* 34: 28-35.

Grochala W., Edwards P. P. (2004). Thermal Decomposition of the Non-Interstitial Hydrides for the Storage and Production of Hydrogen, *Chem. Rev.* 104: 1283-1315.

Groven L. J., Pfeil T. L., Pourpoint T. L. (2013). Solution combustion synthesized cobalt oxide catalyst precursor for $NaBH_4$ hydrolysis, *International Journal of Hydrogen Energy* 38: 6377-80.

Guo S. X., Liu Y., Bond A. M., Zhang J., Karthik P. E., Maheshwaran I., Kumar S. S., Phani K. L. N. (2014). Facile electrochemical co-deposition of a graphene-cobalt nanocomposite for highly efficient water oxidation in alkaline media: direct detection of underlying electron transfer reactions under catalytic turnover conditions, *Phys. Chem. Chem. Phys.* 16: 19035-19045.

Gupta A., Shervani S., Amaladasse F., Sivakumar S., Balani K., Subramaniam A. (2009). Enhanced reversible hydrogen storage in nickel nano hollow spheres, *International Journal of Hydrogen Energy* 44: 22032-22038.

Hino S., Ichikawa T., Tokoyoda K., Kojima Y., Fujii H. (2007). Quantity of NH_3 desorption from the Li-N-H hydrogen storage system examined by Fourier transform infrared spectroscopy, *Journal of Alloys and Compounds* 446-447: 342-344.

Hsueh C. L., Liu C. H., Chen B. H., Chen C. Y., Kuo Y. C., Hwang K. J., Ku J. R. (2009). Regeneration of spent- $NaBH_4$ back to $NaBH_4$ by using high-energy ball milling, *International Journal of Hydrogen Energy* 34: 1717-1725.

Hsueh C. L., Liu C. H., Chen B. H., Lee M. S., Chen C. Y., Lu Y. W., Tsau F., Ku J. R. (2011). A novel design of solid-state NaBH₄ composite as a hydrogen source for 2W PEMFC applications, *Journal of Power Sources* 196: 3530-3538.

Humphries T. D., Kalantzopoulos G. N., Jansa I. L., Olsen J. E., and Hauback B. C. (2013). Reversible Hydrogenation Studies of NaBH₄ Milled with Ni-Containing Additives, *J. Phys. Chem. C* 117: 6060-6065.

Hung A. J., Tsai S. F., Hsu Y. Y., Ku J. R., Chen Y. H., Yu C. C. (2008). Kinetics of sodium borohydride hydrolysis reaction for hydrogen generation, *International Journal of Hydrogen Energy* 33: 6205-6215.

Huot J., Ravnsaek D. B., Zhang J., Cuevas F., Latroche M., Jensen T. R. (2013). Mechanochemical synthesis of hydrogen storage materials, *Progress in Materials Science* 58: 30-75.

Ingersoll J. C., Mani N., Thenmozhiyal J. C., Muthaiah A. (2007). Catalytic hydrolysis of sodium borohydride by a novel nickel-cobalt-boride catalyst, *Journal of Power Sources* 173: 450-457.

Irfan M., Li A., Zhang L., Wang M., Chen C., Khushk S. (2019). Production of hydrogen enriched syngas from municipal solid waste gasification with waste marble powder as a catalyst, *International Journal of Hydrogen Energy* 44: 8051-8061.

Jain I. P., Jain P., Jain A., (2010). Novel hydrogen storage materials: A review of lightweight complex hydrides, *Journal of Alloys and Compounds* 503: 303-339.

Jansa I. L., Aliouane N., Deledda S., Fonnelop J. E., Frommen C., Humphries T., Lieutenant K., Sartori S., Sorby M. H., Hauback B. C. (2012). Chloride substitution induced by mechanochemical reactions between NaBH₄ and transition metal chlorides, *Journal of Alloys and Compounds* 530: 186-192.

Jena P., (2011). Materials for hydrogen storage: Past, Present, and Future, *J. Phys. Chem. Lett.* 2: 206-11.

Jeon E., Cho Y. W. (2006). Mechanochemical synthesis and thermal decomposition of zinc borohydride, *Journal of Alloys and Compounds* 422: 273-275.

Jeong S. U., Cho E. A., Nam S. W., Oh I. H., Jung U. H., Kim S. H. (2007). Effect of preparation method on Co-B catalytic activity for hydrogen generation from alkali NaBH₄ solution, *International Journal of Hydrogen Energy* 32: 1749-54.

Jeong S. U., Kim R. K., Cho E. A., Kim H. J., Nam S. W., Oh I. H., Hong S. A., Kim S. H. (2005). A study on hydrogen generation from NaBH₄ solution using the high-performance Co-B catalyst, *Journal of Power Sources* 144: 129-134.

Jepsen L. H., Skibsted J., Jensen T. R. (2013). Investigations of the thermal decomposition of MBH₄-2NH₃BH₃, M = Na, K, *Journal of Alloys and Compounds* 580: 5287-5291.

Kalantzopoulos G. N., Guzik M. N., Deledda S., Heyn R. H., Mullera J. and Hauback B. C. (2014). Destabilization effect of transition metal fluorides on sodium borohydride, *Phys. Chem. Chem. Phys.* 16: 20483-20491.

Kalidindi S. B., Indirani M., and Jagirdar B. R. (2008). First Row Transition Metal Ion-Assisted Ammonia-Borane Hydrolysis for Hydrogen Generation, *Inorg. Chem.* 47: 7424-7429.

Karabulut A., Guru M., Boynuegri T.A., Aydin M. Y. (2016). Synthesis of Ca(BH₄)₂ from synthetic colemanite used in hydrogen storage by Mechanochemical Reaction. *J. Elec. Mat.* 45(8): 3957-3963.

Karuppaiah M., Murugan R., Sakthivel P., Asaithambi S., Yuvakkumar R., Ravi G. (2018). Rapid microwave assisted synthesis of Mn₂O₃ and Co₃O₄ nanoparticles and their structural, optical and magnetic properties, *International Journal of Advance Engineering and Research Development* 5(7): 1-5.

Khafidz N. Z. A. K., Yaakob Z., Lim K. L., Timmiati S. N. (2016). The kinetics of lightweight solid-state hydrogen storage materials: A review, *International Journal of Hydrogen Energy* 41: 13131-13151.

Khan Z., Al-Thabaiti, S.A., Hussain S. (2016). Nanoscale water soluble self-assembled zero-valent iron: role of stabilizers in their morphology, *RSC Adv.* 6: 7267.

Kim D. R., Cho K. W., Choi Y. I., Park C. J. (2009). Fabrication of porous Co-Ni-P catalysts by electrodeposition and their catalytic characteristics for the generation of hydrogen from an alkaline NaBH₄ solution, *International Journal of Hydrogen Energy* 34: 2622-2630.

Kim H., Na Y. J., Song E. J., Kim K. B., Bae J. M., Kim C. (2014). A single colorimetric sensor for multiple target ions: the simultaneous detection of Fe^{2+} and Cu^{2+} in aqueous media, RSC Adv. 4: 22463-70.

Kim J. H., Jin S. A., Shim J. H., Cho Y. W. (2008). Thermal decomposition behavior of calcium borohydride $\text{Ca}(\text{BH}_4)_2$, Journal of Alloys and Compounds 461: L20-L22.

Kim J., Kim T. (2015). "Compact PEM fuel cell system combined with all-in-one hydrogen generator using chemical hydride as a hydrogen source", Applied Energy 160: 945-953.

Kim T. (2014). NaBH_4 (sodium borohydride) hydrogen generator with a volume-exchange fuel tank for small unmanned aerial vehicles powered by a PEM (proton exchange membrane) fuel cell, Energy 69: 721-727.

Kim Y., Lee E. K., Shim J. H., Cho Y. W., Yoon K. B. (2006). Mechanochemical synthesis and thermal decomposition of $\text{Mg}(\text{AlH}_4)_2$, Journal of Alloys and Compounds 422: 283-287.

Knight D. A., Teprovich Jr J. A., Summers A., Peters B., Ward P. A., Compton R. N. and Zidan R. (2013). Synthesis, characterization, and reversible hydrogen sorption study of sodium-doped fullerene, Nanotechnology 24: 455601. (43)

Kojima Y., Haga T. (2003). Recycling process of sodium metaborate to sodium Borohydride, International Journal of Hydrogen Energy 28: 989-93.

Kojima Y., Suzuki K. I., Fukumoto K., Sasaki M., Yamamoto T., Kawai Y., Hayashi H. (2002). Hydrogen generation using sodium borohydride solution and metal catalyst coated on metal oxide, International Journal of Hydrogen Energy 27: 1029-1034.

Kojima Y., Suzuki K.-I, Fukumoto K., Kawai Y., Kimbara M., Nakanishi H., Matsumoto S., (2004). "Development of 10 kW-scale hydrogen generator using chemical hydride, Journal of Power Sources 125: 22-26.

Kovendhan M., Kang H., Youn J. S., Cho H., Jeon K. J. (2019). Alternative cost-effective electrodes for hydrogen production in saline water condition, International Journal of Hydrogen Energy 44: 5090-5098.

Kumar A., Raju N. N., Muthukumar P., Selvam P.V. (2019). Experimental studies on industrial scale metal hydride based hydrogen storage system with embedded cooling tubes, International Journal of Hydrogen Energy 44: 13549-13560.

Kumar E. M., Rajkamal A., Thapa R. (2017). Screening based approach and dehydrogenation kinetics for MgH_2 : Guide to find suitable dopant using first-principles approach, *Scientific Reports* 7: 15550.

Kumar S., Jain A., Miyaoka H., Ichikawa T., Kojima Y. (2017). Study on the thermal decomposition of NaBH_4 catalyzed by ZrCl_4 , *International Journal of Hydrogen Energy* 42(35): 22432-22437.

Kumar S., Jain U., Jain A., Miyaoka H., Ichikawa T., Kojima Y., Dey G.K. (2017). Development of Mg-Li-B based advanced material for onboard hydrogen storage solution, *International Journal of Hydrogen Energy* 42: 3963-3970.

Kumar S., Kojima Y., Dey G.K. (2017). Synergic effect of ZrCl_4 on thermal dehydrogenation kinetics of KBH_4 , *Journal of Alloys and Compounds* 718: 134-38.

Kumar S., Singh A., Kojima Y., Dey G. K. (2017). Tailoring the Thermodynamics and Kinetics of Mg-Li Alloy for a MgH_2 -Based Anode for Lithium-Ion Batteries, *Energy Technol.* 5: 1546-1551.

Kumar S., Singh A., Nakajima K., Jain A., Miyaoka H., Ichikawa T., Dey G. K., Kojima Y. (2017). Improved hydrogen release from magnesium borohydride by ZrCl_4 additive, *International Journal of Hydrogen Energy* 42(35): 22342-22347.

Lee J., Kong K. Y., Jung C. R., Cho E., Yoon S. P., Han J., Lee T. G., Nam S. W. (2007). A structured Co-B catalyst for hydrogen extraction from NaBH_4 solution, *Catalysis Today* 120: 305-10.

Lei Q., Wang B., Wang P., Liu S. (2019). Hydrogen generation with acid/alkaline amphoteric water electrolysis, *Journal of Energy Chemistry* 38: 162-169.

Li C., Meng W., Hu G., Wang Y., Cao Z., Zhang K. (2018). Preparation and characterization of nanostructured Co-Mo-B thin film catalysts for the hydrolysis of ammonia borane, *International Journal of Hydrogen Energy* 43: 17664-17672.

Li H. W., Yan Y., Orimo S. I., Zuttel A. and Jensen C. M. (2011). Recent Progress in Metal Borohydrides for Hydrogen Storage, *Energies* 4: 185-214.

Li L., Li S., Tan Y., Tang Z., Cai W., Guo Y., Li Q., Yu X. (2012). Hydrogen generation from hydrolysis and methanolysis of guanidinium borohydride, *J. Phys. Chem. C* 116: 14218-23.

Li Y., Qiu W., Qin F., Fang H., Hadjiev V. G., Litvinov D., Bao J. (2016). Identification of Cobalt Oxides with Raman Scattering and Fourier Transform Infrared Spectroscopy, *J. Phys. Chem. C* 120: 4511-4516.

Li Z. P., Liu B. H., Morigasaki N., Suda S. (2003). "Preparation of potassium borohydride by a mechano-chemical reaction of saline hydrides with dehydrated borate through ball milling", *Journal of Alloys and Compounds* 354: 243-247.

Li Z., Li H., Wang L., Liu T., Zhang T., Wang G., Xie G. (2014). Hydrogen generation from catalytic hydrolysis of sodium borohydride solution using supported amorphous alloy catalysts (Ni-Co-P/ γ -Al₂O₃), *International Journal of Hydrogen Energy* 39: 14935-14941.

Liang Y., Wang P., Dai H. B. (2010). Hydrogen bubbles dynamic template preparation of a porous Fe-Co-B/Ni foam catalyst for hydrogen generation from hydrolysis of alkaline sodium borohydride solution, *Journal of Alloys and Compounds* 491: 359-65.

Liang Y., Wang P., Dai H. B. (2010). Hydrogen bubbles dynamic template preparation of a porous Fe-Co-B/Ni foam catalyst for hydrogen generation from hydrolysis of alkaline sodium borohydride solution, *Journal of Alloys and Compounds* 491: 359-365.

Liu B. H., Li Q. (2008). A highly active Co-B catalyst for hydrogen generation from sodium borohydride hydrolysis, *International Journal of Hydrogen Energy* 33: 7385-91.

Liu B. H., Li Z. P. (2009). A review: Hydrogen generation from borohydride hydrolysis reaction, *Journal of Power Sources* 187: 527-534.

Liu B. H., Li Z. P., Suda S. (2009). Improving MgH₂ formation kinetics and its effect on NaBH₄ synthesis, *Journal of Alloys and Compounds* 474: 321-325.

Liu R. S., Lai H. C., Bagkar N. C., Kuo H. T., Chen H. M., Lee J. F., Chung H. J., Chang S. M., Weng B. J. (2008). Investigation on Mechanism of Catalysis by Pt-LiCoO₂ for Hydrolysis of Sodium Borohydride Using X-ray Absorption, *J. Phys. Chem. B* 112: 4870-4875.

Lo Y. L., Hwang B. J. (1994). Decomposition of NaBH₄ in an electroless nickel bath, *Ind. Eng. Chem. Res.* 33:56-61.

Logager T., Holcman J. Sehested K., Pedersen T. (1992). Oxidation of ferrous ions by ozone in acidic solutions, *Inorg. Chem.* 31: 3523-29.

- Loghmani M. H., Shojaei A. F. (2014). Hydrogen production through hydrolysis of sodium borohydride: Oleic acid stabilized Co-La-Zr-B nanoparticle as a novel catalyst, *Energy* 68: 152-159.
- Lu Y. C., Chen M. S., Chen Y. W. (2012). Hydrogen generation by sodium borohydride hydrolysis on nanosized CoB catalysts supported on TiO₂, Al₂O₃ and CeO₂, *International Journal of Hydrogen Energy* 37: 4254-4258.
- Lu Z. H., Li J., Zhu A., Yao Q. Huang W., Zhou R., Zhou R., Chen X. (2013). Catalytic hydrolysis of ammonia borane via magnetically recycle copper iron nanoparticles for chemical hydrogen storage, *International Journal of Hydrogen Energy* 38: 5330-5337.
- Ma J. L., Li N., Zhang Q., Zhang X. B., Wang J., Li K., Hao X. F., Yan J. M. (2018). Synthesis of porous and metallic CoB nanosheets towards a highly efficient electrocatalyst for rechargeable Na-O₂ batteries, *Energy Environ. Sci.* 11: 2833-2838.
- Ma X., Zhao X., Gu J., Shi J. (2019). Co-gasification of coal and biomass blends using dolomite and olivine as catalysts, *Renewable Energy* 132: 509-514.
- Mahato S., Banerjee B., Pugazhenti G., Banerjee T. (2015). Optimization and quantum chemical predictions for the dehydrogenation kinetics of Ammonia Borane-Ionic Liquid mixtures, *International Journal of Hydrogen Energy* 40: 10390-10340.
- Manna J., Roy B., Sharma P. (2015). Efficient hydrogen generation from sodium borohydride hydrolysis using silica sulfuric acid catalyst, *Journal of Power Sources* 275: 727-733.
- Mao J., Gregory D. H. (2015). Recent Advances in the Use of Sodium Borohydride as a Solid State Hydrogen Store, *Energies* 8: 430-453.
- Mao J., Gu Q., Guo Z. and Liu H. K. (2015). Sodium borohydride hydrazinates: synthesis, crystal structures, and thermal decomposition behaviour, *J. Mater. Chem. A* 3: 11269-11276.
- Mao J., Guo Z., Nevirkovets I. P., Liu H. K., Dou S. X. (2012). Hydrogen De-/Absorption Improvement of NaBH₄ Catalyzed by Titanium-Based Additives, *J. Phys. Chem. C* 116: 1596-1604.
- Martelli P., Caputo R., Remhof A., Maun P., Borgschulte A., Zuttel A. (2010). Stability and Decomposition of NaBH₄. *J. Phys. Chem. C* 11: 7173-7177.

McNulty D., Geaney H., Carroll E., Garvey S., Lonergan A., Odwyer C. (2017). The effect of particle size, morphology and C-rates on 3D structured Co_3O_4 inverse opal conversion mode anode materials, *Mater. Res. Express* 4: 025011.

Meena P., Jangir M., Kumar A., Singh R., Sharma V. K., Jain I. P. (2017). Improved dehydrogenation kinetics of MgH_2 due to NiMnAl , *Mater. Res. Express* 4: 116520.

Metin O., Ozkar S. (2009). Hydrogen Generation from the Hydrolysis of Ammonia-borane and Sodium Borohydride Using Water-soluble Polymer-stabilized Cobalt(0) Nanoclusters Catalyst, *Energy & Fuels* 23: 3517-3526.

Mitov M., Rashkov R., Atanassov N., Zielonka A. (2007). Effects of nickel foam dimensions on catalytic activity of supported Co-Mn-B nanocomposites for hydrogen generation from stabilized borohydride solutions, *J Mater Sci* 42: 3367-3372.

Muir S. S., Chen Z., Wood B. J., Wang L., Lu G. Q. (M.), Yao X. (2014). New electroless plating method for preparation of highly active Co-B catalysts for NaBH_4 hydrolysis, *International Journal of Hydrogen Energy* 39: 414-25.

Murthy S. S. (2012). Heat and Mass Transfer in Solid State Hydrogen Storage: A Review, *Journal of Heat Transfer* 134(3): 031020-11.

Naik M. U. D., Rather S. U., Zacharia R., So C. S., Hwang S. W., Kim A. R., Nahm K. S. (2009). Comparative study of dehydrogenation of sodium aluminium hydride wet-doped with ScCl_3 , TiCl_3 , VCl_3 , and MnCl_2 , *Journal of Alloys and Compounds* 471: L16-L22. (49)

Nakamori Y., Miwa K., Ninomiya A., Li H., Ohba N., Towata S. I., Zuttel A., Orimo S. I. (2006). Correlation between thermodynamical stabilities of metal borohydrides and cation electronegativities: First-principles calculations and experiments, *Physical Review B* 74: 045126.

Nale A., Pendolino F., Maddalena A., Colombo P. (2016). Enhanced hydrogen release of metal borohydrides $\text{M}(\text{BH}_4)_n$ ($\text{M} = \text{Li}, \text{Na}, \text{Mg}, \text{Ca}$) mixed with reduced graphene oxide, *International Journal of Hydrogen Energy* 41: 11225-11231.

Nanda S., Rana R., Hunter H. N., Fang Z., Dalai A. K., Kozinski J. A. (2019). Hydrothermal catalytic processing of waste cooking oil for hydrogen-rich syngas production, *Chemical Engineering Science* 195: 935-945.

Netskina O. V., Ozerova A. M., Komova O. V., Odegova G. V., Simagina V. I. (2015). Hydrogen storage systems based on solid-state $\text{NaBH}_4/\text{Co}_x\text{B}$ composite: Influence of catalyst properties on hydrogen generation rate, *Catalysis Today* 245: 86-92.

Niaz S., Manzoor T., Pandith A. H. (2015). Hydrogen storage: Materials, methods and perspectives, *Renewable and Sustainable Energy Reviews* 50: 457-469.

Ocon J. D., Tuan T. N., Yi Y., Leon R. L. D., Lee J. K., Lee J. (2013). Ultrafast and stable hydrogen generation from sodium borohydride in methanol and water over Fe-B nanoparticles, *Journal of Power Sources* 243: 444-50.

Oh S., Song D., Kim H., Sohn D., Hong K., Lee M., Son S., Cho E., Kwon H. (2019). Cobalt-iron-phosphorus catalysts for efficient hydrogen generation from hydrolysis of ammonia borane solution, *Journal of Alloys and Compounds* 806: 643-649.

Olsen J. E., Sorby M. H., Bjorn C. Hauback B. C. (2011). Chloride-substitution in sodium borohydride, *Journal of Alloys and Compounds* 509: L228–L231.

Ozerova A. M., Sigmagina V. I., Komova O. V., Netskina O. V., Odegova G. V., Bulavchenko O. A., Rudina N. A. (2012). Cobalt borate catalysts for hydrogen production via hydrolysis of sodium borohydride, *Journal of Alloys and Compounds* 513: 266-72.

Palmer S. J., Reddy B. J., Frost R. L. (2009). Characterisation of red mud by UV–vis–NIR spectroscopy, *Spectrochimica Acta Part A* 71: 1814-1818.

Panigrahi P., Naqvi S. R., Hankel M., Ahuja R., Hussain T. (2018). Enriching the hydrogen storage capacity of carbon nanotube doped with polyolithiated molecules, *Applied Surface Science* 444: 467-473.

Pareek K., Zhang Q., Rohan R., Xu G., Cheng H. (2014). Room Temperature Hydrogen Physisorption on Exposed Metals in A Highly Cross-Linked Organo-Iron Complex, *Adv. Mater. Interfaces* 1: 1400107.

Parker S. F. (2010). Spectroscopy and bonding in ternary metal hydride complexes-Potential hydrogen storage media, *Coordination Chemistry Reviews* 254: 215-234.

Paskevicius M., Ley M. B., Sheppard D. A., Jensen T. R., Buckley C. E. (2013). Eutectic melting in metal borohydrides, *Phys. Chem. Chem. Phys.* 15: 19774-19789.

Patel N., Fernandes R., Guella G., Kale A., Miotello A., Patton B., Zanchetta C. (2008). Structured and Nanoparticle Assembled Co-B Thin Films Prepared by Pulsed Laser Deposition: A Very Efficient Catalyst for Hydrogen Production, *J. Phys. Chem. C* 112: 6968-6976.

Patel N., Fernandes R., Guella G., Miotello A. (2010). Nanoparticle-assembled Co-B thin film for the hydrolysis of ammonia borane: A highly active catalyst for hydrogen production, *Applied Catalysis B: Environmental* 95: 137- 43.

Patel N., Fernandes R., Miotello A. (2009). Hydrogen generation by hydrolysis of NaBH_4 with efficient Co-P-B catalyst: A kinetic study, *Journal of Power Sources* 188: 411-420.

Pei Z., Bai Y., Wang Y., Wu F., Wu C. (2017). Insight to the Thermal Decomposition and Hydrogen Desorption Behaviors of $\text{NaNH}_2\text{-NaBH}_4$ Hydrogen Storage Composite, *ACS Appl. Mater. Interfaces* 9: 31977-31984.

Pendolino F. (2012). "Boron Effect" on the Thermal Decomposition of Light Metal Borohydrides MBH_4 ($M = \text{Li, Na, Ca}$), *J. Phys. Chem. C* 116: 1390-1394.

Peng S., Fan X., Zhang J., Wang F. (2013). A highly efficient heterogeneous catalyst of Ru/MMT: Preparation, characterization, and evaluation of catalytic effect, *Applied Catalysis B: Environmental* 140-141: 115-124.

Petitpas G., Aceves S. M., Matthews M. J., Smith J. R. (2014). Para- H_2 to ortho- H_2 conversion in a full-scale automotive cryogenic pressurized hydrogen storage up to 345 bar, *International Journal of Hydrogen Energy* 39: 6533-6547.

Pfeil T. L., Pourpoint T. L., Groven L. J. (2014). Effects of crystallinity and morphology of solution combustion synthesized Co_3O_4 as a catalyst precursor in hydrolysis of sodium borohydride, *International Journal of Hydrogen Energy* 39: 2149-59.

Pinto A. M. F. R., Falcao D. S., Silva R. A., Rangel C. M. (2006). Hydrogen generation and storage from hydrolysis of sodium borohydride in batch reactors, *International Journal of Hydrogen Energy* 31: 1341-1347.

Prasad D., Patil K. N., Sandhya N., Chaitra C. R., Bhanushali J. T., Samal A. K., Keri R. S., Jadhav A. H., Nagaraja B. M. (2019). Highly efficient hydrogen production by hydrolysis of NaBH_4 using eminently competent recyclable Fe_2O_3 decorated oxidized MWCNTs robust catalyst, *Applied Surface Science* 489: 538-551.

- Qiao L., Swihart M. T. (2017). Solution-phase synthesis of transition metal oxide nanocrystals: Morphologies, formulae, and mechanisms, *Advances in Colloid and Interface Science* 244: 199-266.
- Qureshy A. M. M. I., Ahmed M., Dincer I. (2019). Performance assessment study of photo-electrochemical water-splitting reactor designs for hydrogen production, *International Journal of Hydrogen Energy* 44: 9237-9247.
- Raikwar D., Munagala M., Majumdar S., Shee D. (2019). Hydrodeoxygenation of guaiacol over Mo, W and Ta modified supported nickel catalysts, *Catalysis Today* 325: 117-130.
- Rambabu K., Hai A., Bharath G., Banat F., Show P. L. (2019). Molybdenum disulfide decorated palm oil waste activated carbon as an efficient catalyst for hydrogen generation by sodium borohydride hydrolysis, *International Journal of Hydrogen Energy* 44: 14406-14415.
- Ren J., Musyoka N. M., Langmi H. W., Mathe M., Liao S. (2017). Current research trends and perspectives on materials-based hydrogen storage solutions: A critical review, *International Journal of Hydrogen Energy* 42: 289-311.
- Rivarolo M., Improta O., Magistri L., Panizza M., Barbucci A. (2018). Thermo-economic analysis of a hydrogen production system by sodium borohydride (NaBH_4), *International Journal of Hydrogen Energy* 43: 1606-1614.
- Ro G., Kim Y. (2019). H_2 generation using Pt nanoparticles encapsulated in $\text{Fe}_3\text{O}_4@\text{SiO}_2@\text{TiO}_2$ multishell particles, *Colloids and Surfaces A* 577: 48-52.
- Sahin O., Baytar O., Hansu F., Saka C. (2014). Hydrogen Generation from Hydrolysis of Sodium Borohydride with Ni(0) Catalyst in Dielectric Barrier Discharge Method, *Energy Sources, Part A: Recovery, Utilization, and Environmental Effects* 36: 1886-1894.
- Sahin O., Saka C., Baytar O., Hansu F. (2013). Influence of plasma treatment on electrochemical activity of Ni (o)-based catalyst for hydrogen production by hydrolysis of NaBH_4 , *Journal of Power Sources* 240: 729-735.
- Sahiner N., Yasar A. O. (2014). H_2 generation from NaBH_4 and NH_3BH_3 using metal catalysts prepared within p(VI) capsule particles, *Fuel Processing Technology* 125:148-54.
- Schlapbach L., Zuttel A. (2001). Hydrogen-storage materials for mobile applications, *NATURE* 414: 353-358.

Schlesinger H. I., Brown H. C., Finholt A. E. (1953). The Preparation of Sodium Borohydride by the High Temperature Reaction of Sodium Hydride with Borate Esters, Contribution from the George Herbert Jones Laboratory of the University of Chicago 75: 205-209.

Seven F., Sahiner N. (2014). Enhanced catalytic performance in hydrogen generation from NaBH₄ hydrolysis by super porous cryogel supported Co and Ni catalysts, Journal of Power Sources 272: 128-136.

Seven F., Sahiner N. (2014). Superporous P(2-hydroxyethyl methacrylate) cryogel-M (M:Co, Ni, Cu) composites as highly effective catalysts in H₂ generation from hydrolysis of NaBH₄ and NH₃BH₃, International Journal of Hydrogen Energy 39: 15455-15463.

Sharma K. (2019). Carbohydrate-to-hydrogen production technologies: A mini-review, Renewable and Sustainable Energy Reviews 105: 138-143.

Shi L., Chen Z., Jian Z., Guo F., Gao C. (2019). Carbon nanotubes-promoted Co-B catalysts for rapid hydrogen generation via NaBH₄ hydrolysis, International Journal of Hydrogen Energy 44: 19868-19877.

Shi L., Xie W., Jian Z., Liao X., Wang Y. (2019). Graphene modified Co-B catalysts for rapid hydrogen production from NaBH₄ hydrolysis, International Journal of Hydrogen Energy 44: 17954-17962.

Si C. D., Gao H. T., Zhou J., Liu G. J. (2010). Catalytic properties of Co/activated carbon catalyst prepared from wheat stalk, Reac Kinet Mech Cat 101: 183-93.

Siddiqui O., Dincer I. (2019). A well to pump life cycle environmental impact assessment of some hydrogen production routes, International Journal of Hydrogen Energy 44: 5773-5786.

Singh A., Maiya M. P., Murthy S. S. (2017). Experiments on solid state hydrogen storage device with a finned tube heat exchanger, International Journal of Hydrogen Energy 42: 15226-15235.

Singh P. K., Das T. (2017). Generation of hydrogen from NaBH₄ solution using metal-boride (CoB, FeB, NiB) catalysts, International Journal of Hydrogen Energy 42: 29360-29369.

Singh S. K. and Xu Q. (2009). Complete Conversion of Hydrous Hydrazine to Hydrogen at Room Temperature for Chemical Hydrogen Storage, J. Am. Chem. Soc. 131: 18032-18033.

Siriwardane R., Poston J. (2019). Monazam E., Richards G., Production of hydrogen by steam oxidation of calcium ferrite reduced with various coals, *International Journal of Hydrogen Energy* 44: 7158-7167.

Sljukic B., Santos D. M. F., Sequeira C. A. C., Banks C. E. (2013). Analytical monitoring of sodium borohydride, *Anal. Methods* 5: 829-839.

Soria M. A., Barros D., Madeira L. M. (2019). Hydrogen production through steam reforming of bio-oils derived from biomass pyrolysis: Thermodynamic analysis including in situ CO₂ and/or H₂ separation, *Fuel* 244: 184-195.

Soykal I. I., Sohn H., and Ozkan U. S. (2012). Effect of Support Particle Size in Steam Reforming of Ethanol over Co/CeO₂ Catalysts, *ACS Catal.* 2: 2335-2348.

Toche F., Chiriac R., Demirci U. B., Miele P. (2012). Ammonia borane thermolytic decomposition in the presence of metal (II) chlorides, *International Journal of Hydrogen Energy* 37: 6749-6755.

Tuan T. N., Yi Y., Lee J. K., Lee J. (2013). Fe-B catalyst fabricated by hybrid capacitive adsorption-chemical reduction method and its application for hydrogen production from NaBH₄ solution, *Catalysis Today* 216: 240- 245.

Umegaki T., Xu Q., Kojima Y. (2013). In situ synthesized spherical nickel-silica composite particles for hydrolytic dehydrogenation of ammonia borane, *Journal of Alloys and Compounds* 580: S313-S316.

Umegaki T., Yan J. M., Zhang X. B., Shioyama H., Kuriyama N., Xu Q. (2010). Co-SiO₂ nanosphere-catalyzed hydrolytic dehydrogenation of ammonia borane for chemical hydrogen storage, *Journal of Power Sources* 195: 8209-8214.

Umegaki T., Yan J. M., Zhang X. B., Shioyama H., Kuriyama N., Xu Q. (2009). Hollow Ni-SiO₂ nanosphere-catalyzed hydrolytic dehydrogenation of ammonia borane for chemical hydrogen storage, *Journal of Power Sources* 191: 209-216.

Urgnani J., Torres F. J., Palumbo M., Baricco M. (2008). Hydrogen release from solid state NaBH₄, *International Journal of Hydrogen Energy* 33: 3111-3115.

Varin R. A., Mattar D. K., Bidabadi A. S., Polanski M. (2017). Synthesis of amorphous manganese borohydride in the (NaBH₄-MnCl₂) system, its hydrogen generation properties and crystalline transformation during solvent extraction, *Journal of Energy Chemistry* 26: 24-34.

Varkolu M., Burri D. R., Kamaraju S. R. R., Jonnalagappa S. B., Vanzyl W. E. (2017). Hydrogenation of Levulinic Acid Using Formic Acid as a Hydrogen Source over Ni/SiO₂ Catalysts, *Chem. Eng. Technol.* 40: 719-26.

Walter J. C., Zurawski A., Montgomery D., Thornburg M., Revankar S. (2008). Sodium borohydride hydrolysis kinetics comparison for nickel, cobalt, and ruthenium boride catalysts, *Journal of Power Sources* 179: 335-9.

Wang C., Zhang S., Yuji S., Zhang Z. (2014). Analysis of a complex produced in the Fenton oxidation process, *Water Science and Technology* 69.5: 1115-9.

Wang K., Kang X., Zhong Y., Hu, J. Ren C., Wang P. (2014). Unexpected Dehydrogenation Behaviors of the 2LiBH₄-MgH₂ Composite Confined in a Mesoporous Carbon Scaffold, *J. Phys. Chem. C* 118; 26447-26453.

Wang L., Cao S., Guo K., Wu Z., Ma Z., Piao L. (2019). Simultaneous hydrogen and peroxide production by photocatalytic water splitting, *Chinese Journal of Catalysis* 40: 470-475.

Wang W., Zhao Y., Chen D., Wang X., Peng X., Tian J. (2014). Promoted Mo incorporated Co-Ru-B catalyst for fast hydrolysis of NaBH₄ in alkaline solutions, *International Journal of Hydrogen Energy* 39: 16202-11.

Wang Y. P., Wang Y. J, Ren Q. L., Li L., Jiao L. F., Song D.W., Liu G., Han Y., Yuan H. T. (2010). Ultrafine Amorphous Co-Fe-B Catalysts for the Hydrolysis of NaBH₄ Solution to Generate Hydrogen for PEMFC, *Fuel Cells* 10: 1, 132-138.

Wen Y., Qu D., An L., Gao X., Jiang W., Wu D., Yang D., Sun Z. (2019). Defective g-C₃N₄ Prepared by the NaBH₄ Reduction for High- Performance H₂ Production, *ACS Sustainable Chem. Eng.* 7: 2343-2349.

Wilcox M. J., Groven L. J. (2017). Solution Combustion Synthesized Lithium Cobalt Oxide As A Catalytic Precursor For The Hydrolysis Of Sodium Borohydride, *International Journal of Hydrogen Energy* 42: 6765-6770.

Wu C., Bai Y., Liu D. X., Wu F., Pang M. L., Yi B. L. (2011). Ni-Co-B catalyst-promoted hydrogen generation by hydrolyzing NaBH₄ solution for in situ hydrogen supply of portable fuel cells, *Catalysis Today* 170: 33-9.

Wu C., Bai Y., Wu F. (2008). Fast hydrogen generation from NaBH₄ solution accelerated by ferric catalysts, *Materials Letters* 62: 4242-4.

Wu C., Wu F., Bai Y., Yi B., Zhang H. (2005). Cobalt boride catalysts for hydrogen generation from alkaline NaBH₄ solution, *Materials Letters* 59: 1748-51.

Wu H., Zhou X., Rodriguez E. E., Zhou W., Udovic T. J., Yildirim T., Rush J. J. (2016). A new family of metal borohydride guanidinate complexes: Synthesis, structures and hydrogen-storage properties, *Journal of Solid State Chemistry* 242: 186-192.

Wu Z., Ge S. (2011). Facile synthesis of a Co-B nanoparticle catalyst for efficient hydrogen generation via borohydride hydrolysis, *Catalysis Communications* 13: 40-3.

Yadav P. K., Das T. (2019). Production of syngas from carbon dioxide reforming of methane by using LaNi_xFe_{1-x}O₃ perovskite type catalysts, *International Journal of Hydrogen Energy* 44: 1659-1670.

Yan J. M., Zhang X. B., Han S., Shioyama H., Xu Q. (2009). Synthesis of Longtime Water/Air-Stable Ni Nanoparticles and Their High Catalytic Activity for Hydrolysis of Ammonia-Borane for Hydrogen Generation, *Inorg. Chem.* 48: 7389-93.

Yang B., Li S., Wang H., Xiang J., Yang Q. (2013). Effect of MWCNTs additive on desorption properties of Zn(BH₄)₂ composite prepared by mechanical alloying. *J. Mater. Sci. Technol.* 29(8): 715-719.

Yang C. C., Chen M. S., Chen Y. W. (2011). Hydrogen generation by hydrolysis of sodium borohydride on CoB/SiO₂ catalyst, *International Journal of Hydrogen Energy* 36: 1418-1423.

Yang C. H., Tsai W. T., Chang J. K. (2011). Hydrogen desorption behavior of vanadium borohydride synthesized by modified mechano-chemical process, *International Journal of Hydrogen Energy* 36: 4993-4999.

Yang Z., Hu J., Li Y., Chen Y., Qian K., Yang H., Chen H. (2019). Catalytic steam gasification of Mengdong coal in the presence of iron ore for hydrogen-rich gas production, *Journal of the Energy Institute* 92: 391-402.

Yao Q., Lu Z.-H., Huang W., Chen X., Zhu J. (2016). High Pt-like activity of the Ni-Mo/grapheme catalyst for hydrogen evolution from hydrolysis of ammonia borane, *J. Mater.Chem. A* 4: 8579-8583.

Yao Q., Lu Z.-H., Jia Y., Chen X., Liu X. (2015). In situ facile synthesis of Rh nanoparticles supported on carbon nanotubes as highly active catalysts for H₂ generation from NH₃BH₃ hydrolysis, *International Journal of Hydrogen Energy* 40: 2207-2215.

Yao Q., Lu Z.-H., Zhang Z., Chen X., Lan Y. (2014). One-pot synthesis of core-shell Cu@SiO₂ nanospheres and their catalysis for hydrolytic dehydrogenation of ammonia borane and hydrazine borane, *Scientific Reports* 4:1-8, DOI:10.1038/srep07597.

Yousefi S.R., Ghanbari D., Salavati-Niasari M., Hassanpour M. (2016). Photo-degradation of organic dyes:simple chemical synthesis of Ni(OH)₂ nanoparticles, Ni/Ni(OH)₂ and Ni/NiO magnetic nanocomposites, *J. Mater Sci: Mater Electron* 27: 1244-53.

Zhang J., Li C., Li L., Du X., Song B., and Xu H. (2014). Multi-shaped Amorphous Alloy Ni-B: Ultrasonically Aided Complexing-reduction Preparation, Catalytic Ability for NaBH₄ Hydrolysis Yielding H₂ Gas, *Z. Anorg. Allg. Chem.* 640(2):456-61.

Zhang Q., and Mohring R. M. (2009). Reaction Chemistry Between Aqueous Sulfuric Acid and Solid Sodium Borohydride, *Ind. Eng. Chem. Res.* 48: 1603-1607.

Zhang Q., Wu Y., Sun X., and Ortega J. (2007). Kinetics of Catalytic Hydrolysis of Stabilized Sodium Borohydride Solutions, *Ind. Eng. Chem. Res.* 46: 1120-1124.

Zhang X., Wei Z., Guo Q., Tian H. (2013). Kinetics of sodium borohydride hydrolysis catalyzed via carbon nanosheets supported Zr/Co, *Journal of Power Sources* 231: 190-196.

Zhang Y., Shimoda K., Miyaoka H., Ichikawa T., Kojima Y. (2010). Thermal decomposition of alkaline-earth metal hydride and ammonia borane composites, *International Journal of Hydrogen Energy* 35: 12405-12409.

Zhang Z. G., Wang H., Liu J. W., Zhu M. (2013). Thermal decomposition behaviors of magnesium borohydride doped with metal fluoride additives, *Thermochimica Acta* 560: 82-88.

Zhang Z. G., Wang H., Zhu M., (2011). Hydrogen release from sodium borohydrides at low temperature by the addition of zinc fluoride, *International Journal of Hydrogen Energy* 36: 8203-8208.

Zhao J., Ma H., Chen J. (2007). Improved hydrogen generation from alkaline NaBH₄ solution using carbon-supported Co-B as catalysts, *International Journal of Hydrogen Energy* 32: 4711-16.

Zheng H., Huang X., Gao H., Dong W., Lu G., Chen X., Wang G. (2019). Decorating cobalt phosphide and rhodium on reduced graphene oxide for high-efficiency hydrogen evolution reaction, *Journal of Energy Chemistry* 34: 72-79.

Zheng Y., Zhu Y., Wang A. (2015). Evolution of Fe³⁺-hydrogel for catalytic reduction of 4-nitrophenol, *Colloid Polym Sci* 293: 2009-2016.

Zhuang D. W., Zhang J. J., Dai H. B., Wang P. (2013). Hydrogen generation from hydrolysis of solid sodium borohydride promoted by a cobalt-molybdenum-boron catalyst and aluminum powder, *International Journal of Hydrogen Energy* 38: 10845-10850.

Zied B. M. A., Alamry K. A. (2019). Green synthesis of 3D hierarchical nanostructured Co₃O₄/carbon catalysts for the application in sodium borohydride hydrolysis, *Journal of Alloys and Compounds* 798: 820-831.

Zou J. J., He H., Cui L., Du H. Y. (2007). Highly efficient Pt/TiO₂ photocatalyst for hydrogen generation prepared by a cold plasma method, *International Journal of Hydrogen Energy* 32: 1762-1770.

Zou Y. C., Nie M., Huang Y. M., Wang J. Q., Liu H. L. (2011). Kinetics of NaBH₄ hydrolysis on carbon-supported ruthenium catalysts, *International Journal of Hydrogen Energy* 36: 12343-12351.

Zuttel A. (2004). Hydrogen storage methods, *Naturwissenschaften* 91: 157-172.

APPENDIX A

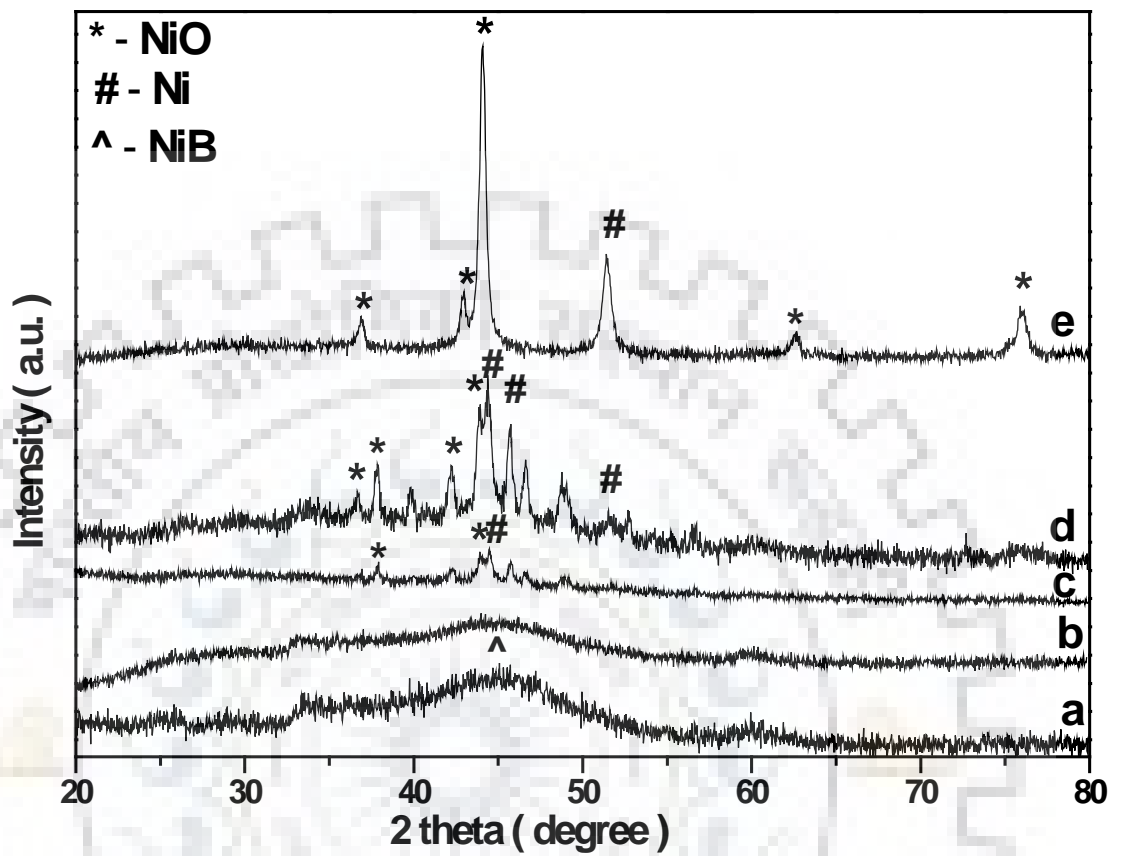


Fig. A1: XRD patterns of NiB-BS catalysts calcined at various calcinations temperature a) 373 K, b) 473 K, c) 573 K, d) 673 K and e) 773 K for 1 h.

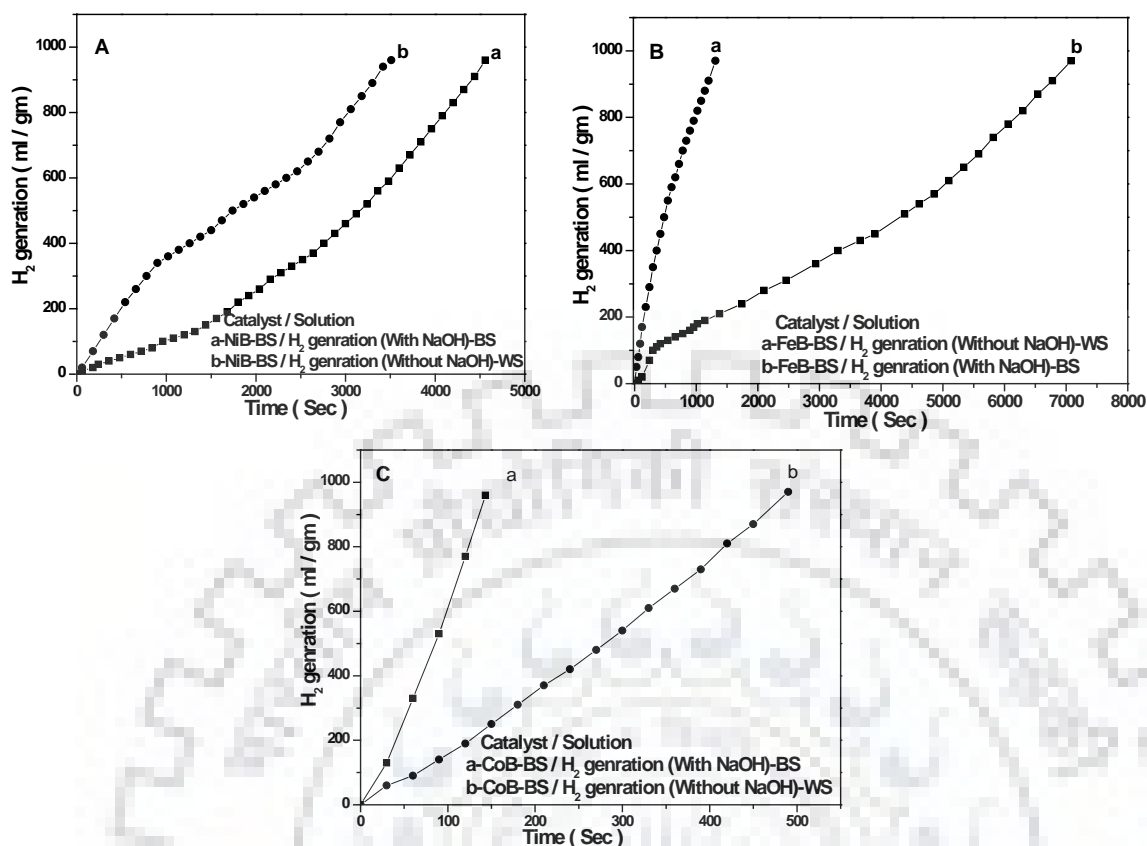


Fig. A2: Hydrogen generation rate of A) NiB catalysts synthesized using base (BS) stabilized sodium borohydride solution and the hydrolysis reaction using with(BS)/without (WS) base stabilized sodium borohydride solution, B) FeB catalysts synthesized using base (BS) stabilized and the hydrolysis reaction using with(BS)/without (WS) base stabilized sodium borohydride solution, and C) CoB catalysts synthesized using base (BS) stabilized sodium borohydride solution and the hydrolysis reaction using with(BS)/without (WS) base stabilized sodium borohydride solution. The catalysts were vacuum desiccator dried for 24 h, followed by calcined at 393 K for 2 h. The hydrogen generation study was conducted at 303 K using 10 mg of each catalyst.

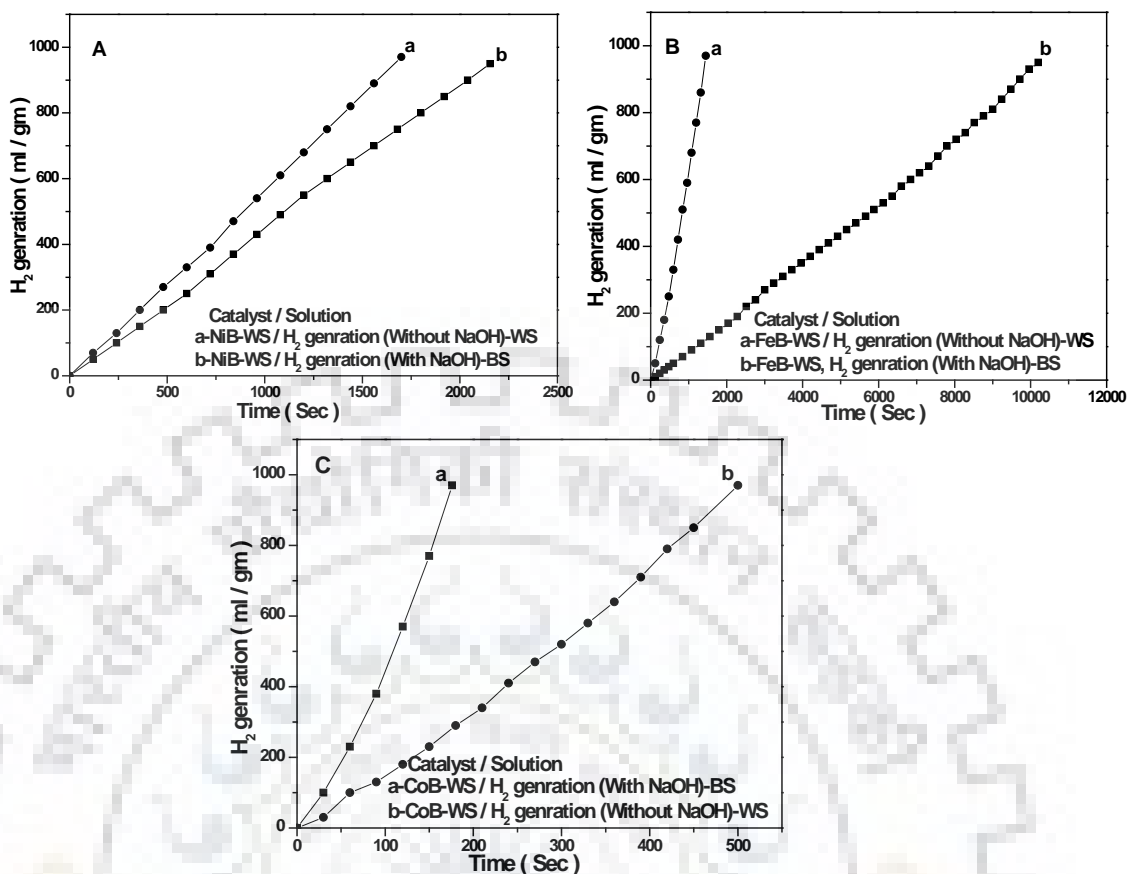


Fig. A3: Hydrogen generation rate of A) NiB catalysts synthesized using without base (WS) stabilized sodium borohydride solution and the hydrolysis reaction using with(BS)/without (WS) base stabilized sodium borohydride solution, B) FeB catalysts synthesized using without base (WS) stabilized and the hydrolysis reaction using with(BS)/without (WS) base stabilized sodium borohydride solution, and C) CoB catalysts synthesized using without base (WS) stabilized sodium borohydride solution and the hydrolysis reaction using with(BS)/without (WS) base stabilized sodium borohydride solution. The catalysts were vacuum desiccator dried for 24 h, followed by calcined at 393 K for 2 h. The hydrogen generation study was conducted at 303 K using 10 mg of each catalyst.

APPENDIX B

Table B1: The Specific surface area of the synthesized catalysts

Catalyst	Specific surface area (sq.m/gm)	Catalyst	Specific surface area (sq.m/gm)
5CoB/ Al ₂ O ₃ - 473 K	152	50CoB/ Al ₂ O ₃ - oven dried	103
10CoB/ Al ₂ O ₃ - 473 K	150	50CoB/ Al ₂ O ₃ - 373 K	95
20CoB/ Al ₂ O ₃ - 473 K	146	50CoB/ Al ₂ O ₃ - 473 K	110
30CoB/ Al ₂ O ₃ - 473 K	134	50CoB/ Al ₂ O ₃ - 573 K	112
40CoB/ Al ₂ O ₃ - 473 K	118	50CoB/ Al ₂ O ₃ - 673 K	115
50CoB/ Al ₂ O ₃ - 473 K	110	50CoB/ Al ₂ O ₃ - 773 K	71
60CoB/ Al ₂ O ₃ - 473 K	75	50CoB/Al ₂ O ₃ - 473 K	110
70CoB/ Al ₂ O ₃ - 473 K	65	50CoB/SiO ₂ - 473 K	113
80CoB/ Al ₂ O ₃ - 473 K	60	50CoB/MgO - 473 K	31
90CoB/ Al ₂ O ₃ - 473 K	56	Al ₂ O ₃	175
SiO ₂	180	MgO	41



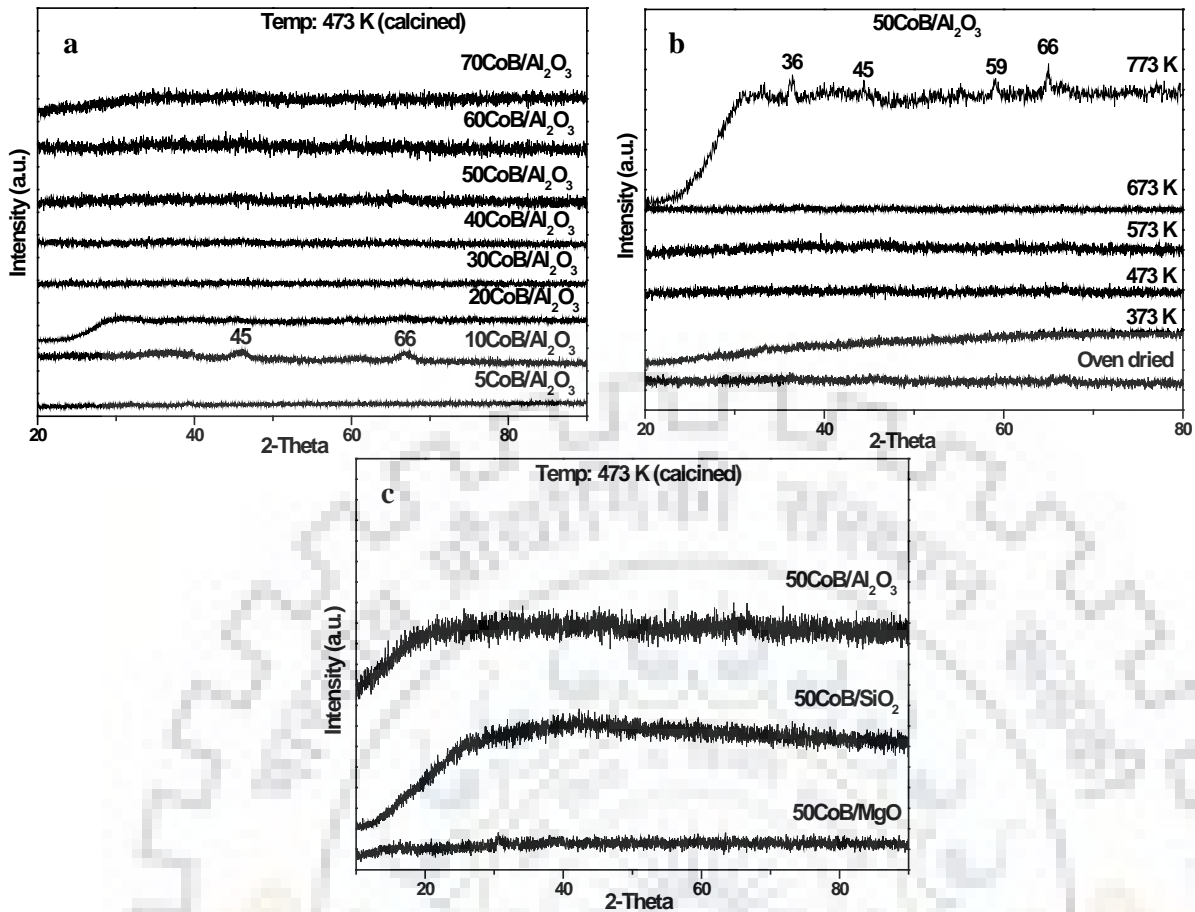


Fig.B1: X-ray diffraction patterns of a) $x\text{CoB}/\text{Al}_2\text{O}_3$ with different loading (of CoB) calcined at 473 K, b) $50\text{CoB}/\text{Al}_2\text{O}_3$ with various calcination temperature (T: oven dried to 773 K), and c) $50\text{CoB}/(\text{support})$ with various supports (SiO_2 , Al_2O_3 , MgO) calcined at 473 K. Where, x is wt percent of CoB in support (5 wt%, 10 wt%, 20 wt%, 30 wt%, 40 wt%, 50wt%, 60wt% and 70 wt%).

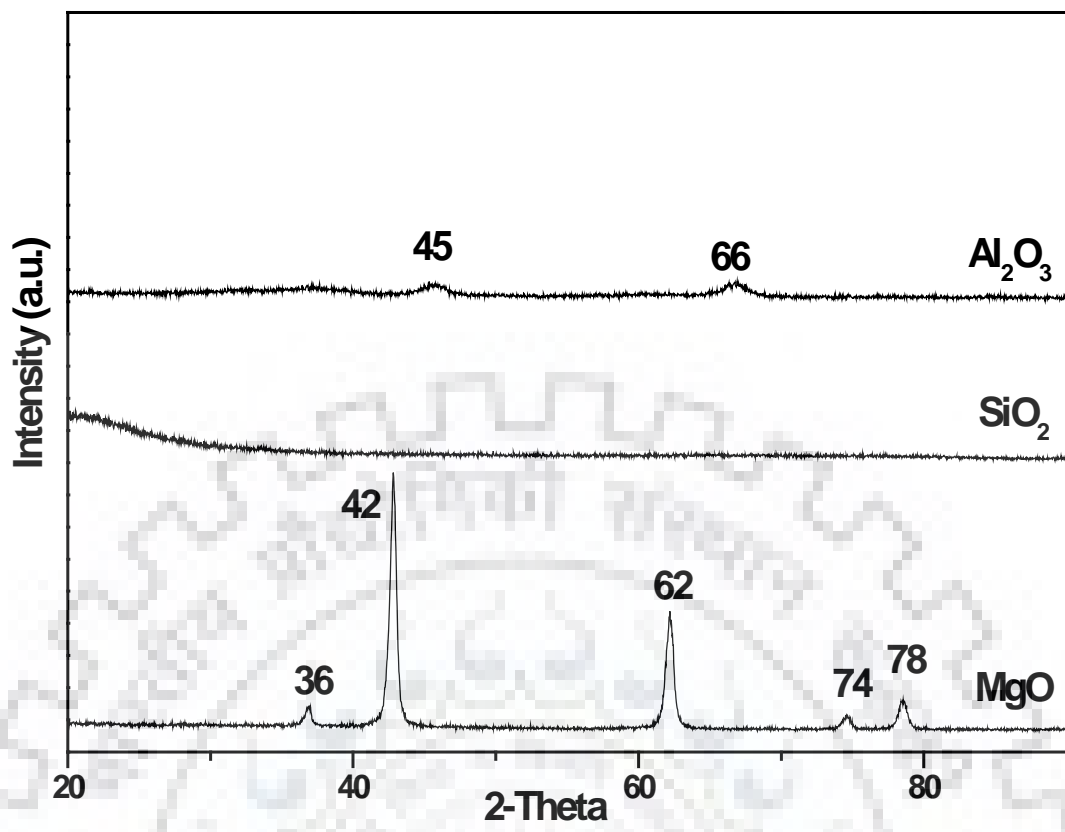


Fig.B2: X-ray diffraction patterns of various supports (MgO , SiO_2 and Al_2O_3).

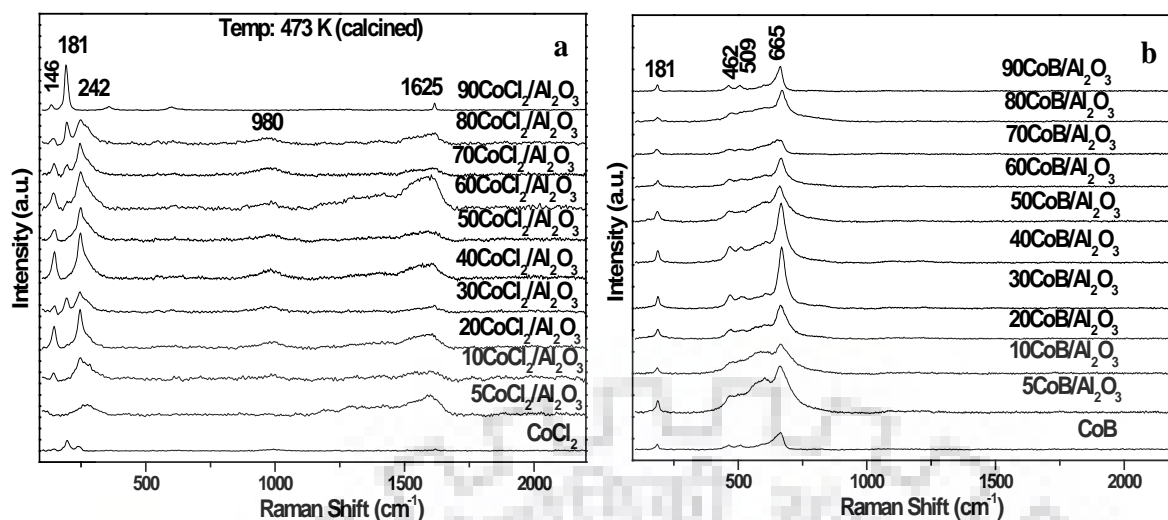


Fig.B3: The Raman spectra of a) $x\text{CoCl}_2/\text{Al}_2\text{O}_3$ samples calcined at 473 K for 2 h, b) after reduction with NaBH_4 solution of each catalyst reported in Fig.B3 a. Where, x is the wt percent of CoB in support (5 wt%, 10 wt%, 20 wt%, 30 wt%, 40 wt%, 50wt%, 60wt% 70wt%, 80wt% and 90 wt%).

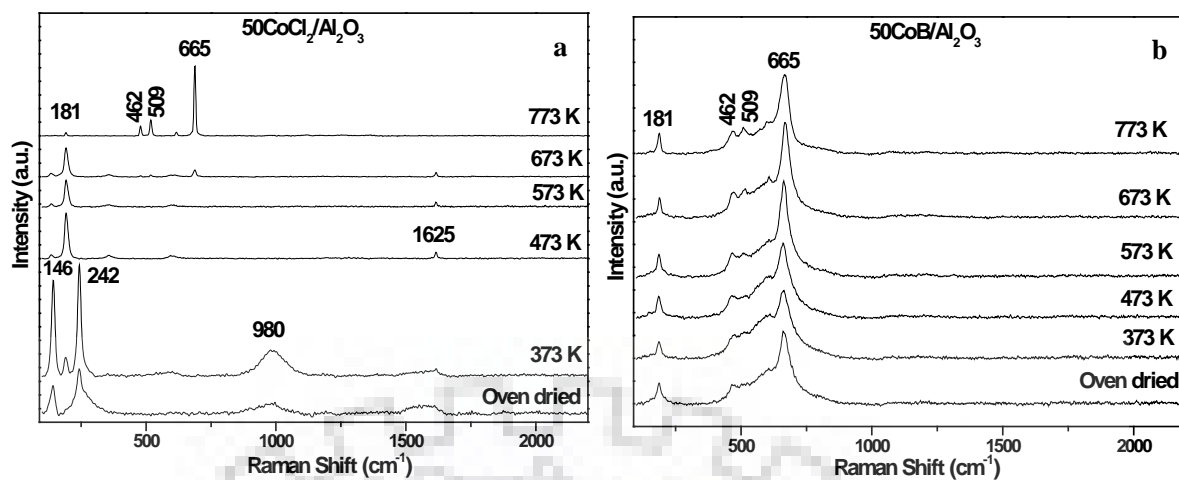


Fig.B4: The Raman spectra of a) 50CoCl₂/Al₂O₃ samples calcined at various temperature for 2 h, b) after reduction with NaBH₄ solution of each catalysts reported in Fig.B4 a. The calcinations temperature was varied from oven dried to 773 K.

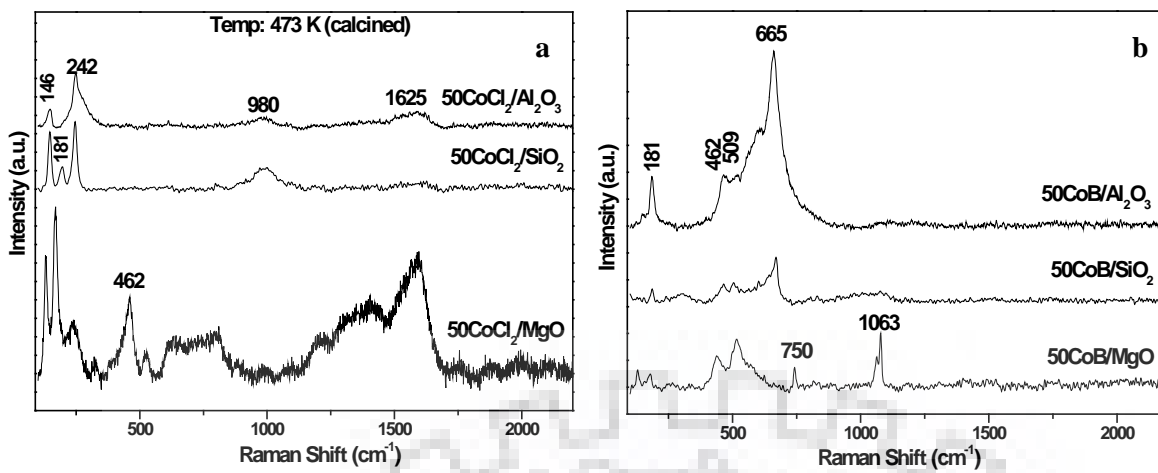


Fig.B5 The Raman spectra of a) 50CoCl₂/(support) samples calcined at 473 K, b) after reduction with NaBH₄ solution of each catalysts reported in Fig.B5 a. The supports used were SiO₂, Al₂O₃, and MgO.

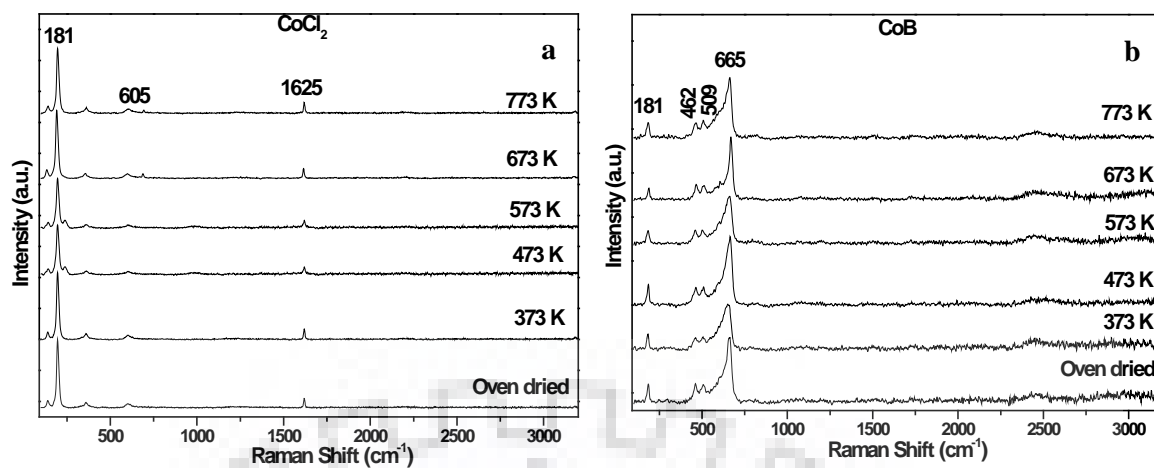


Fig.B6: The Raman spectra of a) CoCl_2 samples calcined at various temperature for 2 h, b) after reduction with NaBH_4 solution of each catalysts reported in Fig.B6 a. The calcinations temperature was varied from oven dried to 773 K.

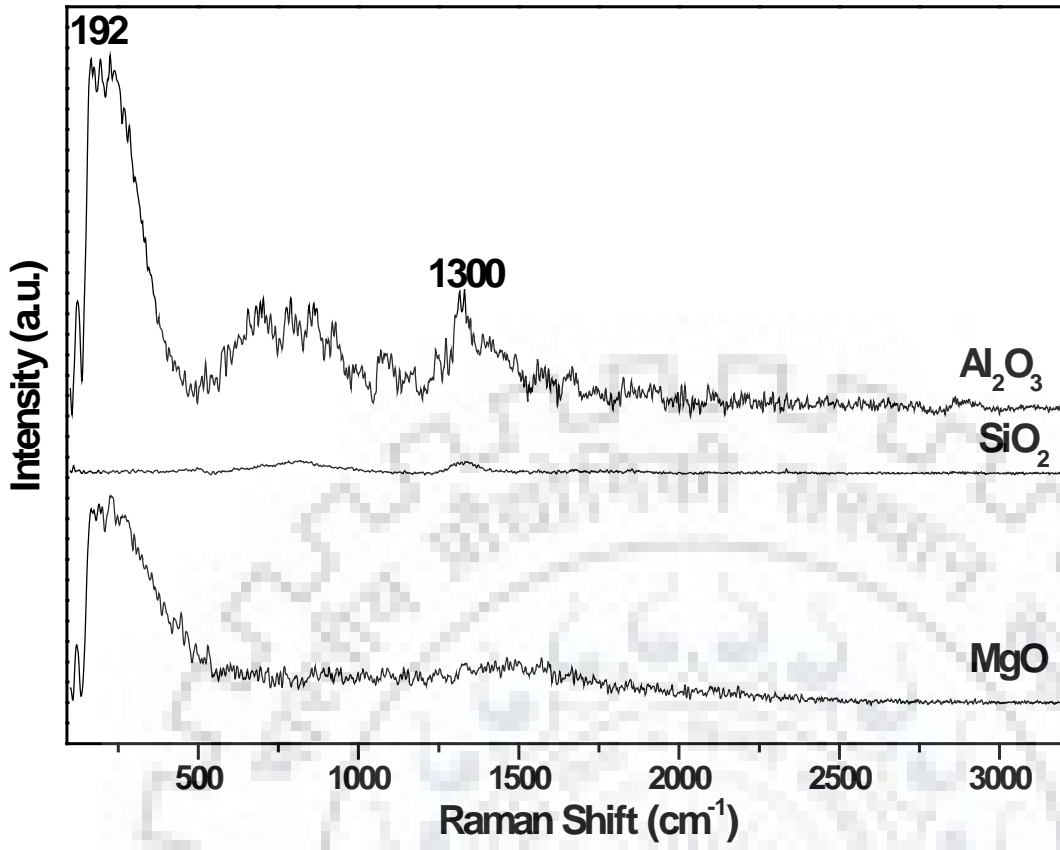


Fig.B7: The Raman spectra of various support (MgO , SiO_2 and Al_2O_3).

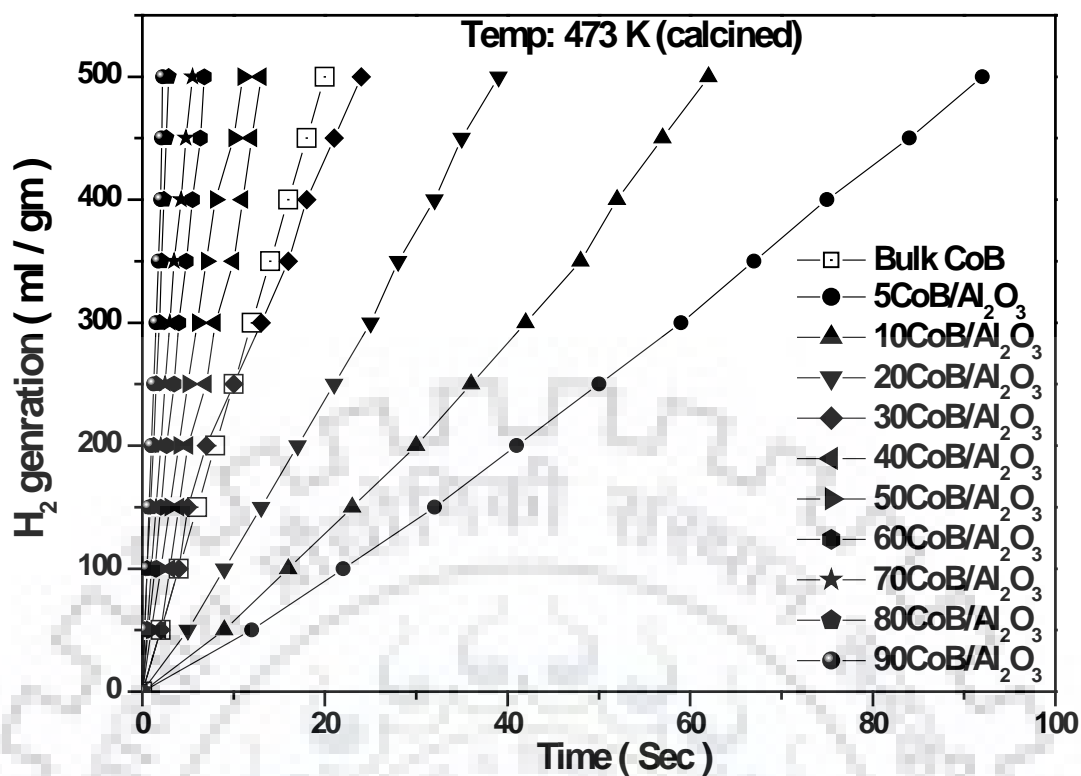


Fig.B8: The generation of hydrogen using $x\text{CoB}/\text{Al}_2\text{O}_3$ catalysts with changing total loading of CoB and bulk CoB catalyst. The generation of hydrogen study was conducted with the temperature at 303 K using 20 mg of catalyst calcined at 473 K. The total loading was varied from 5 wt% to 90 wt% of CoB in support.

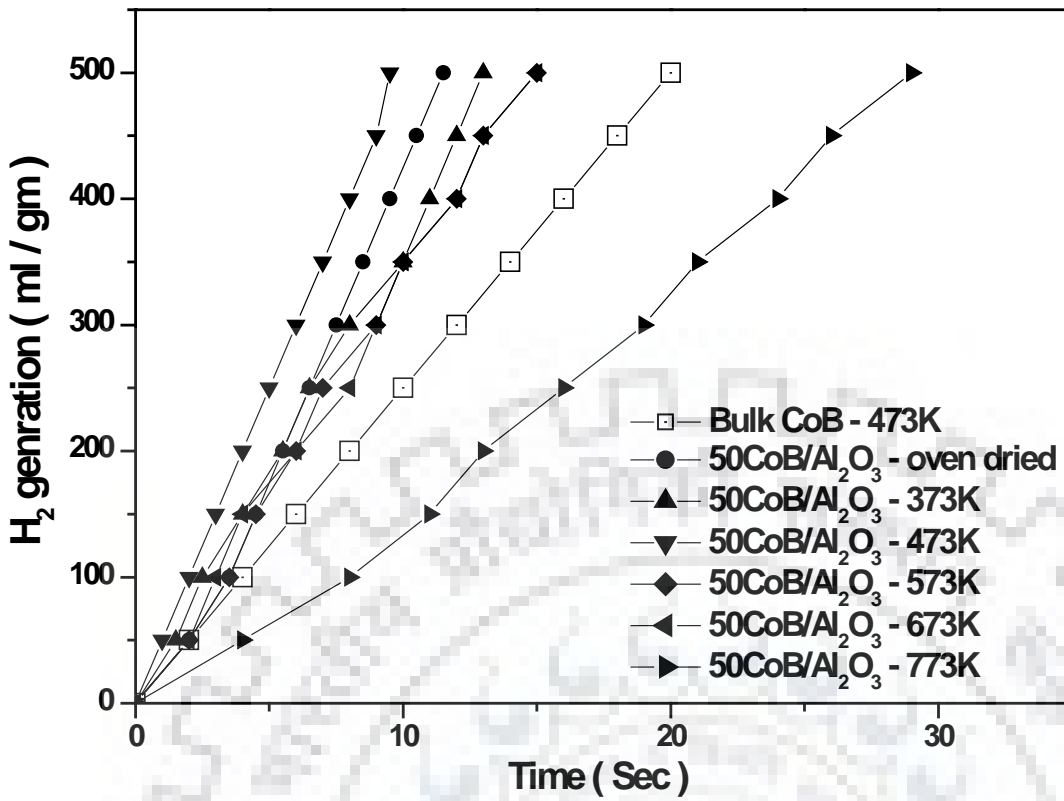


Fig.B9: The generation of hydrogen using 50CoB/Al₂O₃ catalyst with changing calcinations temperature from oven dried to 773 K. The generation of hydrogen study was conducted with the temperature at 303 K using 20 mg of catalyst.

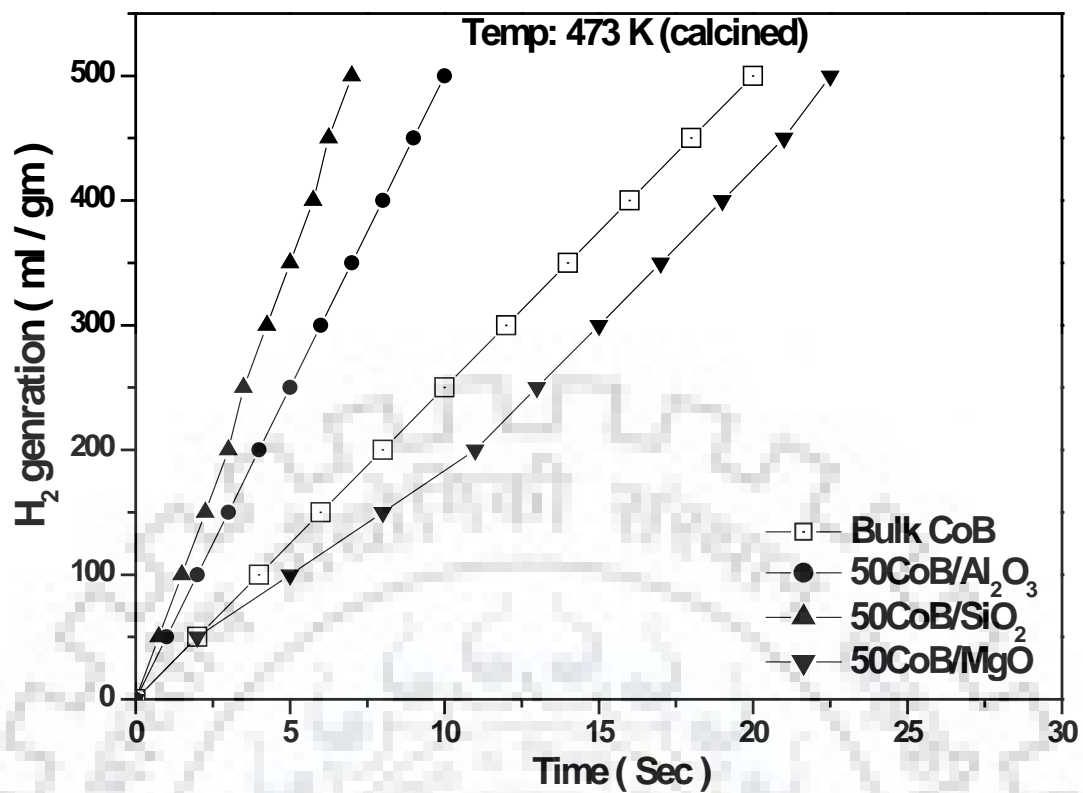


Fig.B10: The generation of hydrogen using 50CoB/(support) catalysts with changing supports (SiO₂, Al₂O₃, and MgO). The generation of hydrogen study was conducted with the temperature at 303 K using 20 mg of catalyst calcined at 473 K.

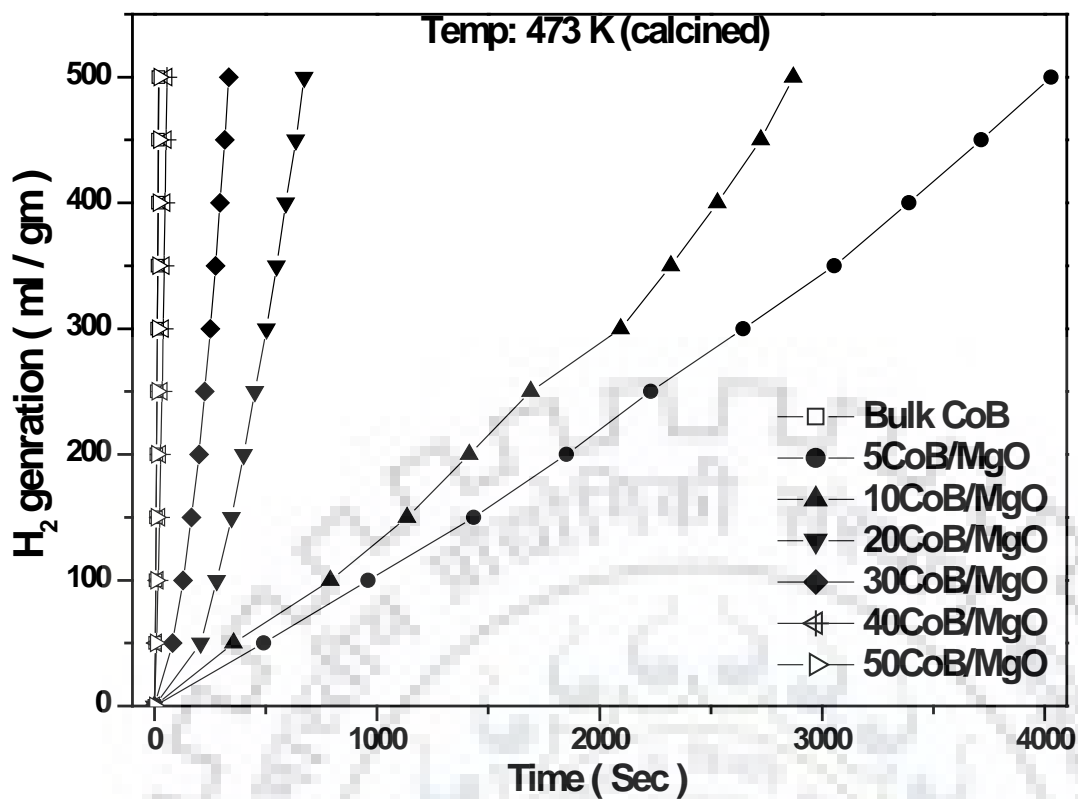


Fig.B11: The generation of hydrogen using xCoB/MgO catalysts with changing total loading of CoB and bulk CoB catalyst. The generation of hydrogen study was conducted with the temperature at 303 K using 20 mg of catalyst calcined at 473 K.

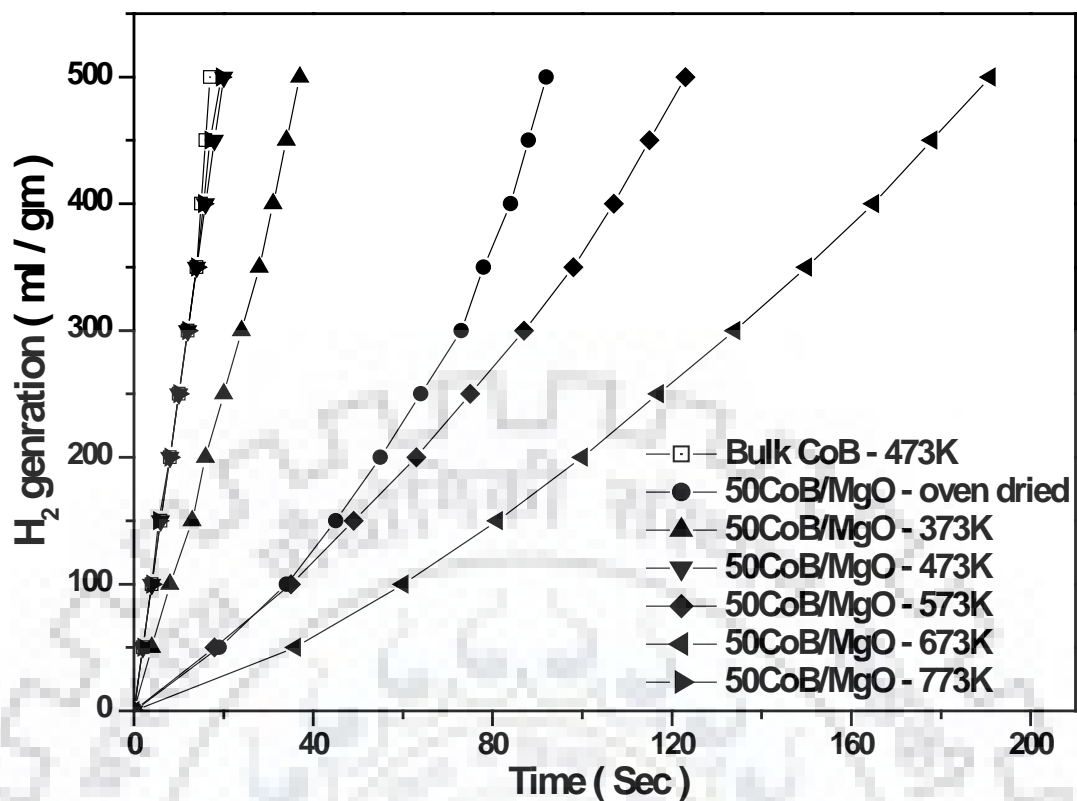


Fig.B12: The generation of hydrogen using 50CoB/MgO catalyst with changing calcinations temperature from oven dried to 773 K. The generation of hydrogen study was conducted with the temperature at 303 K using 20 mg of catalyst.

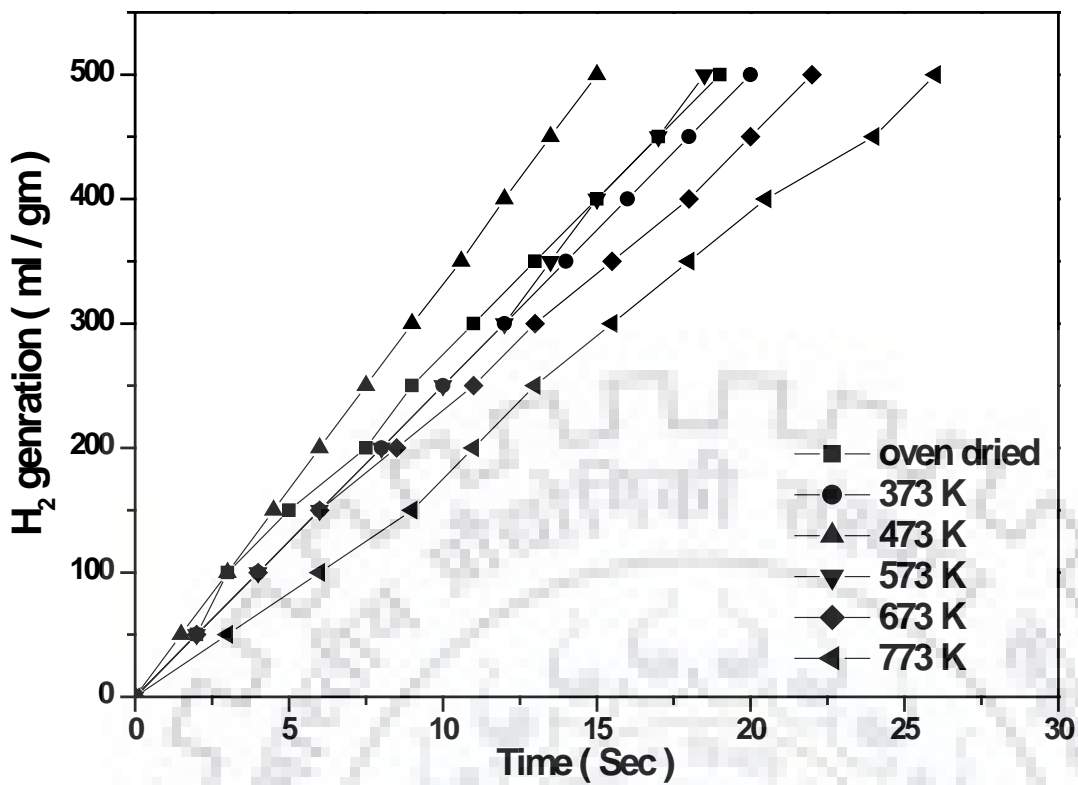


Fig.B13: The generation of hydrogen using bulk CoB catalyst with changing calcinations temperature from oven dried to 773 K. The generation of hydrogen study was conducted with the temperature at 303 K using 20 mg of catalyst.

Appendix-C

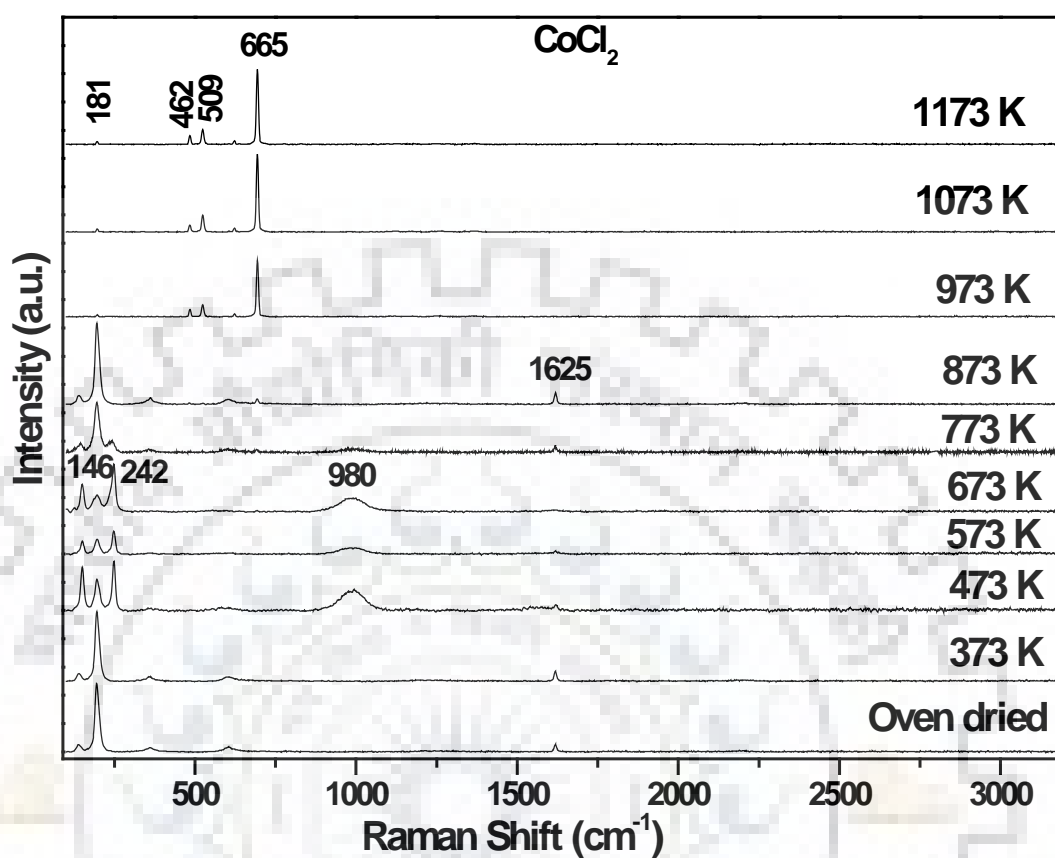


Fig. C1: The Raman spectra of CoCl_2 samples calcined at various temperatures. The calcinations temperature was varied from oven dried to 1173 K for 1 h at each temperature.

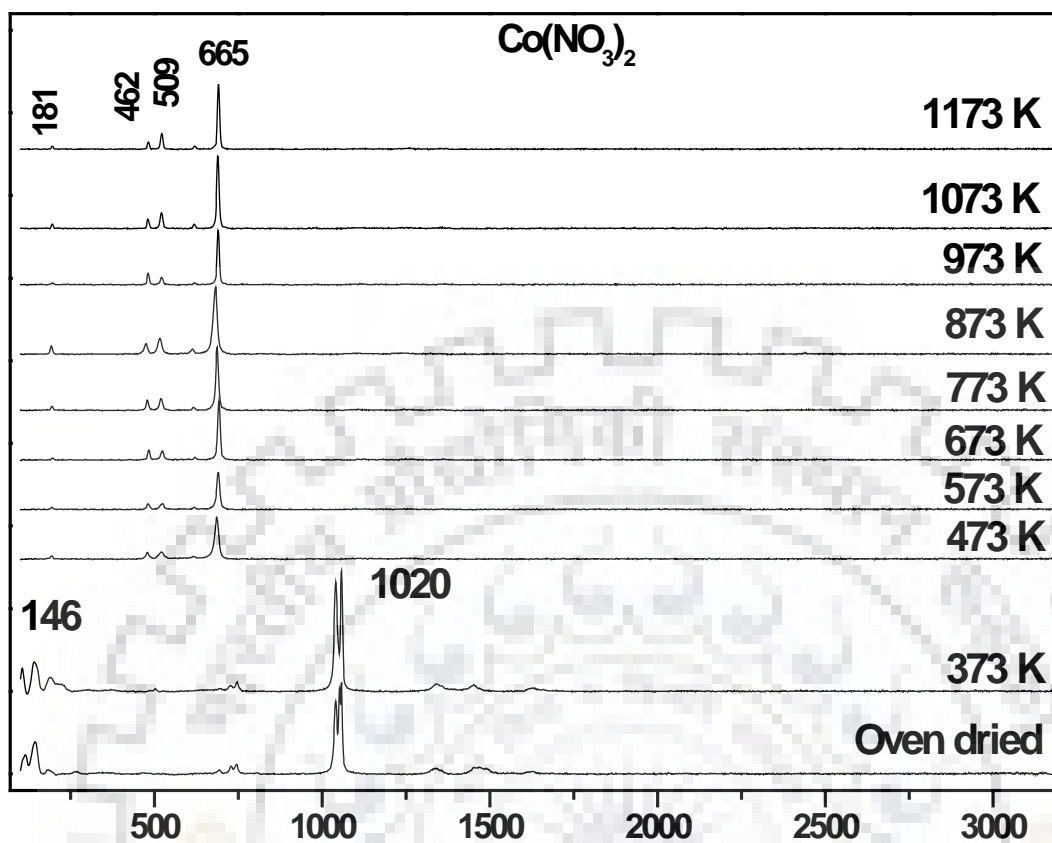


Fig. C2: The Raman spectra of $\text{Co}(\text{NO}_3)_2$ samples calcined at various temperatures. The calcinations temperature was varied from oven dried to 1173 K for 1 h at each temperature.

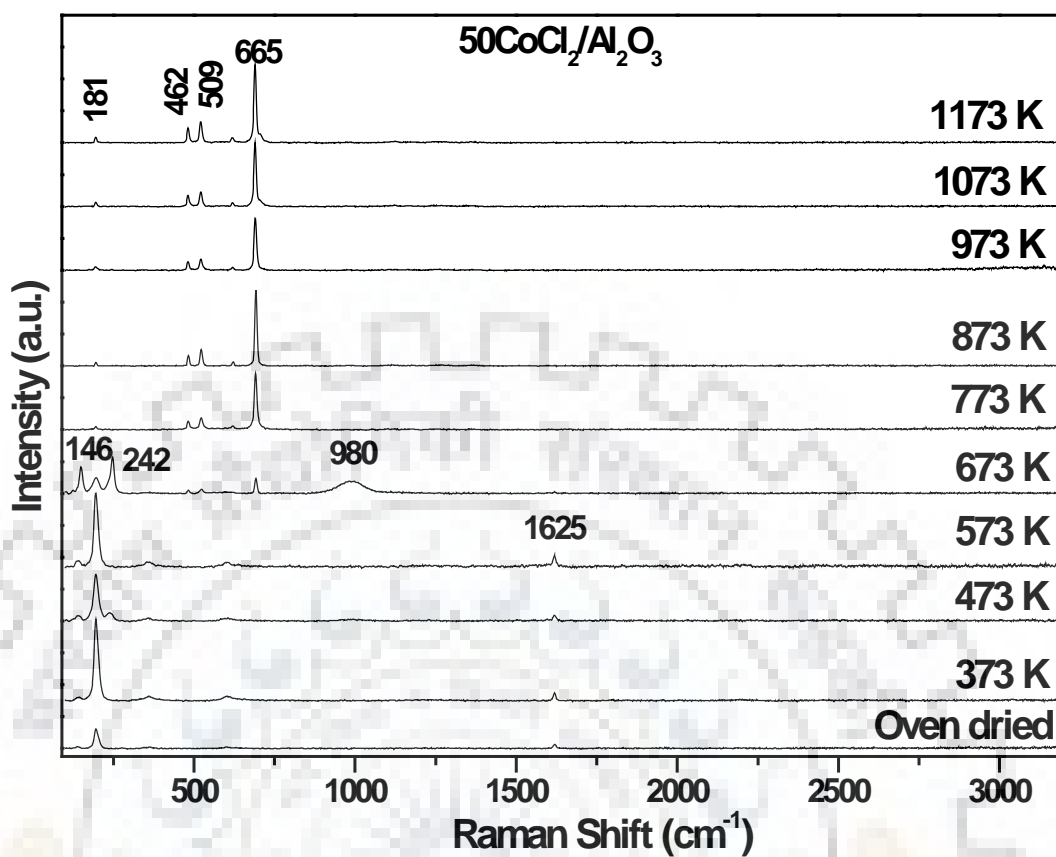


Fig. C3: The Raman spectra of 50CoCl₂/Al₂O₃ samples calcined at various temperatures. The calcinations temperature was varied from oven dried to 1173 K for 1 h at each temperature.

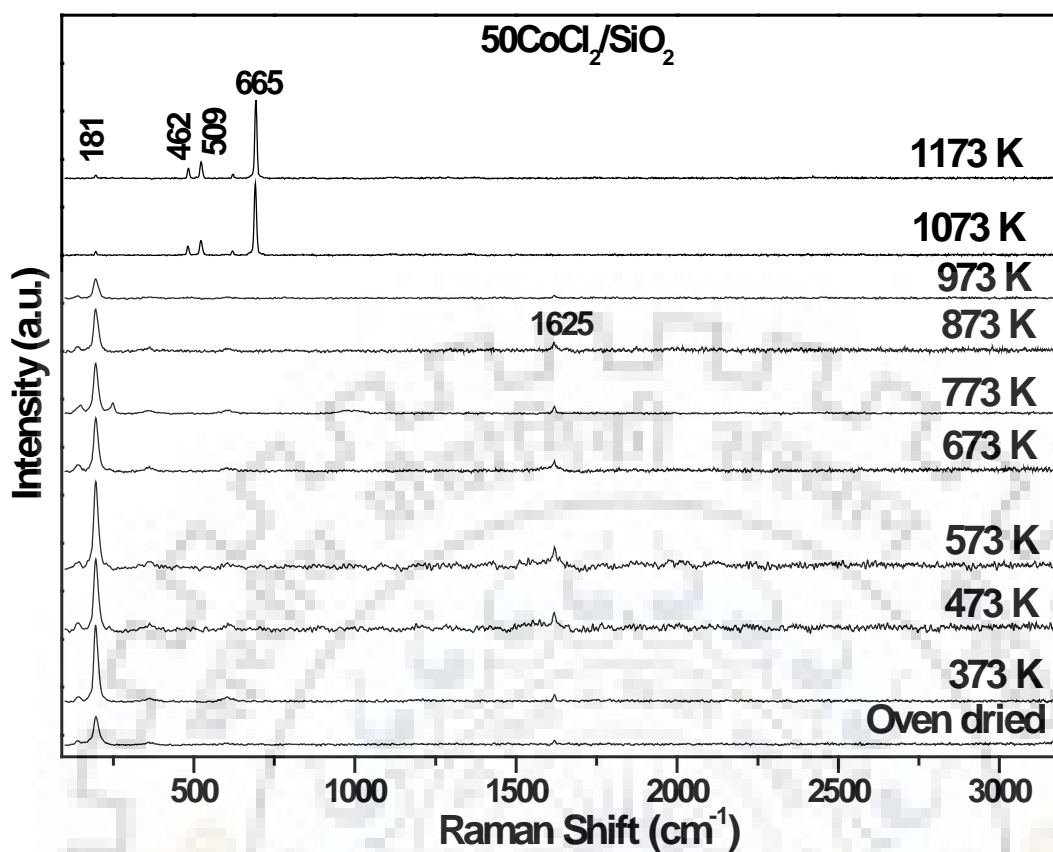


Fig. C4: The Raman spectra of 50CoCl₂/SiO₂ samples calcined at various temperatures. The calcinations temperature was varied from oven dried to 1173 K for 1 h at each temperature.

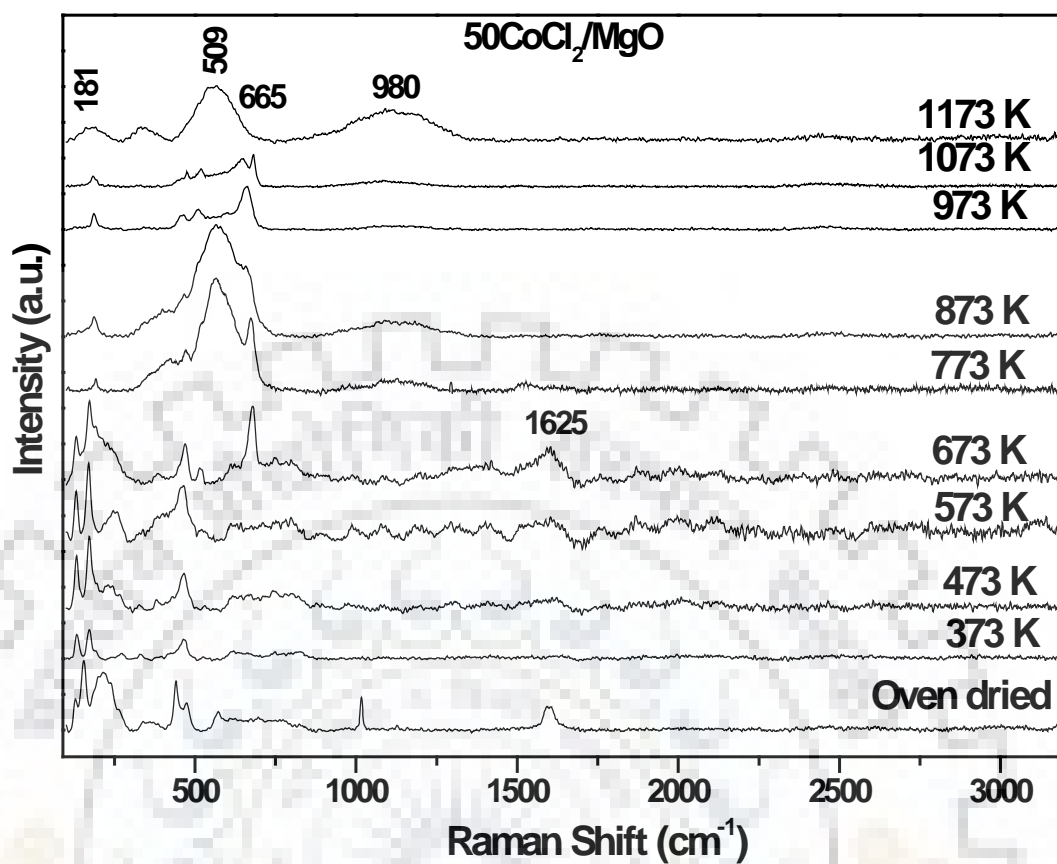


Fig. C5: The Raman spectra of $50\text{CoCl}_2/\text{MgO}$ samples calcined at various temperatures for 1 h at each temperature. The calcinations temperature was varied from oven dried to 1173 K.

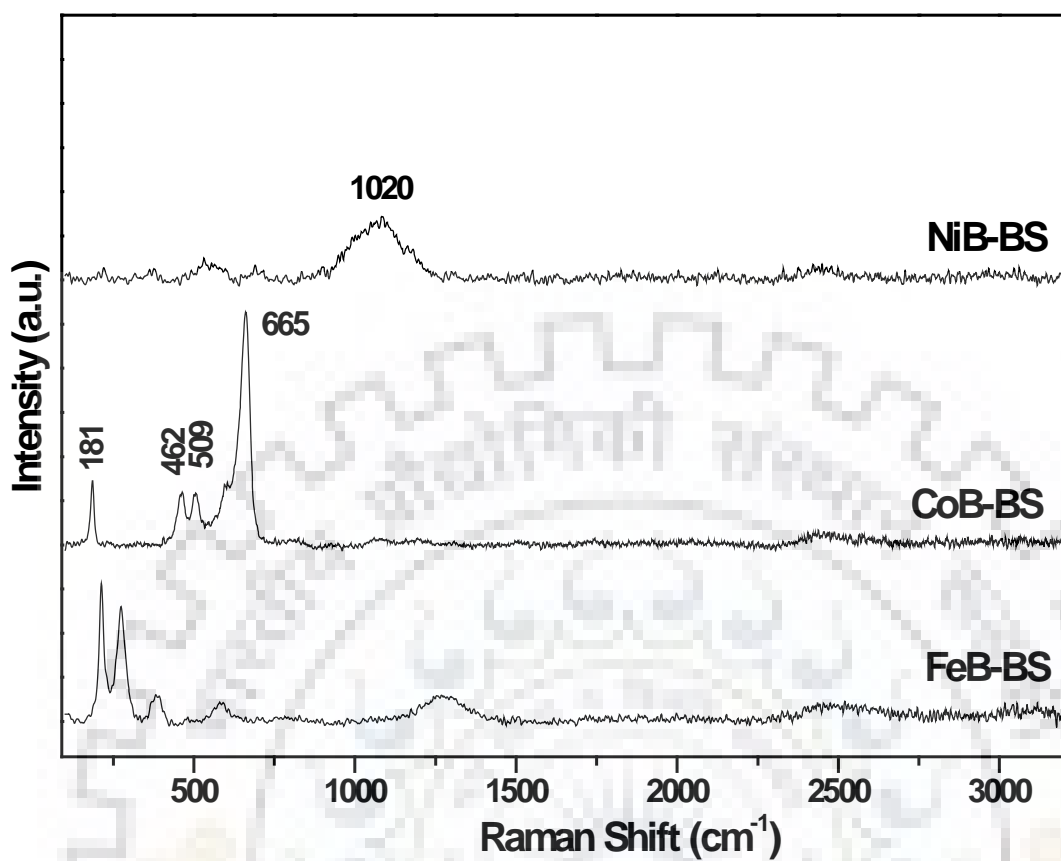


Fig. C6: The Raman spectra of the synthesized catalysts FeB-BS, CoB-BS, and NiB-BS catalysts.

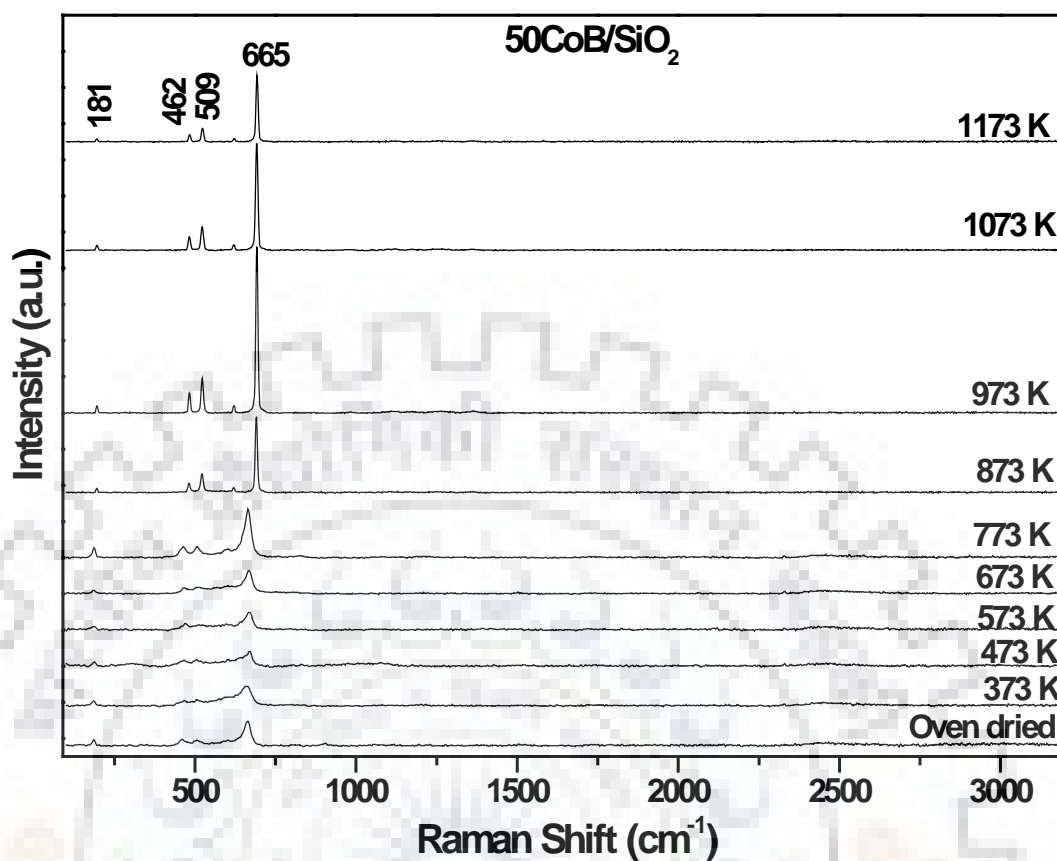


Fig. C7: The Raman spectra of 50CoCl₂/SiO₂ samples calcined at various temperatures followed by reduction with NaBH₄ solution of each catalyst. The final synthesized catalyst was denoted as 50CoB/SiO₂. The calcinations temperature was varied from oven dried to 1173 K for 1 h at each temperature.

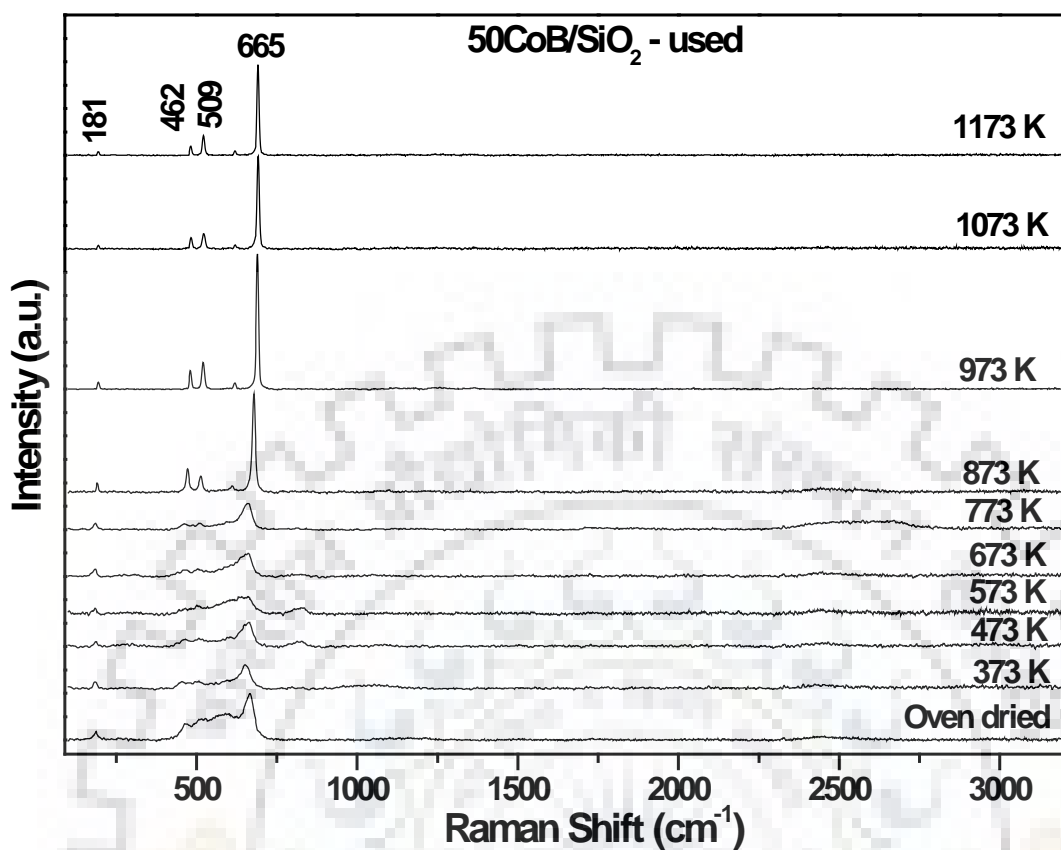


Fig. C8: The Raman spectra of the used samples shown in Fig.C7. The supported catalysts were synthesized (by calcined in air followed by reduction with NaBH₄ solution before use for the generation of hydrogen).

APPENDIX D

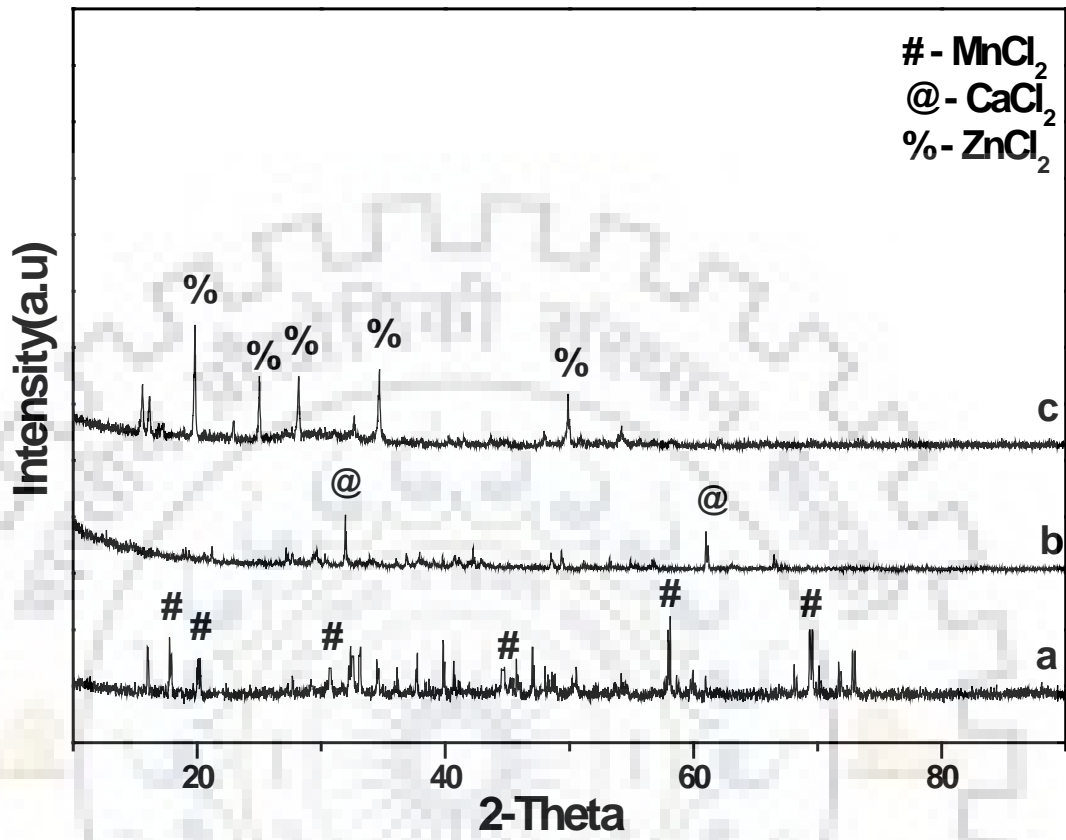


Figure D1: The XRD Patterns of various materials (a) MnCl_2 , (b) CaCl_2 and (c) ZnCl_2 . All of the materials were collected at room temperature.

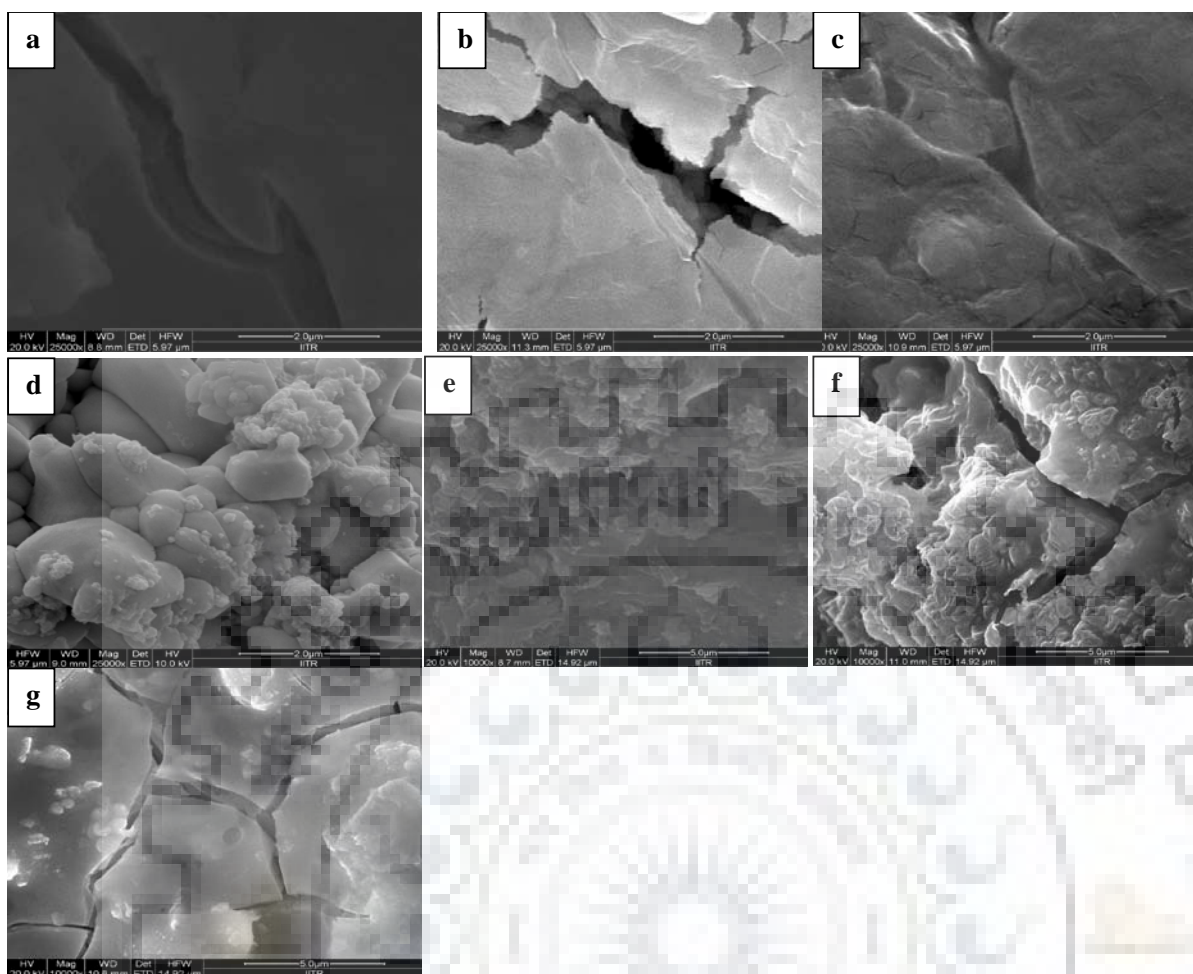


Figure D2: Field Emission Scanning Electron Microscopy (FE-SEM) images of various material (a) P-NaBH₄, (b) MnCl₂, (c) CaCl₂ and (d) ZnCl₂, (e) 20MnCl₂/NaBH₄, (f) 20CaCl₂/NaBH₄ and (g) 20ZnCl₂/NaBH₄.

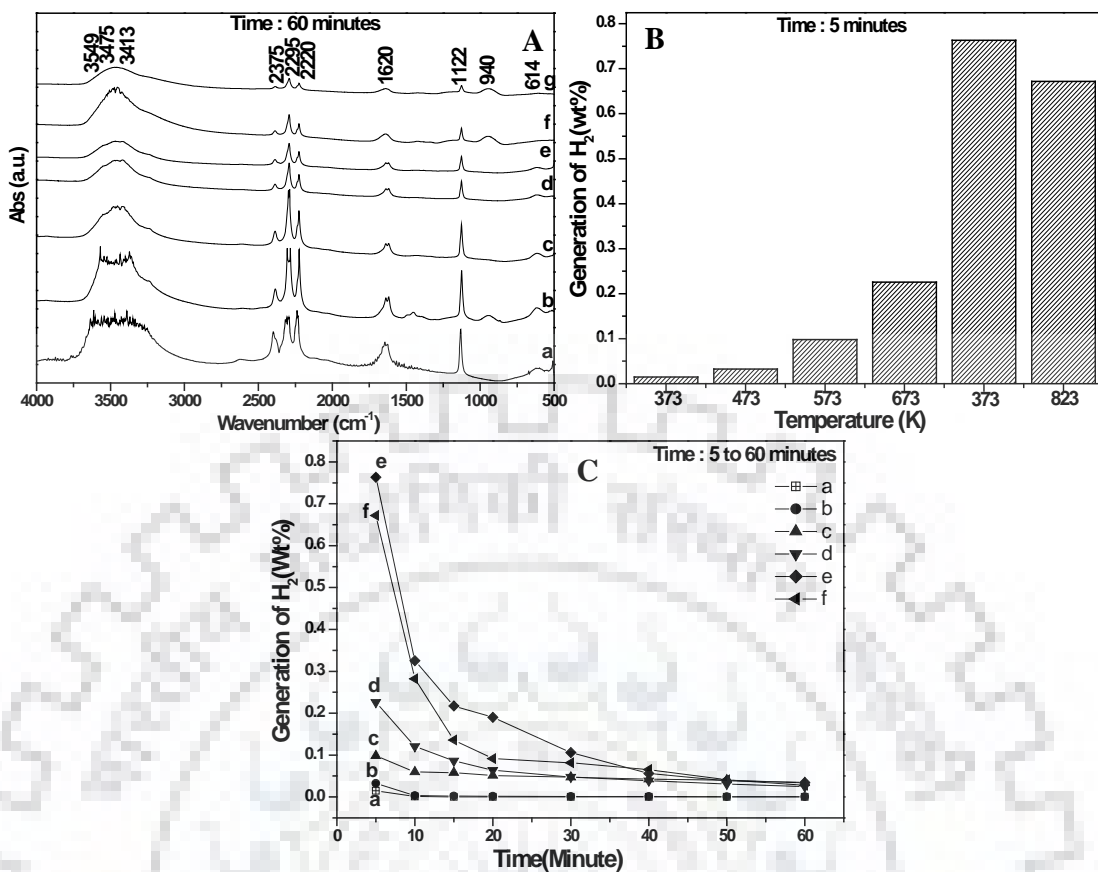


Figure D3: The FTIR spectra of $10\text{MnCl}_2/\text{NaBH}_4$ at various decomposition temperature with nitrogen gas flow through reactor (HVC-DRM-5) for 1 h at (a) 303 K, (b) 373 K, (c) 473 K, (d) 573 K, (e) 673 K, (f) 773 K and (g) 823 K, (B) The generation of hydrogen from $10\text{MnCl}_2/\text{NaBH}_4$ at different thermal decomposition temperature after 5 min, (C) The generation of hydrogen from $10\text{MnCl}_2/\text{NaBH}_4$ at different thermal decomposition temperature (a) 373 K, (b) 473 K, (c) 573 K, (d) 673 K, (e) 773 K and (f) 823 K.

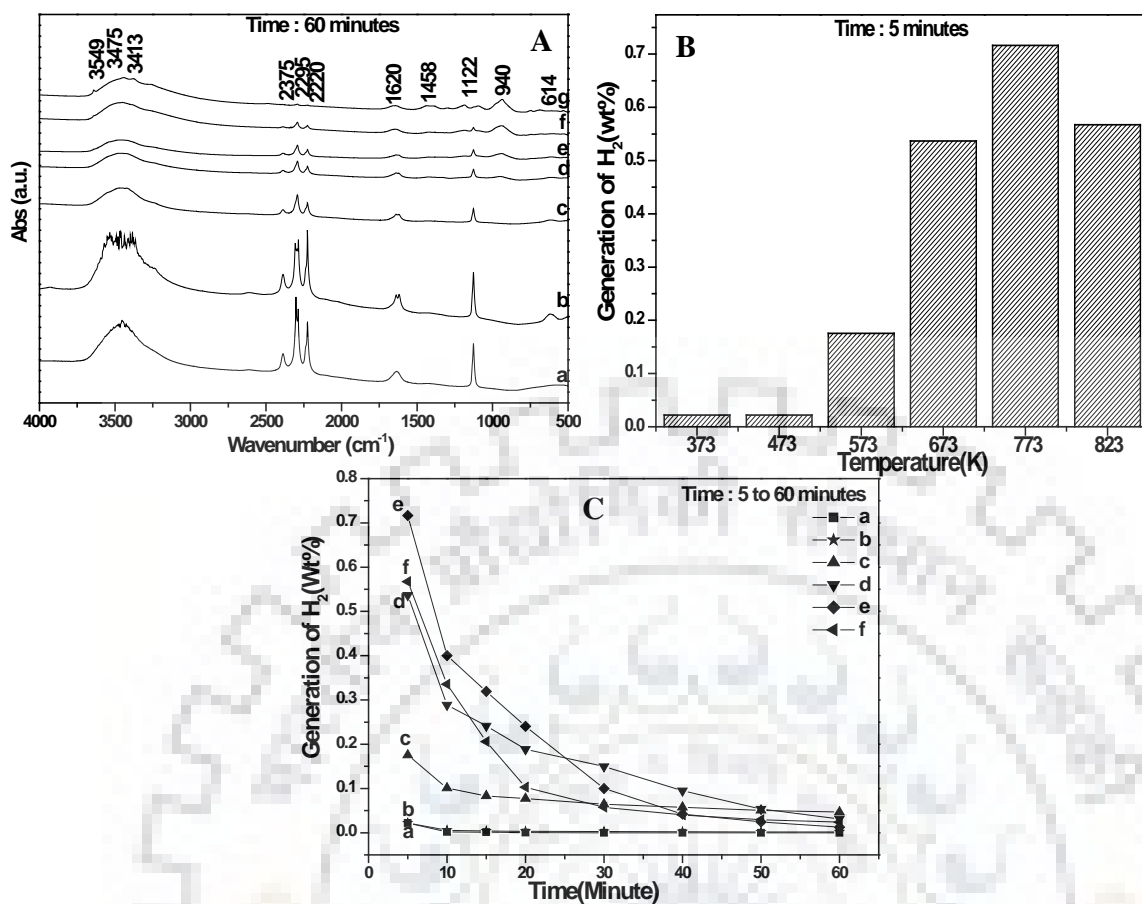


Figure D4: The FTIR spectra of $30\text{MnCl}_2/\text{NaBH}_4$ at various decomposition temperature with nitrogen gas flow through reactor (HVC-DRM-5) for 1 h at (a) 303 K, (b) 373 K, (c) 473 K, (d) 573 K, (e) 673 K, (f) 773 K and (g) 823 K, (B) The generation of hydrogen from $30\text{MnCl}_2/\text{NaBH}_4$ at different thermal decomposition temperature after 5 min, (C) The generation of hydrogen from $30\text{MnCl}_2/\text{NaBH}_4$ at different thermal decomposition temperature (a) 373 K, (b) 473 K, (c) 573 K, (d) 673 K, (e) 773 K and (f) 823 K.

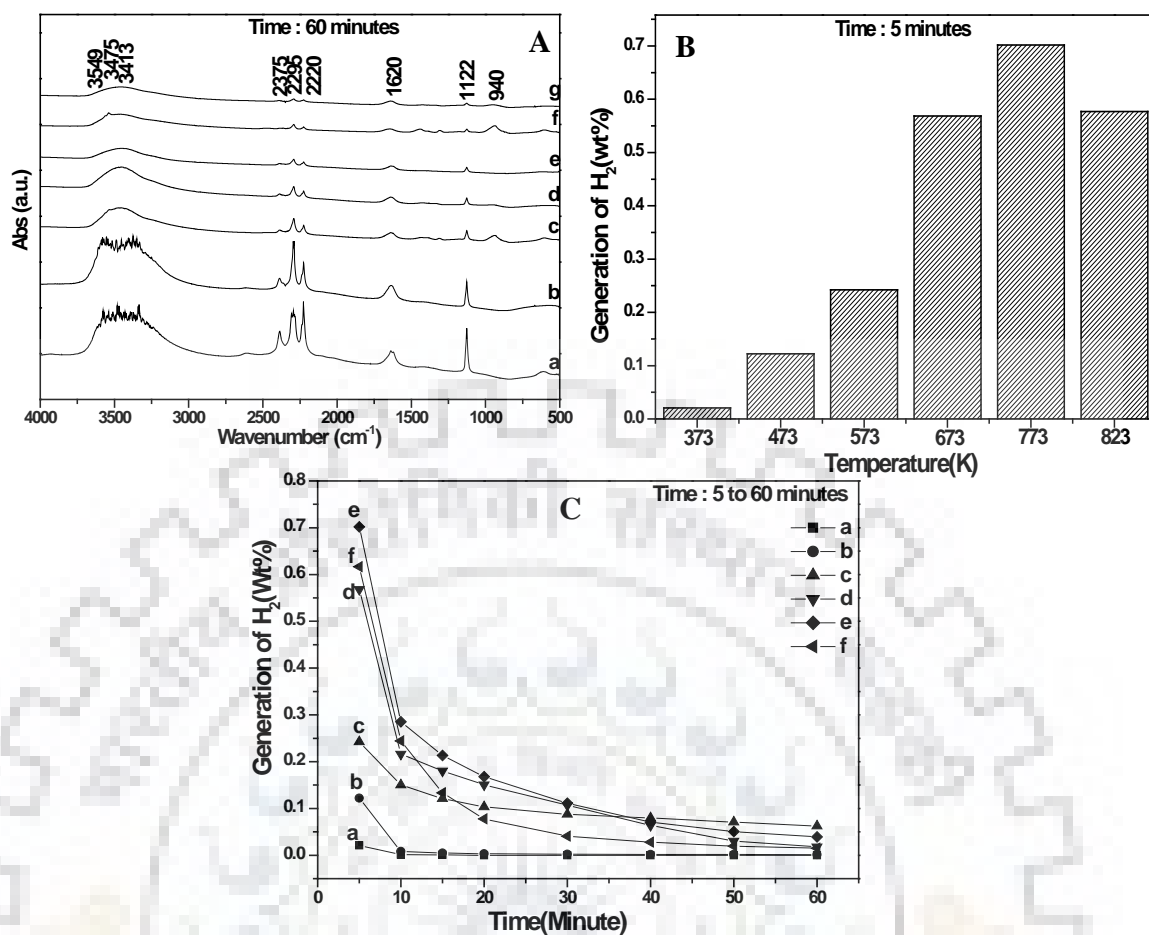


Figure D5: The FTIR spectra of $40\text{MnCl}_2/\text{NaBH}_4$ at various decomposition temperature with nitrogen gas flow through reactor (HVC-DRM-5) for 1 h at (a) 303 K, (b) 373 K, (c) 473 K, (d) 573 K, (e) 673 K, (f) 773 K and (g) 823 K, (B) The generation of hydrogen from $40\text{MnCl}_2/\text{NaBH}_4$ at different thermal decomposition temperature after 5 min, (C) The generation of hydrogen from $40\text{MnCl}_2/\text{NaBH}_4$ at different thermal decomposition temperature (a) 373 K, (b) 473 K, (c) 573 K, (d) 673 K, (e) 773 K and (f) 823 K.

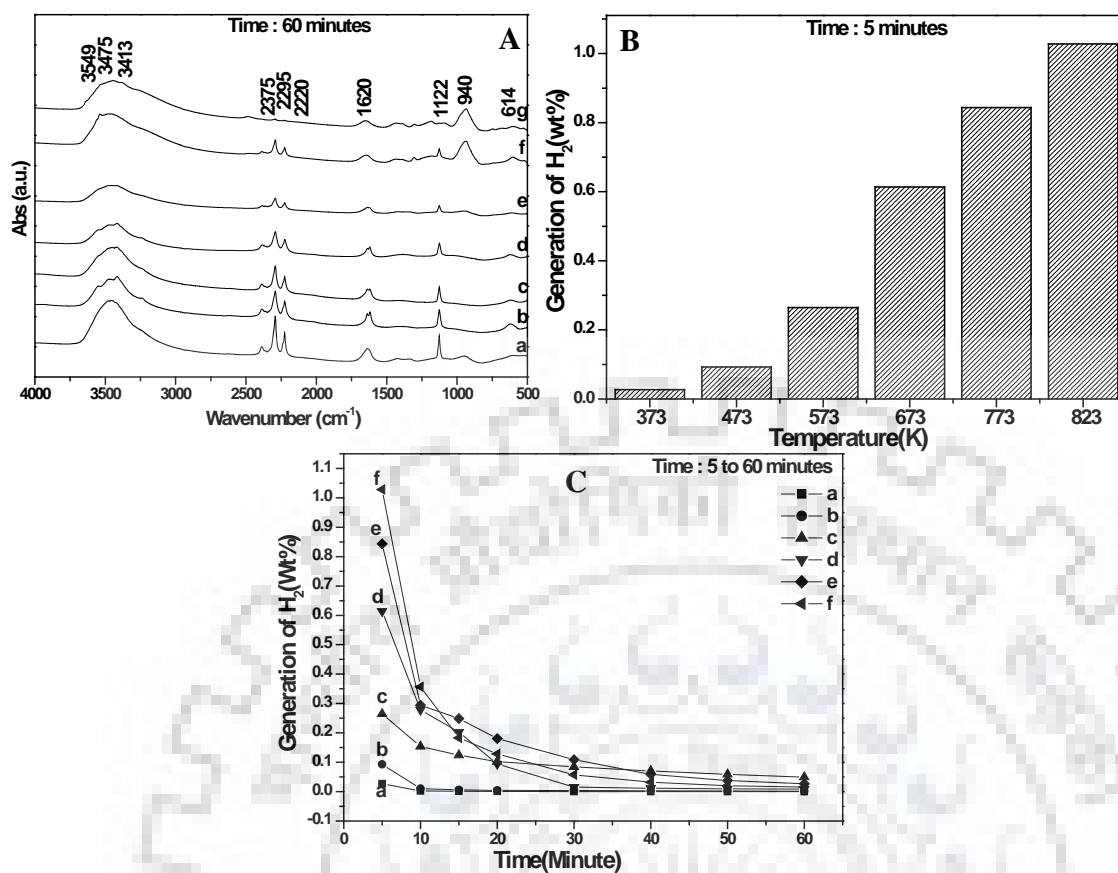


Figure D6: The FTIR spectra of $50\text{MnCl}_2/\text{NaBH}_4$ at various decomposition temperature with nitrogen gas flow through reactor (HVC-DRM-5) for 1 h at (a) 303 K, (b) 373 K, (c) 473 K, (d) 573 K, (e) 673 K, (f) 773 K and (g) 823 K, (B) The generation of hydrogen from $50\text{MnCl}_2/\text{NaBH}_4$ at different thermal decomposition temperature after 5 min, (C) The generation of hydrogen from $50\text{MnCl}_2/\text{NaBH}_4$ at different thermal decomposition temperature (a) 373 K, (b) 473 K, (c) 573 K, (d) 673 K, (e) 773 K and (f) 823 K.

Appendix-E

Calculations for Hydrolysis of NaBH_4 :

Hydrogen generation rate was measured using water displacement method. The figure described in chapter-2. Hydrogen was measured against time.

Catalyst pallet was taken ~10 mg (CoB-BS)

Time (sec)	Volume (ml)	H_2 generation (ml/gm)
0	0	0
30	1.3	130
60	3.3	330
90	5.3	530
120	7.8	780
143	9.6	960

Above data was ml/mg but it has been converted in to ml/gm so the hydrogen generation $1.3 \text{ ml} * 100 = 130 \text{ ml}$.

Similarly, the calculation was done for other catalysts also:

CoB-BS		NiB-BS		FeB-BS	
Time (sec)	H_2 generation (ml/gm)	Time (sec)	H_2 generation (ml/gm)	Time (sec)	H_2 generation (ml/gm)
0	0	0	0	0	0
30	130	1320	130	540	130
60	330	2400	330	2940	360
90	530	3240	520	4620	540
120	780	4080	790	6060	780
143	960	4560	960	7080	970

Calculations for Thermolysis of NaBH₄:

The complete hydrogen desorption reaction of NaBH₄ can be expressed as follows:



37.83 gm 4.032 gm

Basis: 0.055 gm NaBH₄

Weight of hydrogen gas in 1gm of NaBH₄ = 0.1060 gm of H₂ gas

So, weight of hydrogen gas in 0.055gm of NaBH₄ = 5.862×10^{-3} gm of H₂ gas

Weight of hydrogen gas in 0.055gm of NaBH₄ with 97% purity = 5.7097×10^{-3} gm of H₂ gas

As we know that at STP 1mol of a H₂ gas containing 22.4 ltr volume of gas

22.4 ltr of H₂ gas having weight = 2.016 gm

1 ltr of H₂ gas having weight = 0.09 gm

So, weight of 1ml of hydrogen gas = 0.09×10^{-3} gm of H₂ gas

Area in 1 ml of pure hydrogen gas in GC = 4245645.583 unit square

i.e., 4245645.583 area of 1ml hydrogen gas in GC = 0.09×10^{-3} gm of H₂ gas

Weight of hydrogen gas desorbed from 0.055 gm of p-NaBH₄ at different reaction temperature is

$$= \frac{0.09 \times 10^{-3}}{4245645.583} \times \text{Area obtained from GC}$$

Wt% of hydrogen gas desorbed from 0.055 gm of p-NaBH₄ / or mixed with metal additives (MnCl₂, CaCl₂ and ZnCl₂) at different reaction temperature

$$= \frac{\text{wt. of hydrogen gas obtained in 1ml of reacted gas sample}}{\text{wt. of hydrogen gas in 0.055 gm of sodium borohydride}} \times 100$$

Calibration curve plot:

So, 2968448.313 area of 0.70 ml of pure hydrogen gas in GC having hydrogen gas wt

$$= \frac{0.09 \times 10^{-3}}{4245645.583} \times 2968448.313$$

= 0.06298×10^{-3} gm of H₂ gas

2088548.542 area of 0.50 ml of pure hydrogen gas in GC having H₂ gas wt = 0.0443×10^{-3} gm

1231620.917 area of 0.30 ml of pure hydrogen gas in GC having H₂ gas wt = 0.026×10^{-3} gm

843880.877 area of 0.20 ml of pure hydrogen gas in GC having H₂ gas wt = 0.0179×10^{-3} gm

Similarly, we had calculated the weight of hydrogen gas release at different temperature obtained from GC. Following graph showing that weight calculation obtained at different volume of hydrogen gas from GC area is correct.

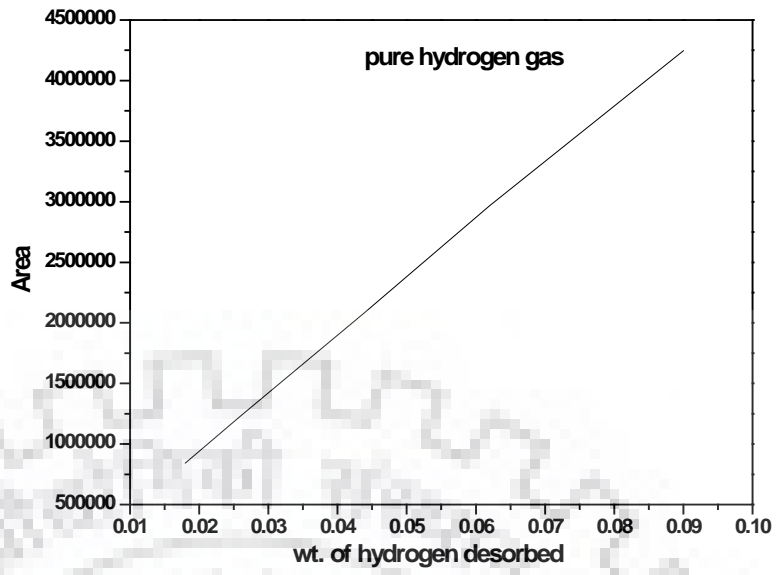
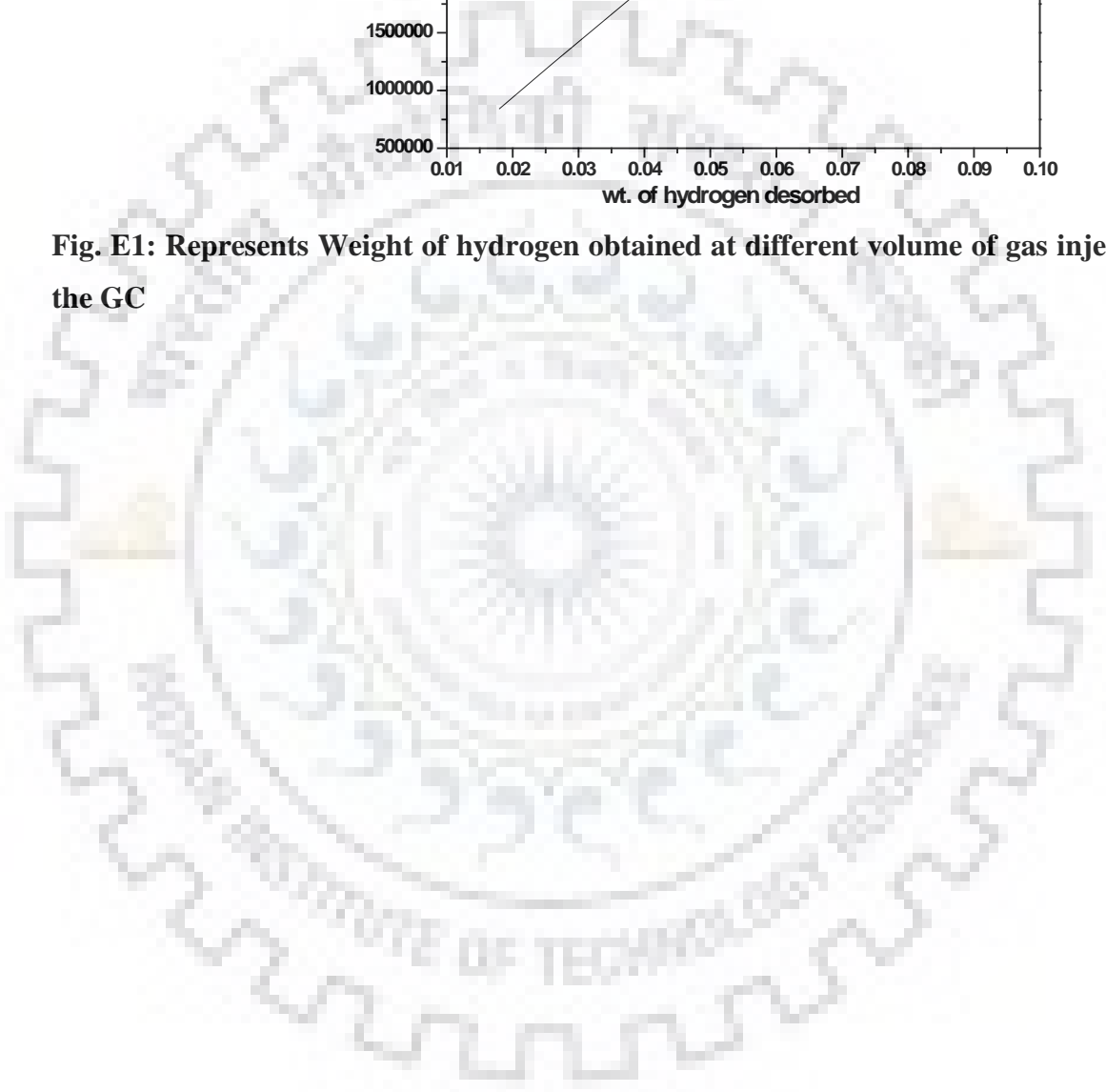


Fig. E1: Represents Weight of hydrogen obtained at different volume of gas injected into the GC



List of Tables

Table.E1: Generation of H₂ (wt%) from 0.055 gm weight of p-NaBH₄ sample in small HVC-DRM-5 reactor after 5 minute at each temperature from 373 K to 823 K as listed above in the table.

Temperature (K)	Area of H ₂ generated using Gas Chromatograph	Weight of H ₂ gas Release (gm)	Generation of H ₂ (wt%) from p-NaBH ₄
373 K	0	0	0
473 K	11836.05	2.51E-07	0.004394
573 K	28059.25	5.95E-07	0.010417
673 K	106609.75	2.26E-06	0.039581
773 K	224053.906	4.75E-06	0.083184
823 K	313523.188	6.65E-06	0.116401

Sample Calculations:

Weight of hydrogen gas desorbed from 0.055 gm of p-NaBH₄ at different reaction temperature is

$$= \frac{0.09 \times 10^{-3}}{4245645.583} \times \text{Area obtained from GC}$$

Weight of H₂ release from NaBH₄ after 5 minute of reaction at 473K = $\frac{0.09 \times 10^{-3}}{4245645.583} \times$

11836.05

$$= 2.51 \times 10^{-7} \text{ gm}$$

Wt% of hydrogen gas desorbed from 0.055 gm of p-NaBH₄ /or mixed with MnCl₂ at different reaction temperature

$$= \frac{\text{wt of hydrogen gas obtained in 1ml of reacted gas sample}}{\text{wt. of hydrogen gas in 0.055 gm of sodium boro hydride}} \times 100$$

$$\text{Weight percentage of H}_2 \text{ released after 5 minute at 473K from NaBH}_4 = \frac{2.51 \times 10^{-7}}{5.7097 \times 10^{-3}} \times 100$$

$$= 0.004394 \text{ wt\%}$$

Table.E2: Generation of H₂ (wt%) from 0.055 gm weight of 20MnCl₂/NaBH₄ sample in small HVC-DRM-5 reactor after 5 minute at each temperature from 373 K to 823 K as listed above in the table.

Temperature (K)	Generation of H ₂ (wt%)
373 K	0.031003479
473 K	0.025111597
573 K	0.255413342
673 K	0.75688182
773 K	0.879230249
823 K	0.951168191

Table.E3: Generation of H₂ (wt%) from 0.055 gm weight of 20ZnCl₂/NaBH₄ sample in small HVC-DRM-5 reactor after 5 minute at each temperature from 373 K to 823 K as listed above in the table.

Temperature (K)	Generation of H ₂ (wt%)
373 K	0.028707754
473 K	0.007549105
573 K	0.031054326
673 K	0.076199319
773 K	0.38680475
823 K	0.373605306

Table.E4: Generation of H₂ (wt%) from 0.055 gm weight of 20CaCl₂/NaBH₄ sample in small HVC-DRM-5 reactor after 5 minute at each temperature from 373 K to 823 K as listed above in the table.

Temperature (K)	Generation of H ₂ (wt%)
373 K	0.037703127
473 K	0.024714346
573 K	0.048576237
673 K	0.069877543
773 K	0.30301868
823 K	0.683420061

Table.E5: Generation of H₂ (wt%) from 0.055 gm weight of xMnCl₂/NaBH₄, 20ZnCl₂/NaBH₄, 20CaCl₂/NaBH₄ and p-NaBH₄ sample in small HVC-DRM-5 reactor after 5 minute at 373 K temperature.

Sample	Generation of H₂ (wt%)
p-NaBH ₄	0
10MnCl ₂ /NaBH ₄	0.014594439
20MnCl ₂ /NaBH ₄	0.031003479
30MnCl ₂ /NaBH ₄	0.021774171
40MnCl ₂ /NaBH ₄	0.020797519
50MnCl ₂ /NaBH ₄	0.02718846
20ZnCl ₂ /NaBH ₄	0.028707754
20CaCl ₂ /NaBH ₄	0.037703127

Table.E6: Generation of H₂ (wt %) from 0.055 gm weight of p-NaBH₄ at different temperature and time as given in the table.

Time (Minute)	Generation of H ₂ (wt%)					
	373 K	473 K	573 K	673 K	773 K	823 K
5	0	0.004394	0.010417	0.039581	0.083184	0.116401
10	0	0.001482	0.007785	0.024346	0.055421	0.10025
15	0	0.001319	0.005449	0.014843	0.041724	0.09075
20	0	0.000732	0.003208	0.009678	0.031844	0.05662
30	0	0.000484	0.001815	0.006397	0.023605	0.01973
40	0	0.000399	0.001009	0.005047	0.021371	0.00921
50	0	0.000328	0.000829	0.00438	0.01993	0.00636
60	0	0.000273	0.000661	0.003658	0.017203	0.00424

Table.E7: Generation of H₂ (wt%) from 0.055 gm weight of 20MnCl₂/NaBH₄ at different temperature and time as given in the table.

Time (Minute)	Generation of H ₂ (wt%)					
	373 K	473 K	573 K	673 K	773 K	823 K
5	0.031003479	0.025111597	0.255413342	0.75688182	0.879230249	0.951168191
10	0.001546732	0.003492836	0.12650523	0.336004109	0.372495011	0.409621637
15	0.000750738	0.002337307	0.084579652	0.246054973	0.074933301	0.109307504
20	0.000547061	0.001680388	0.059294731	0.246054973	0.041203501	0.048691999
30	0.000323707	0.001441033	0.048822128	0.125424068	0.013955454	0.028835247
40	0.000241527	0.001218496	0.047277231	0.066435463	0.009951235	0.020069856
50	0	0.001101621	0.042670078	0.031217886	0.006108379	0.013274587
60	0	0.000983893	0.038814402	0.019252607	0.004497371	0.01016941

Table.E8: Generation of H₂ (wt %) from 0.055 gm weight of 20ZnCl₂/NaBH₄ at different temperature and time as given in the table.

Time (Minute)	Generation of H ₂ (wt%)					
	373 K	473 K	573 K	673 K	773 K	823 K
5	0.02870775 4	0.007549105	0.031054326	0.076199319	0.38680475	0.373605306
10	0.00071153 2	0.001296759	0.010816359	0.018157964	0.185289824	0.24048946
15	0	0.000584689	0.005697341	0.012147739	0.13720915	0.223726046
20	0	0	0.00311433	0.00973681	0.109849333	0.189045844
30	0	0	0.001828895	0.007460614	0.091278815	0.089276205
40	0	0	0.001372608	0.006422349	0.07532135	0.051066299
50	0	0	0.001094753	0.005781173	0.071125391	0.036218656
60	0	0	0.000888552	0.005335003	0.064399288	0.026170985

Table.E9: Generation of H₂ (wt %) from 0.055 gm weight of 20CaCl₂/NaBH₄ at different temperature and time as given in the table.

Time (Minute)	Generation of H ₂ (wt%)					
	373 K	473 K	573 K	673 K	773 K	823 K
5	0.037703127	0.024714346	0.048576237	0.069877543	0.30301868	0.683420061
10	0.003252775	0.001701179	0.007891469	0.007707747	0.077235059	0.257675352
15	0.002170088	0.001293195	0.005202239	0.004298781	0.060837418	0.123295297
20	0.001628931	0.000872661	0.004221966	0.003186764	0.061071873	0.063832957
30	0.001305688	0.000579287	0.003477503	0.002452771	0.060744468	0.029806387
40	0.001060893	0	0.002744512	0.002247757	0.053051164	0.019629292
50	0.000825993	0	0.002273041	0.002133816	0.044938828	0.013861968
60	0.000703141	0	0.001961251	0.002008198	0.037677918	0.010984395

Table.E10: Generation of H₂ (wt%) from 0.055 gm Wt. of sample of p-NaBH₄ and xMnCl₂/NaBH₄ Mixture at 373 K of temperature under N₂ flow rate of 15ml/min through reactor.

Time (Minute)	Generation of H ₂ (wt%)					
	p-NaBH ₄	10MnCl ₂ /NaBH ₄	20MnCl ₂ /NaBH ₄	30MnCl ₂ /NaBH ₄	40MnCl ₂ /NaBH ₄	50MnCl ₂ /NaBH ₄
5	0	0.014594439	0.031003479	0.021774171	0.020797519	0.02718846
10	0	0.001095161	0.001546732	0.001654882	0.00123589	0.00190101
15	0	0	0.000750738	0.001064866	0.00087138	0.00117613
20	0	0	0.000547061	0.000319363	0	0.00093288
30	0	0	0.000323707	0	0	0
40	0	0	0.000241527	0	0	0
50	0	0	0	0	0	0
60	0	0	0	0	0	0

Table.E11: Generation of H₂ (wt%) from 0.055 gm Wt. of sample of p-NaBH₄ and xMnCl₂/NaBH₄ Mixture at 473 K of temperature under N₂ flow rate of 15ml/min through reactor.

Time (Minute)	Generation of H ₂ (wt%)					
	p-NaBH ₄	10MnCl ₂ /NaBH ₄	20MnCl ₂ /NaBH ₄	30MnCl ₂ /NaBH ₄	40MnCl ₂ /NaBH ₄	50MnCl ₂ /NaBH ₄
5	0.004394	0.032383682	0.025111597	0.021942988	0.122257863	0.0927035
10	0.001482	0.003228661	0.003492836	0.0054777	0.008411297	0.01001001
15	0.001319	0.002120135	0.002337307	0.003729889	0.004818516	0.00608145
20	0.000732	0.001611593	0.001680388	0.003017615	0.003404289	0.00445642
30	0.000484	0.001214393	0.001441033	0.002575957	0.002475158	0.00341778
40	0.000399	0.000984412	0.001218496	0.002114992	0.001936525	0.00260943
50	0.000328	0.000864531	0.001101621	0.001947329	0.001663588	0.0021262
60	0.000273	0.000612775	0.000983893	0.001735967	0.001477937	0.00173916

Table.E12: Generation of H₂ (wt%) from 0.055 gm Wt. of sample of p-NaBH₄ and xMnCl₂/NaBH₄ Mixture at 573 K of temperature under N₂ flow rate of 15ml/min through reactor.

Time (Minute)	Generation of H ₂ (wt%)					
	p-NaBH ₄	10MnCl ₂ /NaBH ₄	20MnCl ₂ /NaBH ₄	30MnCl ₂ /NaBH ₄	40MnCl ₂ /NaBH ₄	50MnCl ₂ /NaBH ₄
5	0.010417	0.098144584	0.255413342	0.175384626	0.242222136	0.26486557
10	0.007785	0.059456191	0.12650523	0.100749225	0.150324258	0.15362593
15	0.005449	0.058165914	0.084579652	0.083162343	0.120891789	0.12400661
20	0.003208	0.051040682	0.059294731	0.077182467	0.103095512	0.10208352
30	0.001815	0.04684957	0.048822128	0.064339718	0.087722902	0.08422803
40	0.001009	0.042263205	0.047277231	0.057666821	0.079624454	0.07064696
50	0.000829	0.040171047	0.042670078	0.05078941	0.070612505	0.05851719
60	0.000661	0.033317509	0.038814402	0.046831601	0.062223743	0.04908106

Table.E13: Generation of H₂ (wt%) from 0.055 gm Wt. of sample of p-NaBH₄ and xMnCl₂/NaBH₄ Mixture at 673 K of temperature under N₂ flow rate of 15ml/min through reactor.

Time (Minute)	Generation of H ₂ (wt%)					
	p-NaBH ₄	10MnCl ₂ /NaBH ₄	20MnCl ₂ /NaBH ₄	30MnCl ₂ /NaBH ₄	40MnCl ₂ /NaBH ₄	50MnCl ₂ /NaBH ₄
5	0.039581	0.225947958	0.75688182	0.536918627	0.568323251	0.61404181
10	0.024346	0.120706806	0.336004109	0.288790527	0.216222546	0.27826172
15	0.014843	0.086376615	0.246054973	0.241562025	0.180351546	0.20236735
20	0.009678	0.063793602	0.195626457	0.188635119	0.150474807	0.09422203
30	0.006397	0.047421282	0.125424068	0.149613028	0.106714662	0.01498045
40	0.005047	0.038775866	0.066435463	0.094920902	0.064030029	0.01130808
50	0.00438	0.031136375	0.031217886	0.053370006	0.030165088	0.00984071
60	0.003658	0.024651151	0.019252607	0.031515197	0.018148458	0.00886268

Table.E14: Generation of H₂ (wt%) from 0.055 gm Wt. of sample of p-NaBH₄ and xMnCl₂/NaBH₄ Mixture at 773 K of temperature under N₂ flow rate of 15ml/min through reactor.

Time (Minute)	Generation of H ₂ (wt%)					
	p-NaBH ₄	10MnCl ₂ /NaBH ₄	20MnCl ₂ /NaBH ₄	30MnCl ₂ /NaBH ₄	40MnCl ₂ /NaBH ₄	50MnCl ₂ /NaBH ₄
5	0.083184	0.763438289	0.879230249	0.71649348	0.701878027	0.84365988
10	0.055421	0.325110136	0.372495011	0.400344853	0.285484958	0.29471255
15	0.041724	0.217056062	0.074933301	0.35925981	0.213078292	0.2487722
20	0.031844	0.200194494	0.041203501	0.240627362	0.167868202	0.18071114
30	0.023605	0.106333463	0.013955454	0.099718057	0.111277292	0.10898855
40	0.021371	0.056089903	0.009951235	0.042091552	0.070642426	0.05912553
50	0.01993	0.038668254	0.006108379	0.024462029	0.050580312	0.0376797
60	0.017203	0.034585494	0.004497371	0.012623572	0.039053498	0.02668131

Table.E15: Generation of H₂ (wt%) from 0.055 gm Wt. of sample of p-NaBH₄ and xMnCl₂/NaBH₄ Mixture at 823 K of temperature under N₂ flow rate of 15ml/min through reactor.

Time (Minute)	Generation of H ₂ (wt%)					
	p-NaBH ₄	10MnCl ₂ /NaBH ₄	20MnCl ₂ /NaBH ₄	30MnCl ₂ /NaBH ₄	40MnCl ₂ /NaBH ₄	50MnCl ₂ /NaBH ₄
5	0.116401	0.671978006	0.951168191	0.567151442	0.576808078	1.02802996
10	0.265539	0.281975169	0.409621637	0.335515105	0.244424905	0.20692395
15	0.287296	0.13607644	0.109307504	0.205763488	0.133301387	0.1830601
20	0.308666	0.09163939	0.048691999	0.102827388	0.077560155	0.12842356
30	0.229256	0.081355366	0.028835247	0.057346865	0.040924903	0.05718217
40	0.281402	0.065343772	0.020069856	0.040091077	0.028142075	0.03197319
50	0.021382	0.040585861	0.013274587	0.029510655	0.019466566	0.02022592
60	0.184676	0.028014748	0.01016941	0.024152503	0.014943598	0.01546957

Calculation of total generated hydrogen in 60 minute

The generation of H₂ (wt%) from 0.055 gm weight of 20MnCl₂/NaBH₄ sample in small (HVC-DRM-5) reactor after 0 to 60 minute at each temperature at 373 K and 823 K considering Simpson's 1/3 rd rule as listed above in the table-3 and Table-4.

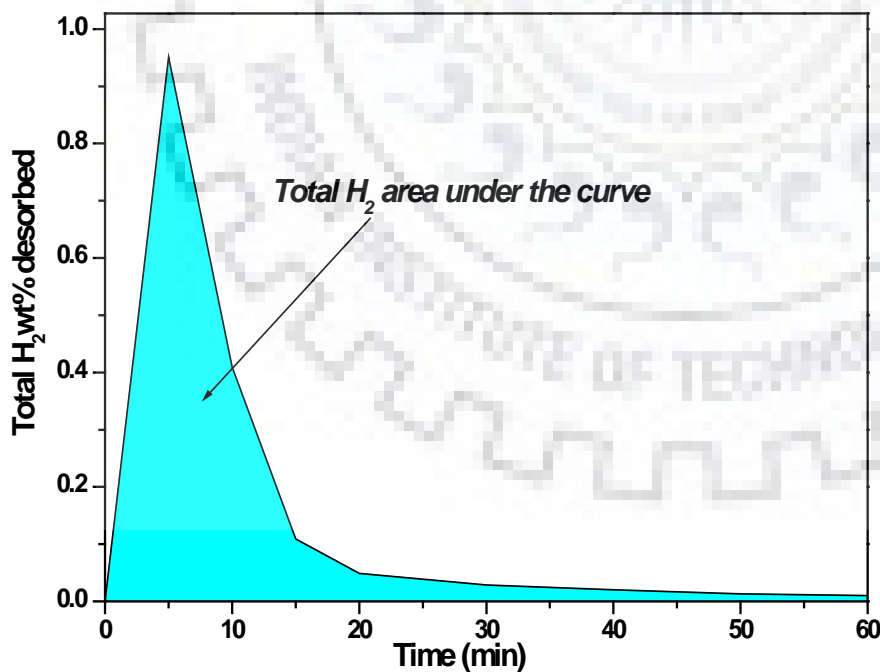
$$\int_{x_0}^{x_n} f(x)dx = h/3[f(x_0) + 4f(x_{i=1,3,5..}) + 2f(x_{i=2,4,6...}) + f(x_n)]$$

Where $h = \frac{x_n - x_0}{n}$, here n = number of interval

Sample calculation:

Time	Wt% desorbed at 823 K
0	0
5	0.951168191
10	0.409621637
15	0.109307504
20	0.048691999
20	0.048691999
30	0.028835247
40	0.020069856
50	0.013274587
60	0.01016941

} I₁
 } I₂



Calculation for I₁:

$$\text{Here, } h = \frac{20-0}{4} = 5$$

$$I_1 = \int_0^{20} f(x)dx = 5/3[0+4*(0.951168191+0.109307504) + 2*(0.409621637) + 0.048691999]$$

$$I_1 = 8.516397$$

Calculation for I₂:

$$\text{Here, } h = \frac{60-20}{4} = 10$$

$$I_2 = \int_{20}^{60} f(x)dx = 10/3[0.048691999 + 4*(0.028835247+0.013274587) + 2*(0.020069856) + 0.01016941]$$

$$I_2 = 0.891468$$

$$I = \int_0^{60} f(x)dx = I_1 + I_2 = 8.516397 + 0.891468$$

$$I = 9.407865$$

The 9.407865 total wt% desorbed of 20MnCl₂/NaBH₄ for 60 minute.

Table.E16: Effect of loading of additive

Metal additive	Time (Minute)	Generation of total desorbed H ₂ (wt %) by Simpson's 1/3 rd rule	
		373 K	823 K
p-NaBH ₄	0 - 60	0	2.421673
10MnCl ₂ /NaBH ₄	0 - 60	0.100947	8.940034
20MnCl ₂ /NaBH ₄	0 - 60	0.225512	9.407865
30MnCl ₂ /NaBH ₄	0 - 60	0.159373	8.291169
40MnCl ₂ /NaBH ₄	0 - 60	0.148579	6.979259
50MnCl ₂ /NaBH ₄	0 - 60	0.200098	10.70263

Table.E17: Effect of various additives

Metal additive	Time (Minute)	Generation of total desorbed H ₂ (wt %) by Simpson's 1/3 rd rule	
		373K	823K
p-NaBH ₄	0 - 60	0	2.421673
20MnCl ₂ / NaBH ₄	0 - 60	0.225512	9.407865
20ZnCl ₂ / NaBH ₄	0 - 60	0.193757	7.830013
20CaCl ₂ / NaBH ₄	0 - 60	0.322648	7.305906



Curriculum vitae

PRASHANT KUMAR SINGH

Ph.D. Research Scholar

Department of Chemical Engineering,

Indian Institute of Technology (IIT) Roorkee, Roorkee, India

Mobile No. - +91 9026835931, +91 9411091044

Email Id: prince04ru@gmail.com, psingh3@ch.iitr.ac.in

Personal Details:

Name in Full : Prashant Kumar Singh

Father Name : Fanish

Singh

Mother Name : Shashiprabha Singh

Permanent Address : 327W, Rajendra Nagar (west), Gorakhnath, Gorakhpur-273015,
U.P., India.

Current Address : Department of Chemical Engineering, Indian Institute of Technology
(IIT) Roorkee, Roorkee, India.

Date of Birth : 12th Nov, 1988

Gender : Male

Marital Status : Single

Nationality : Indian

Educational Qualification:

S.S.C.: GJIC, Gorakhpur (U.P. Board) in 2001.

H.S.C.: GJIC, Gorakhpur (U.P. Board) in 2003.

B.Tech (Chemical Engineering): I. E. T. M. J. P. Rohilkhand University Bareilly in 2008
and
secured 7.12 on 10 point scale.

Post-Graduate Diploma (Cement Technology): National Council for Cement & Building
Materials, Ballabgarh in 2011.

M.Tech (Chemical Engineering): Indian Institute of Technology Roorkee, Roorkee in
2011, Secured 6.91 on 10 point scale.

Doctor of Philosophy (Ph.D.) Chemical Engineering: Indian Institute of Technology
Roorkee, (Persuing).

Research and Project Work:

- **Ph.D Research Topic:** Generation of Hydrogen from Sodium-Borohydride at Low Temperature Using Various Catalysts and Additives for Fuel Cell Applications.
- **M.Tech Dissertation Title:** Modelling of Arsenic Removal in Packed Bed Column using Laterite Soil.
- **M.Tech mini-Project:** Production of Hydrogen from Water.
- **Post-Graduate Diploma Project:** Pollution Control Equipment in Cement Industries.
- **B.Tech Project Title:** Synthesis and Characterization of Biodegradable Polymer.

Research Publication in Journals/Conference:

Proceeding: Research Publication in Journals

- Prashant Kumar Singh, Taraknath Das, Generation of hydrogen from NaBH_4 solution using metal-boride (CoB, FeB, NiB) catalysts, International journal of hydrogen energy 42 (2017) 29360-29369. (**Impact Factor: 4.084**)
- Prashant Kumar Singh, Ishwar Sharan, Mamleshwar Kumar, Taraknath Das, Generation of hydrogen from sodium borohydride at low temperature using metal halides additive, International journal of hydrogen energy 42 (2019) 20191-20202. (**Impact Factor: 4.084**)
- Prashant Kumar Singh, Taraknath Das, Hydrolysis of sodium borohydride using supported cobalt boride catalyst for the generation of hydrogen. (under review)

Research Publication in Conference Proceeding

- (Chemcon-2016)(P. K. Singh, T. Das, "Generation of hydrogen using Co, Fe, and Ni boride catalysts from NaBH_4 solution", 27-30th Dec,2016, Chemcon2016, India)
- (WHEC-2016) (P. K. Singh, A. Jain, T. Das, "Generation and storage of hydrogen from NaBH_4 solution using metal boride catalysts" June 13-16, 2016, 21st WHEC-2016, Zaragoza, Spain)
- (Hypothesis-XIII 2018) (P. K. Singh, Ishwar Sharan, T. Das," Thermolysis of sodium borohydride at low temperature using metal halides as additive", 24-27th July, 2018, Hypothesis-XIII 2018, NTU, Singapore)